Dipl. Ing. Eva Pump

cis-Dihalo Ruthenium Benzylidenes as (*pre*-)Catalysts in Olefin Metathesis Reactions

Doctoral Thesis

Dissertation

zur Erlangung des akademischen Grades einer Doktorin der technischen Wissenschaften an der Technischen Universität Graz

Betreuung: Assoc. Prof. Dipl.-Ing. Dr.techn. Christian Slugovc

Institut für Chemische Technologie von Materialien

August 2014

EIDESSTATTLICHE ERKLÄRUNG

AFFIDAVIT

Ich erkläre an Eides statt, dass ich die vorliegende Arbeit selbstständig verfasst, andere als die angegebenen Quellen/Hilfsmittel nicht benutzt, und die den benutzten Quellen wörtlich und inhaltlich entnommenen Stellen als solche kenntlich gemacht habe. Das in TUGRAZonline hochgeladene Textdokument ist mit der vorliegenden Dissertation identisch.

I declare that I have authored this thesis independently, that I have not used other than the declared sources/resources, and that I have explicitly indicated all material which has been quoted either literally or by content from the sources used. The text document uploaded to TUGRAZonline is identical to the present doctoral dissertation.

Datum / Date

Unterschrift / Signature

abstract

This work is devoted to the study of the chemistry of N-heterocyclic carbene (NHC) bearing *cis*-dihalo ruthenium benzylidenes as a special class of (*pre*-)catalysts for olefin metathesis reactions. Said complexes have to isomerize to their corresponding *trans*-dihalo congeners before an olefin metathesis reaction can occur. Accordingly they can be regarded as a resting state of the actual catalytically active component.

Combined theoretical and experimental studies were conducted with the aim to understand the isomerization process itself and to use this knowledge to explain and in further course to tune the activity of *cis*-dihalo configured (*pre*-)catalysts in olefin metathesis in general and in ring opening metathesis polymerization (ROMP) in particular. For that purpose, several families of ruthenium catalysts in which at least one of the ligands was systematically varied were prepared, characterized and investigated in regard to the above mentioned context.

It was shown that reduction of the steric bulk of the N-heterocyclic carbene ligand shifts the *cis*-*trans* equilibrium towards the *trans*-isomer. Systematic variation of the anionic ligands in such complexes was conducted and results reveal that the highest activity can be observed in systems in which the *cis*-*trans* equilibrium is shifted towards the *trans*-isomer. Further, electronic tuning of the benzylidene ligand was studied and again the same result was retrieved. Summarized, the synopsis of all three parts mentioned is clearly the position of the *cis*-*trans* equilibrium of N-heterocyclic carbene bearing dihalo ruthenium benzylidenes, which is above all decisive for their activity profile.

Beyond that, it has been shown that in NHC bearing *cis*-dihalo ruthenium benzylidenes the halide *trans* to the N-heterocyclic carbene is particularly labile as it can be easily exchanged with neutral donor ligands. The resulting chemical equilibrium of the *cis*-dihalo compound with its cationic counterpart which has been shown to be inactive in catalyzing olefin metathesis reactions is most probably a key for explaining hitherto unexplained solvents effects. Finally, it has been shown, that small amounts of electron donor ligands catalyze the *cis*-*trans* isomerization process which eventually leads to a higher activity of the investigated species in olefin metathesis reactions.

kurzfassung

Diese Arbeit widmet sich einer chemischen Studie über N-heterozyklischer Carben (NHC) tragender *cis*-Dichlor Ruthenium Benzylidene als eine besondere Klasse von Olefin Metathese (*prae*-)Katalysatoren. Besagte Komplexe müssen zu den entsprechenden *trans*-Dihalo Gegenstücken isomerisieren, bevor die Olefin Metathese stattfinden kann. Entsprechend können sie als Ruhezustand der tatsächlich katalytisch aktiven Komponente angesehen werden.

Kombinierte theoretische und experimentelle Studien wurden durchgeführt, um den Isomerisierungsprozess an sich zu verstehen und das Wissen zu nutzen, um die Aktivität von *cis*-Dihalo konfigurierten (*prae*-)Katalysatoren in der Olefin Metathese und im speziellen in der Ring öffnenden Metathesis Polymerisation (ROMP) zu erklären und zu verbessern. Zu diesem Zweck wurde eine Reihe von Katalysatorfamilien hergestellt und charakterisiert, in denen sich zumindest ein Ligand am Ruthenium systematisch verändert. Folglich wurden diese Komplexe hinsichtlich des oben angeführten Zusammenhangs untersucht.

Es konnte gezeigt werden, dass eine Verkleinerung des NHC-Liganden das *cis-trans* Gleichgewicht hin zum *trans*-Isomer verschiebt. Systematische Variationen der anionischen Liganden in solchen Komplexen führten zu dem Resultat, dass die höchste Aktivität in Systemen beobachtet wurde, in denen das *cis-trans* Gleichgewicht zum *trans*-Isomer verschoben war. Außerdem wurden elektronische Tunings am Benzylidene Liganden studiert, die wiederum zum gleichen Ergebnis führten. Daraus geht deutlich hervor, dass die Synapse der drei erwähnten Teile deutlich die Position des *cis-trans* Gleichgewichts der NHC-tragenden Dihalo Ruthenium Benzylidene ist, welches einen massgeblichen Einfluss auf das Aktivitätsprofil der(*prae*-)Katalysatoren hat.

Darüber hinaus wurde gezeigt, dass in diesen Verbindungen besonders das Halid *trans* zum N-heterozyklischen Carben sehr labil ist, nachdem es leicht mit neutralen Donor-Liganden ausgetauscht werden konnte. Das resutlierende chemische Gleichgewicht zwischen *cis*-Dihalo Verbindung und dem kationischen Gegenstück, das in der katalysierenden Olefin Metathese inaktiv ist, ist höchstwahrschinlich der Schlüssel, der bisher unerklärte Lösungsmittel-Effekte erklären könnte. Schließlich konnte gezeigt werden, wie kleine Mengen an Elektronendonor-Liganden die *cis-trans* Isomerisierung katalysieren und folglich eine höhere Aktivität der untersuchten Spezies in der Olefin Metathese hervorrufen.

acknowledgement

It is my pleasure to express my gratitude to all those who helped and supported me in the accomplishment of my PhD thesis. In particular I want to owe this work to my family who has supported me thoughtout this time. Thank you for being there!

I want to thank my supervisor Christian Slugovc. I have experienced extraordinary support and new perspectives during my PhD time. Thanks for the discussions, opportunities and for being patient in times I was impatient. In this context I also thank Franz Stelzer for the opportunity to do this work at ICTM. Cordial thanks to Renate Trebizan and Liane Hochgatterer for their ready help in any organizational request. For the reliable accomplishment of various analyses I thank Roland Fischer and Ana Torvisco, Petra Kaschnitz and Josephine Hobisch. I am grateful for valuable contributions to this work, especially by Michaela Zirngast and Anita Leitgeb.

Many thanks go to all partners and colleagues from the EUMET project to whom I owe joyful hours and fruitful discussions at the project meetings spread all over Europe. In particular, I want to mention César Alejandro Urbina Blanco, Thibault Schmid Simone Manzini and all others. Special thanks go also to project leader Steve Nolan for realizing this project and to Karol Grela (and team) for cooperations in Warsaw and Graz.

Particulary, I want to outline the great time I expired at King Abdullah University of Science and Technology (KAUST) - I never believed it was possible. Special thanks go to Luigi Cavallo and Albert Poater for the extraordinary supervision and for giving me an understanding for theoretical DFT calculations, but also for the amazing free time we shared together. Thanks to Nathalie Gregoire (for perfect organization), the Italian Mafia (Romina Oliva, Anna Vangone, Laura Falviene, Luca Fortunato, Silvano del Gobbo, Michele di Christo and even Carlo Vittorio) and the rest of the Cavallo Group (Mohit Chawla, Sai Chaitanya-Vummaleti, Sheikha Lardhi). Additionally, I want to thank the French Mafia (especially to Violaine Mendez for including me in the French clique, Thomas Maugin, Paco Laveille, Loic Marnat and all others), my Saudi girls (Rawan Olayan, Ghofran Kamal and Roba Binyahib for sharing your culture and thoughts), the nine Austrians I finally found (special thanks to ʒen Kosel and Thomas Theussl), the beach crew (especially Hamada Gharib for the wind surfing sessions), my yoga teacher and all others I met there.

I am indebted to all my friends and colleagues from ICTM for provided help whenever needed, a friendly and inspirational working atmosphere and enjoyable time spent together outside the lab. Special thanks go to Anita Leitgeb (for so many earworms), Julia Wappel (for cutting everything into two halves), Julia Kienberger (for swimming sessions), Simone Strasser (for your extraordinary appetite), Christina Wappl (for your contributions to the german language), David Fast (for making good music), David Reishofer (for perfect organizations), Thomas Bauer (for the "where am I" game), Christopher Fradler (for the Fradius), Katharina Gallas (for the bad hair day), Andreas Dunst (for "simply why not"), Gerwin Passer (for unlocking my computer), Dominik Wohlmuth (for your curls), Florian Preishuber-Pflügl (for the time you went for bike rides with me), Patrick Kosmus (for the photosessions), Mudassir Abbas (for wearing a Lederhose), Sebastijan Kovacic (for the trip to Maribor), Simon Leimgruber (for your tyrolese dialect), Kathrin Bohnemann (for culinaric highlights) and Julia Langer (for sharing your Indian and Japanese experiences) and all others, with whom I shared my time.

Special thanks are also dedicated to my friends outside University, who always were there for me and distracted me from being involved with too much chemistry. Thank you to my sister Lisa (simply for being there), my cousin Claudia (for cooking sessions), Sophie Ederer (for more than 15 years of friendship), Stephanie Gärnter, Bernhard Ludwig and Paula (for being the coolest family I know), Claudia Wagner, Victoria Rezler und Michaela Lorber (for our lady's-nights), Birgit Ungerböck (for help and advice), for Jakob "Jogl" Feuchter (for your irregular working times), Stefan Maurer (for brunching times), Simone Trummer (for bringing me back to my west-styrian routes), Philipp and Karin Lehner (for the best saddle of venison I ever ate), FM4-music and everyone/thing else inspiring me within the last years.

Finally I want to gratefully acknowledge financial support by the European Commision (FP7 no CP-FP 211468-2), Umicore Precious Metal Chemistry, Graz University of Technology and Gesellschaft österreichischer Chemiker (GÖCH), Österreichische Akademie der Wissenschaften (ÖAW) and Springer Verlag for the „Chemical Monthly" Fellowship.

table of content

introduction

into olefin metathesis

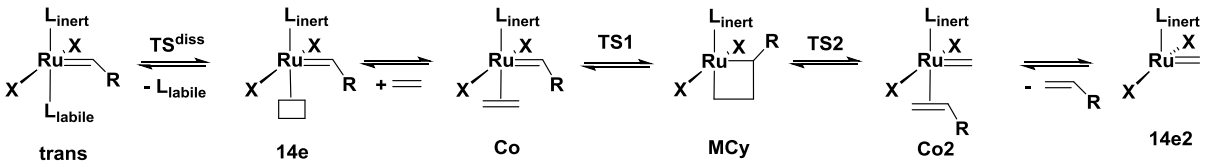

1. General Background

Olefin metathesis has become a powerful reaction for the formation of carbon-carbon (C=C) double bonds in organic chemistry.[1] Several types of reactions can be performed with one and the same alkylidene catalyst, dependent on the substrate and reaction conditions (*cf.* Scheme 1). The importance of metathesis reactions is refelcted in its broad field of applications as various fine chemicals,[2] asymmetric and biologically active compounds,[3] new functionalized materials and various polymers became easily accessible through this reaction.[4]

Scheme 1. Different types of olefin metathesis transformations.

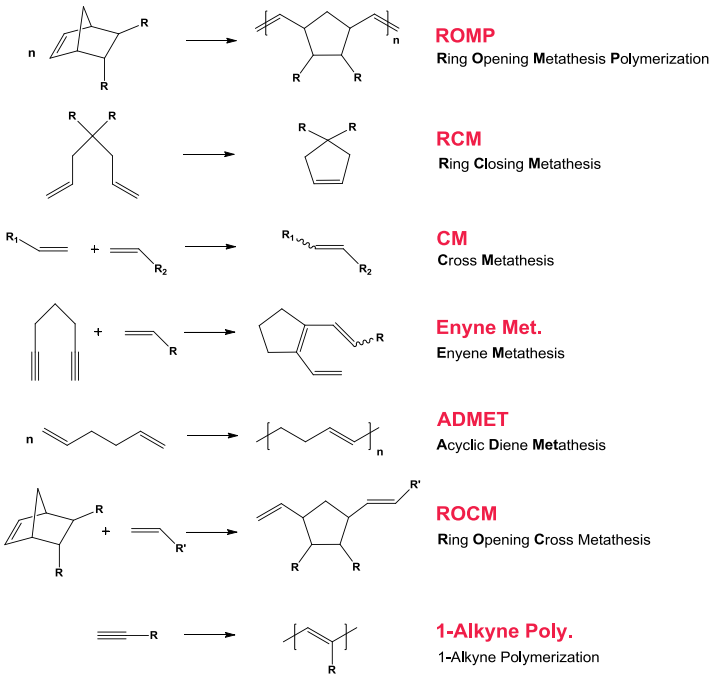

(1) Grubbs, R. H. *Handbook of Olefin Metathesis*, Wiley-VCH, Weinheim, Germany, **2003**.

(2) (a) Connon, S. J. ; Blechert, S. *Angew Chem, Int Ed.* **2003**, 42, 1900-1923. (b) Pozgan, F.; Dixneuf, P. H. Metathesis Chemistry: *From Nanostructure Design to Synthesis of Advanced Materials*, Dordrecht, The Netherlands: Springer **2007**, *243*, 195-222. (c) Mele, G.; Li, J.; Vasapollo, G. *Chim. Oggi.* **2008**, *26*, 72-74.

(3) (a) Giudici, R. E., Hoveyda, A. H. *J. Am. Chem. Soc.* **2007**, *129*, 3824–3825; (b) Keitz, B. K. Grubbs, R. H. *Organometallics* **2010**, *29*, 403–408; (c) Stenne, B.; Timperio, J.; Savoie, J.; Dudding, T.; Collins, S. K. *Org Lett.* **2010**, *12*, 2032–2035; (d) Schmidt, B.; Staude, L. *J. Org. Chem.* **2009**, *74*, 9237-9240.

(4) (a) Leitgeb, A.; Wappel, J.; Slugovc, C. *Polymer* **2010**, *51*, 2927-2946. (b) Bielawski, C. W.; Grubbs, R. H. *Prog. Polym. Sci.,* **2007**, *32*, 1-29. (c) Mol, J. C. *J. Mol. Catal. A.* **2004**, *213*, 39-45. (d) Baughman, T. Wagener, K. B. *Adv. Polym. Sci.* **2005**, *76*, 1-42.

According to the Chauvin mechanism (*cf.* Scheme 2), the principal steps of olefin metathesis involve the transformation of a metal–alkylidene complex and a coordinated olefin into a four-membered metallacycle. The subsequent opening of the metallacylce in the forward direction leads to the formation of the observed products.[5]

Scheme 2. Olefin Metathesis mechanism proposed by Chauvin.

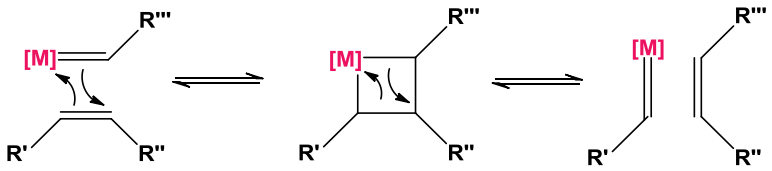

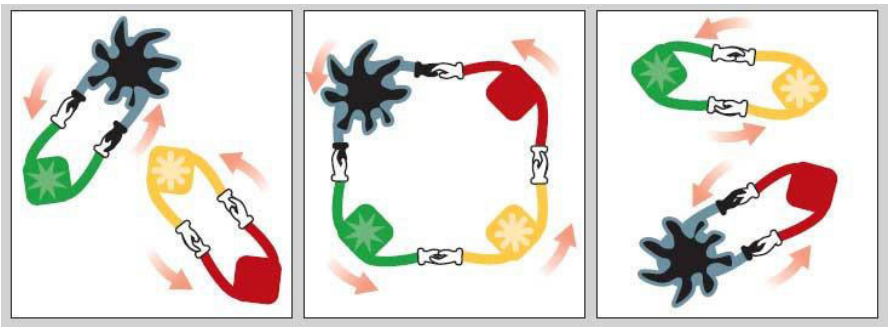

In 2005 Chauvin, Schrock and Grubbs were awarded with the Nobel prize for Chemistry for their affords connected with the clarification of the reaction mechanism and the development of highly efficient transition metal (molybdenum, ruthenium) catalysts.[6] Focusing on Ru-based complexes, a high variety of catalysts were developed in the last decade, which paved the way for widespread major-industrial applications of olefin metathesis in pharmaceutical chemistry (e.g. synthesis of a complex Hepatitis C drug)[7] as well as in polymer industry (Norsorex)[8] or even in petrochemical industry.

(5) Hérisson, P. J. L.; Chauvin, Y. *Die Makromol. Chem.* **1971**, *141*, 161-176.

(6) (a) The Nobel Prize in Chemistry 2005, 5 Oct 2005, http://nobelprize.org, 19. June 2014. (b) R. R. Schrock, *Angew. Chem. Int. Ed,,* **2006**, 45, 3748–3759. (c) R. H. Grubbs, *Angew. Chem. Int. Ed.,* **2006**, 45, 3760–3765. (d) Y. Chauvin, *Angew. Chem. Int. Ed.,* **2006**, *45*, 3740–3747.

(7) Medivir AB „Phase III Data for Simeprevir Demonstrating Efficacy and Safety in Genotype 1 Hepatitis C Patients“ December 20, 2012.

(8) http://astrotech.at/index.php/norsorex.html, June 5, 2014.

2. Well-Defined Ruthenium Catalysts

2.1. Design of Typical, Homogenous Ruthenium Catalysts

The development of homogenous olefin metathesis catalysts based on ruthenium (L_2X_2Ru=CHR-type) commenced in 1992,[9] when the first well-defined complexes were isolated by Grubbs and co-workers. Ruthenium was selected as transition metal due to its excellent functional group tolerance, for water as well as - with some restrictions - for oxygen.[10] All other properties of the catalyst are defined by five ligands which are arranged around the transition metal center in a planar pyramidal geometry: a carbene as active site, two neutral (phosphines, N-heterocyclic carbene) and two anionic ligands (in most cases chlorides). The typical structure and some examples can be found in Figure 1.

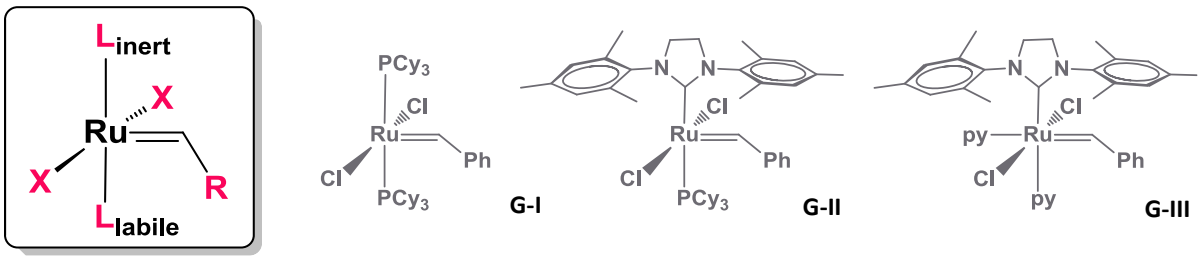

Figure 1. Typical structure of an homogenous Ru based catalyst (left) and famous examples (Grubbs **G-I**, **G-II** and **G-III** catalysts).

By changing the steric and electronic properties of the ligands, special catalysts with improved stability, reactivity and/or selectivity can be designed.[11] For the inert ligand (L_{inert}) the introduction of a N-heterocyclic carbene (NHC) - independently by Herrmann,[12] Grubbs[13]

(9) Nguyen, S. T.; Johnson, L. K.; Grubbs, R. H. *J. Am. Chem. Soc.*. **1992**, *114*, 3974-3975.

(10) Vougioukalakis, G. C.; Grubbs, R. H. *Chem. Rev.* **2010**, *110*, 1746-1787.

(11) Sanford, M. S.; Love, J. A.; Grubbs, R. H. *Organometallics* **2001**, *20*, 531-538.

(12) (a) Weskamp, T.; Kohl, F. J.; Hieringer, W.; Gleich, D.; Herrmann, W. A. *Angew. Chem., Int. Ed.* **1999**, *38*, 2416-2419. (b) Weskamp, T.; Kohl, F. J.; Herrmann, W. A. *J. Organomet. Chem.* **1999**, 582, 362-365. (c) Ackermann, L.; Fürstner, A.; Weskamp, T.; Kohl, F. J.; Herrmann, W. A. *Tetrahedron Lett.* **1999**, *40*, 4787-4898. (d) Frenzel, U.; Weskamp, T.; Kohl, F. J.; Schattenmann, W. C.; Nuyken, O.; Herrmann, W. A. *J. Organomet. Chem.* **1999**, *586*, 263-265.

(13) Scholl, M.; Trnka, T. M.; Morgan, J. P.; Grubbs, R. H. *Tetrahedron Lett.* **1999**, *40*, 2247-2250.

and Nolan[14] - was a major breakthrough in olefin metathesis. Mixed NHC-phosphine complexes (2nd generation of catalysts) were found to possess greater metathesis activity and enhanced thermal stability than the previous generation. It is believed that the higher basicity of the saturated imidazole ligands is translated into an increased activity of the desired catalysts due to a preferential dissociation of the labile ligand (*trans*-effect). Examining the labile ligand more carefully it was shown that in combination with mixed NHC-phophine complexes, the phosphine σ-donor strength and the rate of catalyst initiation correlates leading to enhanced activity in the following order: $P(n\text{-}Bu)_3 < PCy_3 < P(p\text{-}CH_3OC_6H_4)_3 < P(p\text{-}CH_3C_6H_4)_3 < PPh_3, P(p\text{-}FC_6H_4)_3 < P(p\text{-}ClC_6H_4)_3 < P(p\text{-}CF_3C_6H_4)_3$.[15] Considering the anionic ligands, in most cases chloro ligands were exchanged for sulfonates or fluorocarboxylates,[16] phenolates,[17] as well as other halides.[18] Generally it can be predicted, that the catalytic activity increases with smaller and more electron withdrawing anionic ligands from F > Cl > Br > I.[19] Also the carbene ligand R has a big influence on the initiation rate of the catalyst and increases for Grubbs 1st generation catalysts from -H > $-CH=C(Me)_2$ > -Ph > $-CH_2CH_3$.[18a] Nowadays, mainly benzylidene (Materia)[20] and indenylidene (Umicore)[21]

(14) (a) Huang, J.; Stevens, E. D.; Nolan, S. P.; Petersen, J. L. *J. Am. Chem. Soc.* **1999**, *121*, 2674-2678. (b) Huang, J.; Schanz, H.-J.; Stevens, E. D.; Nolan, S. P. *Organometallics* **1999**, *18*, 5375-5380.

(15) Love, J. A.; Sanford, M. S.; Day, M. W.; Grubbs, R. H. *J. Am. Chem. Soc.* **2003**, *125*, 10103-10109.

(16) Krause, J. O.; Nuyken, O.; Wurst, K.; Buchmeiser, M. R. *Chem. Eur. J.* **2004**, *10*, 777–784

(17) (a) Conrad, J. C.; Amoroso, D.; Czechura, P.; Yap, G. P. A.; Fogg, D. E. *Organometallics* **2003**, *22*, 3634–3636. (b) Monfette, S.; Camm, K. D.; Gorelsky, S. I.; Fogg, D. E. *Organometallics* **2009**, *28*, 944–946.

(18) (a) Sanford, M. S.; Love, J. A.; Grubbs, R. H. *J. Am. Chem. Soc.* **2001**, *123*, 6543–6554. (b).Seiders, T. J.; Ward, D. W.; Grubbs, R. H. *Org. Lett.* **2001**, *3*, 3225–3228. (c) Gillingham, D. G.; Kataoka, O.; Garber, S. B.; Hoveyda, A. H. *J. Am. Chem. Soc.* **2004**, *126*, 12288–12290; (d) van Veldhuizen, J. J.; Campbell, J. E.; Giudici, R. E.; Hoveyda, A. H. *J. Am. Chem. Soc.* **2005**, *127*, 6877–6882. (e) Funk, T. W.; Berlin, J. M.; Grubbs, R. H. *J. Am. Chem. Soc.* **2006**, *128*, 1840–1846.

(19) (a) Dias, E. L.; Nguyen, S. T., Grubbs, R. H.; *J. Am. Chem. Soc.* **1997**, 119, 3887-3897. (b) Wappel, J.; Urbina-Blanco, C.A.; Abbas, M.; Albering, J. H.; Saf, R.; Nolan, S. P.; Slugovc, C. *Beilstein J. Org. Chem.* **2010**, *6*, 1091-1098.

(20) http://www.materia-inc.com/wp-content/uploads/materia-catalysts-2011.pdf, June 5, 2014.

(21) http://chemistry.umicore.com/products/#tax_reactiontype_ms=Metathesis, June 5, 2014.

Ru catalysts are used commercially, but also many other alkylidene ligands bring along a series of special catalysts for specific applications.[22]

2.2. Reaction Mechanism of Olefin Metathesis

The mechanism of Chauvin is generally accepted until today, however, it was complemented by describing the reaction steps more sophisticatedly.[23] The first experimental proof for the existence of the metallacycle was only characterized in 2010 by the group of Piers. They applied low temperature NMR spectroscopy for spotting intermediates during ring closing metathesis. Based on their experimental findings they succeeded in describing the kinetics of one full RCM turnover.[24] Theoretical density functional theory (DFT) calculations could precisely reproduce the found results and even complement the full mechanism for this conversion.[25]

In general, the accepted mechanism of olefin metathesis for Grubbs catalysts can be divided into three parts: initiation, propagation and termination. Bearing in mind that after one catalytic turnover the active species for NHC ruthenium catalysts is the same, it is obvious that main differences in reactivity occur in the initiation step. Pecularities of the initiation step will be discussed in the following Paragraph 2.2.1. To control the configuration of the new-formed C=C bond it is one of the most important and difficult targets to fully understand the origin of regio- and stereoselectivity. It is based on the key steps of the olefin metathesis process: the generation of the 14e species, the alkene coordination, the [2+2] cycloaddition generating a metallacycle and the corresponding reverse steps as shown in Scheme 3.[26]

(22) Diesendruck, C. E.; Tzur, E.; Lemcoff, N. G. *Eur. J. Inorg. Chem.* **2009**, 28, 4185–4203.

(23) Cavallo, L. *J. Am. Chem. Soc.* **2002**, *124*, 8965–8973.

(24) van der Eide, E. F.; Piers, W. E. *Nature Chemistry* **2010**, *2,* 571-576.

(25) Poater, A.; Pump, E.; Cavallo, L. *J. Chem. Theory Comput.* **2014**, submitted.

(26) (a) Basset, J. M.; Bilhou, J. L.; Mutin, R.; Theolier, A. *J. Am. Chem. Soc.* **1975**, *97*, 7376-7377. (b) Bilhou, J. L.; Basset, J. M. Mutin, R.; Graydon, W. F. *J. Chem. Soc. Chem. Commun.* **1976**, 970-971.

Scheme 3. First turnover of cross metathesis of [Ru] complex with ethene.

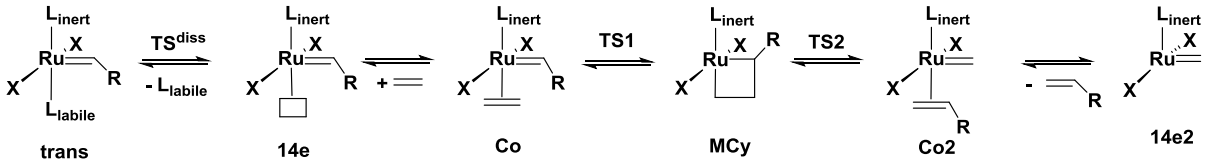

A comprehensive study of Cavallo et al. pointed out the influence of geometric but also energetic aspects of olefin metathesis intermediates on the reactivity and selectivity of the catalyst.[27] The chemoselectivity mainly depends on the preferential coordination of the substrate to the 14e species. Additionally, the progress of the reaction can be read out from respective energy profiles which allow for predictions regarding regio- and stereochemistry of the simplest substrate/Ru backbone combinations. It was found that the metallacycle is the most crucial intermediate. However, also respective transition states and coordination intermediates contribute (partly) to channel the direction of reaction progress. Theoretical DFT calculations suggest for example the origin of the preferential formation of *trans*-olefins in the product release step, which prevents the initially formed *cis*-olefin from escaping the metal to finally form the more stable *trans*-olefin.[28]

2.2.1. Initiation Mechanism

More advanced work has been done to describe the initiation mechanism into detail, as these reaction steps are the most crucial to describe the behavior of a (*pre*-)catalyst. Fast initiating catalysts are exemplary suited for controlled and living polymerization,[4a] while slow initiating complexes are used in high temperature conversions of sterical demanding substrates.[29] The latest state of the art regarding the initiation mechanisms are summarized in Scheme 4.

(27) Pump, E.; Bahri, N.; Credendino, R.; Poater, A.; Cavallo, L. **2014**, to be submitted.

(28) Bahri, N.; Credendino, R.; Cavallo, L. *Beilstein J Org Chem.* **2011**, *7*, 40–45.

(29) Songis, O., Slawin, A. M. Z.; Cazin, C. S. J. *Chem. Commun.* **2012**. *48*, 1266-1268.

Scheme 4. Three possible initiation mechanisms of olefin metathesis.

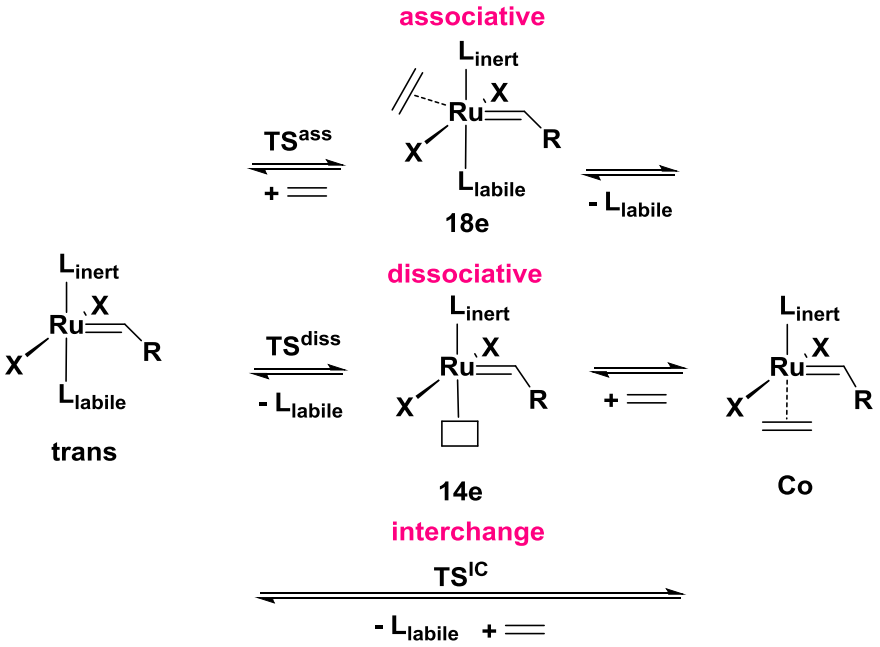

Early works from Grubbs predicted two pathways (associative and dissociative) to eventually occur during the initiation mechanism. Their results provided no evidence that an associative pathway contributes significantly to the metathesis reaction for typical Grubbs type catalysts.[30] Later works by Thiel et al. extended the potential initiation pathway by an interchange mechanism. They investigated the activation of electronically and sterically modified Grubbs-Hoveyda-type catalysts and the substrate diethyl diallylmalonate (DEDAM), butylvinylether (BuVe), 1-hexene, styrene and neohexene, finding that metathesis follow two parallel pathways (dissociative and interchange). The preference for one activation mode depends mainly on steric and electronic properties of the respective ruthenium complex and the olefin employed for metathesis.[31] A theoretical work of Nunez-Zarur et al outlined the major differences in initiation between Grubbs and Grubbs-Hoveyda type catalysts.[32] Similar findings were described by Urbina-Blanco et al for indenylidene Ru complexes. They showed that not even for the same class of catalysts the same initiation

(30) Sanford, M. S.; Love, J. A.; Grubbs, R. H. *J. Am. Chem. Soc.* **2001**, *123*, 749-750.

(31) Thiel, V.; Hendann, M.; Wannowius, K. J.; Plenio, H. *J. Am. Chem.Soc.* **2012**, *134*, 1104−1114.

(32) Nuñez-Zarur, F.; Solans-Monfort, X.; Rodriguez-Santiago, L.; Sodupe, M. *Organometallics* **2012**, *31*, 4203-4215

mechanism was found which highlights the importance of steric and electronic properties of so-called spectator ligands.[33]

3. *cis*-Dichloro Ruthenium Complexes

The study of latent metathesis catalysts and the means to activate them has important practical applications. The desire to enhance the catalyst stability to gain control over the catalytic process is essential when operation control is needed. A lower initiation rate can be exemplary adventagearous in ring opening metathesis polymerization (ROMP) to enhance the processing and storage time of the monomer/catalyst formulation, before the polymerization starts.[34] A deeper understanding, especially of the initiation mechanism of metathesis has yielded a class of latent ruthenium (*pre*-)catalysts with delayed initiation and switchable activity. Several concepts were elaborated to reduce the initiation rate of the catalyst, as shown in Figure 2. Depending on the applied concept, operation control can be regulated by e.g. thermal activation,[35] light[36] or activation agents, as acid.[37]

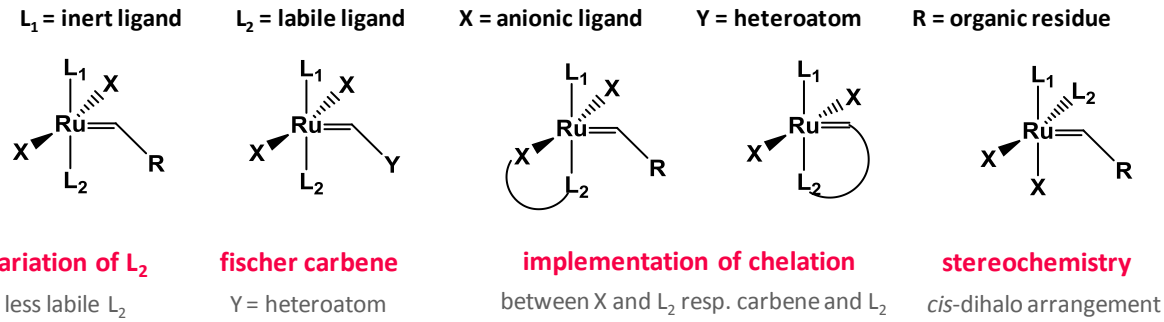

Figure 2. Exemplary designs of latent olefin metathesis initiators.

(33) Urbina-Blanco, C. A.; Poater, A.; Lebl, T.; Manzini, S.; Slawin, A. M.; Cavallo, L.; Nolan, S. P. *J. Am. Chem. Soc.* **2013**, *135*, 7073–7079.

(34) Ung, T., Hejl, A., Grubbs, R., H., Schrodi, Y. *Organometallics* **2004**, *23*, 5399-5401.

(35) (a) Slugovc, C.; Burtscher, D.; Stelzer, F.; Mereiter, K. *Organometallics* **2005**, *24*, 2255-2258; (b) Gstrein, X.; Burtscher, D.; Szadkowska, A.; Barbasiewicz, M.; Stelzer, F.; Grela, K.; Slugovc, C. *J. Polym. Sci. A* **2007**, *45*, 3494–3500.

(36) Ben-Asuly, A.; Aharoni, A.; Diesendruck, C. E.; Vidavsky, Y..; Goldberg, I.; Straub, B. F.; Lemcoff, N. G. *Organometallics* **2009**, *28*, 4652-4655.

(37) Monsaert, S.; Lozano Vila, A.; Drozdzak, R.; Van Der Voort, P. Verpoort, F. *Chem. Soc. Rev.* **2009**, *38*, 3360–3372.

The most trivial example is based on the variation of the Ru-L_2 bond strength (a). The more labile L_2, the more prone is the complex to undergo metathesis (and consequently the less stable it is). Hence, the catalysts stability increases with the following order of labile ligands: PF_3 < py < $P(OMe)_3$ < PMe_3 < PCy_3.[38] Another strategy (b) concerns the metal-alkylidene bond: by introducing a Fischer carbene the activity of the catalyst decreases tremendously. However, those complexes are limited to low temperature applications of electron rich olefins.[39] The most common concept to gain latent complexes is the implementation of a chelating ligand (c). A notable example from literature is a so called Schiff-base catalyst, bearing a L_2-X chelation, which can be activated by the addition of HCl.[37] However, the main methodology developed for this purpose has been the introduction of tethered carbene (L_2-R chelating) ligands. The evolution of ruthenium based metathesis catalysts bearing chelating alkylidenes provided a high variety of stable catalysts, starting from the early oxygen Hoveyda type benzylidenes[40] towards latent sulphur containing complexes.[41] However, for the latter case another phenomenon arose: two stereoisomers were found to coexist independently (d). For both isomers the general scaffold of a typical homogenous ruthenium catalyst remains on L_2X_2Ru=CHR-basis, however, the position of the ligands is interchanged. Most of the conventional available olefin metathesis active catalysts bear *trans*-dichloro structure featureing two chlorides feature in an approximately 160° degree angle to each other. In contrast, chlorides of its *cis*-dichloro counterpart are arranged in orthogonal configuration. Describing the arrangement of both isomers on the basis of the octahedron, the structural difference lies in the position of the halides, which are placed side

(38) Falviene, L.; Poater, A.; Cazin, C. S. J.; Slugovc, C.; Cavallo, L. *Dalton Trans.* **2013**, *42*, 7312-7317.

(39) Louie, J.; Grubbs, R. H. *Organometallics* **2002**, *21*, 2153-2164.

(40) Kingsbury, J. S., Harrity, J. P. A.; Bonitatebus, P. J.; Hoveyda, A. H. *J. Am. Chem. Soc.* **1999**, *121*, 791-799.

(41) (a) Ben-Asuly, A.; Tzur, E.; Diesendruck, C. E.; Sigalov, M.; Goldberg, I.; Lemcoff, N. G. *Organometallics* **2008**, *27*, 811–813. (b) Kost, T.; Sigalov, M.; Goldberg, I.; Ben-Asuly, A.; Lemcoff, N. G. *J. Organomet. Chem.* **2008**, *693*, 2200–2203. (c) Diesendruck, C. E.; Vidavsky, Y.; Ben-Asuly, A.; Lemcoff, N. G. *J. Polym. Sci., Part A: Polym. Chem.* **2009**, *47*, 4209–4213. (d) Ben-Asuly, A.; Aharoni, A.; Diesendruck, C. E.; Vidavsky, Y.; Goldberg, I.; Straub, B. F.; Lemcoff, N. G. *Organometallics* **2009**, *28*, 4652–4655. (e) Vidavsky, Y.; Lemcoff, N.G. *Beilstein J. Org. Chem.* ***2010***, *6*, 1106-1119. (f) Aharoni, A.; Vidavsky, Y.; Diesendruck, C. E.; Ben-Asuly, A.; Goldberg, I.; Lemcoff, N. G. *Organometallics* **2011**, *30*, 1607–1615. (g) Ginzburg, Y.; Anaby, A.; Vidavsky, Y.; Diesendruck, C. E.; Ben-Asuly, A.; Goldberg, I.; Lemcoff, N. G. *Organometallics* **2011**, *30*, 3430–3437.

by side in *cis*-dichloro complexes and opposite to each other in the *trans*-dichloro counterparts (*cf.* Figure 3). Although electronic properties remain similar, the impact on the catalyst performance is tremendous.

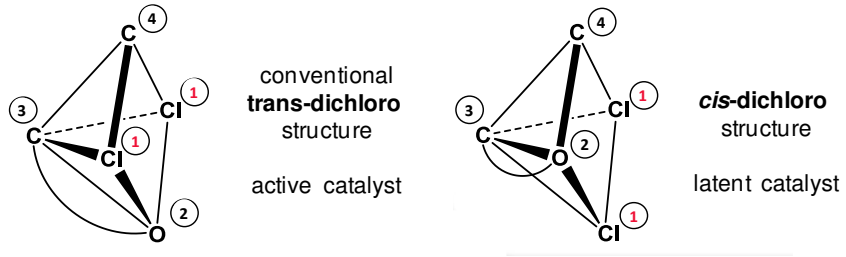

Figure 3. Coordination geometries of *trans*- (left) and *cis*-dichloro isomer (right).

The coexistence of *trans*- and *cis*-dichloro isomers was firstly described in 1993 when Grubbs et al. carried out derivatizations on first generation Grubbs complexes.[42] It remained unclear, if the *cis*-isomers could exist as a stable, non-interconverting species, until Hansen et al. isolated the first Grubbs-type metathesis catalyst with a fixed *cis*-stereochemistry of the chloride ligands.[43] Since then, several complexes have been isolated, bearing *cis*-dichloro stereochemistry, mainly connected with heterocyclic back bond chelating alkylidenes (O[44], S,[41] Se[45], N,[34] Br, I[46] and P[47]), but also with non-chelating phosphine ligands.[48] Generally, the

(42) Nguyen, S. T.; Grubbs, R. H. *J. Am. Chem. Soc.* **1993**, *115*, 9858-9859.

(43) Hansen, S. M; Rominger, F.; Metz, M.; Hofmann, P. *Chem. Eur. J.* **1999**, 5, 557-566.

(44)(a) Stefan Prühs, S.; Lehmann, C. W.; Fürstner, A. *Organometallics* **2004**, *23*, 280–287. (b) Slugovc, C.; Perner, B.; Stelzer, F.; Mereiter, K. *Organometallics* **2004**, *23*, 3622–3626; (c) Leitgeb, A.; Mereiter, K.; Slugovc, C. *Monatsh. Chem.* **2012**, *143*, 901–908. (d) Burtscher, D.; Perner, B.; Mereiter, K.; Slugovc, C. *J. Organomet. Chem.* **2006**, *691*, 5423–5430. (e) Abbas, M.; Slugovc, C. *Tetrahedron Lett.* **2011**, *52*, 2560–2562. (f) Abbas, M.; Slugovc, C. *Monatsh. Chem.* **2012**, *143*, 669–673. (g) Zirngast, M.; Pump, E.; Leitgeb, A.; Albering, J. H.; Slugovc, C. *Chem. Commun.* **2011**, *47*, 2261–2263. (h) Pump, E.; Fischer, R. C.; Slugovc, C. *Organometallics* **2012**, *31*, 6972-6979.

(45) Diesendruck, C. E.; Tzur, E.; Ben-Asuly, A.; Goldberg, I.; Straub, B. F.; Lemcoff, N. G. *Inorg. Chem.* **2009**, *48*, 10819–10825.

(46) (a) Barbasiewicz, M.; Michalak, M.; Grela, K. *Chem.-Eur. J.* **2012**, *18*, 14237-14241. (b) Barbasiewicz, M.; Malińska, M.; Błocki, K. *J. Organomet. Chem.* **2013**, *745-746*, 8-11. (c) Barbasiewicz, M.; Błocki, K.; Malińska, M.; Pawłowski' R. *Dalton Trans.* **2013**, *42*, 355-358.

(47) (a) DeHope, A.; Donnadieu, B.; Bertrand, G. *J. Organomet. Chem.* **2011**, *696*, 2899-2903. (b) Lexer, C.; Burtscher, D.; Perner, B.; Tzur, E.; Lemcoff, N. G.; Slugovc, C. *J. Organomet. Chem.* **2011**, *696*, 2466–2470.

catalytic activity of *cis*-dichloro catalysts in metathesis is by far not as high as that of their *trans*-dichloro counterparts. This can be explained either due to a different mechanism (side bound mechanism) or to an accessory activation step (*cis*-*trans* isomerization). Both possibilities will be discussed in the following paragraph 3.1.

DFT calculations were accomplished to study the relative stability of *cis*- and *trans*-dichloro X-chelated Hoveyda-type ruthenium complexes (X = O, S, Se, N and P). It was found that S, Se, N and P chelating benzylidenes thermodynamically prefer to exist in *cis*-dichloro form, whereas O-chelated complexes were only observed in their *trans*-configuration.[45] Additionally, it will be discussed how ligands (Chapter I-III), but also how donor molecules (Chapter IV) can influence the activity of *cis*-dichloro complexes.

3.1. Reaction Mechanism of *cis*-Dichloro Ruthenium Complexes

In this paragraph, two potential activation mechanisms of *cis*-dichloro ruthenium catalysts will be examined. It is believed that *cis*-dichloro complexes react either through a side bound-mechanism, where the olefin coordinates *cis* to the NHC ligand or through a bottom bound-mechanism after isomerization to its *trans*-dichloro counterpart. Investigating the thermodynamic stabilities of two main intermediates in the olefin metathesis cycle indicated no preferential trend according the (*cis*- or *trans*-) dichloro configuration (*cf*. Figure 4). It was revealed that the coordination intermediate (**Co**) definitely prefers a *cis*-coordination of ethene to the NHC ligand (2.7 kcal/mol), whereas the metallacycle (**MCy**) is thermodynamically more stable in *trans*-configuration (-3.2 kcal/mol).[38]

(48) (a) Bantreil, X.; Schmid, T. E.; Randall, R. A. M.; Slawin, A. M. Z.; Cazin, C. S. J. *Chem. Commun.* **2010**, *46*, 7115–7117. (b) Songis, O.; Slawin, A. M. Z.; Cazin, C. S. J. *Chem. Commun.* **2012**, *48*, 1266-1268; (c) Bantreil, X.; Poater, A.; Urbina-Blanco, C. A.; Bidal, Y. D.; Falivene, L.; Randall, R. A. M.; Cavallo, L.; Slawin, A. M. Z.; Cazin, C. S. J. *Organometallics* **2012**, *31*, 7415-7426. (d) Varnado, J. C. D.; Rosen, E. L.; Collins, M. S.; Lynch, V. M.; Bielawski, C. W. *Dalton Trans.* **2013**, *42*, 13251-13264.

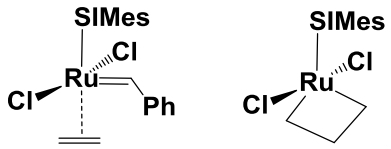

Co MCy

Figure 4. Structure of coordination intermediate of **G-II** catalyst (**Co**) and the simplest, second generation metallacycle (**MCy**).

This simple example shows that the probability to observe both isomers during a reaction is independent from the starting configuration of the complex and influenced by the substrate or impurities present in the reaction mixture. Potential initiation pathways for each isomer were already perused in previous works and will be treated in the following. These results should provide information to find the most apparent activation mechanism of *cis*-dichloro ruthenium complexes.

3.1.1. Side vs Bottom Bound Mechanism

DFT studies from Cavallo and Correa concluded that the preferential reaction pathway - either bottom- or side-bound - is a delicate balance between electronic, steric and solvent effects.[49] Also, studies of Goddard are indicating the relevance of both pathways, as the respective 14e species was found for both isomers.[50] The same group examined in 2008 both pathways more closely (see reaction intermediates and transition states in Figure 5), showing that the rates for metathesis of E- or Z-2-butene via a *cis*-chloride pathway would be infinitesimal compared to the dominant *trans*-chloride pathway.[51] For Z-olefins the gap of the time limiting transition state $\mathbf{TS_{CD}}$ needs around 16 kcal/mol more energy, for E-olefins the difference amounts still 6 kcal/mol, as can be taken from Figure 6.

(49) Correa, A.; Cavallo, L. *J. Am. Chem. Soc.* **2006**, *128*, 13352–13353.

(50) Benitez, D.; Goddard, W. A. *J. Am. Chem. Soc.* **2005**, *127*, 12218-12219.

(51) Benitez, D.; Tkatchouk, E.; Goddard, W. A. *Chem. Comm.* **2008**, 6194-6196.

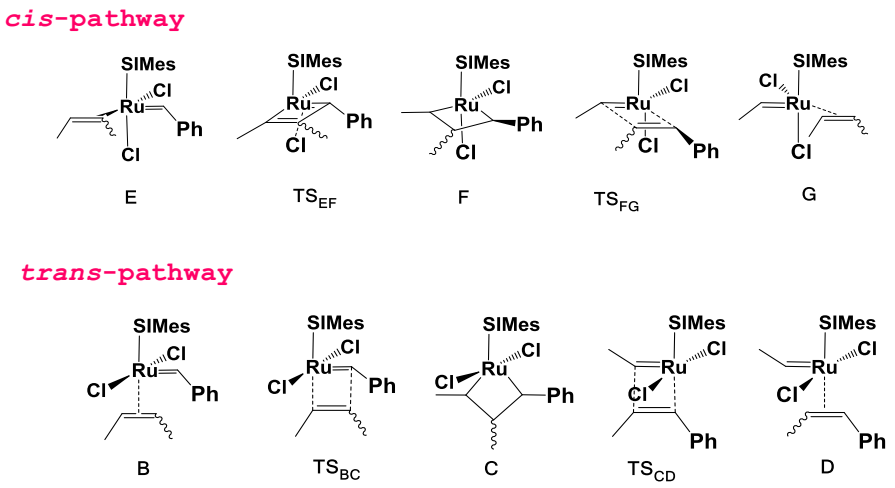

Figure 5. Intermediates and transition states of *cis* and *trans*-metathesis pathway.

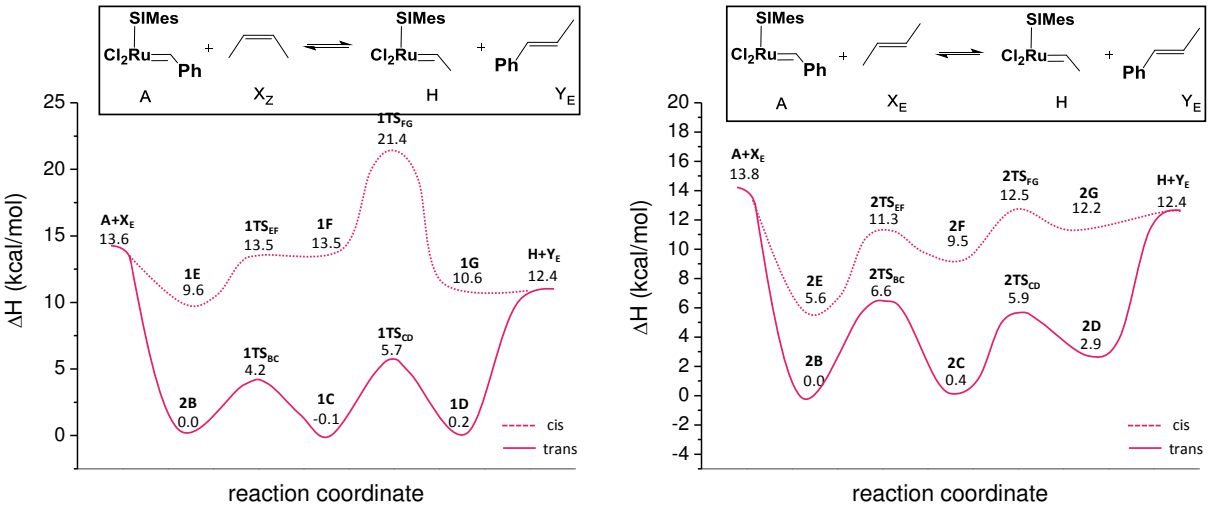

Figure 6 Energy profiles of *cis*- and *trans*-pathway using Z- (left) and E-2-butene (right) as substrate (M06, ΔH in CH_2Cl_2 kcal/mol).

Summarizing these results suggest that the rates for the side bound pathway for E and Z-2-butene would be infinitesimal compared to the dominant bottom bound pathway. Just in case of prevention of the *trans*-dichloro pathway and concurrent stabilization of the *cis*-dichloro geometry, the side-bound mechanism will occur, leading to a retention of the diastereochemistry of the stubstrate.

3.1.2. *cis-trans* Isomerization

The structure/activity relationship in Ru-catalyzed olefin metathesis was mainly investigated by Schrodi[34] and Grela[52]. It was proved that both isomers can be converted into each other in solvents (as CH_2Cl_2). Hence, another explanation for the (always) lower initiation rate for *cis*-dichloro complexes compared to the *trans*-counterpart could indicate an activation mechanism, connected to *cis-trans* isomerization. Potential pathways for the *cis-trans* isomerization were examined by Poater et al, revealing that either a concerted or a dissociative pathway occurs.[53] Isomerization is possible in both directions, however, associated with considerably high activation energies. Moreover, a differentiation of the chelating ligand needs to be done, as their flexibility and the σ-donor strength of the heteroatom influences the mechanism and the energy barriers, respectively.

In the following, two five-membered metal chelate ring catalysts bearing different ligands will be discussed. On the one hand, the catalyst bears a flexible pyridyl ligand ($\mathbf{A}^{py}$) and on the other hand a more rigid quinoline ligand ($\mathbf{A}^{quin}$). All containing reaction steps are exemplary shown in Figure 7.

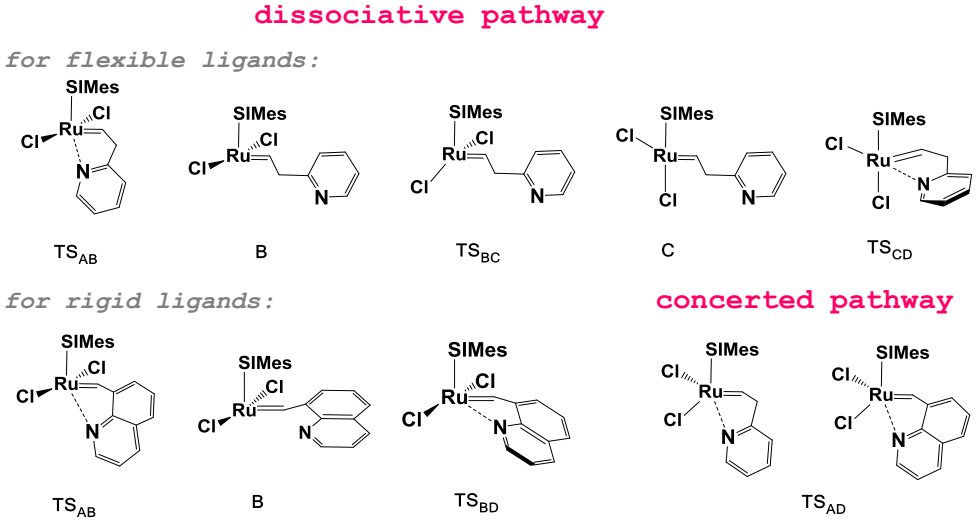

Figure 7. Intermediates and transition states of *cis* and *trans*-metathesis pathway.

(52) Barbasiewicz, M.; Szadkowska, A.; Bujok, R.; Grela, K. *Organometallics* **2006**, *25*, 3599–3604.

(53) Poater, A.; Ragone, F.; Correa, A.; Szadkowska, A.; Barbasiewicz, M.; Grela, K.; Cavallo, L. *Chem. Eur. J.* **2010**, *16*, 14354-14364.

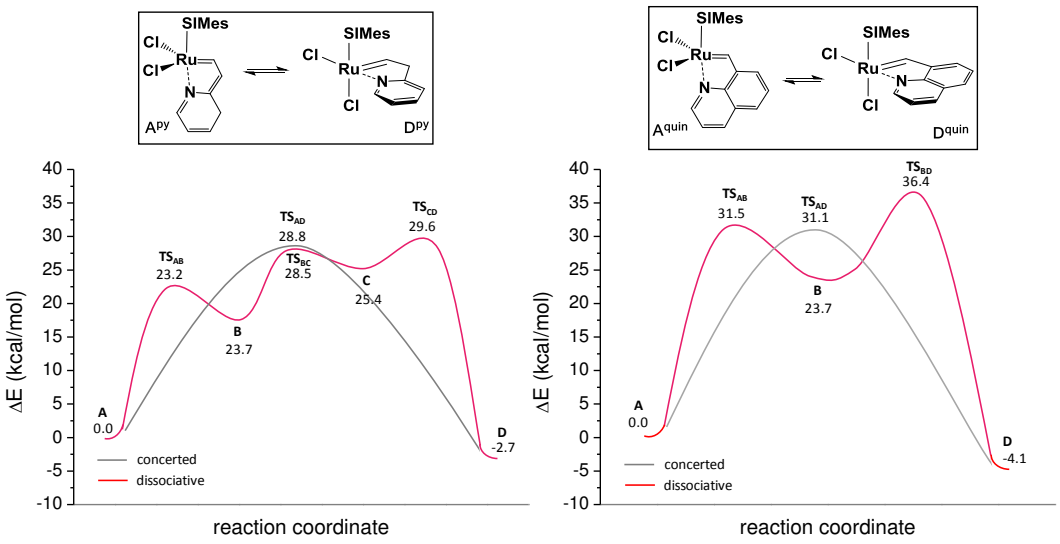

Figure 8. Energy profiles of *trans-cis* isomerization, using a flexible (left) and a rigid chelating ligand (right) (M06, ΔE in CH_2Cl_2 kcal/mol).

Comparing the energy profiles of the isomerization for $\mathbf{A}^{\mathbf{quin}}$ and $\mathbf{A}^{\mathbf{py}}$ (*cf.* Figure 8) the first pronounced differentiation was found for the dissociative pathway. For flexible ligands, two (*cis*- and *trans*-)14e species were found to occur during the isomerization, whereas for rigid ligands just one intermediate in *trans*-configuration was observed. When comparing energy differences between *cis*- and *trans*-species, it is obvious that the σ-donor strength of $\mathbf{A}^{\mathbf{py}}$ ($\Delta H_{D\text{-}A}$ = -2.7 kcal/mol) is less pronounced as for $\mathbf{A}^{\mathbf{quin}}$ ($\Delta H_{D\text{-}A}$ = -4.1 kcal/mol).[45] Comparing both catalysts, the time limiting transition states differ by 7 kcal/mol (dissociative pathway) and still by 2 kcal/mol (concerted pathway) in favor of the pyridyl complex. Dependent on the chelating ligand, both pathways compete more ($\mathbf{A}^{\mathbf{py}}$: concerted pathway is favored by 0.8 kcal/mol) or less ($\mathbf{A}^{\mathbf{quin}}$: concerted pathway is favored by 5.3 kcal/mol) with each other.

results and discussion

In the following chapters, some practical examples where *cis*-*trans* isomerization becomes important will be discussed: Chapter I outlines the role of isomerization for maintaining the stability of *trans*-dichloro ruthenium initiatiors at elevated temperatures. Chapter II treats with the role of unfavorable halide dissociation. The next chapter deduces a correlation between thermodynamic *cis*-*trans* stability of the isomer and the activity of the initiator. Finally, the impact of donor molecules (impurities or conscious addition) to accelerate/decelerate metathesis will be discussed in Chapter IV.

CHAPTER I

nhc series - influence of *trans-cis* isomerization

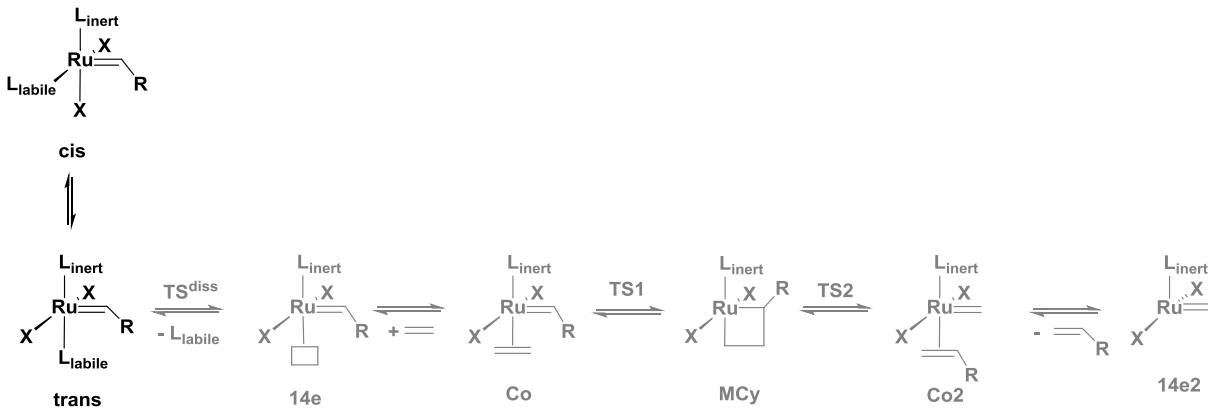

1. Abstract

The impact of inert ligands, as tricyclohexylphosphine (PCy_3, **trans-I**), N,N'-bis (2,4,6-(trimethyl)phenyl) imidazolin-2-ylide (SIMes, **trans-II**), and its 2,6-(diisopropyl)phenyl- (SIPr, **trans-III**), 2-methylphenyl- (SI*o*tol, **trans-IV**) and 2,5-dimethylphenyl- (SIXyl, **trans-V**) derivatives on the activity of latent catalysts bearing a rigid chelating 10-vinylbenzo(h)quinoline ligand is described within a comprehensible study at elevated temperatures. The influence of electronic and sterical modifications of the NHC was compared in ring opening metathesis polymerization (ROMP) in respect to a previously reported *trans*-dichloro (κ^2(C,N)-2-(benzo(h)quinoline-10-yl)methylidene)(1,3-bis(2,4,6-trimethyl-phenyl)4,5-dihydro-imidazol-2-ylidene)-ruthenium compound. DFT calculations revealed that reduction of the steric bulk of the N-heterocyclic carbene ligand shifts the *cis-trans* equilibrium towards the *trans*-isomer. A substantial increased thermal stability of ruthenium catalysts bearing sterically more demanding NHCs (as **trans-II** and **trans-III**) was consequentially assigned to a concomitant *trans-cis* isomerization at temperatures higher than 140°C.

2. Introduction

Since the introduction of a N-heterocyclic carbene,[54] olefin metathesis has attracted more and more attention within a broad field of organic chemistry, polymer chemistry and catalysis in general. However, under certain conditions some catalysts are overactive and rapidly degrade at elevated temperature. Latent catalysts (as **trans-II**) have been developed, typically bearing a SIMes ligand together with strong (and rigid, π-conjugated) chelating ligands (as benzo(h)quinolinylidene (**L-I**)),[55] which refuse Ru-N dissociation at ambient temperature. Generally, this kind of complexes is known to be perfectly stable at elevated temperatures and active in olefin metathesis only at temperatures above 100°C. This feature appears useful for high temperature applications in ring-closing metathesis (RCM) reactions

(54) Samojłowicz, C.; Bieniek, M.; Grela, K. *Chem. Rev.* **2009**, *109*, 3708-3742.

(55) Szadkowska, A.; Gstrein, X.; Burtscher, D.; Jarzembska, K.; Wozniak, K.; Slugovc C.; Grela, K. *Organometallics* **2010**, *29*, 117-124.

of sterically demanding substrates.[56] Additionally, in some ring opening metathesis polymerizations (ROMP) thermal activation[35] can be accomplished for operation control.[4a,57] Regarding DCPD, high processing temperatures are not beneficial as evaporation of the monomer occurs in open systems. Hence, a concept was elaborated to combine high stability of the initiator with a lower switching temperature of more moderate 80°C. The stability was maintained by keeping the rigid **L-I** ligand unchanged. Hence, fine-tuning of the activity was accomplished by modifying the inert ligand L^2=SIMes. It is known that the strength of the Ru-N chelation can be controlled by the so-called *trans*-effect. The electron donating ability and the size of the ligand *trans* to the benzo(h)quinoline nitrogen influences the actual strength of the Ru-N interaction. The larger and more basic the *trans*-ligand, the faster the dissociation of the labile ligand occurs and the better the Ru metallacyclobutane intermediate is stabilized, which is crucial for the activation.[18a,30,58] Additionally, the molecular architecture of this ligand is significant to better describe the influence of steric parameters on the catalysts performance.[59] The Cavallo group has introduced the buried volume to quantify the sterical demand of N-heterocyclic carbenes. V_{bur} (in %) gives indication of the space occupied by the NHC ligand in the first coordination sphere of the metal center. The bigger the buried volume the bulkier is the NHC ligand.[60] It can be calculated on-line by the SambVca (Salerno molecular buried volume calculation) software.[61] Five different ancillary ligands (L^1-L^5) were selected, as shown in Figure 9. First generation ligand L^1=PCy_3 was included as dissociation of Ru-PR_3 bonds is known to be 20 to 40 kcal/mol

(56) (a) Vorfalt, T.; Leutheußer, S.; Plenio, H. *Angew. Chem.* **2009**, *121*, 5293 – 5296; *Angew. Chem. Int. Ed.* **2009**, *48*, 5191 – 5194; (b) Sashuk, V.; Peeck, L. H.; Plenio, H. *Chem. Eur. J.* **2010**, *16*, 3983 –3993; (c) Peeck, L. H.; Plenio; H. *Organometallics* **2010**, *29*, 2761 – 2768.

(57) Leitgeb, A.; Szadkowska, A.; Michalak, M.; Barbasiewicz, M.; Grela, K.; Slugovc, C. *J. Polym. Sci. Part A: Polym. Chem.* **2011**, *49*, 3448-3454.

(58) (a) Sanford, M. S.; Love, J. A.; Grubbs, R. H. *J. Am. Chem. Soc.* **2001**, *123*, 6543-6554; (b) Lujan, C.; Nolan, S. P. *J. Orgmet. Chem.* **2011**, *696*, 3935-3938.

(59) Clavier, H.; Nolan, S. P. *Chem. Commun.* **2010**, *46*, 841–861

(60) (a) Hillier, A. C.; Sommer, W. J.; Yong, B. S.; Petersen, J. L.; Cavallo, L.; Nolan, S. P. *Organometallics* **2003**, **22**, 4322-4326. (b) Poater, A.; Cosenza, B.; Correa, A.; Giudice, S.; Ragone, F.; Scarano, V.; Cavallo, L. *Eur. J. Inorg. Chem.* **2009**, 1759-1766. (c) Cavallo, L.; Correa, A.; Costabile, C.; Jacobsen, H. *J. Organomet. Chem.* **2005**, *690*, 5407-5413.

(61) Poater, A.; Cosenza, B.; Correa, A.; Giudice, S.; Ragone, F.; Scarano, V.; Cavallo, L.*; Eur. J. Inorg. Chem. **2009**, 1759*. See: https://www.molnac.unisa.it/OMtools/sambvca.php, 19. June 2014.

more favored in comparison to a Ru-NHC bonds.[62] Two possibilities arise from this constellation: firstly, a lower Ru-N bond strength which leads to a faster dissociation of the chelating ligand or secondly, a stabilization of the very same interaction which results in a preferential dissociation of the PCy_3 ligand rather than of the chelating ligand. The latter case would imply an additional activation method induced by the addition of Cu(I)Cl.[63]

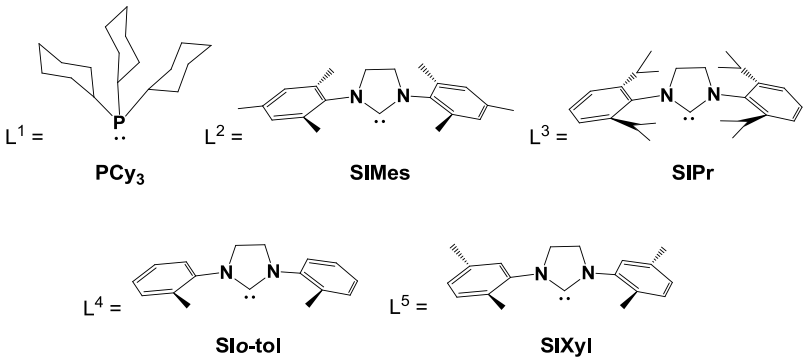

Figure 9. Commonly used inert ligands in ruthenium olefin metathesis.

Another more straightforward option to improve the activity is to tune the electronic and steric properties of the NHC ligand. Recently, some works have been published treating with bulkier NHC ligands and their behavior in olefin metathesis. Generally, an increased initiation rate was found in cross metathesis for 2nd generation phosphine resp. pyridine ruthenium initiators, bearing bulkier NHC ligands (L^3=SIPr).[64] However, in combination with a chelating ester ligand the initiator shows a similar latent behavior in ROMP and RCM as its *cis*-dichloro congener[65] making a prediction about the actual activity for this combination rather difficult. Less hindered NHCs, as L^4=SI*o*-tol (N,N'-bis(2-methylphenyl)imidazolin-2-ylidene) were shown to be more active in RCM of sterical demanding substrates.[66] However,

(62) Weskamp, T.; Schattenmann, W. C.; Spiegler, M.; Hermann, W. A. *Angew. Chem., Int. Ed.* **1999**, 38, 262-268.

(63) Rivard, M.; Blechert, S. *Eur. J. Org. Chem.* **2003**, 2225–2228.

(64) (a) Dinger, M. B.; Mol, J. C. *Adv. Synth. Catal.* **2002**, *344*, 671-677; (b) Urbina-Blanco, C. A.; Leitgeb, A.; Slugovc, C.; Bantreil, X.; Clavier, H.; Slawin, A. M. Z.; Nolan, S. P. *Chem. Eur. J.* **2011**, *17*, 5045-5053.

(65) Leitgeb, A.; Abbas, M.; Fischer, R. C.; Poater, A.; Cavallo, L.; Slugovc, C. *Catal. Sci. Technol.* **2012**, *2*, 1640-1643.

(66) (a) Stewart, I. C.; Ung, T.; Pletnev, A. A.; Berlin, J. M.; Grubbs, R. H.; Schrodi, Y. *Org. Lett.* **2007**, *9*, 1589-1592, (b) Torborg, C.; Szczepaniak, G.; Zielinski, A.; Malinska, M.; Wozniaka, K.; Grela, K. *Chem. Commun.* **2013**, *49*, 3188-3190.

a concomitant C-H deactivation of the N-aryl substituent with the active site on the other hand compensates the enhanced reactivity.[67] This problem can be somewhat reduced by exchanging the N-*o*-tol by a N-Xyl substituent, as the rotation of the xylyl residue is restricted by the second methyl group, preventing a decomposition by C-H activation.

3. Synthesis and Characterization

The synthesis of the presented initiators was straight-forward and is based on well-known transformations.[55] The carbene precursor 10-vinylbenzo(h)quinoline (**L-I**) was reacted with the respective L^1-L^5-functionalized tricyclohexylphosphine (**trans-I**, **trans-IV**, **trans-V**) resp. pyridine (**trans-II**, **trans-III**) indenylidene ruthenium complex, as shown in Scheme 5. Similar to the literature protocol, **trans-II** (L^2=SIMes) was obtained from the appropriate third generation precursor (**M31**) by mixing with 1.2 eq of **L-I** in dichloromethane under inert conditions at room temperature. After 48 h full conversion was detected and the green product was isolated by precipitation in Et_2O and subsequent column chromatography (CH_2Cl_2:MeOH, 10:1 (v:v)) in good yield (63 %). The typical ^{1}H NMR carbene shift in $CDCl_3$ was revealed at 19.19 ppm.

Scheme 5. Synthesis of Ru-Initiator **trans-I** – **trans-V.**

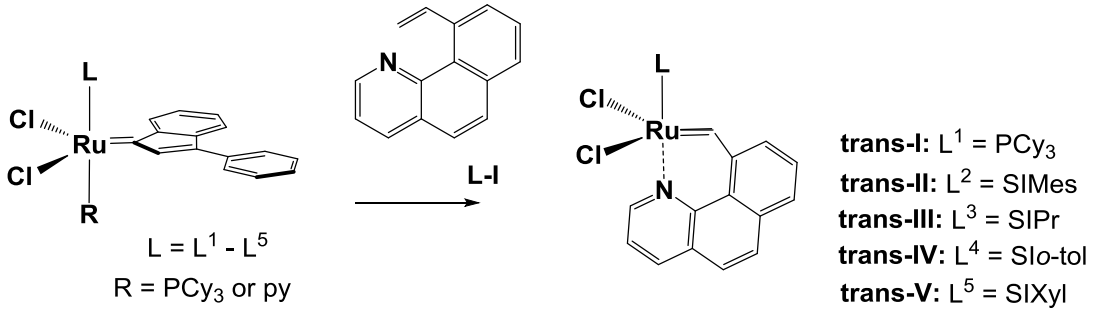

Similar reaction conditions were applied for the preparation of the SIPr analogue **trans-III** starting from the pyridine-containing precursor **M32**. Light green crystals were observed after column chromatography on silica gel (cyclohexane:ethyl acetate, 3:1 (v:v)) in 81 % yield. The complex was characterized via elemental analysis and ^{1}H and ^{13}C{^{1}H} NMR

(67) (a) Vehlow, K.; Gessler, S.; Blechert, S. *Angew. Chem. Int. Ed.* **2007**, *46*, 8082-8085. (b) Hong, S. H.; Chlenov, A.; Day, M. W.; Grubbs, R. H. *Angew. Chem. Int. Ed.* **2007**, *46*, 5184-5186.

spectroscopy in $CDCl_3$, comprising a sharp singlet at 19.06 ppm. Moreover, a *trans*-dichloro stereochemistry could be derived from signals of the NHC pattern, which are consistent with a typical C_s symmetric structure. For preparing **trans-I**, **trans-IV** and **trans-V**, a trihexylphosphine indenylidene ruthenium with the appropriate inert ligand (L^1=PCy_3, L^4=SI*o*-tol and L^5=SIXyl) was used. For gaining compound **trans-I**, the commercially available first generation initiator **M1** was reacted with 1.2 eq of **L-I** in degassed, dry toluene at 80°C with the assistance of 1.0 eq Cu(I)Cl. After a reaction time of 17 h, a full conversion was detected, however, accompanied by decomposition material. After standard purification steps,[68] a dark green microcrystalline powder was isolated in 41% yield. The characteristic carbene proton NMR shift of **trans-I** was detected to be a doublet at 19.53 ppm ($^3J_{HH}$ = 10.4 Hz), which is typical for phosphine initiators. Compounds **trans-IV** and **trans-V** were synthesized under similar reaction conditions in less than 20 min reaction time. **Trans-IV** (L^4=SI*o*-tol) was isolated in 50 % yield by simple filtration of a dark green precipitate, formed during the reaction. In contrary, light green crystals were isolated for the L^5=xylyl sibling **trans-V** by *re*-dissolving the dry, crude product in acetone and subsequent precipitation with *n*-pentane in 74 % yield. Relatively broad ^{1}H NMR signals were found for the carbene protons with a shift at 19.01 ppm (**trans-IV**) and 19.05 ppm (**trans-V**). Compound **trans-V** even showed a second signal at 19.32 ppm, which was not separable by column chromatography. However, this specialty can be assigned to switching between four stable conformations of the reduced, asymmetric NHC ligand (each two *syn* and two *anti*)which is not classifiable by NMR spectroscopy. Additionally, stereochemistry of the chlorides was not distinguishable by spectroscopic means for **trans-I**, **trans-IV** and **trans-V**. Hence, single-crystal X-ray crystallographic measurements were performed to clarify the stereochemistry. Suitable crystals were grown by dichloromethane-*n*-pentane diffusion revealing *trans*-dichloro stereochemistry in all cases. The most stable conformers for *o*-tol (**trans-IV**) resp. xylyl (**trans-V**) functionalized NHCs were confirmed to bear *syn*-conformation, as expected from literature.[66b] Important bond length and angles are presented in Table 1.

(68) If not mentioned differently all complexes were purified by dissolving the crude product in acetone for removing [$CuCl{\cdot}PCy_3$)], column chromatography (CH_2Cl_2:MeOH, 10:1 (v:v)) and subsequent precipitation upon addition of *n*-pentane.

The influence of different inert ligands (L^1-L^5) on the Ru-N dissociation can be deduced from these data.[69] From the electronic aspect, a higher chance for dissociation of the neutral ligand is related to a stronger π-interaction between Ru and the inert ligand (L^1-L^5). Compound **trans-I** bears the longest Ru-X(1) distance with 2.346(5)Å, followed by NHC complexes **trans-II** and **trans-III** (Ru-X(1) = 2.039(8)Å) and **trans-V** and **trans-IV** with similarly short Ru-NHC lengths (Ru-X(1) = 2.027(3)Å and 2.026(2)Å, respectively). When comparing the actual Ru-N(1) bond length, we predict a decrease in activity for the NHC complexes from **trans-IV** and **trans-V** (Ru-N = 2.118(2)Å), to **trans-III** (Ru-N = 2.116(6)Å) and **trans-II** (2.107(3)Å). It has to be noted that steric effects will additionally influence the Ru-N(1) dissociation. The phosphine complex **trans-I** has to be considered separately.

Table 1. Selected bond lengths (Å) and bond angles (deg) for complexes **trans-I** – **trans-V**.

	trans-I	**trans-II**	**trans-III**	**trans-IV**	**trans-V**
Ru–C(22)	1.825(2)	1.814(4)	1.827(2)	1.826(2)	1.824(1)
Ru–X(1)	2.3465(5)	2.039(4)	2.039(8)	2.026(2)	2.027(2)
Ru–N(3)	2.127(2)	2.107(3)	2.116(6)	2.118(2)	2.118(1)
Ru–Cl(1)	2.3572(5)	2.339(1)	2.374(3)	2.3554(5)	2.3522(4)
Ru–Cl(2)	2.3527(5)	2.346(1)	2.356(3)	2.3640(5)	2.3581(4)
X(1)-Ru-C(22)	95.58(6)	99.42(18)	100.98(9)	97.49(8)	99.0(2)
N(1)–Ru–Cl(2)	86.04(4)	84.46(9)	89.78(6)	86.81(5)	87.34(4)
C(22)–Ru–N(3)	90.04(8)	88.82(17)	89.40(9)	90.16(8)	90.14(5)
C(22)–Ru–Cl(1)	101.50(6)	99.22(13)	96.82(7)	97.57(6)	99.37(4)
C(22)–Ru–Cl(2)	103.32(6)	99.29(13)	102.09(7)	104.21(6)	100.08(4)
Cl(1)–Ru–Cl(2)	154.41(2)	160.28(5)	160.22(3)	157.59(2)	160.16(2)

The buried volume (V_{bur} in %) was determined from the XRD and from the DFT calculated structures. Values can be found in Table 2 and are in accordance with expected sterical bulkiness of the inert ligand decreasing from **trans-I** and **trans-III** to **trans-II** and finally to **trans-IV** and **trans-V**.

(69) Urbina-Blanco, C. A.; Poater, A.; Lebl, T.; Manzini, S.; Slawin, A. M. Z.; Cavallo, L.; Nolan, S. P. *J. Am. Chem. Soc.* **2013**, *135*, 7073−7079.

Table 2. Buried volumes for inert ligands L^1-L^5.

	trans-I	trans-II	trans-III	trans-IV	trans-V
$\%V_{bur}$ XRD	34.5	31.9	34.6	30.6	30.5
$\%V_{bur}$ DFT	32.4	30.4	31.8	29.1	29.0

To visualize the buried volume and the effect of sterical hinderance of the different inert ligand, sterical maps of **trans-I – trans-V** were drawn. They can be considered as classical geographic physical maps as various landforms are outlined by different colors, lines, tints, shading and spot elevations. The Ru center (xy-plane) is at level zero (green area) with the ligand under investigation below the metal (z-direction). Brown areas indicate zones where the ligand exceeds the level of the ruthenium, whereas blue parts of the ligand are below the ruthenium xy-level.[70] Interestingly, it seems that the inert ligands of **trans-IV** and **trans-V** hinder the ruthenium more than **trans-I - trans-III** (*cf.* Figure 10). Their NHC ligand makes advantage of the free space by flipping the o-tol respectively xyl-residue in this direction. Striking differences were also found when comparing XRD and DFT calculation, as packing effects manipulate the geometry of the complex.

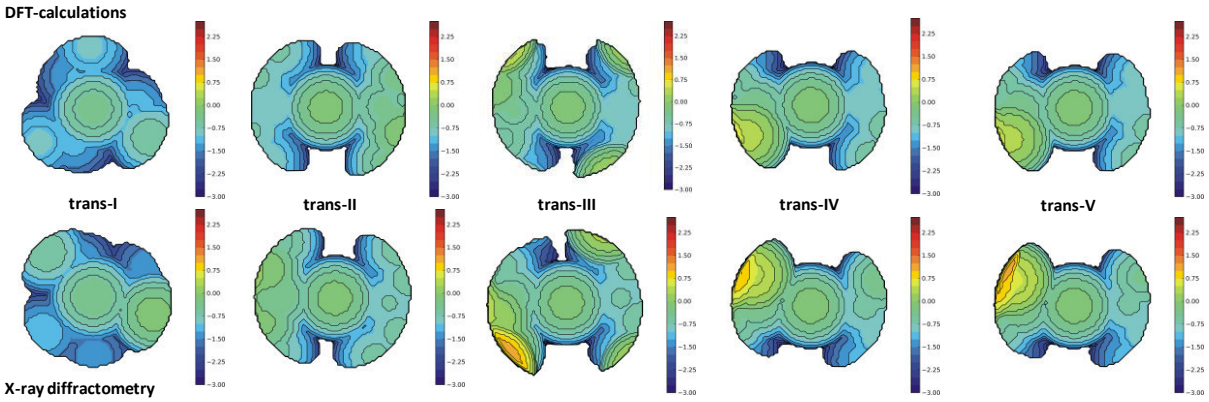

Figure 10. Steric maps of DFT and XRD structures of **trans-I-V**.

(70) Poater, A.; Falviene, L.; Urbina-Blanco, C. A.; Manzini, S.; Nolan, S. P.; Cavallo, L. *Procedia Computer Science* **2013**, *18*, 845-854.

4. Polymerization

Determination of the actual activities of **trans-I – trans-V** was accomplished by a comparative activity study in ring opening metathesis polymerization (ROMP). Three monomers were selected for benchmark reactions (*cf.* Figure 11).

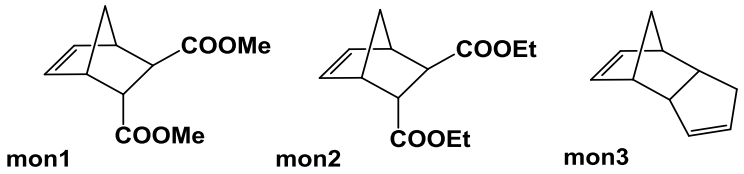

Figure 11. Monomers used in ROMP.

A general impression about the thermostability of initiator **trans-I** – **tran-II** was gained by simultaneous thermal analysis (STA) of a bulk polymerization of liquid monomer (±)-*endo*,*exo*-bicyclo[2.2.1]hept-5-ene-2,3-dicarboxylic acid diethyl ester (**mon2**) with a monomer to initiator ratio of 500. The "switching temperature" for the initiators was equalized to the onset temperature of the exothermic heat flow. Figure 12 shows the corresponding graphs,

Table 3 summarizes the results. According to literature,[55] polymerization initiated with **trans-II** was characterized by an onset of the exothermal heat-flow at 89°C and a mass loss (from retro-Diels Alder) of 15%. In contrast, its first generation analogue **trans-I** did not show any exotherm, however, a mass loss not higher than 66%, indicated partial polymerization. Attempts to initiate olefin metathesis by Ru-PCy_3 dissociation rather than dissociation of the chelating ligand (Ru-N bond break) were carried out by the addition of 1 eq of Cu(I)Cl. However, no changes in the polymerization behavior were found. A similar, latent behavior was observed for the largest (**trans-III**) and the smallest (**trans-IV**) NHC derivatives. For **trans-III**, no onset temperature was found as evaporation of monomer **mon2** occurred before polymerization started (mass loss 80%).

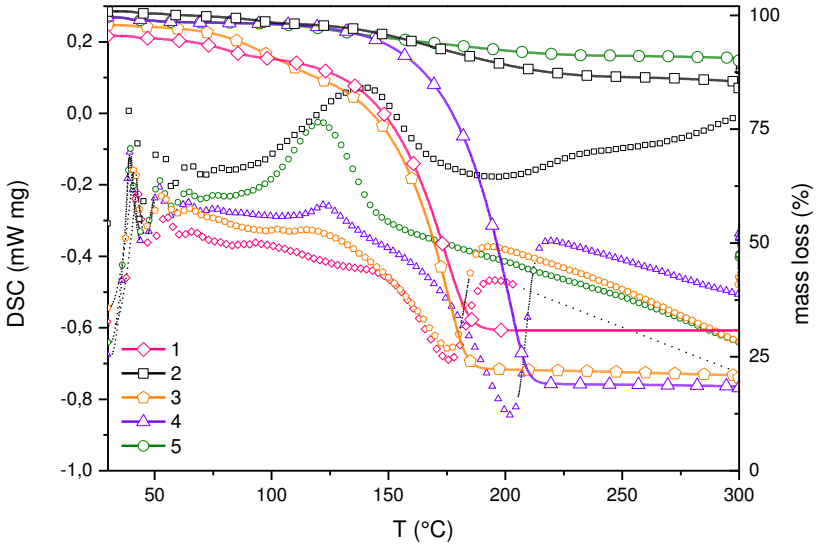

Figure 12. STA analysis of polymerization of **mon2**, initiated by **trans-I** – **trans-V**. Reaction conditions: [**mon2**]:[initiator] = 500:1. Heating rate: 3 K/min. Big symbols: thermogravimetric analysis (TGA); small symbols: differential scanning calorimetry (DSC).

In case of **trans-IV** a small exotherm with an onset temperature of 112°C was observed, however, with a concomittant mass loss of 82%. These data suggest that the majority of the initiator was decomposed. The xylyl functionalized complex **trans-V** revealed a similar activity to **trans-II** with an onset temperature at 88°C and a mass loss of only 10%.

A deeper understanding of the polymerization behavior of initiators **trans-I – trans-V** was gained in solution using monomer **mon1** ((±)-*endo*,*exo*-bicyclo[2.2.1]hept-5-ene-2,3-dicarboxylic acid dimethyl ester) in toluene under standard conditions. As TLC displayed no complete conversion in all cases, the exact progress of the conversion was detected by recording ^{1}H NMR spectra in $CDCl_3$ every day.

Table 3. STA results of **mon2** with initiators **trans-I**- **trans-V.**

Initiator	Onset (°C)	Peak (°C)	Δm (%)
trans-I	-	-	66
trans-II	89	140	15
trans-III	-	-	80
trans-IV	112	124	82
trans-V	88	122	10

Therefore, 200 µL samples were removed and terminated by the addition of 50 µL ethylvinylether and subsequently dried in vacuo. After 6 days, only initiators **trans-II** and **trans-V** showed progress of polymerization Althought the polymerizations did not reach completion, the graphs of the polymerization progress indicate peculiarities in both cases. As can be taken from Figure 13, compound **trans-V** showed a high polymerization rate in the beginning, as already revealed by STA. Termination of **trans-V**-initiated polymerization suggested that this initiator is not thermostable at 110°C for more than 12 h. In comparison, the progress of the polymerization with **trans-II** decelerated after 18 h, however, a steady ascent of the propagation rate was observed leading to a 47% conversion of **poly1** after 6 d.

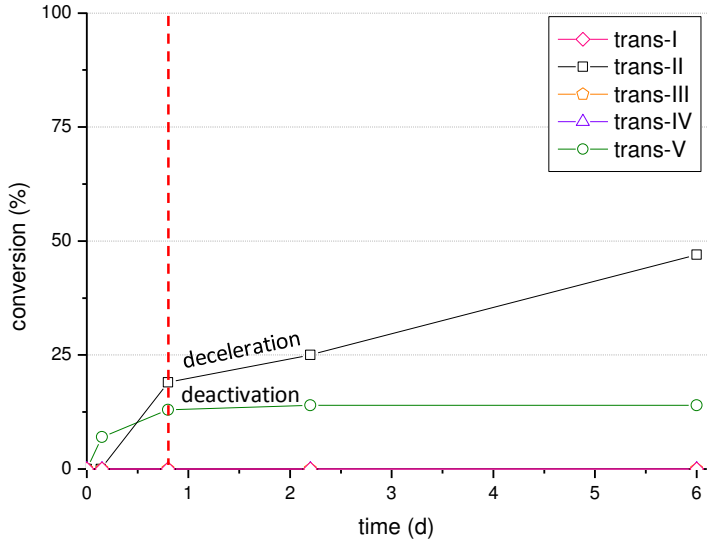

Figure 13. [**mon1**]:[initiator] = 300:1; [**mon1**] = 0.10 mol/L; reaction temperature = 110°C, solvent: toluene; inert atmosphere of N_2.

The series of benchmark reactions with monomers **mon1** and **mon3** led to a general idea about the thermostability of compounds **trans-I** – **trans-V**. Consequentially, initiators were tested for practical applications with DCPD (**mon3**) as a different behavior was expected for this monomer.[71] STA measurements were accomplished for determining the switching temperature of curing DCPD with relatively high catalyst loadings of 100 ppm. Analyses failed as the monomer decomposes at 69°C to the volatile Retro-Diels Alders product cyclopentadiene which evaporated before initiation was detected. In real life

(71) Slugovc, C.; Demel, S.; Riegler, S.; Hobisch, J.; Stelzer, F. *Macromol. Rapid. Commun.* **2004**, *25*, 475-480.

applications (e.g. RIM), typically closed moulds are used to prevent a mass loss by evaporation of the monomer. Qualitative *pre*-tests with 50 ppm of **trans-II** revealed that curing of DCPD for 24 h at 110°C is generally feasible in a closed system. Evaluation of mechanical properties of *poly*-DCPD was subsequently accomplished by compression and tensile tests. Compression tests are limited by a maximal force of 5000 N giving a maximal achievable stress of 10±1 MPa for each test cylinder. This method is only suited for incompletly cured, elastic materials. Fully cured, duroplastic *poly*-DCPD samples were tested by tensile strength analysis. Compression test cylinders with a diameter of 25 mm and a height of 8 mm in 20 mL screw-lid glass vessels were produced with all five initiators **trans-I – trans-V** (50 ppm, 110°C, 24 h). The commercially available catalyst **M2**[72] was utilized as reference material, as mechanical properties are conform to industrally produced *poly*-DCPD norms.[73] Results of compression tests initiated with **trans-I** – **trans-V** and **M2** are depicted in Figure 14 and summarized in Table 4. The maximal reachable compressive strength was obtained with reference initiator **M2** (120±10 MPa). According to previous results with monomer **mon1** and **mon2**, activities of compounds **trans-I** and **trans-IV** are not sufficient for polymerization yielding liquid resp. gelatinous test cylinders. The most potential initiator according to STA, **trans-V**, resulted in a rubbery test piece with a compressive strength of 0.4±0.1 MPa. This result was not improved by enhancing (140°C) or by decreasing (80°C) the reaction temperatures. In contrast, the material properties of **poly3** initiated with **trans-III** (0.8 ± 0.2 MPa) was improved by elevating the temperature to 140°C (5.5 ± 1.2 MPa). Initiator **trans-II** (110°C and 140°C) turned out to reach similar results as obtained with **M2**. Moreover it was shown that this initiator allows for storing the DCPD/initiator formulation for two weeks before curing reaching the very same compression strength as the immediately thermoactivated resin (120±10 MPa).

(72) (a) Fürstner, A.; Grabowski, J.; Lehmann, W. *J. Org. Chem.* **1999**, *64*, 8275-8280. (b) Jafarpour, L.; Schanz, H. J.; Stevens, E. D.; Nolan, S. P. *Organometallics* **1999**, *18*, 5416-5419. (c) http://chemistry.umicore.com/Products/product/587/587.html, 24. June 2014.

(73) Young's modulus of industrial applicable *poly*-DCPD: (E) 1.6-1.9 GPa and maximal stress (R_m) of 40-50 MPa, elongation at yield or break 4-5%).
Data were stated on polymer material property database EFUNDA, 24. June 2014:
(http://www.efunda.com/materials/polymers/properties/polymer_datasheet.cfm?MajorID=PDCP&MinorID=1)

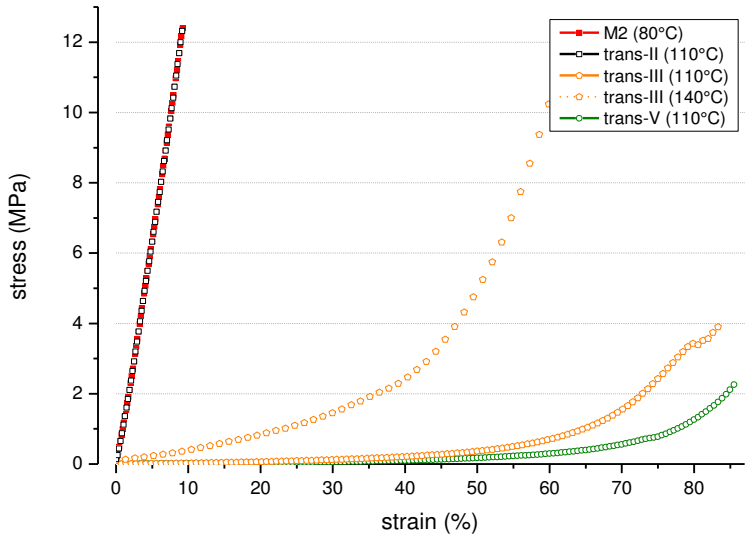

Figure 14. Compressive strength diagram for **poly3**, initiated with **M2**, **trans-II**, **trans-III** and **trans-V**.

Tensile strength tests of resulting **poly3** work pieces were performed. Accordingly, shoulder test bars were prepared with **M2** and **trans-II** under the same reaction conditions as for compression tests. The formulation of liquid DCPD **mon3** (30 $\mu L_{toluene}/mL_{DCPD}$) and initiator **trans-II** (dissolved in the appropriate amount of toluene) was filled in steel molds and closed with a glass plate to prevent vaporization of the monomer. The mould was placed in the oven for 24 h at 110°C. Shoulder bars, prepared with the reference initiator **M2** were accomplished by a reaction temperature of 80°C. Results of **trans-II**-initiated *poly*-DCPD test bars exhibited a Young's modulus of 1.48±0.5 GPa and an R_m value of 36±5 MPa. The activity was maintained when storing the monomer/initiator formulation for one week at room temperature: the maximal stress value for cured **poly3** slightly declined (ΔR_m = 2 MPa), however, the Young's modulus remained steady at 1.48±0.5 GPa. All values are summarized in Table 4.

Table 4. Mechanical properties of **poly3**, obtained after incubating monomer/catalyst resin for 24 h under the listed reaction conditions.

Initiator	Loading (ppm)	T (°C)	Mechanical Appearance	Conversion (%)	Compressive Strenght (MPa)
M2	20	80	hard solid	> 99	120 ± 10
trans-I	50	110	liquid	0	-
trans-II	50	110	hard solid	> 99	120 ± 10

trans-II	50	140	solid	> 99	120 ± 10
trans-II	50	110	soft solid	34	0.8 ± 0.2
trans-III	50	140	solid	80	5.5 ± 1.2
trans-IV	50	110	gel	5	-
trans-V	50	80	liquid gel	< 5	-
trans-V	50	110	soft solid	15	0.4 ± 0.1

5. Thermodynamic Stability

Polymerization of monomers **mon1, mon2** and **mon3** indicated deceleration resp. deactivation of all five initiators. Hence, compounds **trans-I – trans-V** were investigated regarding side reactions resp. decomposition at elevated temperatures. At 50°C only changes for **trans-IV** (in $CDCl_3$) were observed: the complex underwent *trans-cis* isomerization after 12 h (*cis*-content: 13%) which was increased after 16 more hours at 80°C (*cis*-content: 48%). In contrary, neither isomerization nor decomposition occurred at these temperatures for systems **trans-I – trans-III** and **trans-V**. From previous experiments it is known that *trans-cis* isomerization of **trans-II** is generally feasible.[74] Theoretical DFT calculations revealed that the *cis*-content decreases from **trans-II, trans-III** and **trans-V** to be thermodynamically more stable in $CHCl_3$ (*cf.* Table 5). Summarized, it seems that reduction of the steric bulk of the N-heterocyclic carbene ligand shifts the *cis-trans* equilibrium towards the *trans*-isomer.

Table 5. Theoretically (M06/TVZP, pcm=$CHCl_3$) and experimentally (in $CDCl_3$) determined values isomerized resp. deactivated complexes **trans-I** - **trans-V**.

Initatior	calculated[a]		experimental	
	$\Delta E_{trans\text{-}cis}$ (kcal/mol)	[cis]/([cis]+[trans]) (%)	[cis]/([cis]+[trans]) (%)	deactivated (%)
I	-2.4	1	0	100
II	4.4	100	22	-
III	2.8	100	17	-

(74) **Cis-II** was isolated after column chromatography (silica gel, CH_2Cl_2:MeOH, 10:1 (v:v)) of crude **trans-II**, prepared from the pyridine containing **M31** (*cf.* Experimental Section).

IV	-0.6	18	0[b]	100
V	0.3	70	41	30

[a]solvent = $CHCl_3$, solvation model = PCM; [b]after 12 h at 50°C: 13%; after further 16 h at 80°C: 48%.

To overcome the apparently high energy barriers, isomerization experiments were performed in microwave at 140°C. Stock solution of the respective *trans*-compounds **trans-I** – **trans-V** with a concentration of 7 mM were prepared in $CDCl_3$ and exposed for 1 h. Subsequently, the composition of the solution was determined by recording ^{1}H NMR spectra within the carbene region. Results are summarized in Table 5. They display a lower experimental *cis*-content as proposed by DFT calculations, which can be explained by a high isomerization transition state barrier (*cf.* results for **L-II**=quinoline-derivative).[53] These results are indicating that the actual thermodynamic equilibrium was not reached after exposing the complexes for only 1 hour.

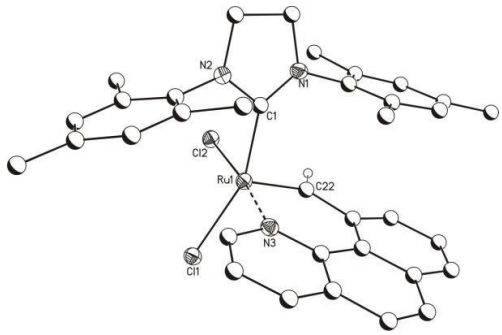

Figure 15. Crystal structures of **cis-II**. All non-carbon atoms are shown as 30% ellipsoids. Hydrogen atoms were removed for clarity. Selected bond lengths (Å) and angles (deg): Ru-C(22)=1.811(4), Ru-C(1)=2.039(5), Ru-N(3)=2.057(4), Ru-Cl(1)=2.399(1), Ru-Cl(2)=2.398(1); C(1)-Ru-C(22)=95.7(2), N(1)-Ru-Cl(2)=85.8(1), C(22)-Ru-N(3)=91.2, C(22)-Ru-Cl(1)=91.7(2), C(22)-Ru-Cl(2)=105.9(1), Cl(1)-Ru-Cl(2)=88.65(4).

Extending the exposure times up to 8 hours, it was revealed that **trans-II** and **trans-III** were perfectly stable under these reaction conditions. At 140°C solely isomerization to the *cis*-species occurred, however, with a different product distribution. After 5 h, a full and selective conversion to **cis-II** was found, whereas only 39% of the *cis*-species occurred for **trans-III** after 8 h. In contrary, **trans-I** decomposed to a dark precipitate with unidentifiable NMR signals. Also initiators **trans-IV** and **trans-V** were subjected to degrade: at room temperature they decompose with O_2 (formation of benzo(h)quinoline-10-carbaldehyde with a signal at 11.26 ppm), whereas at elevated temperatures they underwent CH-deactivation trough intramolecular carbene-arene bond formation.[67] The xylyl-residue in

trans-V lowers the chance of deactivation: nearly full conversion to **deact-IV** was observed for **trans-IV**, whereas only 30% of the starting material was deactivated for **trans-V** after treating the initiator (dissolved in $CDCl_3$) for 1 h in the microwave at 140°C (*cf.* Scheme 6).

Scheme 6. Potential deactivation pathways of complex **trans-IV** and **trans-V**.

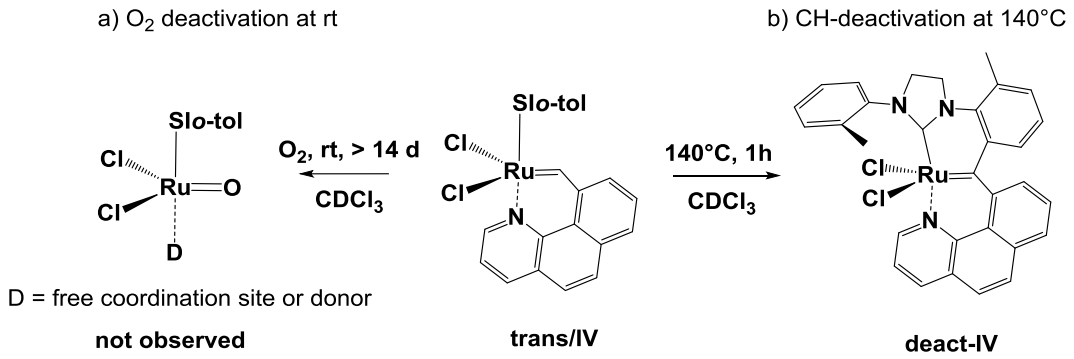

The activity of the **cis**-**II** was reduced in respect to its *trans*-counterpart, as proofed by STA analysis with monomer **mon2** (*cf.* Figure 16). Although the onset temperatures of **cis-II** (94°C) was surprisingly found to be in a similar range as for **trans-II** (89°C), different mass losses were obtained (24% and 15%, respectively). The broad shape of the *trans*-initiated DSC curve indicated that polymerization only terminated at 189°C. Contrary, the offset temperature of polymerization initiated with **cis-II** was found at 150°C. However, as the monomer is known to decompose at 120°C, the arising positive energy amount of the polymerization might partly compensate the exotherm of the polymerization. For the activity of **cis-II** these results imply that the needed thermodynamical amount of **trans-II** is formed at 94° which enables initiation of the polymerization. Consequentially, the activity is much lower which is reflected in a higher mass loss of **cis-II** and a cut off exotherm. Hence, the obtained results are not surprising, as both isomers coexist in thermodynamic equilibrium (*cf.* Introduction).

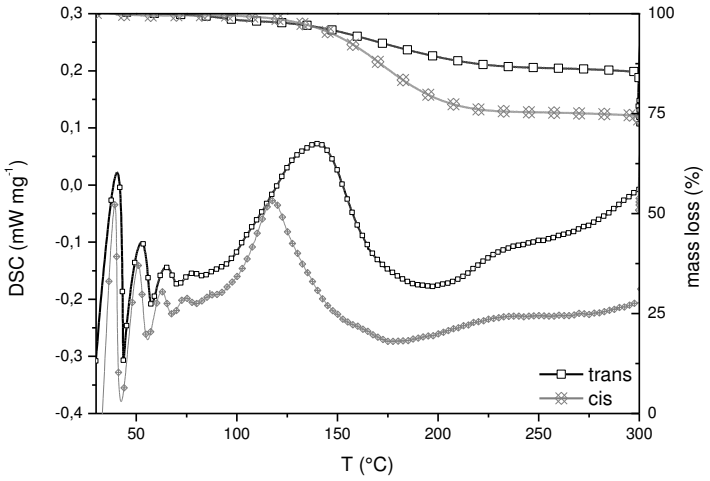

Figure 16. STA analysis of polymerization of **mon2**, initiated by **trans-II** and **cis-II**. Reaction conditions: [mon2]:[initiator] = 500:1. Heating rate: 3 K/min. Large icons: thermogravimetric analysis (TGA); small cubes: differential scanning calorimetry (DSC).

Generally, the lower activity of *cis*-complexes can be explained by a stronger Ru-N interaction. As can be taken from XRD data, the Ru-N bond length is distinctly stronger for **cis-II** (2.057(4) Å) in comparison to **trans-II** with 2.107(3) Å. As the *trans*-effect from the SIMes ligand in **trans-II** accomplishes these terms rather than the chloride for **cis-II,** dissociation of the chelated benzo(h)quinoline is less favored.

6. Conclusion

The influence of changing electronic and steric properties of the inert ancillary ligand (L^1-L^5) on a known, thermoswitchable ruthenium system (**trans-II**) has been reported. Expected improvements in the activity of initiators **trans-I**, **trans-III**, **trans-IV** and **trans-V** could not be found. Only **trans-V** displayed a somewhat enhanced initiation rate in comparison to **trans-II**. Benchmark reactions revealed either deceleration or complete deactivation of all initiator after less than one day. Experimental studies on the catalyst per se revealed that isomerization to the *cis*-isomer occurred at elevated temperatures, however, differently pronounced. Computational results confirmed that the *cis*-isomer is more stable for **trans-II, trans-III** and **trans-V**. Consequentially, a decelerated activity originates from a changed *trans*- to *cis*-stereochemistry during the reaction. On the other hand, a prematurely termination in polymerization with initiators bearing small NHCs (**trans-**

IV and **trans-V**) can be explained by either oxygen or CH-deactivation. Accordingly, compound **trans-II** remains the most potential initiator within this series. It combines a reasonable activity and a good stability at temperatures > 110°C. The concomittant *trans-cis* isomerization occurring under these conditions impacts positively on the catalytic behavior of the complex as it protects the complex from decomposition. Besides, even the *cis*-counterpart is activateable in ROMP at elevated temperatures.

Scheme 7. *trans-cis* Isomerization for stabilizing the complex at elevated temperatures.

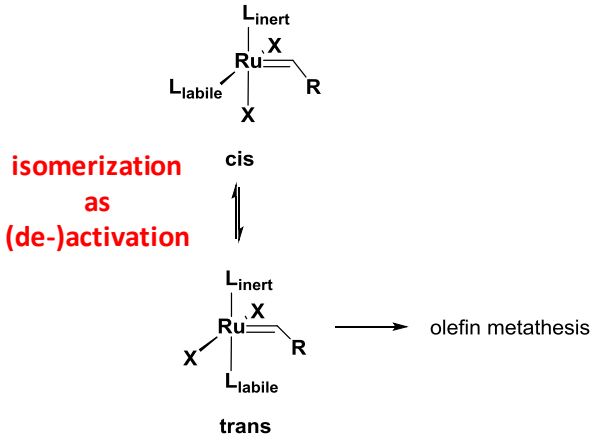

In fact, a higher loading and activation temperature was needed to obtain mechanical characteristics comparable to industrially produced *poly*-DCPD samples. However, the initiator can be stored together with the monomer up to two weeks at room temperature, without observing decomposition or polymerization. After thermoactivation at 110°C, no pronounced changes in the mechanical properties of *poly*-DCPD were found. Hence, this feature might open the door for applications, where monomer and initiator need to be stored together before activation leads to the desired product.

CHAPTER II

halide series - influence of halide dissociation[44h]

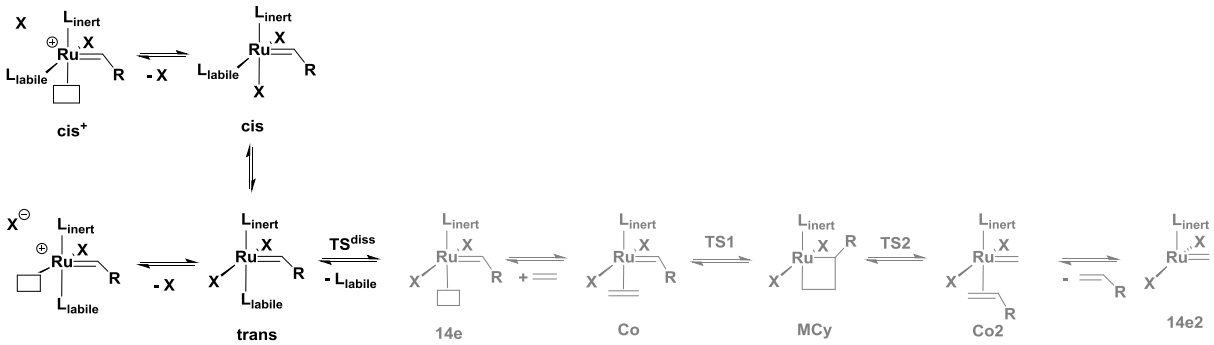

1. Abstract

This chapter discusses the lability of the anionic ligands in second generation (N,N'-bis[2,4,6-(trimethyl)phenyl]imidazolin-2-ylidene] (SIMes)) *cis*-dihalo ruthenium benzylidene complexes bearing an ester chelating benzylidene ligand. A simple halide exchange reaction with iodide salts was used to assess the lability of the halide in this type of complexes. The starting *cis*-dichloro compound (**cis2**) underwent rapid and selective exchange of the chloride *trans* to the SIMes ligand to form **cis2b**. The substitution of the second chloride (*cis* to the NHC ligand) to form **cis2c** was found to be much slower. To complete the family of *cis*-dihalo compounds, a fast and selective exchange of the iodide *trans* to the NHC led to the selective formation **cis2d**, after adding a chloride source to the dissolved complex. All four compounds have been fully characterized and their catalytic activity was accessed using ring opening metathesis polymerization (ROMP). It was found that the activity of the initiators decreases in the order **cis2d** > **cis2** > **cis2b** > **cis2c** and seems to be related to the formation of the corresponding *trans*-dihalo species, which are the actual active initiators.

2. Introduction

At first glance the sterical and electronical properties seem to be similar for *cis*- and *trans*-dichloro isomers. The fact that both isomers are deviant in their activity is a sign for some pronounced distinctions existing. The main difference between *cis*- and *trans*-dichloro compounds lies in the changed position of chloride (X) and labile ligand (L_{labile}), as can be found in Figure 17. This ligand arrangement has tremendous concequences due to its influence on the preferential dissociation of the ligands. It is well recognized that commonly applied NHC (L_{inert}) ligands are strong σ-donors promoting a dissociation of the ligand *trans* to it. This so-called *trans*-effect suggests a preferential L_{labile} dissociation in case of *trans* complexes, whereas for *cis*-compounds the halide (X) in *trans* position of the inert ligand is prone to dissociate.

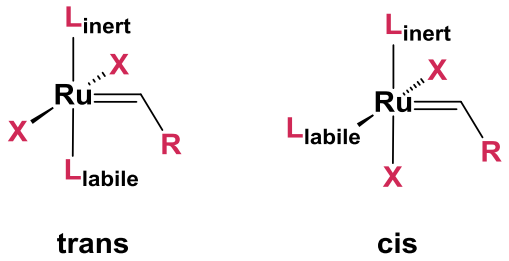

Figure 17. Differences between *cis*- and *trans*-stereochemistry.

Consequently, it is believed that *cis*-dichloro ruthenium complexes easily exchange their halides in *trans* position to the NHC ligand. In comparison to a creeping halide exchange which was observed for *trans*-dichloro isomers, the behavior of *cis*-compounds is more selective, providing some future implications for mechanistical impacts.

3. Synthesis and Characterization

For the current study a *cis*-dichloro complex bearing a chelating ester substituted benzylidene ligand (*cf*. Experimental Section, **cis2**) was used. Compound **cis2** was prepared via carbene exchange of the commercially available complex **M31** with 1.5 eq of ethyl 5-methoxy-2-vinylbenzoate in CH_2Cl_2 as the solvent at 20°C. After a reaction time of 8 h, **cis2** was obtained upon separation from **cis2$^+_{py}$** via column chromatography as a green microcrystalline powder in 78% yield (*cf.* Experimental Section)[75]. The complex was characterized via elemental analysis, ^{1}H- and ^{13}C{^{1}H}-NMR spectroscopy. Characteristic signals from the ^{1}H-NMR spectrum in $CDCl_3$ comprise a carbene carbon proton at 18.92 ppm and a typical *cis*-dichloro pattern for the aromatic protons of the mesityl rings (one of those considerably up-field shifted to 6.03 ppm) as well as for the diastereotopic CH_2-groups of the imidazolyl and the ester-moieties. These data strongly suggest the presence of the *cis*-dichloro stereoisomer in solution. The structural identity of **cis2** was finally confirmed by single crystal X-ray diffraction measurement (*cf*. below).

(75) Previously a very similar *cis*-dichloro benzylidene derivative was discussed, bearing an *iso*-propyl ester (**cis2-iPr**) instead of the ethyl ester derivative **cis2** (*cf.* Ref. 44g). Herein we used **cis2** as the starting material because it could be obtained in higher yield than the *iso*-propyl ester derivative. The higher yield can be traced back to less by-product formation (**cis2$^+_{py}$**) during the carbene exchange reaction and will be discussed more into detail in Chapter III.

Scheme 8. Preparation of the complexes under investigation[a]

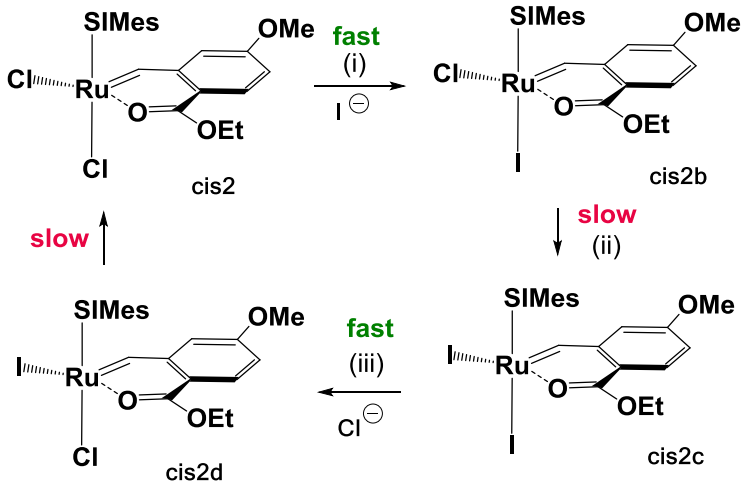

[a]i) CH_2Cl_2, aq. KI, extraction, 1 min, Conversion: 94% **cis2b**, or MeOH, KI (30eq), 10 min, Yield: 90% **cis2b**; ii) CH_2Cl_2, KI (30 eq), 3d, column chromatography, Yield 42% **cis2c**; iii) CH_2Cl_2, aq. KCl, extraction, 1 min, Yield: 85% **cis2d**.

In a next step the exchange of chloride for iodide ligands was examined by using different protocols. The first attempt was based on the works on Hoveyda-type *trans*-dichloro compounds.[19b] They added excess of potassium iodide (KI) to a suspension of **cis2** in methanol and stirred the reaction mixture at room temperature. In case of *cis*-dichloro compounds, an immediate colour change appeared upon addition of KI from dark green to grass green. The formation of at least one new product was confirmed by thin layer chromatography by a pronounced decrease of the spot for **cis2**. By removing of the solvent after 10 min and *re*-dissolving the residue in $CDCl_3$, a novel compound was characterized in pure form by means of NMR spectroscopy. The product of the reaction was identified upon characterization as the mixed *cis*-dihalide complex **cis2b** (*cf*. Scheme 8). The proton of the carbene carbon of the new compound **cis2b** was found by ^{1}H-NMR spectroscopy exhibiting a signal at 18.38 ppm. All other signals resemble the corresponding spectrum of **cis2**. Also the carbon-NMR data of **cis2** and **cis2b** were closely related. Differences in spectra were not exceeding shifts of the carbene carbon and the heterocyclic carbene carbon by more than 3 ppm (**cis2**: 283.5 and 217.6 ppm, **cis2b:** 280.2 and 215.0 ppm;). The final proof of the structure of **cis2b** was retrieved from single crystal X-ray diffraction determination (*cf*. below). In contrary, 2nd generation (*trans*-dichloro) Hoveyda catalysts[19b] gave an unselective

exchange of both chlorides[76] (*cf*. Experimental Section), whereas halide exchange in **cis2** led to a fast and selective substitution of the chloride *trans* to the N-heterocyclic carbene ligand.

When using dry CH_2Cl_2 instead of methanol, the halide exchange reaction was much slower giving only 5% conversion in approximately 2 h. The yield could be increased upon the addition of 2 eq of water (in respect to **cis2**) or by using technical, undried CH_2Cl_2. Consequentially, the reaction proceeded faster and reached conversions higher than 90% in about 2 h, however, accompanied by another, yet unidentified complex characterized by a carbene's proton resonance of 18.54 ppm (*cf*. below). This experiment shows the great importance of the presence of water, which was in the following evidenced by a simple extraction experiment. For this attempt, **cis2** (dissolved in CH_2Cl_2) and an aqueous KI solution (5 w-%) were poured into an extraction funnel and subsequently shaken for 5 sec, leading again to an immediate color change of the organic phase. The conversion towards **cis2b** after one extraction experiment was determined by ^{1}H-NMR spectroscopy to be 94%. A following extraction with freshly prepared KI_{aq}. (5 w-%) revealed that the conversion towards **cis2b** dropped towards the before mentioned complex with the carbene shift at 18.54 ppm. Again, a similar experiment was performed with the 2nd generation *trans*-Hoveyda catalyst.[77] In this case, three repetitions of the extraction process gave only 5% conversion towards the mono iodo substituted Hoveyda-type complex (*cf*. Experimental Section). For identifying the above mentioned, hitherto unknown complex (Ru=C*H* at 18.54 ppm), **cis2** was reacted with 30 eq of KI in undried CH_2Cl_2 as the solvent for 3 days. Under these conditions a mixture of 44% **cis2b** and 56% of the new compound arised. Column chromatography (CH_2Cl_2:MeOH, 10:1 (v:v)) allowed for the separation of the new, yellowish compound in 42% yield (*cf*. Scheme 8). This complex was unambiguously identified as the corresponding *cis*-diiodo derivative **cis2c** from single crystal X-ray analysis (*cf*. below). Moreover, NMR spectroscopy indicated the *cis*-diiodo stereoisomer not only to be present in solid state but also in solution. This result is somewhat surprising since intuition might pretend that a *cis* arrangement of two iodides is an unfavorable arrangement in this kind of complexes. Finally, the last member of the sibling - the mixed *cis*-dihalide complex **cis2d -** was prepared in 85% yield by extraction of a CH_2Cl_2 solution of **cis2c** with aqueous potassium chloride. Single crystal X-ray diffraction

(76) A mixture of *trans*-chloroiodo and trans-diiodo Hoveyda was obtained after 3 h reaction time.

(77) Garber, S. B.; Kingsbury, J. S.; Gray, B. L.; Hoveyda, A. H. *J. Am. Chem. Soc.* **2000**, *122*, 8168-8179.

analysis revealed that **cis2d** is a diastereomer of **cis2b** with an interchanged occupation of the iodid and the chloride. The characteristic carbene proton was found at 19.01 ppm for compound **cis2d**. Similar to **cis2b**, **cis2d** is not stable in solution because of halide-redistribution reactions forming **cis2**, **cis2b** and **cis2c** as the main products (*vide infra*). Thus, acquisition of a clean ^{13}C-NMR spectrum was not feasible.

Finally, single crystal X-ray diffraction measurements confirmed isostructural solid state structures of **cis2** – **cis2d**. Pecularities will be described on the expample of **cis2**: this complex crystallizes as an ansolvate in the orthorhombic space group $P2_12_12_1$ with only one Ru complex in the asymmetric unit. Generally, the compounds exhibit a square pyramidal coordination geometry with a carbene ligand (C22) forming the apex of the pyramid (*cf*. Figure 18). The base of the pyramid is formed by the two halide ligands (X1, X2), the carbonyl oxygen (O1) and the carbon atom of the SIMes ligand (C1). Important bond lengths and angles are shown in Table 6. Of particular interest is the bond length of the halide ligands.

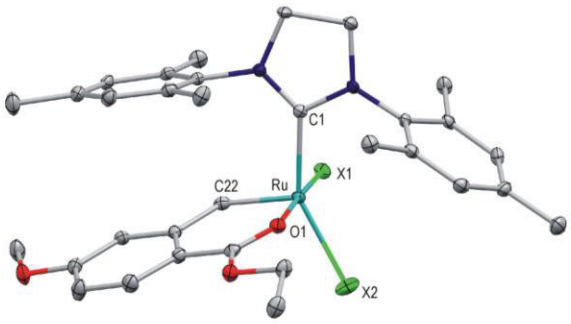

Figure 18. Generalized solid state structure of the compounds under investigation (H-atoms omitted for clarity).

The lability of the chloride in *trans*-position to the NHC-ligand (exerting a strong *trans*-effect) is not reflected by the observed bond-lengths (the *trans*-influence of the NHC is smaller than the *trans*-influence of the O-donor). Exemplary, **cis2** shows a slightly longer Ru-chloride bond of the chloride in *cis*-position to the NHC ligand (Ru-X1 = 2.3632(6)Å) compared to the chloride *trans* to the NHC ligand (Ru-X2 = 2.3447(9) Å).[78] Accordingly, bond lengths of the chlorides in **cis2** are somewhat longer but similar to those in the 2nd generation Hoveyda catalyst (Ru-Cl1 = 2.340(12) and Ru-Cl2 = 2.328(12)).[77] The X-ray crystal

(78) A series of related *cis*-dichloro complexes containing, O, N, S or P donor ligands show the same structural feature, i.e. the chloride in *cis*-position to the NHC ligand exhibits a longer bond-lengths than the chloride *trans*-to the NHC ligand; see ref. 34, 41b, 48a, 52a.

structure of **cis2b** shows the iodide in *trans*-position (X2) to the NHC ligand, which is however partially occupied by iodide (11%) and chloride (89%).[79]

Table 6. Selected bond lengths (Å) and bond angles (°) for complexes **cis2** – **cis2d**.[a]

	cis2	**cis2b**[b]	**cis2c**	**cis2d**[c]
Ru–C(22)	1.824(3)	1.823(4)	1.823(7)	1.82(3)
Ru–C(1)	2.010(2)	2.009(4)	2.026(6)	2.05(5)
Ru–O(1)	2.076(2)	2.089(3)	2.083(4)	2.11(2)
Ru–X(1)	2.3632(6)	2.366(9)	2.6715(5)	2.651(3)
Ru–X(2)	2.3447(9)	2.6603(5)	2.6983(7)	2.35(5)
C(1)-Ru-C(22)	98.7(1)	100.7(2)	100.0(3)	-
O(1)–Ru–X(2)	85.53(6)	86.06(9)	85.0(1)	-
C(22)–Ru–O(1)	89.9(1)	90.0(2)	89.6(2)	-
C(22)–Ru–X(1)	89.6(1)	89.9(3)	90.0(1)	-
C(22)–Ru–X(2)	111.3(1)	106.9(1)	103.8(2)	-
X(1)–Ru–X(2)	91.21(3)	94.0(2)	94.91(2)	-

[a]Complexes **cis2b**, **cis2c**, and **cis2d** from an isostructural series with two Ru-complexes and one CH_2Cl_2 molecule in the asymmetric unit. Only the bond lengths of the first of these two complexes are given. [b]Partial occupation of X1 with 11% iodide; [c]Partial occupation of X2 with 50% iodide; twinned crystals of poor quality, bond angles therefore omitted.

The chloro-ligand exhibits almost the same distance from the ruthenium center as found in **cis2**. The same accounts for the carbene carbon atom (C22) and the NHC-carbene carbon atom (C1). The Ru-I bond lengths is very similar to the Ru-I bonds in the diiodo derivate of the 2nd generation Hoveyda catalyst.[19a] The diiodo-derivative **cis2c** is characterized by similar bond lengths of both iodide ligands. In this case, the iodide in *trans*-position to the NHC is slightly less tightly bonded than the iodide in the other position. For **cis2d** only bad crystals could be grown, which allowed for the principal proof of the proposed coordination geometry, but not for more detailed discussions.[80]

(79) During crystallization the halides are exchanging forming **cis2c**, which co-crystallizes with **cis2b**.

4. Mechanism of the Halide Exchange

Fast halide exchange in *cis*-dichloro compounds was found to preferentially occur in *trans* position to the NHC ligand. However, bond lengths summarized in Table 6 give no clear evidence of which halide is more prone to dissociate from the ruthenium centre. As it will be discussed in Chapter III, not only the *trans*-effect of the NHC ligand (which can not be predicted by the bond length), but also the missing tracability of the the cationic complex where X1 dissociates is responsible for a preferential formation of the selective product formation of **cis2b**. DFT calculations revealed an immediate rearrangement to one and the same cationic complex similar to **cis2**$^{+}_{ROH2}$ (but without ROH) in case of either X1 or X2 dissociation. Consequentially, the slow X1 exchange might be best explained by this phenomenon. The presence of donor molecules (as solvents) has a stabilizing effect on the cationic complex. On the one hand the dissociated X^- (counterion) can be solvated and the solvent molecule can coordinate on the vacant coordination site *trans* to the NHC. The occurrence of by-product **cis2**$^{+}_{py}$ during the synthesis of **cis2** provides evidence for the principal possibility of the halide in *cis*-position to the NHC-ligand dissociating.[44g] Consequentially, either a chloride *re*-coordinates to the cationic species to form **cis2** (degenerative halide exchange) or an iodide forming **cis2b** (productive halide exchange). The reaction pathway is outlined in Scheme 9 and accordingly slower in absence of a coordinating solvent. Contrary, halide dissociation in *cis*-position to the NHC ligand is less favorable for the formed *trans*-species (*cf*. experiments with 2nd generation Hoveyda catalyst).

Scheme 9. Suggested mechanism for the fast halide exchange in the presence of donating solvent molecules.

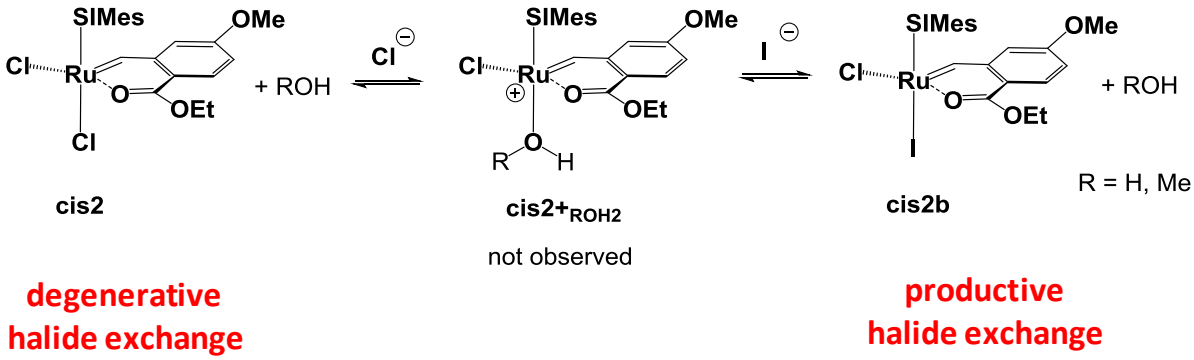

(80) Evaluation of data for **cis2d** revealed a partial occupation of X2 with 50% iodide,only twinned crystals could be obtained; two independent complexes where found in the unit cell, disordered solvent molecules are present.

Another hint which makes the presence of a cationic species in solution plausible was shown when mixing **cis2** and **cis2c** in $CDCl_3$. An immediate halide exchange was observed by the occurance of **cis2b** and **cis2d** (*cf.* Experimental Section) meaning that the halide has to dissociate from the ruthenium center for a short time. Similar results with *trans*-dichloro compounds were already reported in literature.[81]

5. Thermodynamic Stability

Besides the occurance of all four members of the *cis*-dihalo group, also traces of other by-products were observed when storing the *cis*-dihalo complex in solution ($CDCl_3$). Especially during the preparation of primarily **cis2b** and **cis2d** indications about newly introduced compounds were gained. For this purpose ^{1}H-NMR spectroscopy was accomplished by dissolving each complex in $CDCl_3$ under inert atmosphere of nitrogen and monitoring the composition of the solution. Results after 24 h are presented in Table 7. After 1 day, **cis2** gave a new carbene bearing complex (**trans2**) in about 2±1% (*cf*. Experimental Section). This compound was characterized by a carbene's proton resonance of 18.71 ppm and a characteristic doublet ($^4J_{HH}$= 2.5 Hz) at 6.25 ppm which was assigned to the aromatic proton of the chelating benzylidene at the vicinal position to the carbene and the methoxy group. These results are in accordance with a similar *trans*-dichloro ester chelating benzylidene published earlier.[65,82] After 6 days, **trans2** was present in 4±2%. Accordingly, **cis2** is in equilibrium with its *trans*-dichloro diastereomer **trans2**, although the complex was isolated in pure *cis*-configuration (*cf*. Chapter III). Assuming that the equilibrium was reached after that time, the difference in free energy was calculated to be approximately 8±2 kJ/mol in favor of **cis2**. Similarly, **cis2c** formed upon standing for 1 day in $CDCl_3$ (amongst some decomposition), the *trans*-diiodo carbene species (**trans2c**) in about 8±2% reaching an equilibrium after 2 days at about 11±2% (*cf.* Experimental Section). Accordingly, the difference in free energy of **cis2c** and **trans2c** is approximately 5.2±1 kJ/mol and hence about 3 kJ/mol smaller than in case of **cis2** *vs*. **trans2**. The considerably high error margins can be explained by the occurrence of a concurring decomposition reaction which is characterized

(81) Tanaka; K.; Böhm, V. P. W.; Chadwick, D.; Roeper, M.; Braddock, D. C. *Organometallics* **2006**, *25*, 5696-5698.

(82) Fürstner, A.; Thiel, O. R.; Lehmann, C. W. *Organometallics* **2002**, *21*, 331-335.

by the formation of ethyl 2-formyl-4-methoxybenzoate (characteristic peak at 10.71 ppm in the ^{1}H-NMR spectrum, *cf.* Experimental Section). The decomposition also hampered attempts to measure the kinetics towards equilibrium. Typically 3±1% of all ruthenium carbene species present in the reaction mixture had decomposed after 2 days at room temperature.

Table 7. Product distribution obtained after storing **cis2** – **cis2d** for 24 h in $CDCl_3$ at room temperature.

Starting material	Product Distribution[a]							
	cis2	**cis2b**	**cis2c**	**cis2d**	**trans2**	**trans2b**	**trans2c**	**decomp.**[b]
cis2	96 %	-	-	-	2 %	-	-	2 %
cis2b	10 %	76 %	11 %	3 %	< 1 %	< 1 %	< 1%	< 1 %
cis2c	-	-	90 %	-	-	-	8 %	2 %
cis2d	12 %	6 %	14 %	44 %	7 %	6 %	1 %	5 %

[a]determined by 1H-NMR spectroscopy; [b]according to the occurrence of ethyl 2-formyl-4-methoxy benzoate (characteristic 1H-NMR shift: 10.71 ppm (s, 1H, C*H*O))

Complex **cis2b** was behaving differently in terms that hardly any *trans*-dihalide stereoisomers could be observed. Instead, **cis2b** underwent halide exchange reactions and after 24 h in $CDCl_3$ a mixture of 4% **cis2**, 69% **cis2b**, 23% **cis2c** and 3% **cis2d** was observed. After another 24 h the mixture was composed of 3% **cis2**, 49% **cis2b**, 25% **cis2c**, 23% **cis2d.** Only after about 3 days minor amounts of *trans*-dihalide complexes were observed. In coherence, the diastereomer **cis2d** gave a mixture of 7% **cis2**, 9% **cis2b**, 16% **cis2c**, 37% **cis2d**, 11% **trans2**, 2% **trans2c** and 9% **trans2b** after already 24 h. The latter complex was characterized by the carbene's proton resonance at 18.28 ppm and was assigned in analogy to the last hitherto unknown mixed *trans*-dihalide complex **trans2b**. The differently pronounced product distribution when starting from similar complexes **cis2b** and **cis2d** might be explained by the position of the sterical demanding iodide which seems to strongly contribute to the halide dissociation and *cis*-*trans* isomerization, respectively.

6. Polymerization

The isolation of all four complexes of this sibling rendered a comparative reaction study possible: complexes **cis2** – **cis2d** were used to initiate ring opening metathesis polymerization of dimethyl bicyclo[2.2.1]hept-5-ene-2,3-dicarboxylate (**mon1**). Subsequently, the number average molecular weight (M_n) of the polymers was determined to give an indirect, qualitative comparison of the ratios of initiation to propagation rate constants (k_i/k_p) for the initiators under investigation. Reaction conditions and results are given in Table 8. Initiator **cis2** gave a polymer, characterized by a M_n value of 526 000 g/mol and a PDI of 2.0 after a reaction time of 24 h. For comparison, an initiator providing fast and complete initiation (**M31**, characterized by a $k_i/k_p >> 1$) gives a polymer characterized by a M_n of about 54 600 g mol^{-1} and a polydispersity index (PDI) of 1.07 under the same reaction conditions.[44g] The results obtained for **cis2** are typical for initiators with a *cis*-dichloro structure[44,41,45] with a k_i/k_p ratio is distinctly less than 1 (*cf*. Table 8, entry 2).

Table 8. Polymerization data for the polymerization of **mon1**, initiated with the respective *cis*-dihalo compounds.

entry	initiator	time (h)[a]	conversion (%)[a]	M_n (kg/mol)[a,b]	PDI[a,b]	$t_{1/2}$[c]
1	**M31**	< 1	100	54.6	1.07	< 1 min
2	**cis2**	< 24	100	526	2.0	7.3 h
3	**cis2b**	39	100	456	1.9	33 h
4	**cis2c**	168	80	n.d.	n.d.	> 264 h
5	**cis2d**	8	100	146	2.1	1.5 h

[a]Reaction conditions: [**mon1**] : [Initiator] = 300 :1; [**mon1**] = 0.1 mol L^{-1}; reaction temperature = 40°C, solvent: CH_2Cl_2; inert atmosphere of N_2; [b] determined by GPC relative to poly(styrene) standards in THF;[c] determined by monitoring the polymerization progress via ^{1}H-NMR; reaction conditions: [**mon1**] : [Initiator] = 70 :1; [**mon1**] = 0.13 mol L^{-1}; reaction temperature = 25°C, solvent: $CDCl_3$; inert atmosphere of N_2

As revealed by the corresponding M_n values, k_i/k_p increases in the order of k_i/k_p (**cis2**) ≈ k_i/k_p(**cis2b**) <<k_i/k_p (**cis2d**) within this series. Regarding to **cis2c** no point can be made because even after a polymerization time of 7 d at 40°C only 80 % of **mon1** were consumed. Additionally, a kinetic measurement to monitor the polymerization of **mon1** was accomplished via ^{1}H-NMR spectroscopy to better display the reactivity of the respective

catalyst. Obtained half-lives are presented in the last column in Table 8 and a time conversion plot is shown in Figure 19. It was revealed that **cis2d** ($t_{½}$ = 90 min) is by far the most active initiator, followed by **cis2** ($t_{½}$ = 440 min), **cis2b** ($t_{½}$ = 33 h) and finally the *cis*-diiodo compound **cis2c** being the least active initiator ($t_{½}$ > 250 h). Explaining the diverse results for **cis2** and **cis2c** is straightforward: the *cis*-dihalo precursor has to isomerize to its *trans*-dihalo counterpart before becoming active. However, different propagation species will be observed, as the sterical bulkiness of the iodide coligands distinctly retards the propagation.[19] Hence, it is obvious that a small amount of **trans2**, which was formed by **cis2**, led to a faster propagation species as **trans2c**, which isomerized in a higher amount from **cis2c**. Consequently a faster polymerization rate could be obtained for **cis2**. In contrast to the dihalo complexes, the key for explaining the different activity of mono-iodo substituted complexes **cis2b** and **cis2d** lies in the different tendencies to form the corresponding *trans*-dihalo species. While an iodide *trans* to the NHC ligand (**cis2b**) does hardly form any *trans* species, an iodo ligand *cis* to the NHC (**cis2d**) forms considerable amounts of *trans*-species upon standing in solution (*cf*. Table 7). Furthermore, these *trans*-species not only comprise the expected mixed halide compound **trans2b** but also **trans2c** and - in considerably high amounts – the most active (*pre*-)catalyst **trans2** within this series (*cf*. Table 7), which is most probably responsible for the highest activity of **cis2d** in the polymerization of **mon1**.

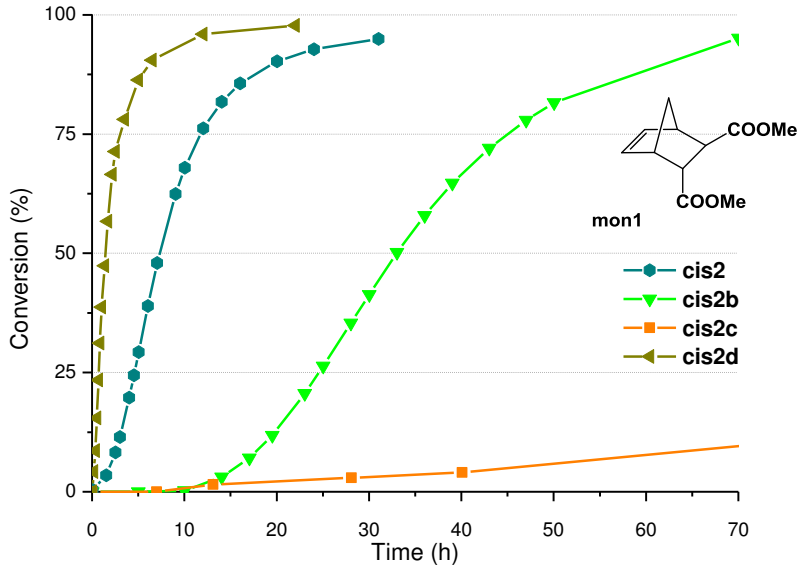

Figure 19. Time conversion plot for the polymerization of mon1 (see inset) with initiators **cis2** – **cis2d**; determined by monitoring the polymerization progress via ^{1}H-NMR; reaction conditions: [**mon1**] : [Initiator] = 70 :1; [mon1] = 0.13mol L^{-1}; reaction temperature = 25°C, solvent: $CDCl_3$; inert atmosphere of N_2

However, it remains unclear why **cis2b** is rather reluctant to form the *trans*-species compared to **cis2d**. It seems that an iodide in *cis*-position to the NHC is more predisposed to open the chelate and consequentially to form the active *trans*-species.

7. Conclusions

Within this work the particularities of the anionic ligands in *cis*-dihalo ruthenium benzylidene complexes bearing a NHC-ligand were discussed. Results indicate a preferential exchange of the halide *trans* to the NHC ligand in the presence of traces of donor solvents such as water or methanol. For this halide exchange a dissociative mechanism is suggested. The halide *cis* to the NHC ligand seems to be less labile and exchange in this position is less pronounced. These observations are attributed to a slower dissociation of the halide in *cis*-position (no pronounced *trans*-effect), but also to the fact that consequentially the halide in *trans*-position has to migrate up to the other position, as no stable intermediate was found.

Exploitation of this knowledge allowed for the isolation of the corresponding mono-iodo, mono-chloro and the diiodo complex and a reactivity study using these complexes as initiators for the ROMP of a norbornene derivative was conducted. While **cis2b** (bearing the iodide *trans* to the NHC) and **cis2c** (bearing two iodides) are less active as the parent dichloro initiator **cis2**, complex **cis2d** (bearing an iodide *cis* to the NHC-ligand and a chloride *trans* to the NHC) is more active than **cis2**. The superiority of **cis2d** can be traced back to its marked tendency to rearrange to all three possible *trans*-dihalo species (i.e. the actually active species) in solution. The degenerate ligand exchange presented here might constitute an unproductive *pre*-equilibrium in olefin metathesis. Dissociation of the halide gives rise to a cationic species, which is metathesis inactive.[83]

(83) (a) Wang, H.-Y.; Yim, W.-L.; Klüner, T.; Metzger, J. O. *Chem. Eur. J.* **2009**, *15*, 10948-10959. (b) Wang, H.-Y.; Yim, W.-L.; Guo, Y.-L.; Metzger, J. O. *Organometallics* **2012**, *31*, 1627-1634.

Scheme 10. Halide dissociation as concurring reaction to *cis-trans* isomerization and entrance into the olefin metathesis cycle.

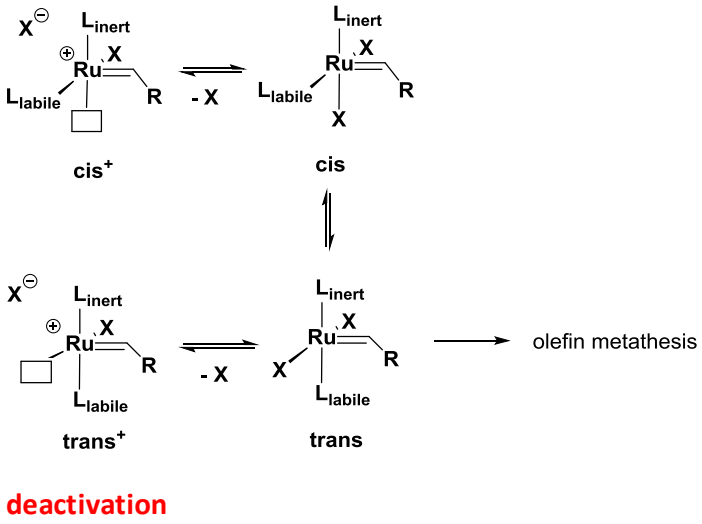

The low activity of *cis*-dichloro ruthenium benzylidenes is at least partly caused by this process (see Scheme 10). Generally it is believed, that the more labile the halide *trans* to the NHC-ligand is (resp. the more stable the cationic complex is) the less active is the catalyst. At the same time the *cis-trans* isomerization seems to be influenced by the nature and position of the anionic ligand. An higher isomerization rate gave an higher reactivity of the *cis*-dihalo compex (*pre*-)initiator. Closer spezifications regarding the isomerization mechanism will be discussed in Chapter III and IV.

CHAPTER III

benzylidene series - activation mechansim of *cis* dichloro (*pre*-)catalysts[84]

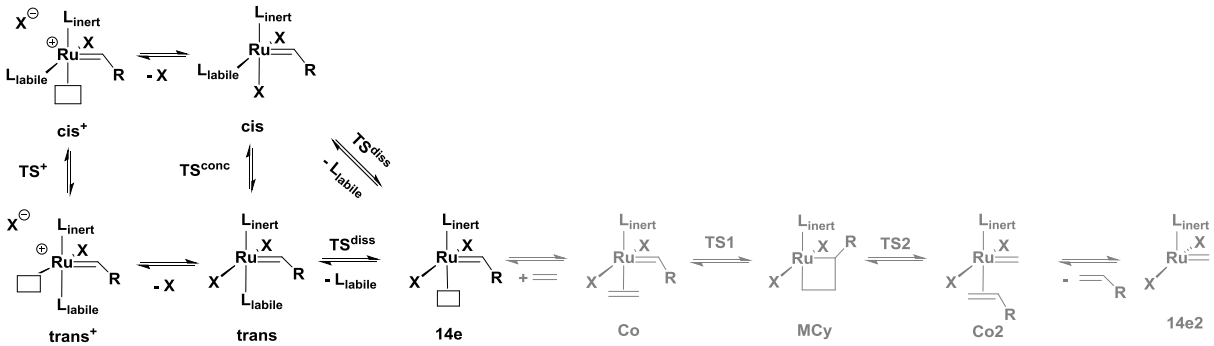

(84) Pump, E.; Poater, A.; Zirngast, M.; Torvisco, A.; Fischer, R.; Cavallo, L.; Slugovc, C. *Organometallics* **2014**, *33*, 2806–2813.

1. Abstract

Herein, the influence of electronically modified second generation *cis*-dihloro ruthenium ester chelating benzylidene complexes was elaborated. The complexes were prepared, characterized and benchmarked in a typical ring opening metathesis polymerization (ROMP) experiment. The effect of the electronic tuning, achieved by the introduction of a methoxy (EDG) or a nitro group (EWG) on the chelating benzylidene ligand was studied experimentally and theoretically. A clear trend was revealed by DFT calculations, showing that the activity of the initiators is dependent on the relative stability between the *cis*- and *trans*-isomer, which can be influenced by electronic modification of the ligands.

2. Introduction

In this work we aim on studying the impact of electronic modification of the chelating carbene ligand on the catalytic properties of the different *cis*-dichloro ruthenium complexes. The influence of electronical tuning on the catalytic activity has already been described experimentally[85] and theoretically[32,86] for *trans*-dichloro-configured second generation Hoveyda-type catalysts.[40] In simplified terms, the activity in this system increases with the implementation of electron withdrawing substitutents on the benzylidene moiety and is lowered in the presence of electron-donating groups. In this coherence differences in the activity were primarily explained by varying the energy of the transition state for the decoordination of the O-donor of the chelating benzylidene ligand. Taking these studies as an inspiration, the effect of the electronic tuning of the benzylidene ligand in *cis*-dichloro species was herein disclosed. Generally, the applicability of *cis*-dichloro ruthenium complexes is limited by their low activity in comparison to their *trans*-dichloro analogues. However, their slow initiation and pronounced thermal stability (*cf.* Introduction) can be used benefically in a number of high temperature and thermally triggered

(85) (a) Zaja, M.; Connon, S. J.; Dunne, A. M.; Rivard, M.; Buschmann, N.; Jiricek, J.; Blechert, B. *Tetrahedron* **2003**, *59*, 6545−6558. (b) Michrowska, A.; Bujok, R.; Harutyunyan, S.; Sashuk, V.; Dolgonos, G.; Grela, K. *J. Am. Chem. Soc.* **2004**, *126*, 9318−9325.

(86) Nuñez-Zarur, F.; Poater, J.; Rodrıǵuez-Santiago, L.; Solans-Monfort, X.; Solà, M. *Comp.Theor. Chem.* **2012**, *996*, 57−67.

applications.[44e,f,48b,c] As already discussed in Chapter I, the lowered initiation is attributed to an accessory activation step, which was experimentally and theoretically shown to correspond to a *cis-trans* isomerisation (*cf.* Introduction).

3. Synthesis and Characterization

Within this work we aimed at the preparation of electronically modified ester-chelating benzylidene complexes. A series of differently substituted 2-vinylbenzoic acid ethyl ester derivatives was prepared as carbene-precursors **L1-3** - **L5-3.** The ester funcionalized benzylidenes featured either an additional substituent (**L1-3**), an electron donating methoxy group in *meta*- (**L2-3**) or in *para*-position (**L3-3**) to the vinyl-group or an electron-withdrawing nitro group in *meta*- (**L4-3**) or in *para*-position (**L5-3**) and were prepared following known protocols (*cf*. Experimental Section).[87] According to Chapter II, complexes **cis1 – cis5** were obtained from a carbene-exchange reaction of **M31** with 1.2 - 1.5 eq of **L1-3** - **L5-3**. The reaction was performed in CH_2Cl_2 at 25°C and is typically finished after 17 h. Extraction of the reaction mixture with HCl_{aq} (5 v-%) allowed for the separation of most pyridine and subsequent precipitation of the products with *n*-pentane yielded the desired complexes **cis1** - **cis5** in crude form. Particularly complexes **cis1**, **cis2** and **cis3** are contaminated with a major impurity (6 – 13 %) which was tentatively assigned to cationic pyridine containing species $\mathbf{cis1^+_{py}}$ – $\mathbf{cis3^+_{py}}$ as shown in Scheme 11 (*cf*. Experimental Section).[88] A similar impurity was not present in the crude product mixtures of **cis4** and **cis5**. Upon subsequent purification by column chromatography analytically pure **cis1 – cis5** were obtained in moderate to good yield. The complexes were characterized by ^{1}H- and ^{13}C-NMR spectroscopy, elemental analysis and single crystal X-ray crystallography.

(87) (a) Cheng, H. X.; Fu, C. J. *Chin. J. Chem.* **2007**, 25, 1762-1765. (b) Wei, H.; Zhang, Y. J.; Wang, F.; Zhang, W. *Tetrahedron: Asymmetry* **2008**, *19*, 482-488. (c) Friedrich, K; Öster, H. *Chem. Ber.* **1961**, *94*, 834-837.

(88) The by-products were not isolated in pure form. NMR spectroscopic data retrieved from the crude product mixtures suggested the formation of cationic pyridine complexes on the basis of a high-field shifted carbene proton resonances (17.41-17.93 ppm) and the presence of signals assigned to a coordinated pyridine (e.g. 8.50-8.55 ppm). A similar complex has been isolated and fully characterized recently, see: Ref. 44g.

Scheme 11. Synthesis of **cis1**-**cis5**.

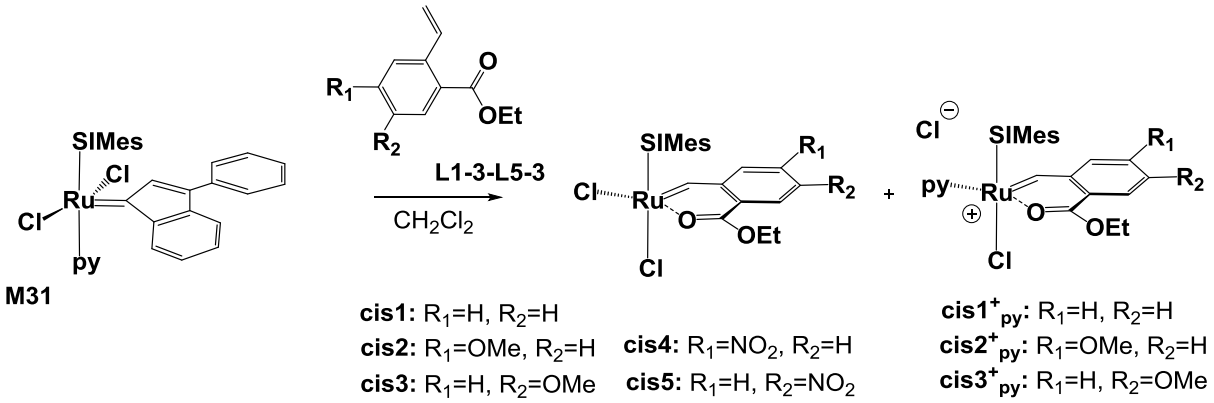

cis1: R_1=H, R_2=H
cis2: R_1=OMe, R_2=H
cis3: R_1=H, R_2=OMe
cis4: R_1=NO_2, R_2=H
cis5: R_1=H, R_2=NO_2

cis1$^+_{py}$: R_1=H, R_2=H
cis2$^+_{py}$: R_1=OMe, R_2=H
cis3$^+_{py}$: R_1=H, R_2=OMe

The typical ^{1}H-NMR pattern suggested a *cis*-dichloro structure in all cases (*cf*. Chapter II). Variation of the electron density of the benzylidene ligand is reflected by the ^{1}H-NMR-shift of the carbene's proton: Electron rich derivatives **cis3** and **cis2** showed the corresponding singlet at 18.57 and 18.92 ppm and the electron poor systems **cis4** and **cis5** exhibited the resonance at lower field at 19.09 and 19.30 ppm, respectively. Unsubstituted complex **cis1** showed the according signal at 18.96 ppm. Similarly, the ^{13}C-resonance of the carbene was shifted according to the electronic modification of the benzylidene ligand. While **cis1** – **cis3** exhibited deshielded carbene resonances of in the range of 282.9 – 283.8 ppm, the nitro-group-bearing derivatives gave a signal at lower fields (278.0 ppm for **cis4** and 276.7 ppm for **cis5**). The same trend could be found for the C=O resonance of the ester group, but less pronounced. Unsubstituted **cis1** showed the carbonyl C peak at 177.0 ppm. Corresponding resonances were found at 176.1 (**cis2**) and 178.2 ppm (**cis3**) for methoxy derivatives. The peak was shifted to higher fields for nitro substituted complexes (176.1 ppm for **cis4** and 175.7 ppm for **cis5**). Comparable carbene proton shifts were obtained for electronically modified Hoveyda-type initiators,[85a] indicating that the highest observable impact on the carbene proton was evoked by *para*-substituted benzylidenes ligands. An EDG functionalization (R^2=O^{i}Pr) is shielding the proton, leading to an up-field shifted carbene-proton (as for **cis3**), while the nitro group has the opposite effect (**cis5**). It deshields the electron density at the carbene proton resulting in a downfield shifted ^{1}H NMR signal in comparison to the substituted Hoveyda system.

Single crystal X-ray diffraction analysis confirmed the structural suggestion from the evaluation of ^{1}H-NMR data (*cf*. Figure 20). The typical *cis*-dichloro arrangement was assigned

by a distorted square pyramidal coordination mode, as it was already discussed in Chapter II. Important bond lengths and angles are presented in Table 12.

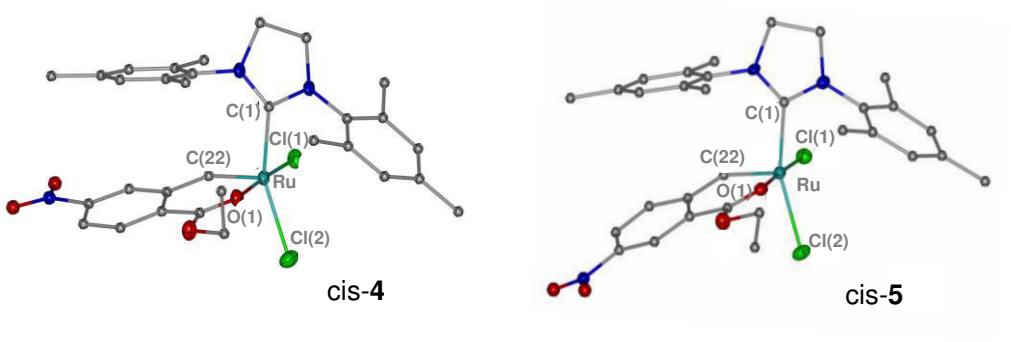

Figure 20. Crystal structures of **cis4** and **cis5**. Hydrogen atoms were omitted for better clarity.

Table 9. Selected bond lengths (Å) and bond angles (deg) for complexes **cis1** – **cis5**.

	cis1[44b]	**cis2**[44h]	**cis3**	**cis4**	**cis5**
Ru–C(22)	1.821(2)	1.824(3)	1.833(9)	1.813(3)	1.805(5)
Ru–C(1)	2.024(2)	2.010(2)	2.008(8)	2.022(3)	2.033(5)
Ru–O(1)	2.088(1)	2.076(1)	2.072(6)	2.093(2)	2.083(3)
Ru–Cl(1)	2.368(1)	2.363(2)	2.374(3)	2.352(1)	2.356(1)
Ru–Cl(2)	2.356(2)	2.344(2)	2.354(3)	2.367(2)	2.351(1)
C(1)-Ru-C(22)	98.68(7)	98.7(1)	97.7(4)	97.5(1)	99.0(2)
O(1)–Ru–Cl(2)	85.81(4)	85.53(6)	84.6(2)	85.63(6)	86.1(1)
C(22)–Ru–O(1)	89.86(7)	89.9(1)	89.4(3)	90.2(1)	90.1(2)
C(22)–Ru–Cl(1)	91.88(6)	89.6(1)	92.4(3)	90.6(1)	92.4(2)
C(22)–Ru–Cl(2)	106.15(6)	111.3(1)	107.9(3)	107.8(1)	102.8(2)
Cl(1)–Ru–Cl(2)	90.49(2)	91.21(3)	92.08(9)	91.69(3)	91.92(5)

The electronic tuning of the benzylidene ligand hardly influenced the Ru-Cl(1) (2.352(1)-2.374(3) Å) and the Ru-Cl(2) (2.344(2)-2.367(2) Å) bond lengths. The same accounted for the Ru-C(22) and Ru-C(1) distances. Minor deviations did not systematically follow the anticipated effect of the substitution. Only the Ru-O(1) distance somehow reassembled the expected tendency of shorter Ru-O bonds for methoxy substituted complexes and longer Ru-O bonds for nitro derivatives. Effects were not very pronounced as can be seen in Table 9. Generally, all solid state structures were very similar, except one particularity worth to be mentioned: the ethyl ester residue in compound **cis4** was out of plane, pointing towards the

NHC ligand, while in all other complexes it was in a coplanar arrangement with the benzylidene ligand. Although this phenomenon might be best explained by packing effects, it nevertheless played a role during the theoretical study described below.

4. Considerations on the Isomerization

As discussed in the introduction, it is generally believed that 2nd generation *cis*-dichloro ruthenium benzylidene complexes have to isomerize to their *trans*-counterparts before they become active in olefin metathesis transformations. Herein we aim at studying the energetic isomerization profiles for the series of electronically modified compounds under investigation. Three plausible *cis-trans* isomerization mechanisms were examined by DFT calculations. Crystal structures were taken as model to obtain optimized geometries of **cis1 - cis5**. The three considered pathways can be characterized as a chloride dissociative pathway through transition state **TS1**, a concerted pathway, through transition state **TS2**, and an oxygen dissociative pathway, through transition states **TS3**, as schematically shown for **cis2** in Figure 21. Results for all complexes are given in Table 10. The first pathway, corresponding to chloride dissociation, was considered because **cis2** exhibits a pronounced lability of the chloride in *trans* position to the NHC-ligand.[44h,89] DFT calculations confirmed that dissociation of either Cl1 or Cl2 leads to the same product **cis**$^{+}$ bearing the newly formed vacant coordination site *trans* to the NHC-ligand. This step is distinctly higher in energy ($\Delta E_{cis\text{-}Cl+\text{-}cis}$ = 33.4 – 38.3 kcal/mol) than the upper transition states observed for the other two pathways. Furthemore, after chloride dissociation another energy barrier of about 15 kcal/mol has to be overcome to finally arrive at the desired *trans* product. Overall the upper barrier window for this first dissociative pathway spans from 49.7 to 53.9 kcal/mol. These data suggest that this isomerization pathway is strongly disfavored.[90] However, calculations reveal a distinctly higher energy demand for chloride dissociation in the nitro-substituted derivatives ($\Delta E_{cis\text{-}Cl+\text{-}cis}$ = 38.3 and 38.1 kcal/mol for **cis4** and **cis5**), when compared to the unsubstituted or methoxy-substituted congeners (33.4 – 35.6 kcal/mol).

(89) For a discussion of the lability of chloride co-ligands in olefin metathesis catalysts in general see: Falivene, L.; Poater, A.; Cazin, C. S. J.; Slugovc, C.; Cavallo, L. *Dalton Trans.* **2013**, *42*, 7312-7317.

(90) This situation might change in the presence of donor ligands: *cf.* Chapter IV.

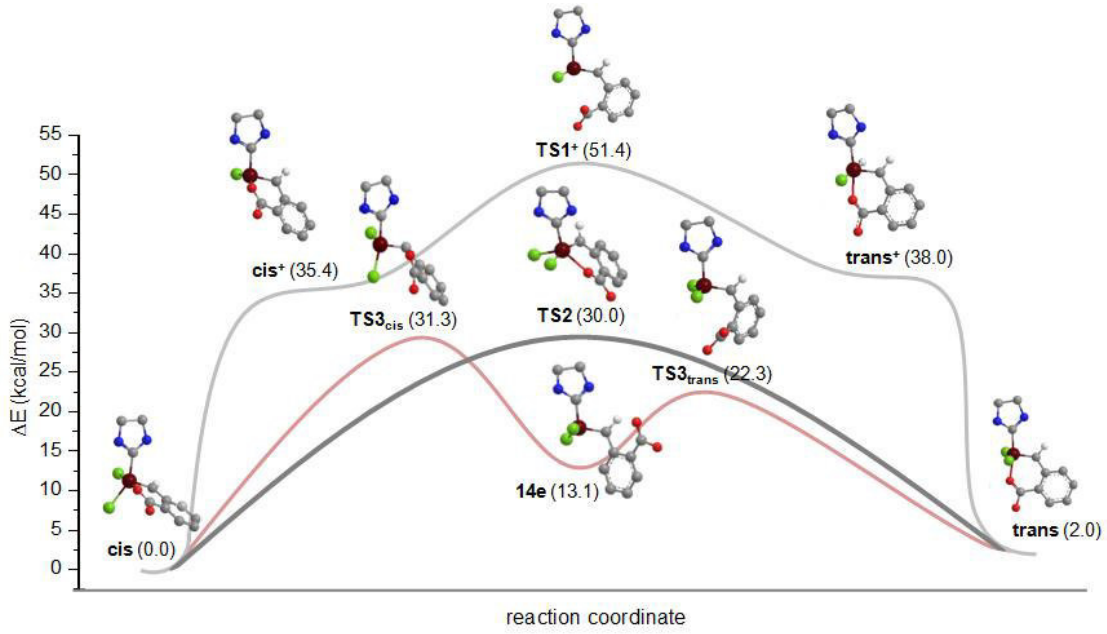

Figure 21. Potential pathways for *cis-trans* isomerization (for **cis2**): halide dissociative (**TS1**$^{+}$), concerted (**TS2**) and oxygen dissociative mechanism (**TS3**).

Table 10. Energies (kcal/mol) of **cis1** - **cis5** according to activation mechanism (bold values highlight the more likely pathway).[a]

Initiator	cis	cis-Cl^{+}	TS1^{+}	trans-Cl^{+}	TS2	TS3$_{cis}$	14e	TS3$_{trans}$	trans	trans$_{exp.}$
1	0.0	35.6	51.1	38.0	29.4	**29.1**	13.9	20.2	1.6	1.6 ± 0.4
2	0.0	35.4	51.4	37.5	**30.0**	31.3	13.1	22.3	2.0	2.3 ± 0.6
3	0.0	33.4	49.7	36.9	28.8	**27.4**	13.7	20.2	0.9	1.3 ± 0.3
4	0.0	38.3	53.9	39.6	30.1	**29.7**	14.4	18.7	0.4	0.4 ± 0.2
5	0.0	38.1	52.9	40.4	**28.7**	29.0	12.2	18.8	0.6	1.0 ± 0.3

[a] solvent = CH_2Cl_2, solvation model = PCM

These findings are the key for understanding why the cationic pyridine complexes **cis4**$^{+}_{py}$ and **cis5**$^{+}_{py}$ were not observed as by-products in the synthesis of the nitro-complexes. The second and the third pathway, i.e. the concerted (**TS2**) and the dissociative mechanism (**TS3$_{cis}$**) show similar upper barriers in the range of 27.4 – 31.3 kcal/mol. Complexes **cis2** and **cis5** might isomerize rather through a concerted transition state[53] to form the *trans*-counterpart. On the other hand complexes **cis1**, **cis3** and **cis4** may pursue an oxygen dissociative pathway, first overcoming the **TS3$_{cis}$**,[91] and then reaching the generally accepted

(91) The corresponding *cis*-14e compound was never observed in any calculation.

olefin metathesis active *trans*-14e complex by overcoming the **TS3$_{trans}$** which is about 10 kcal/mol lower in energy than **TS3$_{cis}$**. However, there is no clear trend to conclude that one of the two pathways is clearly favored, since the transition states **TS2** and **TS3$_{cis}$** differ in energy by less than 1.5 kcal/mol. Further, in some cases **TS2** is slightly lower in energy, in the other **TS3$_{cis}$** is lower in energy, see Table 10. Having established a mechanistic understanding of the isomerization process, now the position of the *cis*-*trans* equilibrium is discussed. A solution of pure **cis1** – **cis5** (c = 6.3 µM) in $CDCl_3$ was prepared and the isomerization progress at room temperature was monitored via ^{1}H-NMR spectroscopy. After three days the equilibrium was balanced for **cis1** – **cis3** and **cis5** (**trans1**: 6%; **trans2**: 2%; **trans3**: 10%; **trans5**: 16%), whereas for **cis4** balancing was finished in 15 days (**trans4**: 33%). From this dataset, the free energies ($\Delta G_{trans-cis}$) were calculated to be between 0.4±0.2 and 2.3±0.6 kcal/mol in favor of the *cis*-isomer and were found to be in good agreement with the corresponding values determined by the DFT calculations ($\Delta E_{trans-cis}$) (*cf*. Table 10). Additionally the speed of the isomerization could be roughly correlated to the energy of the highest transition state for isomerization,[92] by determining the *trans*-content after 1 h (at room temperature in $CDCl_3$). Complex **cis3** (TS = 27.4 kcal/mol) almost reached the equilibrium after that time resulting in 9±0.5% **trans3** (which is 90±5% of the theoretically amount of **trans3**) and 3±0.5% of **trans1** (50±8% of the theoretical amount, TS = 29.1 kcal/mol) and 4±0.5% of **trans5** (25±3%, TS = 28.7 kcal/mol) were present. In contrast, no *trans*-product could be observed in case of **cis4** (TS = 29.7 kcal/mol) and **cis2** (TS = 30.0 kcal/mol).

5. Polymerization

Similar to Chapter II, the isolation of **cis1 - cis5** rendered a comparative activity study possible. Ring opening metathesis polymerization (ROMP) of dimethyl-bicyclo[2.2.1]hept-5-en-2,3-dicarboxylate (**mon1**) was used as the benchmark reaction. First, a kinetic measurement of polymerization of monomer **mon1** was monitored at room temperature with **cis1 - cis5** as (*pre-*)initiators by means of arrayed ^{1}H-NMR spectroscopy. The obtained data are depicted in Scheme 22 in a time/conversion plot and polymerization half-lives are

(92) An experimental determination of the activation energy was not possible due to an unknown concomitant decomposition reaction becoming important at higher temperatures.

given in Table 11. It was found that **cis5** ($t_{1/2}$ = 98 min) was the most active catalyst, followed by **cis4** ($t_{1/2}$ = 122 min), **cis3** ($t_{1/2}$ = 161 min), **cis1** ($t_{1/2}$ = 372 min) and **cis2** ($t_{1/2}$ = 440 min) as the least active initiator of all. The descending order is mainly dependent on the activation energy for the isomerization. This holds true for the activity increase from **cis2** to **cis1** and to **cis3**. However, the two most active initiators, the nitro derivatives **cis4** and **cis5**, show higher barriers for the *cis-trans* isomerization process than **cis3**. The *trans*-species is less disfavored in these two cases which might explain their higher activity compared to **cis1** – **cis3**.

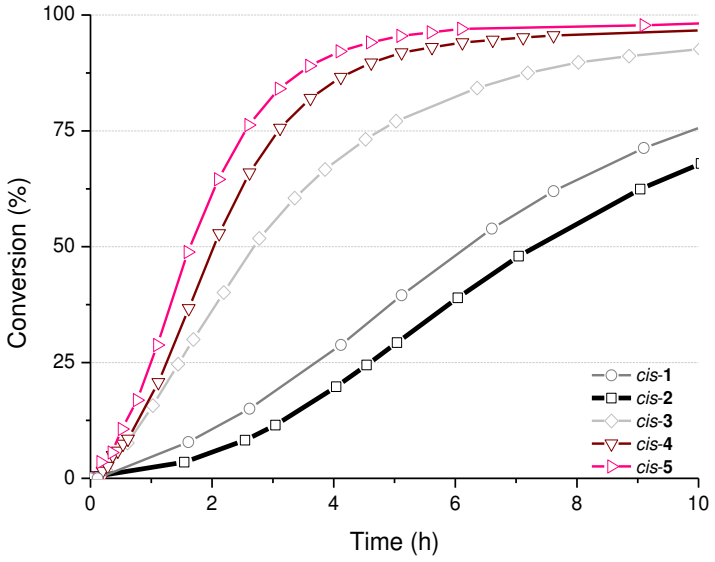

Figure 22. Time/conversion plot for the polymerization of mon1 with initiators **cis1** – **cis5** relying on ^{1}H NMR-data. Reaction conditions: [**mon1**]:[initiator] = 70:1; [**mon1**] = 0.13 mol L^{-1}; reaction temperature = 25°C, solvent: $CDCl_3$; inert atmosphere of N_2.

Table 11. Characterization of **poly1** prepared with **cis1**-**cis5** at elevated temperature.[a]

Initiator	Time (min)[b]	M_n (kg/mol)[c]	PDI[c]
M31	10±2	54	1.1
cis1	30±4	242	1.7
cis2	35±4	281	1.9
cis3	15±3	176	1.6
cis4	12±2	116	1.5
cis5	12±2	144	1.5

[a] Reaction conditions: [**mon1**] : [initiator] = 300 :1; [**mon1**] = 0.1 mol L^{-1}; reaction temperature = 80°C, solvent: toluene; inert atmosphere of N_2; [b] time until conversion is complete (checked by thin layer chromatography); [c]determined by SEC relative to *poly*(styrene) standards in THF.

Also this assumption bears an inconsistency because the said difference between the thermodynamic stability of the *cis*- and the *trans*-species in **cis4** is smaller than in **cis5**. Accordingly **cis5** should be more active than **cis4** which is not the case. Here the thermodynamic stability of the actual initiator, the 14e-species, seems to be decisive because most active **cis5** bears the thermodynamically most favored 14e-species (12.2 kcal/mol) and slightly less active **cis4** leads to a less stable 14e-species (14.4 kcal/mol). Accordingly it is proposed that the stationary concentration of the 14e-species is an important factor for the activity of the initiators under investigation.

To shed more light on the structure-activity relationship discussed so far, another series of polymerizations of **mon1** at elevated temperature of 80°C with a monomer to initiator ratio of 300:1 was carried out. The aim was to provide the system enough energy to overcome the barrier for *cis-trans* isomerization and to assess the initiation efficacy of **cis1** – **cis5**. The polymerization reaction was carried out until complete conversion of **mon1** was assured. Thereupon the polymers were isolated and their number average molecular weights (M_n) were examined by size exclusion chromatography (SEC). Data can be found in Table 11 and Figure 24. Additionally, three published initiators **cis6, trans6** and **trans7** were selected to evaluate the general validity of a potential correlation (see Figure 23).[44c,55]

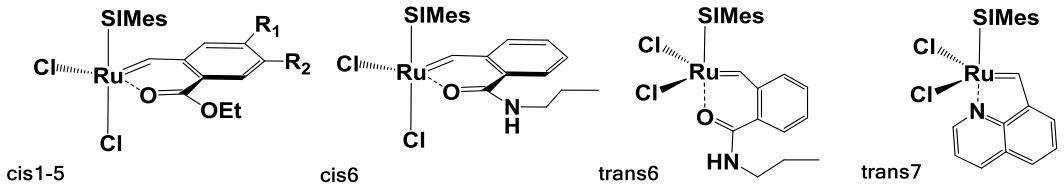

Figure 23. Structures of complexes **1-7.**

This approach allows for an indirect relative assessment of the initiation efficacy because M_n is proportional to the ratio of propagation rate (k_p) and the initiation rate constant (k_i) provided that no secondary metathesis occurs. The propagation rate k_p is the same in all cases, as in all cases the same propagating species occurs. Consequentally, M_n is only dependent on k_i. **M31** was included as a benchmark initiator in this study, because it provides fast and complete initiation ($k_i >> k_p$). The polymer **poly1**, prepared with **M31** at room temperature, is characterized by a M_n-value of 62 kg/mol and a PDI of < 1.1 (relative to *poly*(styrene) standards; [**mon1**]:[**M31**] = 300:1). At 80°C and with **M31** as the initiator, **poly1** showed a similar M_n as at room temperature. The polymerization was finished after about

10 min. Contrary, *cis*-Dichloro initiators under investigation gave **poly1** with higher M_n-values, decreasing from 281 kg/mol (**cis2**) to 116 kg/mol (**cis4**) (*cf*. Table 11 and Figure 24) meaning that the initiation efficacy is in the best case approximately 2 times lower than in case of the fast and fully initiating compound **M31**. In general, low activity at room temperature and moderate initiation efficacy at higher temperature are typical for *cis*-dichloro initiators. Electronic modification is either decreasing (**cis2**) or increasing the initiation efficacy (**cis3** – **cis5**).

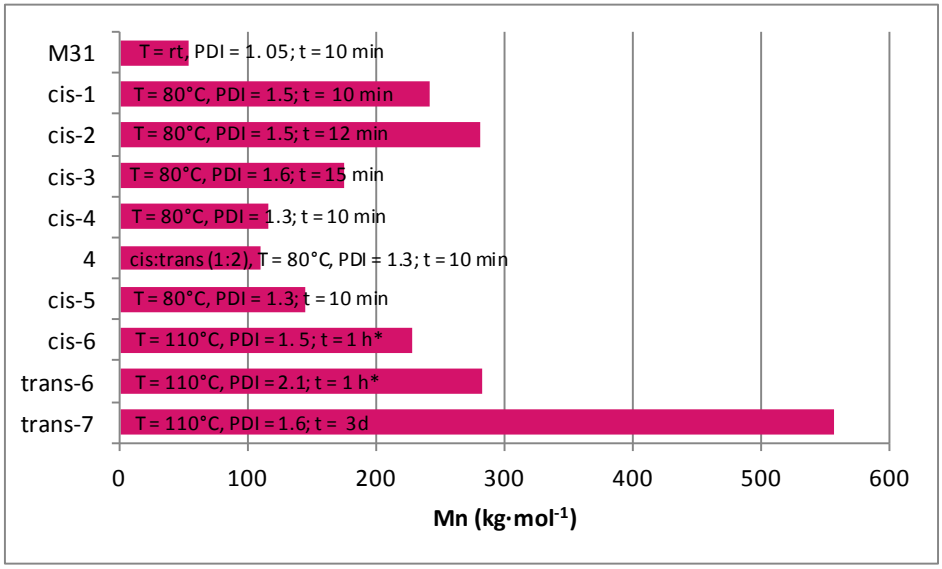

Figure 24. GPC data of **poly1** initiated with **cis1**-**5** and **trans6**-**7**.

Analyzing these data, a linear correlation between the measured M_n-values and the difference between the calculated thermodynamic stabilities of the *trans*-configured and the *cis*-configured isomers ($\Delta E_{trans\text{-}cis}$) can be found (see Figure 25). This means that the initiation efficacy is above all determined by the position of the *cis-trans* equilibrium assuming that the said equilibrium is reached fastly at 80°C. Thus, electronic tuning of the benzylidene ligand translate into altered balancing of the *cis-trans* equilibrium which is in turn responsible for the observed initiation efficacy of the initiators.

The following important implications can be deduced by our findings: a) at a reaction temperature which is high enough to provide a fast (relative to initiation) balancing of the *cis-trans* equilibrium, the initiation efficacy is dependent on the relative thermodynamic stability of the *trans*-isomer in comparison to the *cis*-isomer; b) this postulate should hold true no matter if a pure *cis*-isomer or a pure *trans*-isomer is initially used; accordingly, c) a

trans-configured initiator might be deactivated at elevated temperature if a thermodynamically more stable *cis*-isomer is accessible.

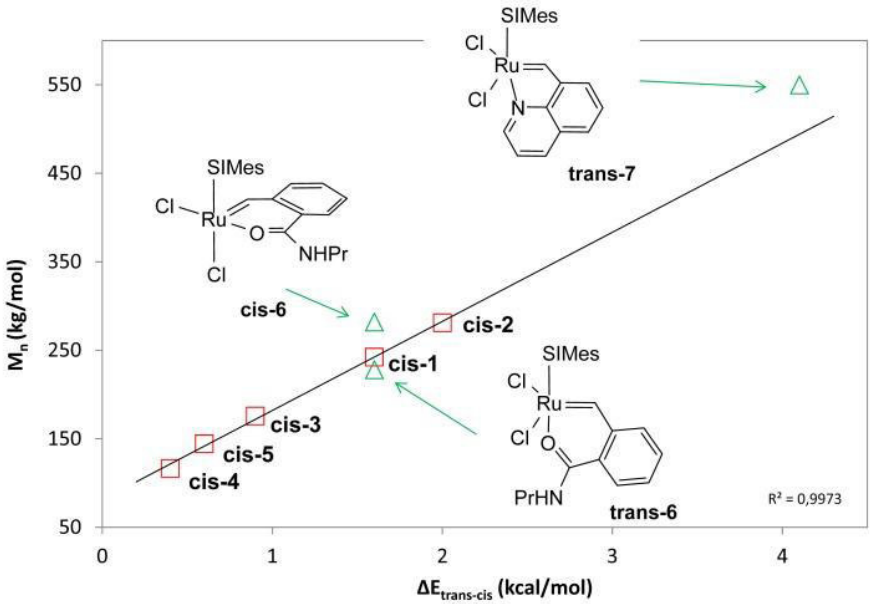

Figure 25. Correlation between activity of (*pre*-)catalysts and theoretically determined thermodynamic *cis-trans* equilibrium constant.

Figure 25 shows that all three external data points **cis6**, **trans6** and **trans7**[93] fit on the plotted trendline, indicating a more general applicability of the postulate that the assessment of the thermodynamic equilibrium position of the *cis-trans* isomerization is suited to predict the initiation efficacy of a *cis*- (but also *trans*-)dichloro ruthenium benzylidene initiators at elevated temperature. Another experiment further confirms this fact as similar M_n values for **poly1** were observed when employing pure **cis4** (M_n = 116 kg/mol, PDI = 1.5, t=12 min) or a mixture of **4** (*trans:cis* = 2:1, M_n=110 kg/mol, PDI=1.3 and t=10 min).

As polymerization experiments at elevated temperature (80°C - 110°C) were performed in toluene, changes in thermodynamic equilibrium were calculated in dependence on the solvent (*cf.* Scheme 26 and Table 12). Differences in thermodynamic equilibrium constants of complexes **1**-**5** were found to be shifted through the *trans* side with decreasing electric dipole moments.[41f]

(93) In literature the higher M_n-value of **poly1** obtained with **trans6** (when compared to **cis6**) was attributed to different solubility of the initiators, *cf.* Ref. 44c.

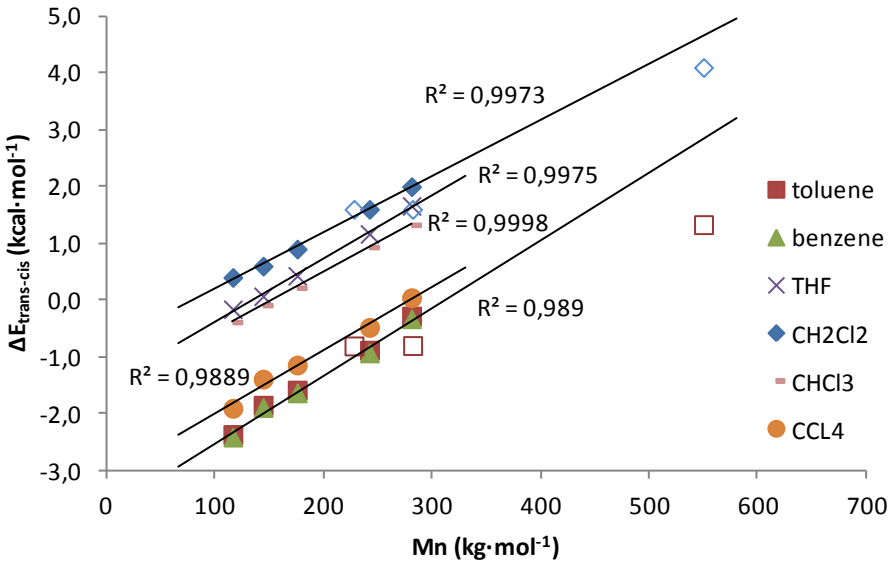

Figure 26. Solvent effects on the thermodynamic equilibrium. Full symbols: complexes **cis1-5,** empty symbols: **cis6**, **trans6** and **trans7**.

Correlations of number molecular weight with the thermodynamic equilibrium constants of complexes **1**-**5** in solvents as toluene ($2.4 \cdot 10^{-30.0}$ Cm), benzene ($2.3 \cdot 10^{-30.0}$ Cm), CCl_4 ($2.2 \cdot 10^{-30.0}$ Cm), $CHCl_3$ ($4.8 \cdot 10^{-30.0}$ Cm), THF ($7.5 \cdot 10^{-30.0}$ Cm), CH_2Cl_2 ($9.1 \cdot 10^{-30.0}$ Cm) were plotted and can be found in Table 12. The coefficient of determination gives in all cases a correlation > 98% (Figure 26), meaning the general trend remains the same in different solvents as already predicted for CH_2Cl_2.

Table 12. Influence of solvent on thermodynamic equilibrium $\Delta E_{trans\text{-}cis}$ (in kcal/mol) for complexes **1-5.**

complex	toluene	benzene	THF	CH_2Cl_2	$CHCl_3$	CCl_4
1	-0.9	-0.9	1.2	1.6	0.9	-0.5
2	-0.3	-0.3	1.7	2.0	1.3	0.0
3	-1.6	-1.6	0.4	0.9	0.2	-1.1
4	-2.4	-2.4	-0.2	0.4	-0.4	-1.9
5	-1.9	-1.9	0.1	0.6	-0.1	-1.4

6. Conclusion

The importance of *cis-trans* isomerization for dormant *cis*-dichloro initiators was studied by experimental and theoretical means. As can be read in the previous chapters, the activation of *cis*-dichloro initiators in olefin metathesis occurs through the appearance of the *trans*-species. Theoretical DFT calculations revealed the mechanism of the isomerization occurring either through an oxygen dissociative or a concerted pathway. The third potential pathway (by halide dissociation) was excluded for further considerations due to high energy barriers (*cf*. Scheme 12).

Scheme 12. Pathways for *cis-trans* isomerization.

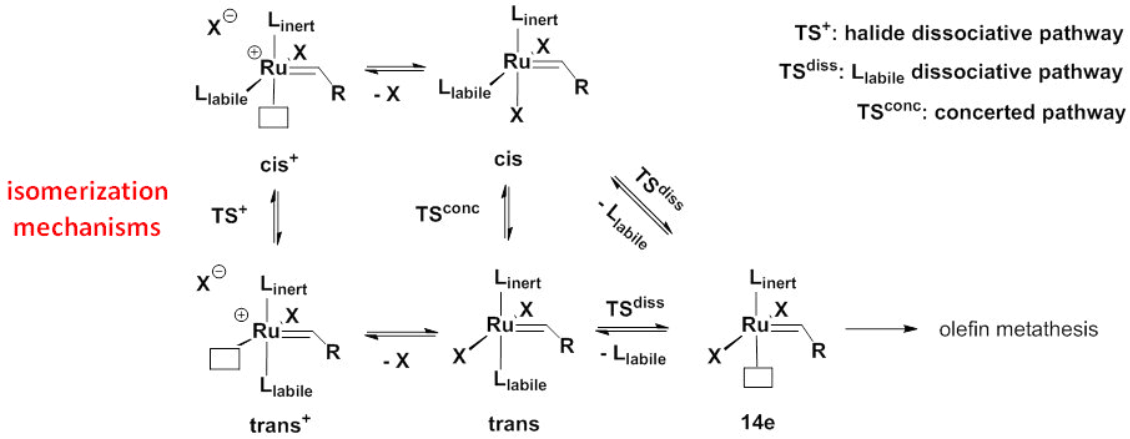

Contrary, no clear trend allowed for concluding which is the favored pathway for isomerization. Experimentally it was shown that energy barriers to overcome the transition state can already be reached at room temperature. However, the reaction time is restricted by the duration of isomerization. By overcoming the responsible transition state, the specific thermodynamic equilibrium of each complex can be reached. This reaction can be accelerated at elevated temperatures. Hence, transition state barriers can be neglected at elevated temperatures, resulting immediately in the specific thermodynamic *cis-trans* isomerization equilibrium of each initiator. Comparing experimental and theoretical results, it was found that the thermodynamic equilibrium constants were in good agreement. Moreover, we showed that this equilibrium is the key for the activity of *cis*-dichloro (*pre*-)catalysts in olefin metathesis. Results in ROMP at T > 80°C outlined coherence between activity and thermodynamic equilibrium of initiators under investigation. Number average molecular weights (M_n) were plotted against theoretically determined $\Delta E_{trans\text{-}cis}$ to find a

correlation of 99.7%. Consequentially, the activity of *cis*- (but also *trans*-) dichloro ruthenium initiators can be predicted by the thermodynamic equilibrium constant for *cis*-*trans* isomerization.

CHAPTER IV

donor molecules - activation/deactivation of (*pre*-)catalyst

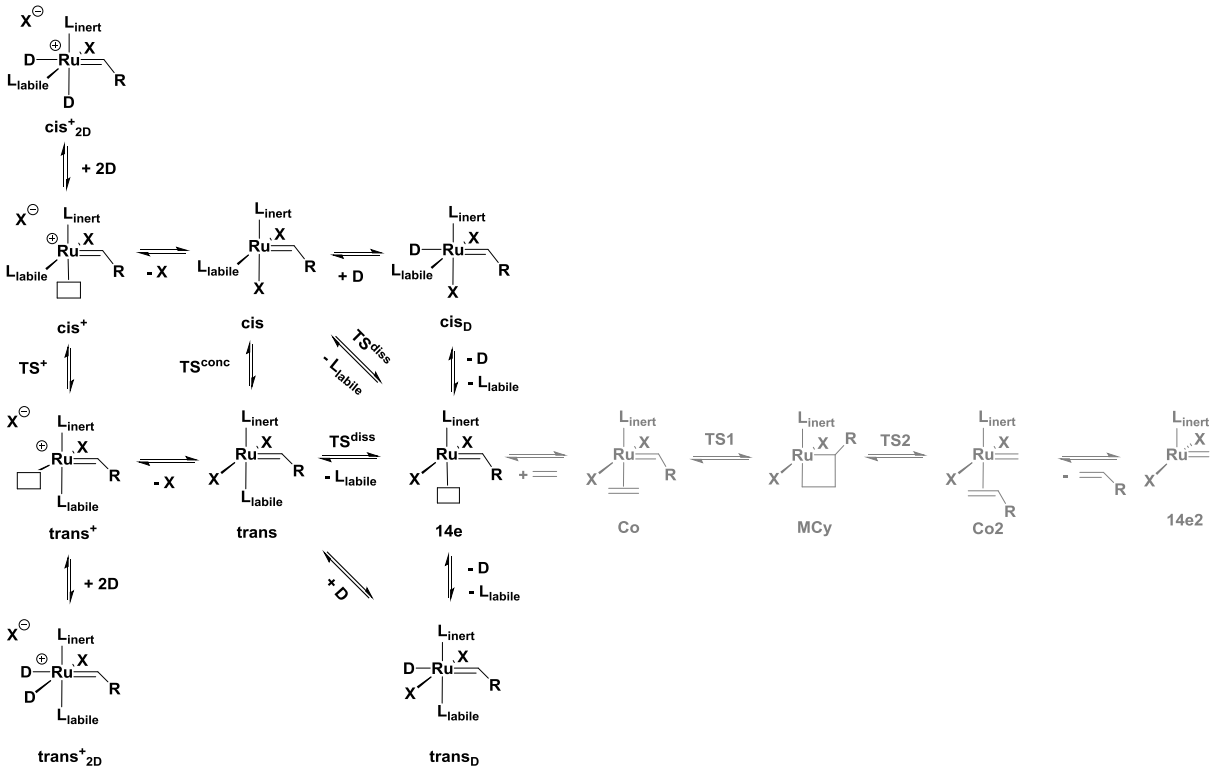

1. Abstract

Cis to *trans*-dichloro isomerization of second generation ruthenium benzylidenes was studied in presence of donor molecules. Solvents and additives are known to constantly influence the stereochemistry of the complex and hence the reactivity of the (*pre*-)catalyst in olefin metathesis. In further consequence, the reproducibility of *cis*-dichloro ruthenium initiated metathesis was revealed to be strongly depent on the presence of donor molecules in the reaction mixture, using pyridine as an example. These changes in activity were examined experimentally and theoretically. Generally, the coordination of one donor molecule at the sixth coordination site was found to facilitate the activation of the (*pre*-)catalyst, whereas two donor molecules (and consequentially the dissociation of one chloride) have the opposite effect. Computational studies presented in this work reveal the mechanistic basis of this phenomenon. Depending on the amount and nature of donor molecule the activation of the (*pre*-)catalyst is either relieved or hampered.

2. Introduction

The third generation of ruthenium complexes arose 2002, when a six-coordinated pyridine modified catalyst **G-III** was obtained after the addition of 3-bromopyridine to the second generation benzylidene complex **G-II**. At that time this type of catalyst was one of the fastest initiators,[94] however the impact of the sixth ligand coordinating on the mechanism of the initiation to obtain high-efficiency catalysts was only examined recently by Grela et al.[95] Important representatives are shown in Figure 27. Dependent on the sterical bulk of the other ligands, either one (**M31**)[96] or two labile ligands (**G-III**[97], **Grela-III**[95a], **Lem-**

(94) Love, J. A.; Morgan, J. P.; Trnka, T. M.; Grubbs, R. H. *Angew. Chem., Int. Ed.* **2002**, *41*, 4035–4037

(95) (a) Szadkowska, A.; Żukowska, K.; Pazio, A. E.; Woźniak, K.; Kadyrov, R.; Grela, K. *Organometallics* **2011**, *30*, 1130– 1138; (b) Zukowska, K.; Szadkowska, A.; Trzaskowski, B.; Pazio, A.; Paczek, L.; Wozniak, K.; Grela, K. *Organometallics* **2013***, 32,* 2192–2196; (c) Trzaskowski, B.; Grela, K. *Organometallics* **2013**, *32*, 3625-3630.

(96) **M31** is commercially available from Umicore.

(97) Choi, T. L. Grubbs, R. H. *Angew. Chem., Int. Ed.* **2003**, *42*, 1743–1746.

III[41f]) can coexist. In this coherence, especially the presence of pyridine containing 18e complexes in *cis*-dichloro complexes is of interest.

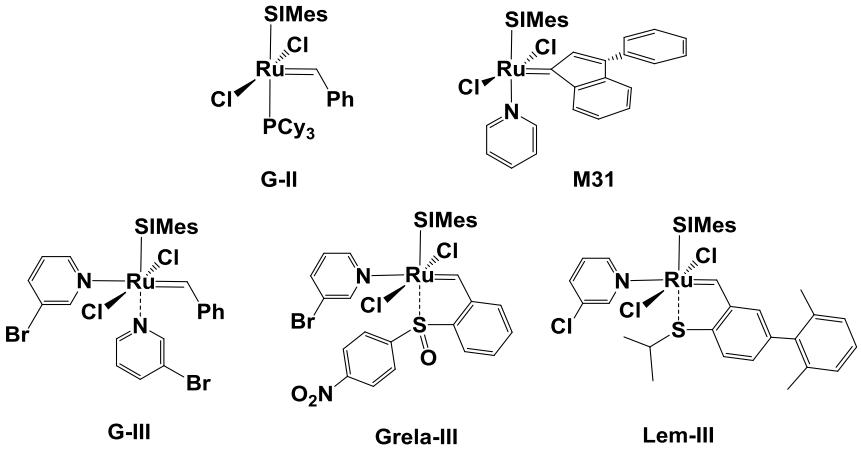

Figure 27. Development of 3rd generation ruthenium complexes.

The role of pyridine on *cis*-dichloro complexes was already disclosed in previous work. During the synthesis of a *cis*-dichloro benzylidene derivative, bearing an isopropyl ester (**cis2-iPr**).[44g] The cationic complex was formed during a ligand exchange reaction, starting from the commercially available pyridine containing complex **M31** (*cf.* Scheme 13). An alternative pathway to reach the cationic species **cis2-iPr$^{+}_{py}$** was found to appear directly from **cis2-iPr** by the addition of excess pyridine, however, only after subsequent column chromatography on silica gel (CH_2Cl_2:MeOH, 8:1 (v:v)) in 25% yield. Without this purification step, only unidentified (*pre*-)products were observed, which seem to hamper the conversion toward the cationic pyridine complex.

Scheme 13. Synthesis of chelating ester ruthenium benzylidenes.

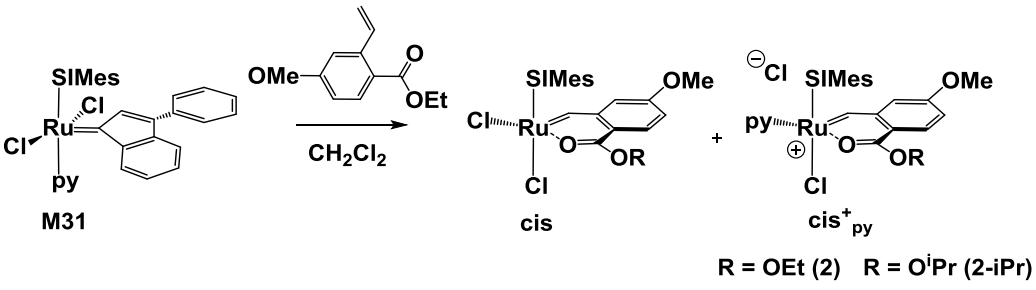

The activity of cationic **cis$^{+}_{py}$**-type compexes in olefin metathesis was found to be dependent on the chloride counterion. Acceleration in respect to the *cis*-complex was observed in presence of a Cl^- counter ion. Contrary, (nearly) complete deactivation occurred

when preventing the back coordination of the counter chloride by a non-coordinating anion, namely PF_6^-. This fact implies an activation mechanism of **cis** through *cis-trans* isomerization rather than through a cationic intermediate.[44g] Accordingly, pyridine seems to have an accelerating effect on the isomerization rate. This effect is already well-known for *trans*-dichloro complexes and was recently reported by Lemcoff et al. He stated that the addition of pyridine, but also other donor molecules as water, DMSO and PCy_3 to *trans*-dichloro catalysts has an accelerating effect on the *cis-trans* isomerization rate. Additionally, an improved activity of the *trans*-dichloro compound was found in the presence of donors.[41f] Grela et al. could finally show that the formation of a neutral 18e complex is responsible for the improved activity.[95] Consequentially, similar impacts of pyridine (and in general donor molecules) on the activation mechanism of *cis*-dichloro olefin metathesis catalysts are expected and were disclosed within this work.

3. Results and Discussion

The accelerating effect of pyridine on the activity of *cis*-dichloro complexes was firstly stated when a cationic, pyridine containing complex **cis2-iPr$^+_{py}$** was isolated and tested in ring opening olefin metathesis. As the cationic species itself was inactive, the role of pyridine (and donor molecules in general) was studied more into detail. Likewise, an accelerating effect was obtained under given reaction conditions when adding 5.0 eq of pyridine to **cis2**. Contrary, an increased excess of pyridine (50 eq) has a decelerating effect on the polymerization (*cf.* below). Thus, we became interested in the pyridine-doped activation and deactivation of *cis*-dichloro ruthenium complexes. Hence, four potential structures were considered to be formed in presence of pyridine (*cf.* Figure 28). The thermodynamic stability was examined by theoretical DFT calculations (pcm = CH_2Cl_2), using pyridine, DMSO, methanol, water and nitrate (NO_3^-) as donor molecules (*cf.* Table 13). In case of pyridine, the obtained results suggest the formation of **cis2$_{py}$** and **cis2$^+_{2py}$** as main products. The fully characterized cationic complex **cis2$^+_{py}$** is thermodynamically slightly favored when referring to the *cis*-dichloro complex. However, its occurance is restricted to (1) either appear as side product during the synthesis of **cis2** (*cf.* above) or to (2) further treatment (column chormatography or extraction with $HCl_{aq.}$) when starting directly from **cis2** and an excess of pyridine. In contrast, the expected formation of **cis2$^+_{py2}$** where the chloride in *trans*-position

to the NHC ligand was exchanged, is thermodynamically not favored and will not be considered for further assignments. DMSO shows a similar, however, less prounced tendency as pyridine to be able to form **cis2$^{+}_{D}$**, **cis2$_{D}$** and **cis2$^{+}_{2D}$**. More polar solvents, as water and methanol, are only prone to form the neutral species **cis2$_{D}$**. The addition of a salt, as NO_3^-, was also considered in this studies. Nitrate is a bidentate ligand and can coordinate on two coordination sites of the complex. Hence, only 18e structures **cis2$_{D}$** and **cis2$^{+}_{2D}$** were regarded. Consequentially, a negative charge was found when NO_3^- coordinates with just one oxygen on the sixth coordination site of **cis2** to form **cis2$^{-}_{NO3}$** and neutral for **cis2$_{NO3}$**, where the nitrate acts as bidentate anionic ligand and compensates the loss of one chloride.

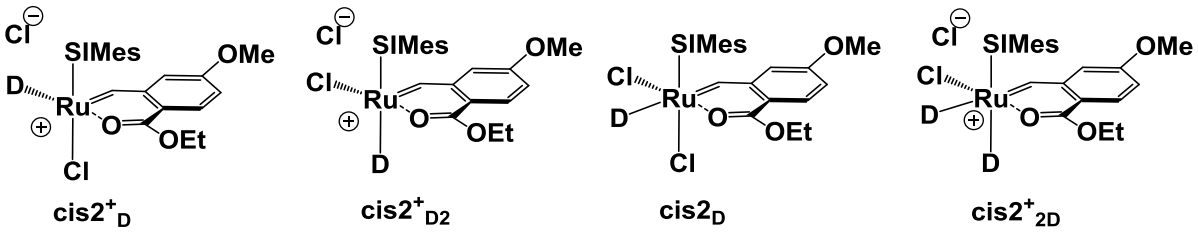

Figure 28. Potential product formation when adding donor molecules to **cis2**.

Table 13. Energies of potential products, when adding donor molecules to **cis2** (ΔE in kcal/mol).

entry	donor	cis2	cis2$^{+}_{D}$	cis2$^{+}_{D2}$	cis2$_{D}$	cis2$^{+}_{2D}$
1	**py**	0.0	-0.8	3.4	-13.0	-15.1
2	**DMSO**[a]	0.0	-1.4	10.1	-2.6	-6.6
3	**H_2O**	0.0	15.5	19.1	-8.6	6.1
4	**MeOH**	0.0	15.1	15.9	-8.5	3.4
5	**NO_3^-**	0.0	-	-	-0.5	-0.8

[a] for DMSO always a preferential coordination of the sulfur atom was found.

A ^{1}H NMR spectroscopic study (300 MHz, $CDCl_3$) of **cis2** was accomplished within the carbene region using an excess of 30 eq pyridine to approve the formation of the aforementioned products (*cf.* Figure 29a). The starting product shows a carbene-proton shift at 18.92 ppm, the **cis2$^{+}_{py}$** proton features a shift at 17.96 ppm. The addition of pyridine led to the immediate formation of a new carbene signal, which is downfield-shifted to 19.69 ppm. When the reaction was extended to three days, the formation of another species with a carbene-H at 20.12 ppm was observed. A similar signal at 20.12 ppm was found when recording a spectrum of **cis2** in pure pyridine-d^5 (*cf.* Figure 29b). The abundant excess of

pyridine implies the formation of the cationic dipyridine complex **cis2$^{+}_{2py}$**. Extended reaction times led to the formation of two more downfield-shifted signals, which are assigned to opened chelate compounds with two or three pyridines coordinating.

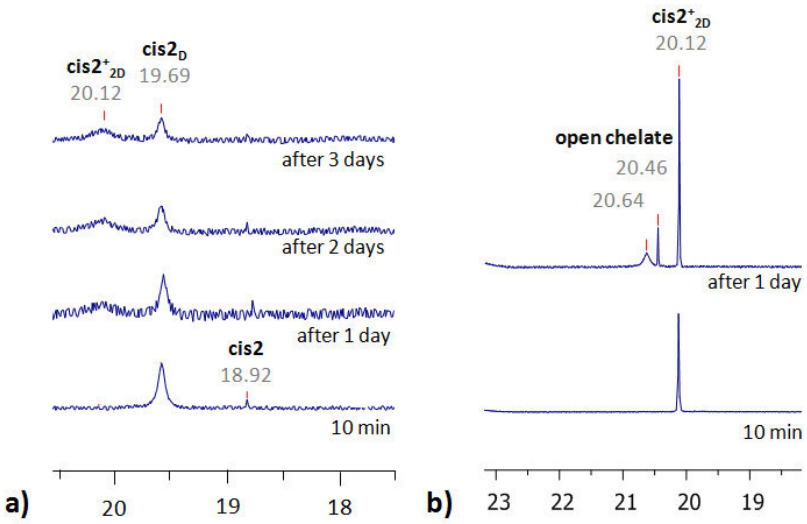

Figure 29. ^{1}H NMR spectra (300 MHz, 25°C) within the carbene region of **cis2** (a) in $CDCl_3$ with 30 eq and (b) in pyridine-d^{5}.

These observations have been confirmed by theoretical NMR simulations with chloroform as a solvent (pcm = $CHCl_3$). The calculated shields (σ) of previously reported complexes correlated to the experimentally found chemical shifts (δ) in 92% (*cf.* Experimental Section). In the following the trend of experimental assignment matched with the theoretically calculated data. Another hint for the formation of **cis2$^{+}_{2py}$** was accomplished, when **cis2$_{NO3}$** was formed from **cis2** by the addition of NH_4NO_3 in methanol (or undried CH_2Cl_2, respectively) or by extraction of the complex **cis2** dissolved in CH_2Cl_2 with a saturated, aqueous solution of NH_4NO_3.[44h] The complex was isolated and fully characterized. The main significant signal by ^{1}H NMR spectroscopy was characterized by a downfield shifted carbene proton resonance at 19.82 ppm. The final proof of the 18e structure was retrieved from single X-ray diffraction determination (*cf.* Figure 30). A reason for not observing crystals of the related **cis2$^{+}_{2py}$** might be connected to its relatively long Ru-N bond length of > 2.3 Å. These data suggest the dissociation of the Ru-N bond to be more likely compared the Ru-O bond in case of **cis2$_{NO3}$**.

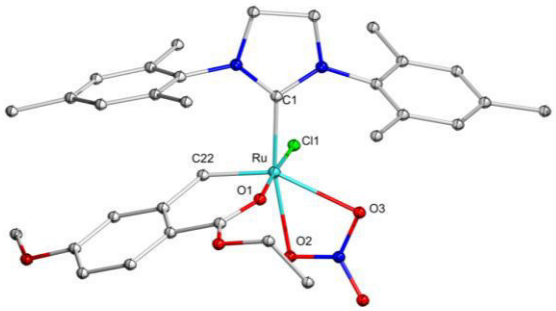

Figure 30. Crystal structure of **cis2$_{NO3}$**. Hydrogen atoms were omitted for better clarity. Important bond lengths (Å): Ru-C(22): 1.828(3), Ru-C(1)= 1.995(4), Ru-O(1)= 2.060(3), Ru-Cl(1)= 2.3676(9), Ru-O(2)= 2.183(3), Ru-O(3)= 2.365(2); bond angles (deg): C(1)-Ru-C(22)= 97.6(1); C(1)Ru-O(3)= 110.2(1), O(1)-Ru-O(2)= 56.6(1); C(22)-Ru-O(1)= 91.0(1); C(22)-Ru-Cl(1)= 90.5(1), C(22)-Ru-O(2)= 95.4(1), C(22)-Ru-O(3)= 151.9(1), Cl(1)-Ru-O(2)= 93.15(7).

Experimental restrictions were found when adding H_2O, methanol as well as DMSO can be attributed to the low solubility of **cis2** in these high polarity-solvents. The addition of excess of water (37 eq) and methanol (520 eq) simply led to a broadening of the **cis2** carbene signal (18.92 – 18.97 ppm) implying the formation of the 18e complex **cis2$_D$**. Recording spectra in deuterated solvents led to the formation of **cis2$^+_{DMSO}$** (16.46 ppm) and a broad **cis2** (18.97 ppm) signal in DMSO-d^6 and **cis2$_{MeOD}$** (19.52 ppm) in pure MeOD. However, the low solubility of the complex questions the trustability of the results.

4. Polymerization

Initiator **cis2** was used for studying the ROMP kinetics of of dimethyl bicyclo[2.2.1]hept-5-ene-2,3-dicarboxylate (**mon1**) under standard conditions. Figure 31 shows acceleration of the polymerization (blue lines) when adding small amounts (5.0 eq) of donor molecules. In case of pyridine the highest acceleration was observed ($t_{1/2}$ = 3.4 h). Likewise, the addition of NO_3^- led to an improvement of the polymerization by 2.7 h in comparison to the starting compound **cis2** ($t_{1/2}$ = 7.3 h).

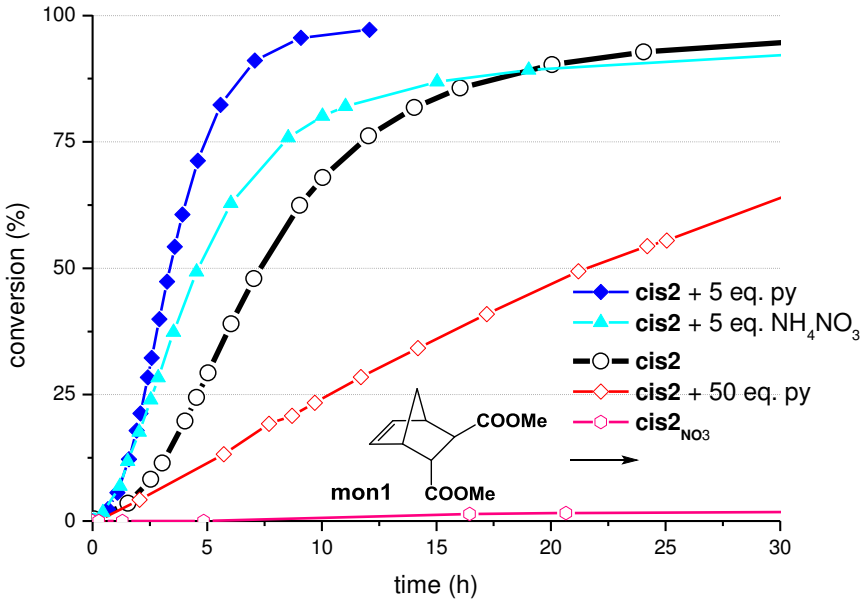

Figure 31. Standard benchmark reaction of **mon1** and **cis2** without (black), with 5 eq (dark blue), 5 eq NH_4NO_3 (cyan), 50 eq pyridine (red) and **cis2**$_{NO3}$ (pink). Conditions: [**mon1**]:[**cis2**$_{(NO3)}$] = 70:1; [**mon1**] = 0.17 mol/L; reaction temperature = 25°C, solvent: CDCl3; inert atmosphere of N_2.

The most obvious explanation for the accelerated polymerization is the formation of the 18e complex (as found for the *trans*-congener) **cis2**$_D$, which was assigned to be the primary product when adding 30 eq of pyridine to **cis2**. Contrary, high excess of donor molecules favors the tendency to form **cis2**$^+_{2D}$, which in turn retards the polymerization (red lines). The addition of 50 eq of pyridine already leads to an increased half life of 21.4 h. Another proof for the latency of this kind of complexes is the reaction with **cis2**$_{NO3}$ which is completely blocked for polymerization under the very same conditions. In presence of a chloride source (benzyl triethyl ammonium chloride, 1.0 eq), the complex can be *re*-activated slowly ($t_{1/2}$ = 50.2 h). This implies that not only a cationic species (**cis2**$^+_{2D}$), but also the neutral **cis2**$_{NO3}$ hinders the reaction. However, NO_3^- is known to be a very labile ligand,[98] which might be also exchanged by two donor molecules, leading to a cationic **cis2**$^+_{2D}$ complex.

(98) (a) Buchmeiser, M. R.; Ahmad, I.; Gurram, V.; Kumar, P. S. *Macromolecules* **2011**, *44*, 4098-4106. (b) Jović, M.; Torker, S.; Chen, P. *Organometallics* **2011**, *30*, 3971-3980. (c) Keitz, B. K.; Fedorov, A.; Grubbs, R. H. *J. Am. Chem. Soc.* **2012**, *134*, 2040-2043.

5. Activation/Deactivation

The *cis-trans* isomerization was already studied in previous experimental and theoretical works (*cf.* Introduction). For *cis*-dichloro ruthenium benzylidenes two isomerization pathways (concerted and oxygen dissociative) were described to preferentially occur.[84] It was assumed that a concerted isomerization mechanism in presence of a sixth ligand is less plausible to occur due to sterical hindrance. Herein we aim at studying the energetic isomerization based on an oxygen dissociative mechanism in presence of pyridine. As described before, the addition of (a small excess of) pyridine led to a preferential formation of a neutral 18e complex **cis2$_{py}$** (-13.1 kcal/mol) followed by the formation of the cationic bipyridyl complex **cis2$^{+}_{2py}$** as secondary product (-15.5 kcal/mol). Comparing the upper energy barriers for the oxygen dissociation, this barrier is decreased in presence of one pyridine molecule from 31.3 to 28.5 kcal/mol. For **cis2$_{py}$** simply pyridine-dissociation is necessary to reach the olefin metathesis active 14e species. A *re*-association consequently leads to the formation of **16e$_{trans+py}$** and finally to the active *trans*-dichloro (*pre*-)catalyst *(cf.* Figure 32). Alternatively, rearrangement of the pyridine from **16e$_{cis+py}$** to **16e$_{trans+py}$** requires comparable energy barriers (*cf.* Experimental Section). The activation path, when starting form the *trans*-(*pre*-)catalyst was already described by Grela et al revealing an energy gain of the time limiting energy barrier in the same range (~ 3 kcal/mol).[95a]

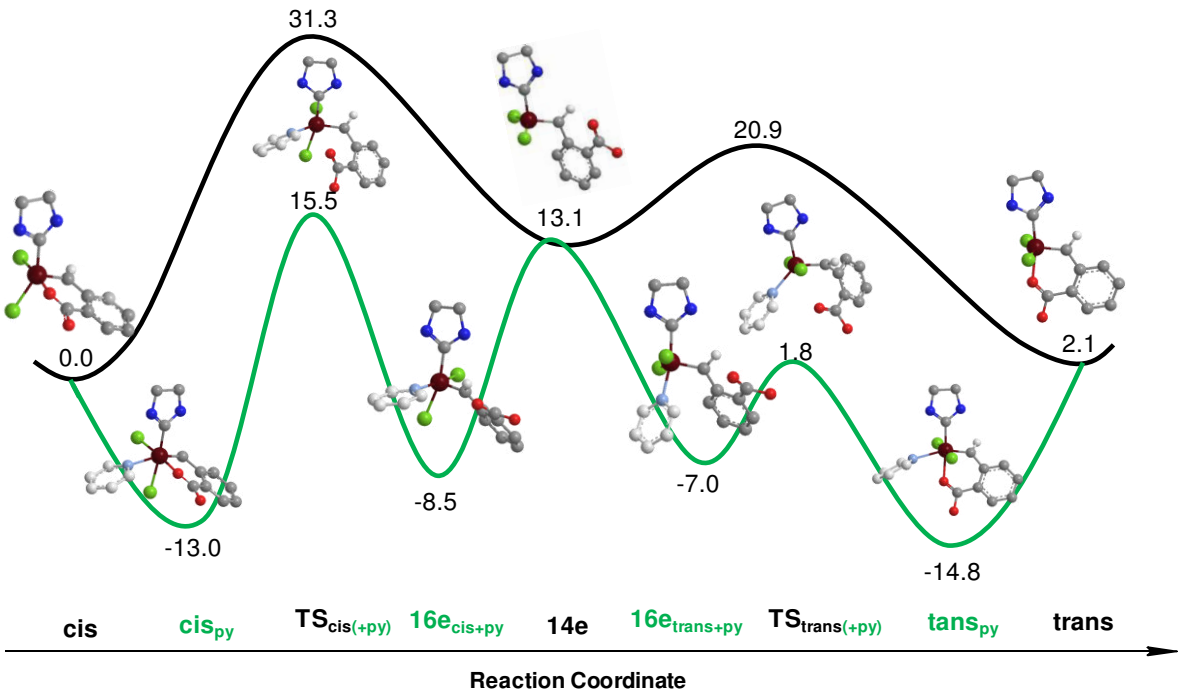

Figure 32. Proposed pathway for donor-accelerated *cis-trans* isomerization.

Accordingly, also aforementioned donor molecules were investigated on how they affect the rate limiting activation step for donor-activated isomerization. The barriers decrease from 28.5 kcal/mol for pyridine to 25.6 kcal/mol for H_2O, 23.3 kcal/mol for MeOH, 23.2 kcal/mol for DMSO and finally 15.9 kcal/mol for NO_3^-. Values of the *cis*-14e pathway are summarized in Table 14. The most pronounced acceleration was experimentally found for pyridine, although its pathway shows the highest energy barrier within this series. NMR measurements suggest a hampered **cis2$_D$** formation for all other donor molecules due to a decreased solubility (*cf.* above). Accordingly, this might be the reason for not observing a more pronounced accelerating effect in case of other donor molecules.

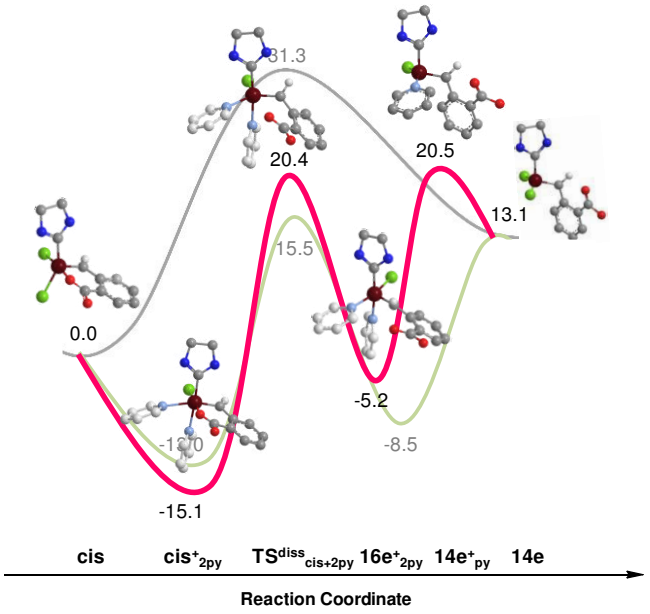

Figure 33. Proposed pathway for donor-decelerated activation of the (*pre*-)catalyst.

Table 14. Energies (kcal/mol) of **cis2** in presence of donor molecules 1-5 according to activation mechanism.

entry	donor	cis	cis$_D$	TS$^{diss}_{cis(+D)}$	16e$_{cis+D}$	14e
	-	0.0	-	31.3	-	13.1
1	**py**	0.0	-13.0	15.5	-8.5	13.1
2	**DMSO**	0.0	-2.6	20.6	-12.5	13.1
3	**H_2O**	0.0	-8.6	17.0	5.4	13.1
4	**MeOH**	0.0	-8.5	15.8	3.7	13.1
5	**NO_3^-**	0.0	-0.5	14.4	10.6	13.1

Contrary, the upper barrier for the oxygen dissociation in presence of two pyridine molecules (**cis2$^+_{2py}$**) is increased from 31.3 to 35.5 kcal/mol when comparing to **cis2**. Besides

this unfavorable transition energy, another factor plays an important role in making **cis1$^{+}_{2py}$** a worse (*pre*-)catalyst as compared to **cis2$_{py}$** and **cis2**: the formation of the active **14e** complex (13.4 kcal/mol) is less accessible, starting from this compound. Although the opening of the chelate leads to a stable, cationic **16e$^{+}_{2py}$** compound (-5.2 kcal/mol), one pyridine molecule needs to dissociate to first of all form a cationic **14e$^{+}_{py}$** species (20.4 kcal/mol), requiring another 25.6 kcal/mol. Subsequently the second pyridine needs to be exchanged by a chloride. Hence, back formation to **16e$^{+}_{2py}$** in presence of an excess of pyridine might be a concurring reaction to the entrance in the metathesis cycle. The respective energy profile can be found in Figure 33.

6. Conclusion

In summary, we disclosed the effect of the addition of donor molecules on the catalytic performance of *cis*-dichloro ruthenium benzylidenes. The activation mechanism of *cis*-dichloro configured olefin metathesis (*pre*-)initiators occurs through isomerization. The mechanism of this process in presence of pyridine was studied by experimental and theoretical means. It was assumed that isomerization in presence of a sixth ligand proceeds rather through an oxygen dissociative mechanism as through a concerted mechanism due to sterical hindrance. DFT calculations revealed that the rate limiting transition energy is the oxygen dissociative transition state starting from the *cis*-dichloro isomer. This barrier can be lowered when one donor molecule is coordinating on the vacant site of the complex to form a neutral 18e complex (see Scheme 14, **activation**). In the case that two donor molecules coordinate to the ruthenium center one chloride has to dissociate to form an inactive species (**cis2$^{+}_{2D}$**)**.** The energy profile for this comound is less favorable and prevents the formation of the active **14e** species (see Scheme 14, **deactivation**).

Scheme 14. Activation and deactivation of (*pre*-)catalyst in presence of donor molecules.

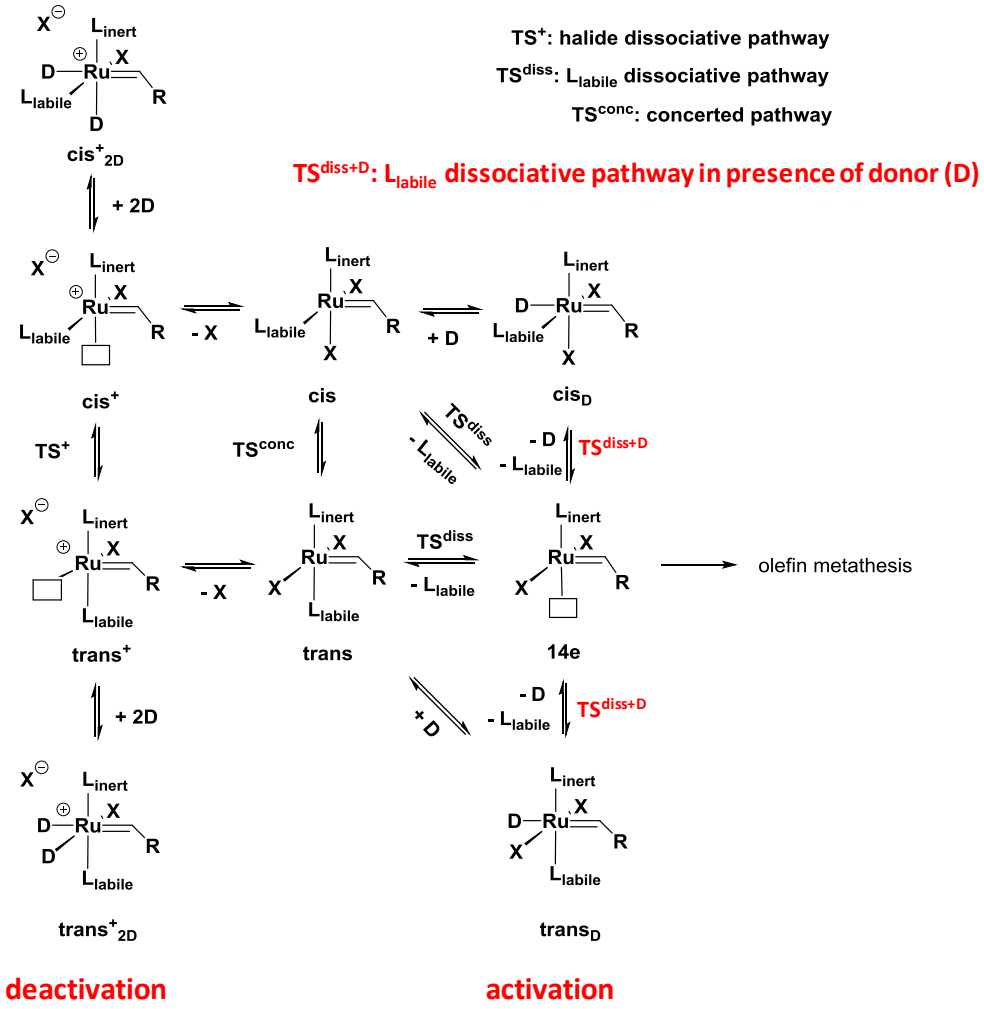

Experimental results were found to be in good agreement with the proposed pathways. A slight excess of pyridine (donor) generates high acceleration, whereas the addition of an increased excess hampers polymerization. The general validity of our results for all (*cis*- and *trans*-)dichloro ruthenium compounds is given, as the isomerization equilibrium can be shifted towards *cis*- or *trans*-compound in presence of impurities or even substrate. Moreover, activation or deactivation might be explained by our findings.

experimental section

Instruments and Materials

All chemicals were purchased from commercial sources (Fluka, Sigma Aldrich or Alfa Aesar) and were used as received. Precursor initiators were either ordered commercially (**M1**, **M2**, **M31**, **M32**) or prepared according to literature or patents.

For polymerization experiments toluene without styrene stabilizers from Sigma Aldrich (Chromasolv for HPLC, 99.9%) was used. DCPD (98%) was ordered from Sigma Aldrich and stored liquefied (30 $\mu L_{toluene}/mL_{DCPD}$) under N_2 atmosphere.

All preparation steps were performed under inert conditions (nitrogen) with dry, degassed solvents, unless otherwise noted. For thin layer chromatography, TLC sheets from Merck (silica gel 60 on aluminium) were used.

Polydispersity indices (PDI) and molecular weight data were determined by gel permeation chromatography, using THF as eluent. The setting consists of the following arrangement: Merck Hitachi L6000 pump (delivery volume: 1 mL/min), separation columns of Polymer Standards Service (5µm grade size), refractive index detector from Wyatt Technology. For calibration polystyrene standards from Polymer Standard Service were used. NMR spectra (^1H, ^{13}C) were recorded on Bruker Avanze 300 MHz spectrometer and Varion INOVA 500 MHz (^1H NMR kinetic measurements), which were referenced to $SiMe_4$ and deuterated $CDCl_3$ (^1H to 7.26 ppm, ^{13}C to 77.0 ppm). Deuterated solvents were obtained from Cambridge Isotope Laboratories Inc.

Ligands

1. Chapter I

1.1. Triflation of Alcohol

1.1.1. Preparation of 10-Trifluoromethane-Sulfonatebenzo(h)quinoline (L-Ia)

Scheme 15. Triflation of 10-hydroxybenzo(h)quinoline.

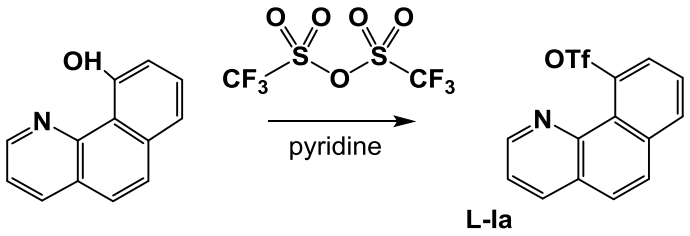

10-Hydroxybenzo(h)quinoline (1.25 g, 6.39 mmol, 1.0 eq) was dissolved in pyridine (10 mL). The yellowish reaction mixture was cooled to 0°C. Subsequently 1.19 mL triflic anhydride (1.98 g, 7.03 mmol, 1.1 eq) were added dropwise. The resulting red-orange solution was brought to room temperature and stirred for 24 h. Next, the solution was poured on H_2O (~100 mL) and subsequently extracted three times with diethyl ether (each 100 mL). The organic phase was neutralized by extracting three times with $HCl_{aq.}$ (5 w-%, each 100 mL). The organic phase was then dried with Na_2SO_4, filtered, the solvent was evaporated and the product was dried in vacuo. Yield: 1.59 g (76 %) yellowish solid.

Analytical data are in accordance with published values.[55]

TLC: R_f = 0.3 (Cy:EA, 5:1 (v:v)).

^{1}H-NMR (δ, 20°C, $CDCl_3$, 300 MHz): 9.10 (dd, 1H, *b*quin^2), 8.21 (d, 1H, *b*quin^4), 7.96 (d, 1H, *b*quin^7), 7.84 (d, 2H, *b*quin^5), 7.78 (d, 2H, *b*quin^6), 7.69 (m, 1H, *b*quin^8), 7.59 (d, 1H, *b*quin^{3,9}).

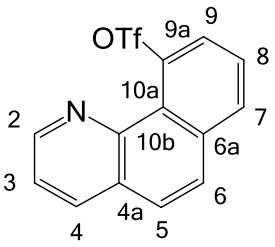

1.2. Vinylation by Suzuki Coupling

1.2.1. Preparation of 10-Vinylbenzo(h)quinoline (L-I)

Scheme 16. Suzuki-coupling of 10-triflatebenzo(h)quinoline.

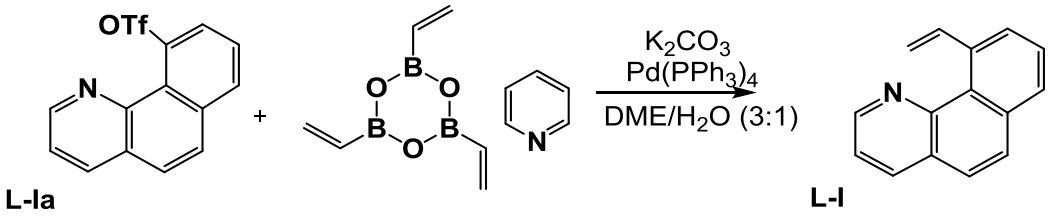

10-Triflatebenzo(h)quinoline (1.59 g, 4.85 mmol, 1.0 eq), K_2CO_3 (1.34 g, 9.70 mmol, 2.0 eq) and vinyl boronic acid anhydride pyridine complex (1.37 g, 5.82 mmol, 1.2 eq) were put in a Schlenk flask and subsequently three times evacuated and flushed with N_2. A degassed mixture of dimethoxy methane/water (3+1 (v+v), 30 mL) was added to the solids. The reaction mixture was heated to 90°C. Then the $Pd(PPh_3)_4$ (168 mg, 0.145, 0.03 eq) was added and the solution was stirred over night (17 h). The next day, the reddish reaction solution was cooled to room temperature and poured over a paper filter to a 500 mL separating funnel. Subsequently H_2O (50 mL) and Et_2O (50 mL) were added and the aqueous phase was extracted three times with Et_2O (each 75 mL). For neutralization, the ether phase was extracted three times with saturated $NaHCO_{3,\ aq.}$ (each 100 mL). Traces of water of the organic layer were removed by adding Na_2SO_4, which was subsequently filtered. The solvent was removed and the reddish, oily crude product (666 mg, 67% yield) was filtered through a frit filled with silica gel conditioned in CH_2Cl_2. The phosphine-free product was eluted with CH_2Cl_2. Yield: 597 mg (60 %) yellowish solid.

Analytical data are in accordance with published values.[55]

TLC: R_f = 0.6 (Cy:EA, 5:1 (v:v)).

^{1}H-NMR (δ, 20°C, $CDCl_3$, 300 MHz): 9.06 (s, 1H, *b*quin^2), 8.61 (dd, $^3J_{HH,trans}$ = 17.2 Hz, $^3J_{HH,cis}$ = 10.8 Hz, 1H, C*H*=CH_2), 8.16 (d, 1H, *b*quin^4), 7.88 (d, 1H, *b*quin^5), 7.81 (d, 2H, *b*quin^{6,7}), 7.67 (d, 2H, *b*quin^{8,9}), 7.49 (m, 1H, *b*quin^3), 5.62 (d, 1H, $^3J_{HH,\ trans}$ = 17.2 Hz, CH=C*H*$_2$), 5.41 (d, 1H, $^3J_{HH,\ cis}$ = 10.8 Hz, CH=C*H*$_2$).

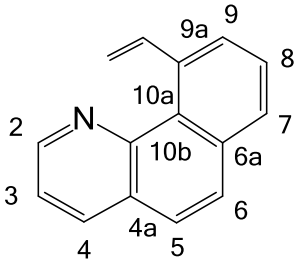

2. Chapter II-IV

2.1. 4-Functionalized Benzoic Acids

2.1.1. Preparation of 2-Bromo-4-Methoxy Benzoic Acid (L2-1)

Scheme 17. Friedel Crafts Acylation (**L2-1a**)

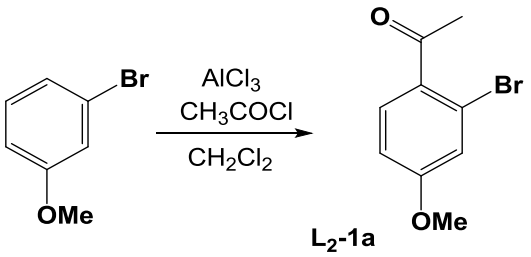

The synthesis of 2-bromo-4-methoxy acetophenone (**L2-1a**) was performed according to literature.[99] 1-Bromo-3-methoxybenzene (5.0 g, 0.026 mol, 1.0 eq) and aluminium chloride (4.38 g, 0.032 mol, 1.2 eq) were dissolved in CH_2Cl_2 (50mL) and cooled to 0°C, then acetyl chloride was added dropwise. The reaction was stirred for 2 h at room temperature. Afterwards the reaction solution was poured on a mixture of ice water (50 mL) and HCl_{conc} (10 mL) and extracted with CH_2Cl_2 (2 x 100 mL). The organic layer was separated, washed with water (100 mL) and aqueous $NaOH_{aq.}$ (10 w-%, 100 mL). Further, the organic layer was dried with Na_2SO_4, filtered and the solvent was evaporated. The oily residue was purified by column chromatography (pentane:Et_2O, 5:1 (v:v) by sampling the spot with R_f = 0.4). Yield: 3.64 g (59 %) clear oil.

Analytical data are in accordance with published values.[99]

TLC: R_f = 0.4 (pentane:Et_2O, 5:1 (v:v)).

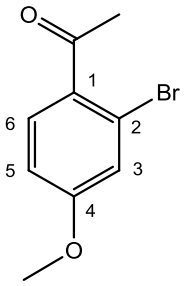

^{1}H-NMR (δ, 20°C, $CDCl_3$, 300 MHz): 7.59 (d, 1H, $^3J_{HH}$ = 8.7 Hz, ph^6), 7.15 (d, 1H, $^4J_{HH}$ = 2.5 Hz, ph^3), 6.88 (dd, 1H, $^3J_{HH}$ = 8.7 Hz, $^4J_{HH}$ = 2.5 Hz, ph^5), 3.84 (s, 3H, OCH_3), 2.62 (s, 3H, C=OCH_3).

(99) Takano, D.; Fukunaga, Y.;, Doe, M.; Yoshihara, K.; Kinoshita, T. *J. Heterocyclic Chem.* **1997**, *34*, 1111-1114.

2.1.2. Preparation of 2-Bromo-4-Methoxy Benzoic Acid (L2-1)

Scheme 18. Haloform reaction (**L2-1**)

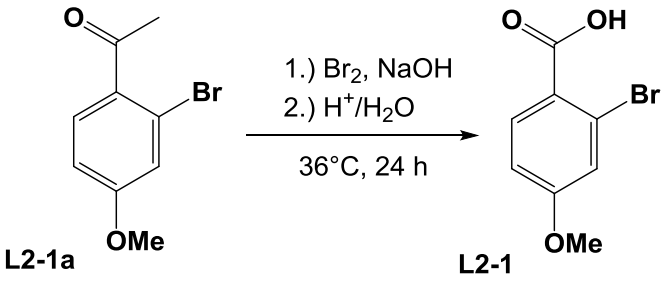

The synthesis of 2-bromo-4-methoxy benzoic acid (**L2-1**) was performed according to literature.[87b] 2-Bromo-4-methoxy-acetophenone (3.63 g, 15.8 mmol, 1.0 eq) was added dropwise to a sodium hypobromit solution (bromine (2.93 mL, 56.9 mmol, 3.6 eq) at 0°C in a $NaOH_{aq.}$-solution (20 w-%, 50 mL) and stirred at 36°C for 24 h. Na_2SO_3 (10 g in 40 mL) was added, then the reaction mixture was extracted with Et_2O. The aqueous phase was acidified with some drops of HCl_{conc}, the precipitate was filtered, washed with water and dried in vacuo. Yield: 2.60 g (71 %) white solid.

Analytical data are in accordance with published values.[87b]

TLC: R_f = 0.4 (Cy:EA, 3:1 (v:v)).

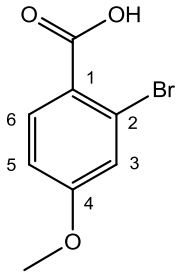

^{1}H-NMR (δ, 20°C, $CDCl_3$, 300 MHz): 8.04 (d, 1H, $^3J_{HH}$ = 8.8 Hz, ph^6), 7.23 (d, 1H, $^4J_{HH}$ = 2.5 Hz, ph^3), 6.90 (dd, 1H, $^3J_{HH}$ = 8.7 Hz, $^4J_{HH}$ = 2.5 Hz, ph^5), 3.87 (s, 3H, OCH_3).

2.1.3. Preparation of 2-Bromo-4-Nitro-Benzoic Acid (L4-1)

Scheme 19. Oxidation of toluene derivative (**L4-1**).

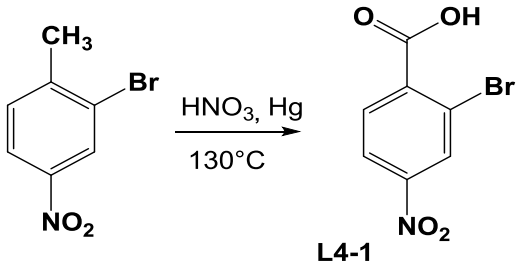

2-Bromo-4-nitro-benzoic acid (**L4-1**) was performed according to literature.[87c] In a reactor 2-bromo-4-nitrotoluene (8.0 g, 0.0370 mol, 1.0 eq) was reacted in HNO_3 (45 w-%, 100 mL) with two drops of elementary mercury. The mixture was heated in an autoclave for 24 h at 130°C. After the reaction cooled down to room temperature, the precipitate was filtered, washed with water (100 mL) and subsequently dissolved in $NaOH_{aq.}$ (10 w-%, 100 mL). $HCl_{aq.}$ (10 v-%) was added to the accruing red solution until colorless needles precipitated, which were again filtered and washed with water (100 mL). Yield: 5.64 g (62 %) colorless needles.

Analytical data in accordance with published values.[87c]

TLC: R_f = 0.4 (*n*-pentane:Et_2O, 5:1 (v:v)).

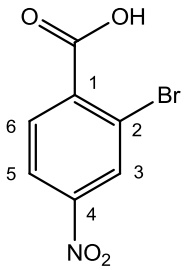

^{1}H-NMR (δ, 20°C, $CDCl_3$, 300 MHz): 8.57 (d, 1H, $^4J_{HH}$ = 2.1 Hz, ph^3), 8.26 (dd, 1H, $^3J_{HH}$ = 8.7 Hz $^4J_{HH}$ = 2.1 Hz, ph^5), 6.88 (d, 1H, $^3J_{HH}$ = 8.7 Hz, ph^5), 1.42 (s, 1H, COO*H*).

2.2. Esterification of Benzoic Acids

2.2.1. 4-Substituted Benzoic Acids

Scheme 20. Esterification of 4-substituted benzoic acids.

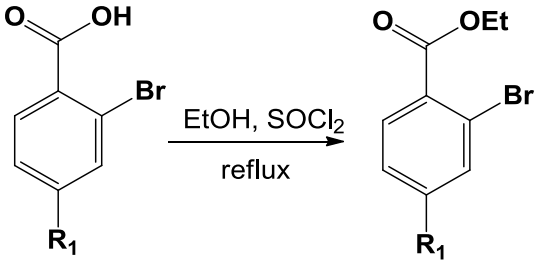

2-Bromo-4-methoxy benzoic acid (1.0 eq) was suspended in the desired alcohol and cooled to 0°C. Afterwards, thionyl chloride (3.6 eq) was added dropwise. The reaction mixture was stirred at reflux temperature until complete conversion was achieved (monitored by TLC). The excess of alcohol and thionyl chloride was distilled. The remaining liquid was dissolved in Et_2O (50 mL), water (50 mL), saturated $NaHCO_{3,aq.}$ (50 mL) and extracted with Et_2O (2 x 100 mL). The organic layer was dried over Na_2SO_4, filtered, evaporated and dried in vacuo.

2.2.1.1. Preparation of 2-Bromo-4-Methoxy Benzoic Acid Ethyl Ester (L2-2)

2-Bromo-4-methoxy benzoic acid ethyl ester was prepared analogously, using thionylchlorid (1.86 g, 15.7 mmol, 3.6 eq) and 2-bromo-4-methoxybenzoic acid (1.05 g, 4.35 mmol, 1.0 eq) in EtOH (8 mL). Yield: 1.04 g (92 %) yellowish oil.

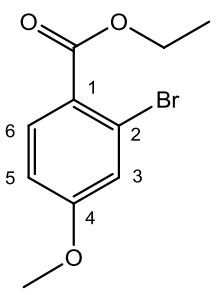

^{1}H-NMR (δ, 20°C, $CDCl_3$, 300 MHz): 7.85 (d, 1H, $^3J_{HH}$ = 8.8 Hz, ph^6), 7.18 (d, 1H, $^4J_{HH}$ = 2.5 Hz, ph^3), 6.86 (dd, 1H, $^3J_{HH}$ = 8.7 Hz, $^4J_{HH}$ = 2.5 Hz, ph^5), 4.36 (q, 2H, $^3J_{HH}$ = 7.1 Hz, C*H*$_2$CH$_3$), 3.83 (s, 3H, OC*H*$_3$), 1.38 (t, 3H, CH$_2$C*H*$_3$, $^3J_{HH}$ = 7.1 Hz, CH$_2$C*H*$_3$). **^{13}C-NMR** (δ, 20°C, $CDCl_3$, 75 MHz): 165.46 (1C, C_q, *C*OOEt), 162.16 (1C, ph^4), 133.10 (1C, ph^{3,5,6}), 123.55, 123.32 (2C, C_q, ph^{1,2}), 119.69, 112.99 (2C, ph^{3,5,6}), 61.20 (1C, *C*H$_2$CH$_3$) 55.37 (1C, OCH$_3$), 52.11 (1C, COO*C*H$_3$), 14.23 (1C, CH$_2$*C*H$_3$)

2.2.1.2. Preparation of 2-Bromo-4-Nitro Benzoic Acid Ethyl Ester (L4-2)

2-Bromo-4-nitro benzoic acid ethyl ester was prepared analogously, using thionyl chlorid (1.044 g, 8.78 mmol, 3.6 eq) and 2-bromo-4-methoxybenzoic acid (0.600 g, 2.44 mmol, 1.0 eq) in EtOH (5 mL). The mixture was heated to 75°C and subsequently purified analogously to the previous preparation. Yield: 0.628 g (94%) yellowish oil.

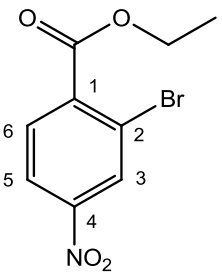

^{1}H-NMR (δ, 20°C, $CDCl_3$, 300 MHz): 8.50 (d, 1H, $^{4}J_{HH}$ = 2.3 Hz, ph^{3}), 8.20 (dd, 1H, $^{3}J_{HH}$ = 8.7 Hz, $^{4}J_{HH}$ = 2.2 Hz, ph^{5}), 7.90 (d, 1H, $^{3}J_{HH}$ = 8.4 Hz, ph^{5}), 4.42 (q, 2H, $^{3}J_{HH}$ = 7.2 Hz, CH_2CH_3), 1.43 (s, 3H, $^{3}J_{HH}$ = 7.2 Hz, CH_2CH_3). **^{13}C-NMR** (δ, 20°C, $CDCl_3$, 75 MHz): 164.8 (1C, C_q, *C*OOEt), 149.1 (1C, C_q, ph^{4}), 138.4 (2C, C_q, ph^{1}), 131.6 (1C, ph^{3}), 129.1 (1C, ph^{6}), 122.0 (2C, ph^{2,5}), 62.5 (1C, CH_2CH_3), 14.1 (1C, CH_2CH_3)

2.2.2. Un- and 5-Substituted Benzoic Acids

Scheme 21. Esterification of un- and 5-substituted benzoic chlorides.

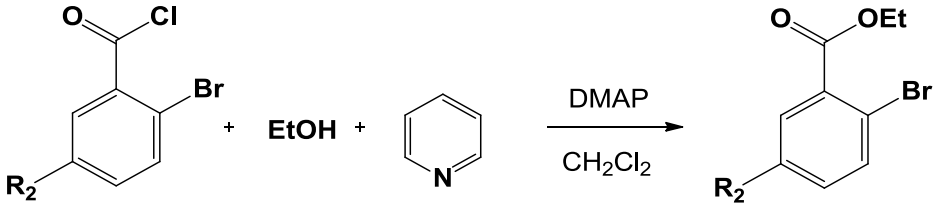

2-Bromo benzoic acid ethyl ester derivatives (**L1-3, L3-3** and **L5-3**) were prepared similar to literature[44b] starting from a 2-bromo benzoyl chloride derivative (1.0 eq), the respective alcohol (1.4 eq), pyridine (2.6 eq) and a catalytic amount of 4-DMAP (0.05 mol), which was added at 0°C. The reaction mixture was refluxed for up to 1 day. Subsequently, the reaction mixture was cooled down to rt, Et_2O (10 mL) was added and the organic layer was washed by extraction with $HCl_{aq.}$ (10 v-%, 3 x 100 mL) and aqueous, saturated $NaHCO_{3,\ aq.}$ (3 x 100 mL). The organic layer was dried with Na_2SO_4, filtered, concentrated and dried in vacuo.

2.2.2.1. Preparation of 2-Bromo Benzoic Acid Ethylester (L1-2)

2-Bromo-benzoic acid ethyl ester was prepared analogously to the abovementioned procedure. 2-Bromo benzoyl chloride (0.806 g, 3.64 mmol, 1.0 eq), pyridine (0.750 g, 9.48 mmol, 2.6 eq), EtOH (0.235 g, 5.10 mmol, 1.4 eq) and a catalytic amount of 4-DMAP (23.1 mg, 0.182 mmol, 0.05 eq) were mixed in cold CH_2Cl_2. Yield: 0.739 g (88%) yellowish oil.

Analytical data are in accordance with published values.[44b]

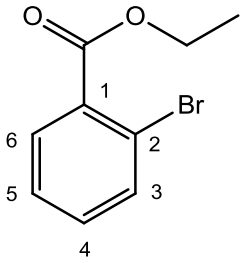

^{1}H-NMR (δ, 20°C, $CDCl_3$, 300 MHz): 7.77 (dd, 1H, $^3J_{HH}$ = 7.2 Hz, $^4J_{HH}$ = 2.4 Hz, ph^6), 7.66 (dd, 1H, $^3J_{HH}$ = 7.6 Hz, $^4J_{HH}$ = 1.6 Hz, ph^3), 7.34 (dq, 1H, $^3J_{HH}$ = 7.6 Hz, $^4J_{HH}$ = 2.1 Hz, ph^{4,5}), 4.41 (q, 2H, $^3J_{HH}$ = 7.2 Hz, CH_2CH_3), 1.41 (s, 3H, $^3J_{HH}$ = 7.2 Hz, CH_2CH_3).

2.2.2.2. Preparation of 5-Methoxy-2-Bromo Benzoic Acid Ethyl Ester (L3-2)

2-Bromo-5-methoxy-benzoic acid ethyl ester was prepared analogously to the abovementioned procedure. 2-Bromo-5-methoxy benzoic acid (1.003 g, 4.01 mmol, 1.0 eq), pyridine (0.824 g, 10.4 mmol, 2.6 eq), EtOH (0.239 g, 5.61 mmol, 1.4 eq) and a catalytical amount of 4-DMAP (24.5 mg, 0.200 mmol, 0.05 eq) were mixed in cold CH_2Cl_2. Yield: 0.875 g (84%) yellowish oil.

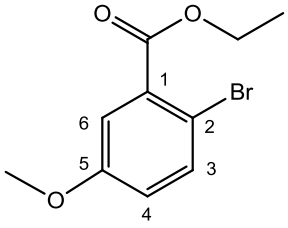

^{1}H-NMR (δ, 20°C, $CDCl_3$, 300 MHz): 7.52 (d, 1H, $^3J_{HH}$ = 8.8 Hz, ph^3), 7.29 (d, 1H, $^4J_{HH}$ = 3.1 Hz, ph^6), 6.88 (dd, 1H, $^3J_{HH}$ = 8.9 Hz, $^4J_{HH}$ = 3.2 Hz, ph^4), 4.40 (q, 2H, $^3J_{HH}$ = 7.1 Hz, CH_2CH_3), 3.82 (s, 3H, OCH_3), 1.41 (s, 3H, $^3J_{HH}$ = 7.1 Hz, CH_2CH_3). **^{13}C-NMR** (δ, 20°C, $CDCl_3$, 75 MHz): 166.1 (1C, C_q, *C*OOEt), 158.5 (1C, C_q, ph^5), 135.0 (1C, ph^3), 133.2 (2C, C_q, ph^1), 118.7 (1C, ph^4), 116.2 (1C, ph^6), 111.8 (1C, C_q, ph^2), 61.7 (1C, CH_2CH_3), 55.6 (1C, OCH_3), 14.2 (1C, CH_2CH_3).

2.2.2.3. Preparation of 5-Nitro-2-bromo Benzoic Acid Ethyl Ester (L5-2)

2-Bromo-5-nitro-benzoic acid ethyl ester was prepared analogously to the abovementioned procedure. 2-Bromo-5-nitro benzoyl chloride (2.505 g, 10.2 mmol, 1.0 eq), pyridine (2.089 g, 26.4 mmol, 2.6 eq), EtOH (0.655 g, 14.25 mmol, 1.4 eq) and a catalytic amount of 4-DMAP (62.1 mg, 0.508 mmol, 0.05 eq) were mixed in cold CH_2Cl_2. Yield: 2.349 g (84%) yellowish oil.

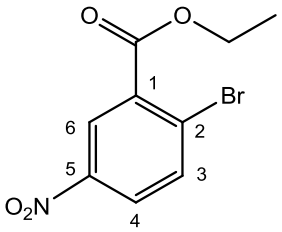

^{1}H-NMR (δ, 20°C, $CDCl_3$, 300 MHz): 8.63 (d, 1H, $^4J_{HH}$ = 2.7 Hz, ph^6), 8.16 (dd, 1H, $^3J_{HH}$ = 8.7 Hz, $^4J_{HH}$ = 2.7 Hz, ph^4), 7.86 (d, 1H, $^3J_{HH}$ = 8.7 Hz, ph^3), 4.46 (q, 2H, $^3J_{HH}$ = 7.1 Hz, C*H*$_2$CH$_3$), 3.82 (s, 3H, OCH_3), 1.45 (s, 3H, $^3J_{HH}$ = 7.1 Hz, CH_2CH_3). **^{13}C-NMR** (δ, 20°C, $CDCl_3$, 75 MHz): 164.2 (1C, C_q, *C*OOEt), 146.1 (1C, C_q, ph^5), 135.6 (1C, ph^4), 133.7 (1C, C_q, ph^1), 129.1 (1C, C_q, ph^2), 126.4 (1C, ph^3), 126.2 (1C, ph^6), 62.6 (1C, *C*H$_2$CH$_3$), 14.2 (1C, CH$_2$*C*H$_3$)

2.3. Vinylation by Suzuki Coupling

Scheme 22. Suzuki coupling of 2-bromo benzoic acid ester derivatives.

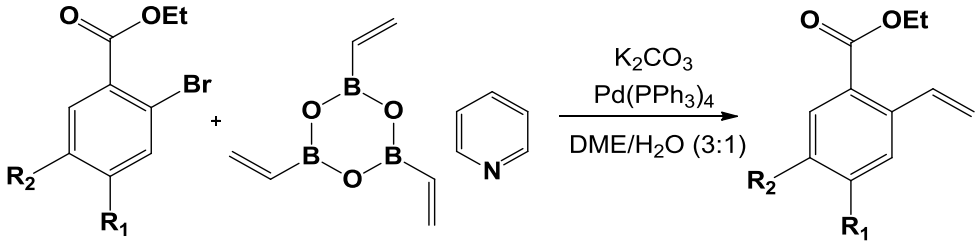

2-Vinyl benzoic acid ethyl ester derivatives were prepared as described in literature[44b] starting from 2-bromo benzoic acid ethyl ester derivatives (1.0 eq), vinylboronic anhydride pyridine complex (1.2 eq) and K_2CO_3 (2.0 eq) dissolved in degassed DME:H_2O, 3:1 (v:v). $Pd(PPh_3)_4$ (0.104 g , 0.090 mmol, 0.03 eq) was added, the reaction mixture was heated to 90°C and stirred for 1-2 d. The reaction mixture was quenched with water (10 mL). Subsequently, Et_2O (10 mL) was added and the organic layer was washed by extraction with

$HCl_{aq.}$ (10 v-%, 3 x 100 mL) and aqueous, saturated $NaHCO_{3,aq.}$ (3 x 100 mL). The organic layer was dried with Na_2SO_4, filtered, concentrated and dried in vacuo.

2.3.1. Preparation of 2-Vinyl Benzoic Acid Ethyl Ester (L1-3)

Ligand **L1-3** was prepared as it was described in the procedure above starting from 2-bromo benzoic acid ethyl ester (0.444 g, 1.93 mmol, 1.0 eq), vinylboronic anhydride pyridine complex (0.560 g, 2.32 mmol, 1.2 eq) and K_2CO_3 (0536 g, 3.88 mmol, 2.0 eq), dissolved in degassed DME:H_2O (3:1 (v:v), 15 mL). $Pd(PPh_3)_4$ (0.067 g, 0.0582 mmol, 0.03 eq) was added and the mixture reacted for 4 h at 90°C. The crude material was purified by column chromatography, using Cy:EA, 20:1 (v:v). Yield: 0.183 g (54 %) yellowish oil.

Analytical data are in accordance with published values.[44b]

^{1}H-NMR (δ, 25°C, $CDCl_3$, 300 MHz): 7.87 (d, 1H, $^3J_{HH}$ = 7.9 Hz , ph^6), 7.58 (d, 1H, $^3J_{HH}$ = 8.5 Hz, ph^3), 7.47 (t, 1H, $^3J_{HH}$ = 8.8, 6.7 Hz, ph^3), 7.32 (d, 1H, $^3J_{HH}$ = 17.6 Hz, $^3J_{HH}$ = 11.0 Hz, C*H*CH_2), 7.64 (z, 1H, $^3J_{HH}$ = 7.6 Hz, ph^5), 6.64 (d, 1H, $^3J_{HH}$ = 17.6 Hz, CHC*H*$_2$), 5.35 (d, 1H, $^3J_{HH}$ = 11.0 Hz, CHC*H*$_2$), 4.37 (q, 1H, $^3J_{HH}$ = 7.1 Hz, C*H*$_2$CH$_3$), 3.86 (s, 6H, OC*H*$_3$, COOC*H*$_3$), 1.39 (t, 3H, $^3J_{HH}$ = 7.1 Hz, CH$_2$C*H*$_3$).

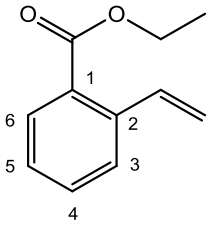

2.3.2. Preparation of 4-Methoxy-2-Vinyl Benzoic Acid Ethyl Ester (L2-3)

Ligand **L2-3** was prepared similar to the described procedure starting from 2-bromo-4-methoxy benzoic acid ethyl ester (1.04 g, 3.76 mmol, 1.0 eq), vinylboronic anhydride pyridine complex (1.09 g, 4.51 mmol, 1.2 eq) and K_2CO_3 (1.04 g, 7.52 mmol, 2.0 eq), dissolved in 45 mL of a degassed mixture of toluene:EtOH:H_2O, 1:1:1 (v:v:v). $Pd(PPh_3)_4$ (0.130 g, 0.113 mmol, 0.03 eq) was added and the mixture reacted for 2 d at 90°C. The crude material was purified by column chromatography, using Cy:EA, 6:1 (v:v). Yield: 0.623 g (80%) yellowish oil.

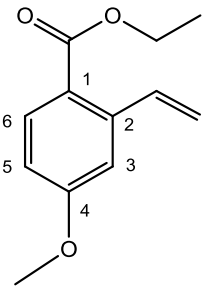

^{1}H-NMR (δ, 20°C, $CDCl_3$, 300 MHz): 7.91 (d, 1H, $^{3}J_{HH}$ = 8.8 Hz , ph^{6}), 7.55 (dd, 1H, $^{3}J_{HH}$ = 17.3, 11.0 Hz, C*H*CH_2), 7.03 (d, 1H, $^{4}J_{HH}$ = 2.6 Hz, ph^{3}), 6.82 (dd, 1H, $^{3}J_{HH}$ = 8.7 Hz, $^{4}J_{HH}$ = 2.6 Hz, ph^{5}), 5.61 (dd, 1H, $^{3}J_{HH}$ = 17.4 Hz, $^{4}J_{HH}$ = 1.1 Hz, CHC*H*$_2$), 5.34 (dd, 1H, $^{3}J_{HH}$ = 10.9 Hz, $^{4}J_{HH}$ = 1.2 Hz, CHC*H*$_2$), 4.33 (q, 2H, $^{3}J_{HH}$ = 7.2 Hz, C*H*$_2$CH$_3$), 3.86 (s, 6H, OC*H*$_3$, COO*C*H$_3$), 1.37 (t, 3H, $^{3}J_{HH}$ = 7.2 Hz, CH$_2$C*H*$_3$). **^{13}C-NMR** (δ, 20°C, $CDCl_3$, 75 MHz): 166.78 (1C, C$_q$, *C*OOEt), 162.34 (1C, C$_q$, ph^{4}), 142.23 (1C, C$_q$, ph^{2}), 136.40 (1C, *C*HCH$_2$), 132.59 (1C, ph^{6}), 121.11 (1C, C$_q$, ph^{1}), 116.17 (1C, *C*H$_2$CH), 112.72, 112.33 (2C, ph^{3,5}), 60.59 (1C, *C*H$_2$CH$_3$) 55.31 (1C, O*C*H$_3$), 14.29 (1C, CH$_2$*C*H$_3$).

2.3.3. Preparation of 5-Methoxy-2-Vinyl Benzoic Acid Ethyl Ester (L3-3)

Ligand **L3-3** was prepared as in the procedure above, starting from 2-bromo-5-methoxy benzoic acid ethyl ester (0.500 g, 1.93 mmol, 1.0 eq), vinylboronic anhydride pyridine complex (0.557 g, 2.32 mmol, 1.2 eq) and K_2CO_3 (0.533 g, 3.86 mmol, 2.0 eq), dissolved in degassed DME+H_2O (3+1, v+v, 15 mL). $Pd(PPh_3)_4$ (66.9 mg, 0.058 mmol, 0.03 eq) was added and the mixture reacted for 1 d at 90°C. The crude material was purified by column chromatography, using Cy:EA, 20:1 (v:v). Yield: 145 mg (37%) yellowish oil.

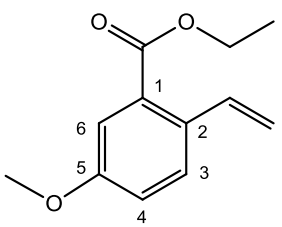

^{1}H-NMR (δ, 20°C, $CDCl_3$, 300 MHz): 7.52 (d, 1H, $^{3}J_{HH}$ = 8.5 Hz , ph^{6}), 7.37 (d, 1H, $^{4}J_{HH}$ = 2.7 Hz,ph^{6}), 7.37 (dd, 1H, $^{3}J_{HH}$ = 17.3, 11.1 Hz, C*H*CH_2), 7.03 (dd, 1H, $^{3}J_{HH}$ = 8.7 Hz, $^{4}J_{HH}$ = 2.7 Hz, ph^{4}), 5.55 (dd, 1H, $^{3}J_{HH}$ = 17.3 Hz, $^{4}J_{HH}$ = 1.2 Hz, CHC*H*$_2$), 5.24 (dd, 1H, $^{3}J_{HH}$ = 11.0 Hz, $^{4}J_{HH}$ = 1.1 Hz, CHC*H*$_2$), 4.37 (q, 2H, $^{3}J_{HH}$ = 7.2 Hz, C*H*$_2$CH$_3$), 3.84 (s, 3H, OC*H*$_3$, COO*C*H$_3$), 1.39 (t, 3H, $^{3}J_{HH}$ = 7.1 Hz, CH$_2$C*H*$_3$). **^{13}C-NMR** (δ, 20°C, $CDCl_3$, 75 MHz): 167.3 (1C, C$_q$, *C*OOEt), 158.7 (1C, C$_q$, ph^{5}), 135.2 (1C, *C*HCH$_2$), 132.0 (1C, C$_q$, ph^{2}), 130.0 (1C, C$_q$, ph^{1}), 128.3 (1C, ph^{3}), 118.2 (1C, ph^{4}), 114.6 (1C, ph^{6}), 114.6 (1C, CH*C*H$_2$), 61.3 (1C, *C*H$_2$CH$_3$) 55.5 (1C, O*C*H$_3$), 14.3 (1C, CH$_2$*C*H$_3$).

2.3.4. Preparation of 4-Nitro-2-Vinyl Benzoic Acid Ethyl Ester (L4-3)

Ligand **L4** was prepared as it was described in the procedure above, starting from 2-bromo-4-nitro benzoic acid ethyl ester (0.628 g, 2.29 mmol, 1.0 eq), vinylboronic anhydride pyridine complex (0.662 g, 2.75 mmol, 1.2 eq) and K_2CO_3 (0.633 g, 4.58 mmol, 2.0 eq), dissolved in degassed DME+H_2O (3+1, v+v, 20 mL). $Pd(PPh_3)_4$ (79.0 g, 0.0687 mmol, 0.03 eq) was added and the mixture reacted for 18 h at 90°C. The crude material was purified by column chromatography, using Cy:EA, 5:1 (v:v). Yield: 0.350 g (69%) yellowish oil.

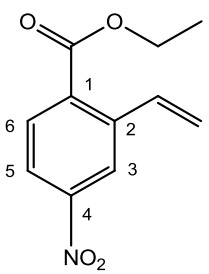

^{1}H-NMR (δ, 20°C, $CDCl_3$, 300 MHz): 8.42 (d, 1H, $^4J_{HH}$ = 2.2 Hz, ph^3), 8.13 (dd, 1H, $^3J_{HH}$ = 8.6 Hz, $^4J_{HH}$ = 2.2 Hz, ph^5), 7.03 (d, 1H, $^3J_{HH}$ = 2.6 Hz, ph^6), 7.43 (dd, 1H, $^3J_{HH}$ = 17.4, 11.0 Hz, C*H*CH_2), 5.83 (d, 1H, $^3J_{HH}$ = 17.3 Hz, CHC*H*$_2$), 5.53 (d, 1H, $^3J_{HH}$ = 11.2 Hz, CHC*H*$_2$), 4.42 (q, 2H, $^3J_{HH}$ = 7.2 Hz, C*H*$_2$$CH_3$), 1.42 (t, 3H, $^3J_{HH}$ = 7.0 Hz, CH_2C*H*$_3$). **^{13}C-NMR** (δ, 20°C, $CDCl_3$, 75 MHz): 165.7 (1C, C_q, *C*OOEt), 149.5 (1C, C_q, ph^4), 145.7 (1C, C_q, ph^2), 134.7 (1C, C_q, ph^1), 133.8 (1C, *C*HCH_2), 131.4 (1C, ph^6), 121.9 (1C, C, ph^{3,5}), 121.7 (1C, ph^{3,5}), 119.2 (1C, *C*H_2CH), 62.0 (1C, *C*H_2CH_3) 14.2 (1C, CH_2*C*H_3).

2.3.5. Preparation of 5-Nitro-2-Vinyl Benzoic Acid Ethyl Ester (L5-3)

Ligand **L5** was prepared as described in the procedure above, starting from 2-bromo-5-nitro benzoic acid ethyl ester (0.995 g, 3.63 mmol, 1.0 eq), vinylboronic anhydride pyridine complex (1.061 g, 4.41 mmol, 1.2 eq) and K_2CO_3 (1.007 g, 7.30 mmol, 2.0 eq), dissolved in degassed DME+H_2O (3+1, v+v, 20 mL). $Pd(PPh_3)_4$ (0.126 g, 0.109 mmol, 0.03 eq) was added and the mixture reacted for 1 d at 90°C. The crude material was purified by column chromatography, using Cy:EA, 20:1 (v:v). Yield: 0.448 g (46%) yellowish oil.

TLC: R_f = 0.65 (Cy:EA, 3:1 (v:v)).

^{1}H-NMR (δ, 20°C, $CDCl_3$, 300 MHz): 8.74 (d, 1H, $^4J_{HH}$ = 2.6 Hz, ph^6), 8.31 (dd, 1H, $^3J_{HH}$ = 8.8 Hz, $^4J_{HH}$ = 2.5 Hz, ph^4), 7.75 (d, 1H, $^3J_{HH}$ = 8.7 Hz, ph^3), 7.54 (q, 1H, $^3J_{HH}$ = 17.2, 11.2 Hz, C*H*CH_2),

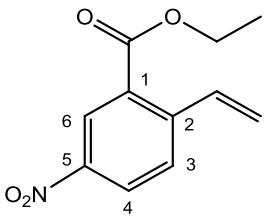

5.82 (d, 1H, $^{3}J_{HH}$ = 17.6 Hz, CHCH_2), 5.34 (dd, 1H, $^{3}J_{HH}$ = 11.2 Hz, CHCH_2), 4.43 (q, 2H, $^{3}J_{HH}$ = 7.2 Hz, CH_2CH$_3$), 1.34 (t, 3H, $^{3}J_{HH}$ = 7.1 Hz, CH$_2$CH_3). **^{13}C-NMR** (δ, 20°C, $CDCl_3$, 75 MHz): 165.3 (1C, C_q, *C*OOEt), 146.7 (1C, C_q, ph^5), 145.6 (1C, C_q, ph^2), 134.2 (1C, *C*HCH$_2$), 129.8 (1C, C_q, ph^1), 128.3 (1C, ph^4), 126.3 (1C, ph^3), 125.7 (1C, ph^6), 120.3 (1C, CH*C*H$_2$), 61.9 (1C, *C*H$_2$CH$_3$) 14.2 (1C, CH$_2$*C*H$_3$).

[Ru] Complexes

1. Chapter I

Scheme 23. General procedure of NHC functionalized [Ru] complexes.

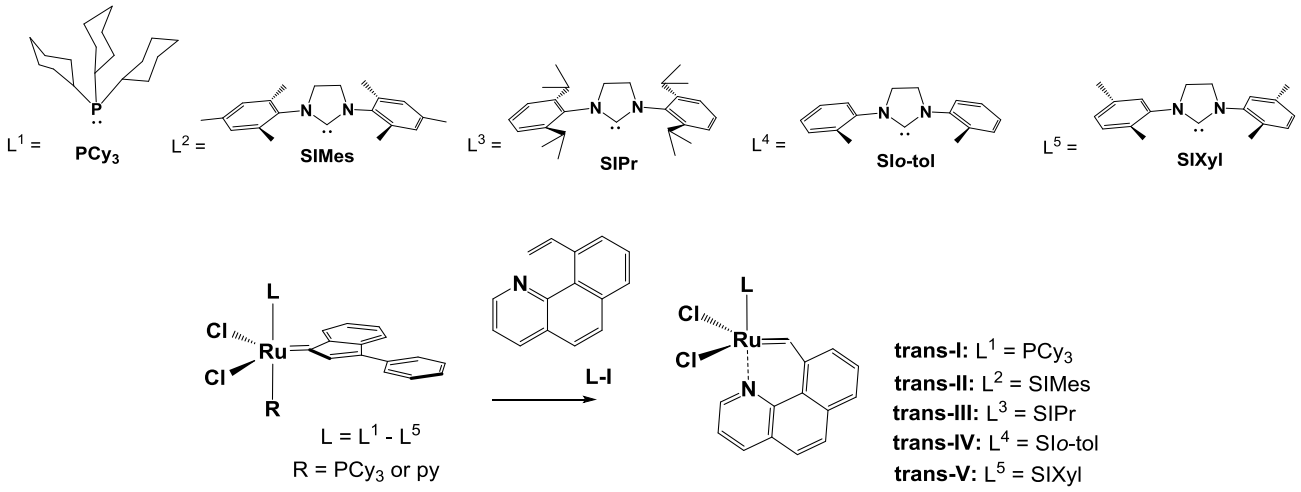

1.2 eq of the carbene precursor 10-vinylbenzo(h)quinoline (**L-I**) was reacted with the respective L^1-L^5-functionalized tricyclohexylphosphine (**trans-I**, **trans-IV**, **trans-V**) resp. pyridine (**II** and **trans-III**) indenylidene ruthenium complex, as shown in Scheme 23.

1.1. Preparation of *trans*-Dichloro-(κ²(C,N)-2-(Benzo(h)Quinolin-10-yl)-Methylidene)(PCy_3)Ru (trans-I)

In a Schlenk flask 280.0 mg of **M1** (0.30 mmol, 1.0 eq), 74.7 mg of ligand **L-I** (0.36 mmol, 1.2 eq) and 30.3 mg of Cu(I)Cl (0.30 mmol, 1.0 eq) were dissolved in dry toluene (14 mL). The reaction mixture was stirred and heated to 80°C. After 2 h a green precipitate was visible which albeit disappeared until the next day (17 h). TLC confirmed full conversion although the reaction mixture was not completely green. The solvent was removed and the precipitate *re*-dissolved in acetone, for removing insoluble [$CuCl{\cdot}PCy_3$] complex. The solvent was removed again and the residue was chromatographically separated on silica gel with

DCM:methanol, 10:1 (v:v) as an eluent. A dark green precipitate appeared, when resolving the residue in DCM and adding *n*-pentane. Yield: 79.5 mg (41%) dark green crystals.

Anal. Calcd. for $C_{32}H_{42}Cl_2NPRu$ (643.63): C, 59.71; H, 6.58; N, 2.18. **Found**: C, 59.57; H, 6.51; N, 2.13. **^{1}H-NMR** (δ, 20°C, $CDCl_3$, 300 MHz): 19.53 (d, Ru=CH), 9.60 (m, 1H, $^3J_{HH}$ = 5.0 Hz, H_{bquin}^{2}), 8.32 (d, 1H, $^3J_{HH}$ = 7.6 Hz, H_{bquin}^{7}), 8.30 (d, 1H, $^3J_{HH}$ = 7.6 Hz, H_{bquin}^{4}), 8.18 (d, 1H, $^3J_{HH}$ = 7.7 Hz, H_{bquin}^{9}), 8.05 (d, 1H, $^3J_{HH}$ = 8.8 Hz, H_{bquin}^{5}), 7.91 (t, 1H, $^3J_{HH}$ = 7.8 Hz, H_{bquin}^{8}), 7.84 (dd, 1H, $^3J_{HH}$ = 5.0 Hz, 7.6 Hz, H_{bquin}^{3}), 7.84(d, 1H, $^3J_{HH}$ = 8.9 Hz, H_{bquin}^{6}), 2.48 (q, 3H, $^3J_{HH}$ = 11.3 Hz, H_{Cy3}^{1}), 2.23 (d, 6H, $^3J_{HH}$ = 11.5 Hz, H_{Cy3}), 2.04-1.82 (m, 12H H_{Cy3}), 1.74 (s, 3H, H_{Cy3}), 1.34 (s, 9H, H_{Cy3}). **^{13}C-NMR** (δ, 22°C, $CDCl_3$, 75 MHz): 295.7 (s, 1C, Ru=CH), 149.0 (1C, C_{bquin}^{2}), 145.1 (1C_q, C_{bquin}^{10b}), 141.7 (1C_q, C_{bquin}^{4a}), 137.8 (1C, C_{bquin}^{7}), 136.5 (1C_q, C_{bquin}^{6a}), 130.3 (1C, C_{bquin}^{8}), 129.9 (1C, C_{bquin}^{4}), 129.5 (1C_q, C_{bquin}^{10a}), 128.7 (1C, C_{bquin}^{9}), 127.4 (1C, C_{bquin}^{5}), 126.1 (1C, C_{bquin}^{6}), 122.7 (1C_q, C_{bquin}^{10}), 121.8 (1C, C_{bquin}^{3}), 53.4 (2C, C_{2HIm}), 34.5, 30.3, 28.0, 26.4 (18C, C_{Cy3}).

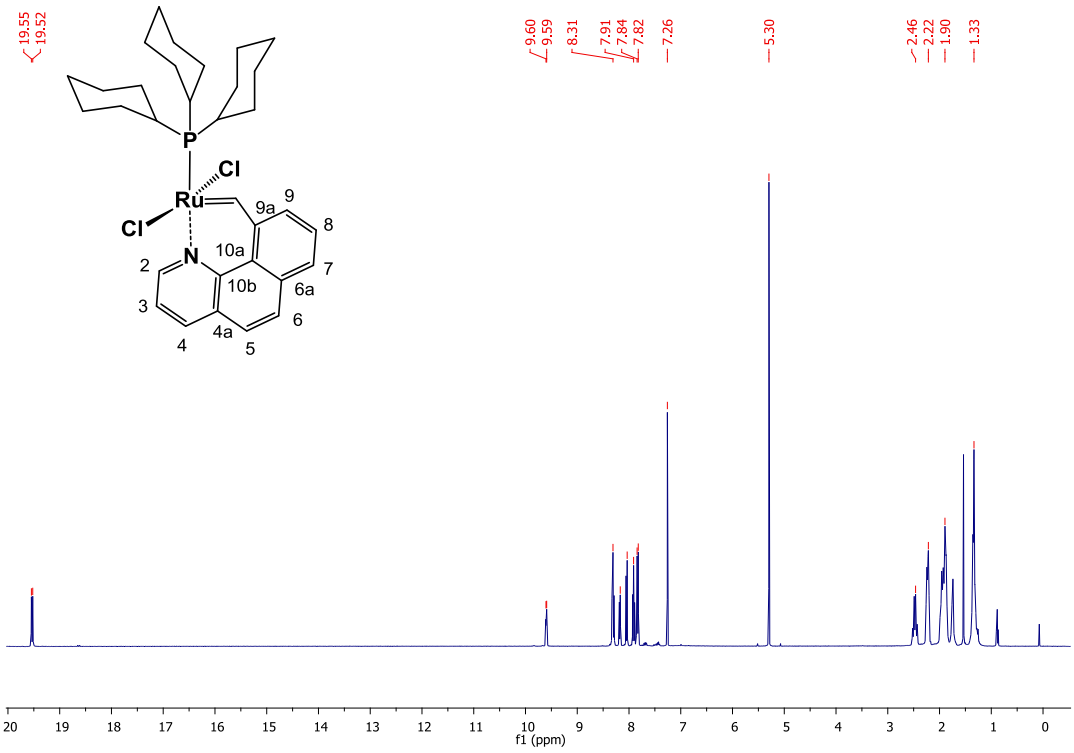

Figure 34. ^{1}H-NMR spectrum of complex **trans-I** (300 MHz, 25°C, $CDCl_3$).

1.2. Preparation of Dichloro-(κ²(C,N)-(2-(Benzo(h)Quinolin-10-yl)-Methylidene)(SIMes))Ru (II)

A Schlenk flask equipped with a stirring bar was charged with **M31** (1.81 g, 2.42 mmol, 1.0 eq) and ligand **L-I** (597 mg, 2.91 mmol, 1.2 eq). The tube was flushed with argon and anhydrous CH_2Cl_2 (30 mL) was added. The purple reaction mixture was stirred at 25°C for 48 h, whereupon the colour changed to dark green. The volume of the solvent was reduced to about 5 mL, and upon addition of Et_2O (50 mL) a green precipitate formed which was filtered off. The residue was washed with Et_2O (3x10 mL) and dried in vacuo. Yield: 1.43 mg (88%) of green solid. Subsequently, column chromatography on silica gel (CH_2Cl_2:MeOH, 10:1 (v:v)) was accomplished, leading to 2 fractions.

Yield of first fraction: 1.05 g (65%) of green solid (**trans-II**).
Analytical data are in accordance to literature.[55]
TLC: R_f = 0.9 (CH_2Cl_2:MeOH, 10:1 (v:v))

^{1}H NMR (δ, 20 C, 500 MHz, $CDCl_3$): 19.19 (s, 1H, Ru=CH), 8.25 (d, 1H, $^3J_{HH}$ = 5.0 Hz, H_{bquin}^2), 8.17 (d, 1H, $^3J_{HH}$ = 7.5 Hz, H_{bquin}^7), 8.07 (d, 1H, $^3J_{HH}$ = 8.0 Hz, H_{bquin}^4), 7.90 (d, 1H, H_{bquin}^5), 7.64 (m, 2H, $H_{bquin}^{6,8}$), 7.44 (dd, 1H, $^3J_{HH}$ = 8.0 Hz, $^3J_{HH}$ = 5.0 Hz, H_{bquin}^3), 7.17 (s, 4H, $H_{mes}^{3,5}$), 7.10 (d, 1H, $^3J_{HH}$ =7.5 Hz, H_{bquin}^9), 4.20 (s, 4H, H_{H2Im}), 2.55 (bs, 12H, $H_{mes\text{-}CH3}$), 2.50 (s, 6H, $H_{mes\text{-}CH3}$).

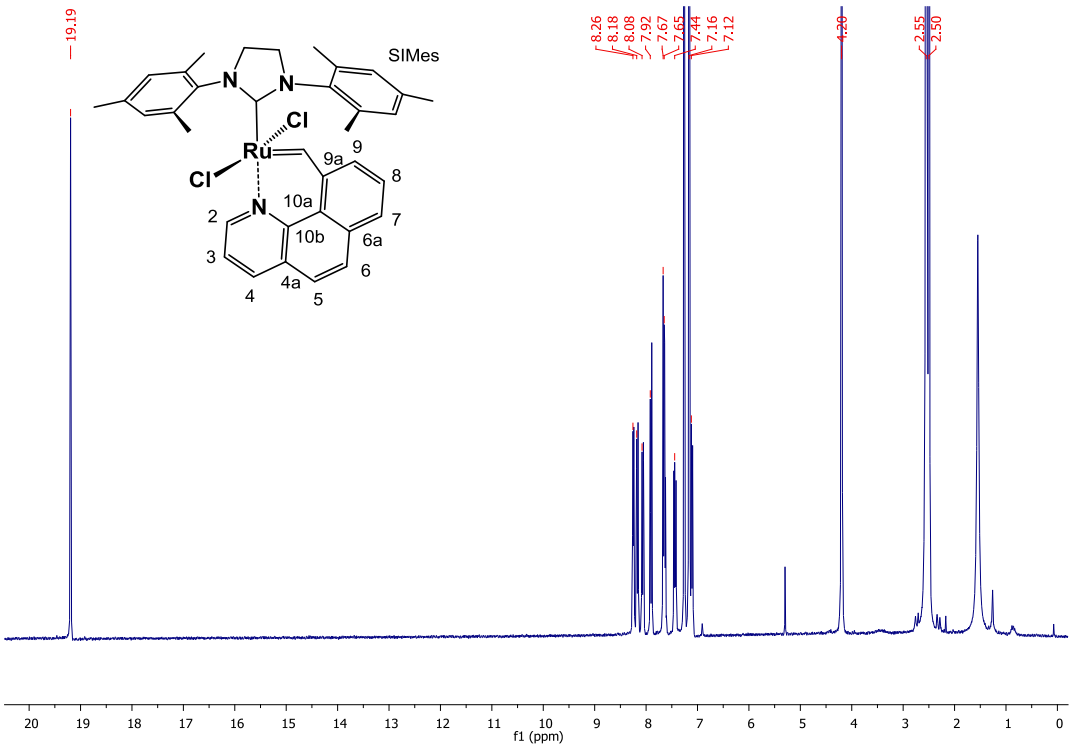

Figure 35. ^{1}H-NMR spectrum of complex **trans-II** (300 MHz, 25°C, $CDCl_3$).

Yield of second fraction: 35 mg (2%) of dark green solid (**cis-II**).

TLC: R_f = 0.6 (CH_2Cl_2:MeOH, 10:1 (v:v))

^{1}H NMR (25°C, 300 MHz, $CDCl_3$): 19.19 (s, 1H, Ru=CH), 8.42 (d, 1H, $^{3}J_{HH}$ = 5.0 Hz, H_{bquin}^{2}), 8.18 (d, 1H, $^{3}J_{HH}$ = 7.9 Hz, H_{bquin}^{5}), 8.10 (d, 1H, $^{3}J_{HH}$ = 7.9 Hz, H_{bquin}^{4}), 7.94 (d, 1H, $^{3}J_{HH}$ = 8.7 Hz, H_{bquin}^{7}), 7.69 (d, 1H, $^{3}J_{HH}$ = 9.5 Hz, H_{bquin}^{9}), 7.68 (t, 1H, $^{3}J_{HH}$ = 7.9 Hz, H_{bquin}^{6}), 7.38 (d, 1H, $^{3}J_{HH}$ = 8.7 Hz, H_{bquin}^{8}), 7.29 (t, 1H, $^{3}J_{HH}$ = 7.5 Hz, H_{bquin}^{3}), 7.34, 7.17, 7.06, 7.01 (s, 4H, H_{mes}), 3.73 (m, 4H, H_{H2Im}), 3.06, 2.72, 2.53, 2.18, 1.38, 0.37 (bs, 18H, $H_{mes\text{-}CH3}$).

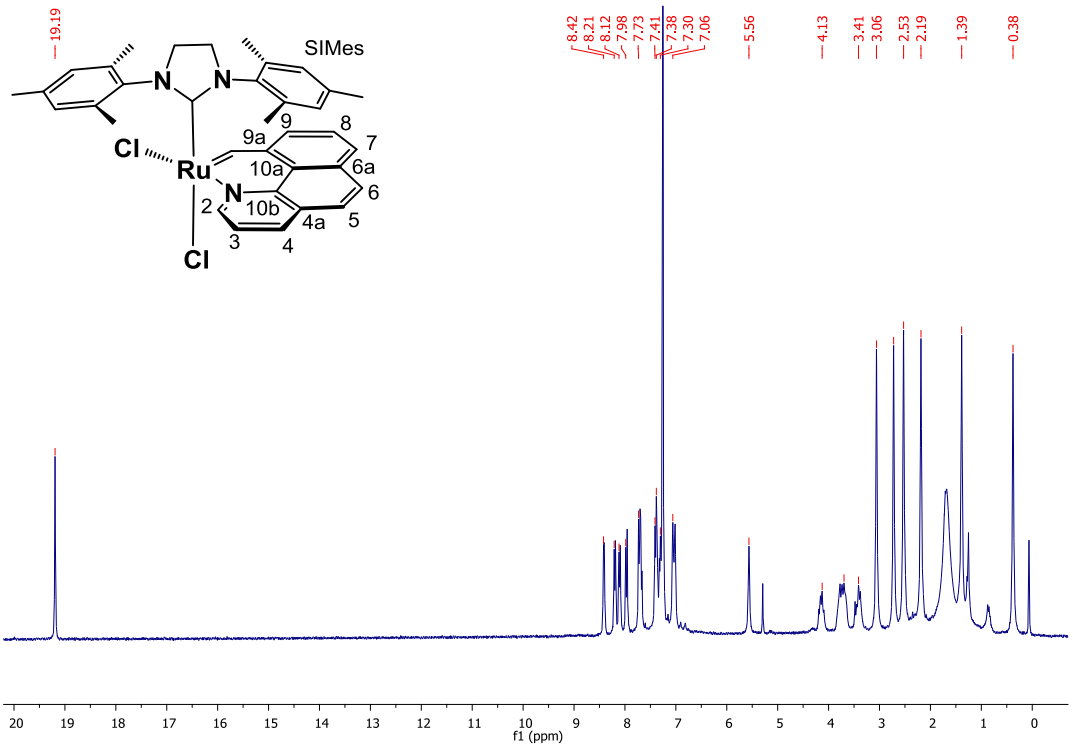

Figure 36. ^{1}H-NMR spectrum of complex **cis-II** (300 MHz, 25°C, $CDCl_3$).

1.2.1. Alternative Protocol for the Preparation of cis-II

15 mg of **trans-II** were dissolved in 1 mL degassed $CHCl_3$. and exposed for 8 h at 140°C in microwave. The mother liquor and the precipitate were dried and *re*-dissolved in CD_2Cl_2, revealing a quantitative formation of **cis-II**, as detected by ^{1}H NMR spectroscopy.

Anal. Calcd for $C_{35}H_{35}N_3Cl_2Ru$ (669.65), C, 62.78; N, 6.27; H, 5.27. **Found**: C, 62.96; N, 6.15; H, 5.41. **^{1}H NMR** (25°C, 300 MHz, CD_2Cl_2): 19.10 (s, 1H, Ru=CH), 8.34 (ds, 1H, $^{3}J_{HH}$ = 5.4 Hz, $^{4}J_{HH}$ = 1.1 Hz, H_{bquin}^{2}), 8.29 (d, 1H, $^{3}J_{HH}$ = 7.8 Hz, H_{bquin}^{7}), 8.19 (d, 1H, $^{3}J_{HH}$ = 7.5 Hz, H_{bquin}^{4}), 8.05 (d, 1H, $^{3}J_{HH}$ = 8.6 Hz, H_{bquin}^{5}), 7.79 (d, 1H, $^{3}J_{HH}$ = 8.6, H_{bquin}^{6}), 7.77 (t, 1H, $^{3}J_{HH}$ = 7.5 Hz, H_{bquin}^{8}), 7.43 (d, 1H, $^{3}J_{HH}$ = 7.3 Hz, H_{bquin}^{9}), 7.37 (dd, 1H, $^{3}J_{HH}$ = 7.9 Hz, H_{bquin}^{3}), 7.39, 7.12, 7.03, 5.59 (s, 4H, H_{mes}), 4.12 (m, 1H, H_{H2Im}), 3.73 (m, 2H, H_{H2Im}), 3.39 (m, 1H, H_{H2Im}), 3.00, 2.69, 2.57, 2.19, 1.39, 0.37 (bs, 18H, $H_{mes\text{-}CH3}$). **^{13}C NMR** (δ, 20°C, 75 MHz, CD_2Cl_2): 291.2 (1C, Ru=CH), 216.7 ($1C_q$,CNN), 154.8 (1C; C_{bquin}^{2}), 146.5 ($1C_q$, C_{bquin}^{10b}), 141.0, 140.9, 139.4, 138.8, 138.7, 136.5, 136.1, 135.8, 135.6, 134.3 ($10C_q$, $C_{mes,}$ $C_{bquin}^{4a,6a}$), 137.5 (1C, C_{bquin}^{4}), 131.7 (1C, C_{mes}), 130.9

(1C, C_{bquin}^{7}), 130.4 (1C, C_{mes}), 130.2 (1C, C_{bquin}^{8}), 130.1 (1C, C_{mes}), 130.0 (1C_q, C_{bquin}^{10a}), 129.3 (1C, C_{mes}), 129.1 (1C, C_{bquin}^{5}), 128.8 (1C, C_{bquin}^{9}), 127.8 (1C, C_{bquin}^{6}), 124.2 (1C_q, C_{bquin}^{10}), 122.2 (1C, C_{bquin}^{3}), 51.8, 51.6 (s, 2C, C_{H2Im}), 21.7, 21.3, 20.6, 19.4, 18.8, 17.2 (6C, $C_{mes\text{-}CH3}$).

1.3. Preparation of *trans*-Dichloro-(κ²(C,N)-(2-(Benzo(h)-Quinolin-10-yl)Methylidene))(SIPr)Ru (trans-III)

SIPr-py complex **M32** (150 mg, 0.18 mmol, 1.0 eq) was dissolved in 9 mL of dry, freshly degassed dichloromethane. Subsequently, the ligand **L-I** (55 mg, 0.26 mmol, 1.5 eq) was added. The mixture was stirred for 48 h at room temperature whilst the color turned from red to bright green. The solvent was evaporated and the crude product was subjected to column chromatography on silica gel (CH:EA, 3:1 (v:v)). Yield: 110 mg (81%) light green powder.

TLC: R_f = 0.43 (CH:EA, 3:1 (v:v)).

Anal. Calcd. for $C_{41}H_{47}Cl_2N_3Ru$ (753.81): C, 65.33; H, 6.28; N, 5.57. **Found:** C, 65.21; H, 6.20; N, 5.51. **^{1}H NMR** (δ, 20°C, $CDCl_3$, 300 MHz): 19.06 (s, 1H, Ru=C*H*); 8.61 (d, 1H, $^3J_{HH}$ = 5.2 Hz, H_{bquin}^{2}), 8.13 (d, 1H, $^3J_{HH}$ = 8.1 Hz, H_{bquin}^{7}), 8.07 (d, 1H, $^3J_{HH}$ = 8.1 Hz, H_{bquin}^{4}), 7.89 (d, 1H, $^3J_{HH}$ = 8.8 Hz, H_{bquin}^{5}), 7.67-7.59 (m, 4H, $H_{bquin}^{6,8}$, H_{SIPr}), 7.52-7.44 (dd, 1H, $^3J_{HH}$ = 8.1 Hz, $^3J_{HH}$ = 5.2 Hz, H_{bquin}^{3}, m, 4H, H_{SIPr}), 6.96 (d, 1H, $^3J_{HH}$ = 6.9 Hz, H_{bquin}^{9}), 4.20 (s, 4H, H_{H2Im}), 3.77 (4H, $H_{iPr\text{-}CH}$), 1.35-1.16 (d, 24H, $H_{iPr\text{-}CH3}$). **^{13}C NMR** (δ, 20°C, $CDCl_3$, 125 MHz): 306.2 (1C, Ru=*C*H), 217.7 (1C, *C*NN), 149.4 (1C; C_{bquin}^{2}), 148.6, 145.9, 141.7, 137.2, 136.1, 129.9, 129.8, 129.5, 129.3, 128.6, 127.0, 125.4, 124.7, 122.8, 121.3 (25C, $C_{bquin}^{2\text{-}10}$, $C_{SIPr}^{1\text{-}6}$), 54.8 (2C, C_{H2Im}), 27.1 (4C, $C_{iPr\text{-}CH}$), 23.9 (8C, $C_{iPr\text{-}CH3}$).

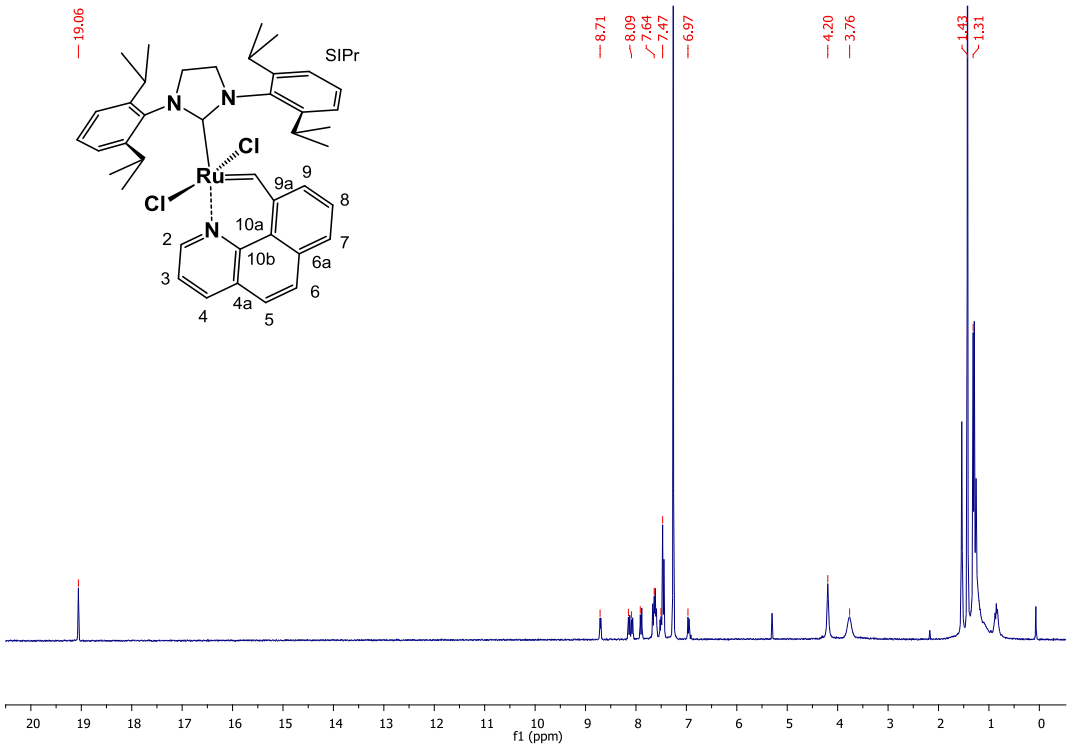

Figure 37. ^{1}H-NMR spectrum of complex **trans-III** (300 MHz, 25°C, $CDCl_3$).

1.4. Preparation of *trans*-Dichloro-(κ²(C,N)-(2-Benzo(h)-Quinolin-10-yl Methylidene))(SIotol) Ru (trans-IV)

In an Argon floated Schlenk flask, 96.5 mg [(SI*o*-tol)$RuCl_2$(PCy_3)(Ind)] (0.11 mmol, 1.0 eq), 36.6 mg ligand **L-I** (0.18 mmol, 1.6 eq) and 14.4 mg Cu(I)Cl (0.14 mmol, 1.3 eq) were dissolved in dry toluene (8 mL). The reaction was heated to 80°C and stirred for 20 min, until a green precipitate was formed, which was filtered and subsequently dried in vacuo. Yield: 33.0 mg (50%) of dark green crystals.

Anal. Calcd. for $C_{31}H_{27}Cl_2N_3Ru$ (613,54): C, 60.69; H, 4.44; N, 6.85. **Found:** C, 60.87; H, 4.52; N, 6.76. **^{1}H NMR** (300 MHz, $CDCl_3$, 25°C): δ 19.01 (bs, 1H, Ru=C*H*), 8.79 (bs, 1H, $H_{o\text{-}tol}$), 8.59 (bs, 1H, H_{bquin}^{2}), 8.16 (d, 1H, $^{3}J_{HH}$ = 7.9 Hz, H_{bquin}^{4}), 8.13 (d, 1H, H_{bquin}^{7}), 7.92 (d, 1H, $^{3}J_{HH}$ = 8.9 Hz, H_{bquin}^{5}), 7.69 (d, 1H, $^{3}J_{HH}$ = 8.9 Hz, H_{bquin}^{6}), 7.61 (t, 1H, $^{3}J_{HH}$ = 7.5 Hz, 7.8 Hz, H_{bquin}^{8}), 7.66-7.44 (bs, 5H, $H_{o\text{-}tol}$), 7.50 (dd, 1H, $^{3}J_{HH}$ = 5.3 Hz, 7.5 Hz, H_{bquin}^{3}), 7.20 (bs, 2H, $H_{o\text{-}tol}$), 6.92 (bs, 1H, H_{bquin}^{9}), 4.44, 4.09 (bs, 4H, H_{H2Im}), 2.69 (s, 6H, $H_{o\text{-}tol\text{-}CH3}$). **^{13}C NMR** (75 MHz, $CDCl_3$, 25°C): δ 290.3 (s, 1C, Ru=CH), 214.7 (1C_q, CNN), 149.1 (1C; C_{bquin}^{2}), 146.2 (1C_q, C_{bquin}^{10b}), 142.1 (1C, C_q,

C_{bquin}^{4a}), 141.5, 138.3 (2C, C_q, $C_{o\text{-}tol}$) 137.2 (1C, C_{bquin}^{7}), 136.0 (1C_q, C_{bquin}^{6a}), 132.5 (1C, $C_{o\text{-}tol}$), 131.0 (1C, $C_{o\text{-}tol}$), 130.0 (1C, $C_{o\text{-}tol}$), 129.9 (1C, C_q, $C_{o\text{-}tol}$), 129.7 (2C, $C_{bquin}^{4,8}$), 129.0 (1C, $C_{o\text{-}tol}$), 128.7 (1C, $C_{o\text{-}tol}$), 128.6 (1C, C_{bquin}^{5}), 128.5 (1C, C_q, C $_{bquin}^{10a}$), 127.8 (1C, 1C_q, $C_{o\text{-}tol}$), 126.9 (1C, C_{bquin}^{6}), 124.3 (1C, C_{bquin}^{9}), 123.2 (1C_q, C_{bquin}^{10}), 121.3 (1C, C_{bquin}^{3}), 54.4, 51.4 (2C, C_{H2Im}), 19.6, 18.4 (2C, $C_{o\text{-}tol\text{-}CH3}$).

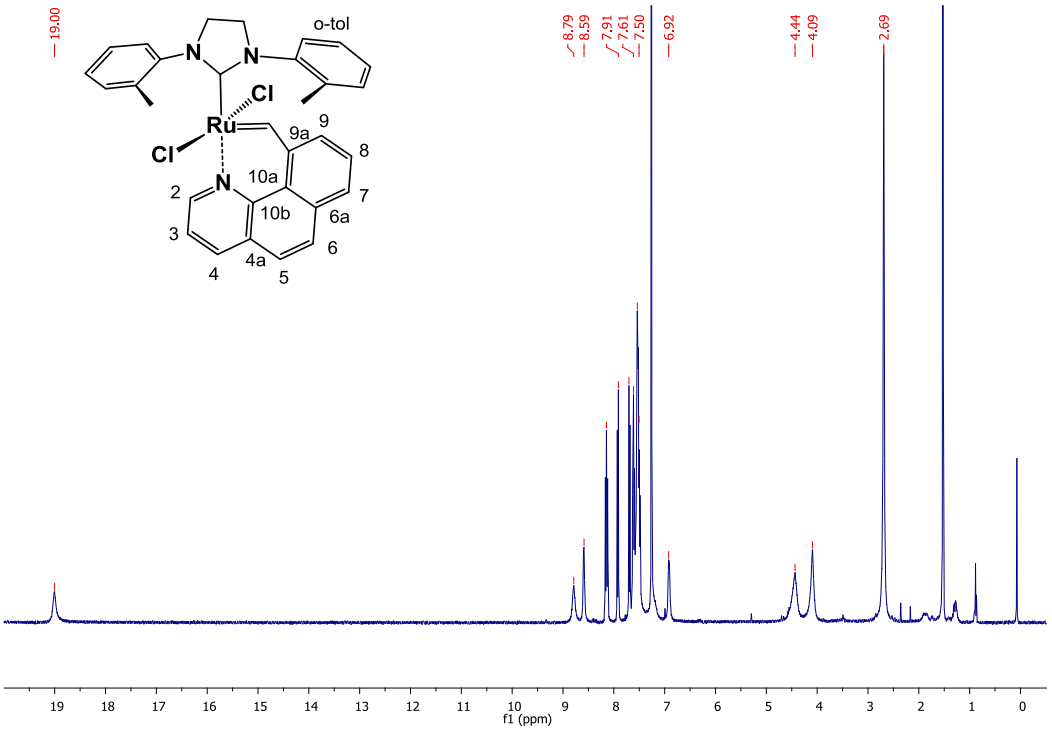

Figure 38. ^{1}H-NMR spectrum of complex **trans-IV** (300 MHz, 25°C, $CDCl_3$).

1.5. Preparation of *trans*-Dichloro-(κ²(C,N)-(2-(Benzo(h)-Quinolin-10-yl)-Methylidene))(SIXyl)Ru (trans-V)

In a Schlenk flask 96.7 mg [(SIXyl)$RuCl_2(PCy_3)$(Ind)] (0.11 mmol, 1.0 eq), 30.0 mg bquin ligand **L-I** (0.15 mmol, 1.3 eq) and 13.2 mg Cu(I)Cl (0.13 mmol, 1.2 eq) were dissolved in 7 mL dry toluene. The reaction was heated to 80°C and stirred for 15 min until the mixture turned green and full conversion was detected by TLC. The solvent was removed and the residue was *re*-dissolved in acetone. The white precipitate [CuCl·PCy_3] was filtered and the solvent was again removed. A concentrated DCM solution was prepared and then layered with *n*-pentane, leading to a green precipitate. Yield: 52.1 mg (74%) of light green crystals.

Anal. Calcd. for $C_{33}H_{31}Cl_2N_3Ru$ (641.60): C, 61.78; H, 4.87; N, 6.55. **Found:** C, 61.82; H, 4.93; N, 6.51. **^{1}H NMR** (300 MHz, $CDCl_3$, 25°C): δ 19.05 (s, 1H, Ru=CH), 8.70 (s, 1H, H_{xyl}) 8.55 (s, 1H, $H_{bquin}{}^{2}$), 8.16 (d, 1H, $^3J_{HH}$ = 8.3 Hz, $H_{bquin}{}^{7}$), 8.13 (d, 1H, $^3J_{HH}$ = 7.7 Hz, $H_{bquin}{}^{4}$), 7.93 (d, 1H, $^3J_{HH}$ = 8.8 Hz, $H_{bquin}{}^{5}$), 7.70 (d, 1H, $^3J_{HH}$ = 8.7 Hz, $H_{bquin}{}^{6}$), 7.62 (t, 1H, $^3J_{HH}$ = 7.7 Hz, $H_{bquin}{}^{8}$), 7.49 (t, 1H, $^3J_{HH}$ = 7.7 Hz, $H_{bquin}{}^{3}$), 7.42 (d, 1H, H_{xyl}), 7.35 (d, 2H, H_{xyl}), 6.91 (d, 1H, $^3J_{HH}$ = 6.6 Hz, $H_{bquin}{}^{9}$), 7.21-6.29 (bs, 2H, H_{xyl}), 4.54, 4.53, 4.03 (bs, 4H, H_{H2Im}), 2.63, 2.53, 2.13 (s, 12H, $H_{xyl\text{-}CH3}$). **^{13}C NMR** (75 MHz, $CDCl_3$, 25°C): δ 289.9 (s, 1C, Ru=CH), 214.7 (1C_q, CNN), 148.8 (1C_q, $C_{bquin}{}^{2}$), 146.5 (1C, C_q, $C_{bquin}{}^{10b}$), 142.1 (1C, $C_{bquin}{}^{4a}$), 141.0 (1C, C_q, C_{Xyl}) 137.8 (1C, C_{Xyl}), 137.1 (1C, $C_{bquin}{}^{7}$), 135.9 (1C, C_q, $C_{bquin}{}^{6a}$), 134.5, 133.4 (2C, C_q, C_{Xyl}), 132.5 (1C, C_{Xyl}), 132.2 (1C, C_q, C_{Xyl}), 131.5 (1C, C_q, C_{Xyl}), 130.6 (1C, C_q, C_{Xyl}), 130.4 (2C, C_{Xyl}), 129.9 (1C, $C_{bquin}{}^{7}$), 129.6 (1C, C_q, $C_{bquin}{}^{10a}$), 129.5 (1C, C_{Xyl}), 129.4 (1C, $C_{bquin}{}^{4,8}$), 128.6 (1C, $C_{bquin}{}^{5}$), 128.4 (1C, C_{Xyl}), 126.8 (1C, $C_{bquin}{}^{6}$), 123.8 (1C, C_q, $C_{bquin}{}^{9}$), 123.3 (1C_q, $C_{bquin}{}^{10}$), 121.2 (1C, $C_{bquin}{}^{3}$), 54.2, 51.0 (2C, C_{H2Im}), 20.8, 20.6, 19.0, 17.8 (4C, $C_{xyl\text{-}CH3}$).

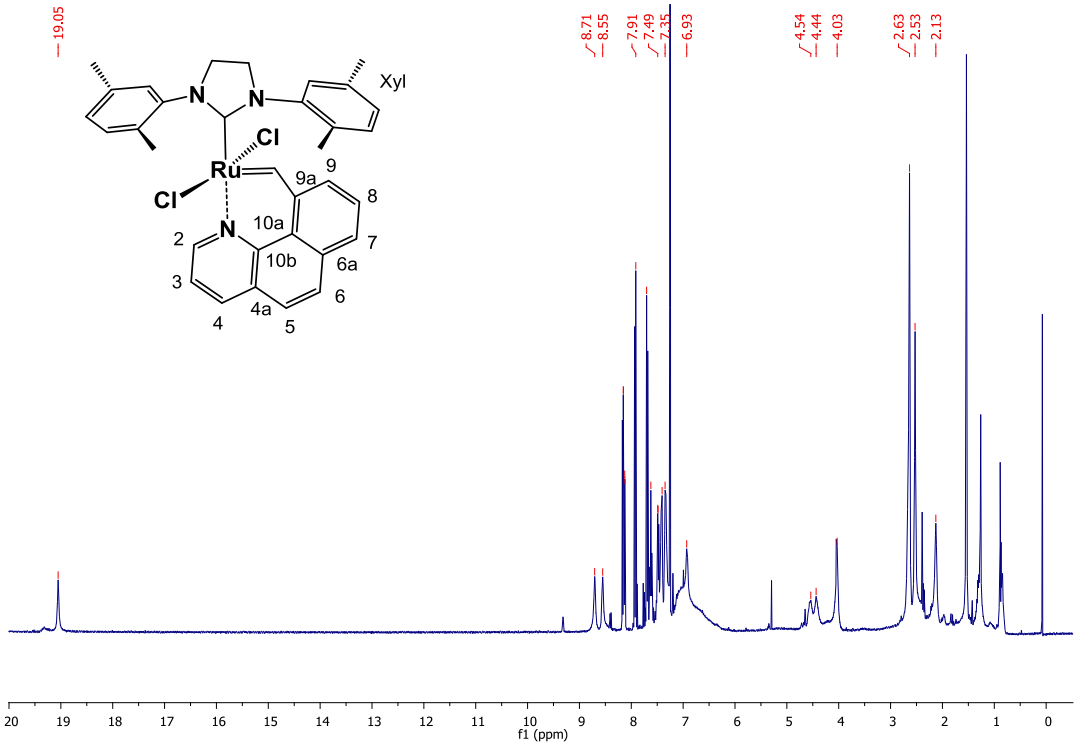

Figure 39. ^{1}H-NMR spectrum of complex **trans-V** (300 MHz, 25°C, $CDCl_3$).

1.6. Decomposition of trans-IV

Scheme 24. CH-deactivation of complex **trans-IV**.

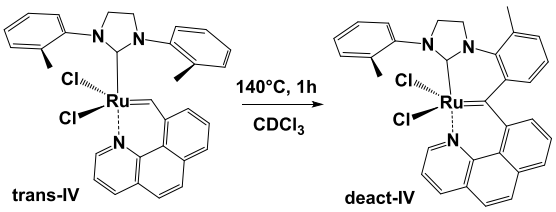

Compound **deact-IV** was obtained, during isomerization experiments, as described in Isomerization Paragraph 0. A 7.0 mM stock solution of the respective *trans*-compound **trans-IV** was prepared in $CDCl_3$ and subsequently exposed in microwave at 140°C for 20 min.

^{1}H NMR (δ, 300 MHz, $CDCl_3$, 25°C): δ 9.12 (s, 1H, $^4J_{HH}$ = 4.3 Hz, H_{bquin2}), 8.71 (s, 0.5H, $H_{o\text{-}tol}$), 8.21 (d, 1H, $^3J_{HH}$ = 7.7 Hz, H_{bquin4}), 8.14 (d, 1H, $^3J_{HH}$ = 7.7 Hz, $H_{o\text{-}tol'}$), 8.01 (s, 0.5H, $H_{o\text{-}tol}$), 7.96 (d, 1H, $^3J_{HH}$ = 8.7 Hz, H_{bquin4}), 7.78 (d, 1H, $^3J_{HH}$ = 7.7 Hz, $H_{o\text{-}tol'}$), 7.76 (d, 1H, $^3J_{HH}$ = 8.7 Hz, H_{bquin6}), 7.68 (t, 1H, $^3J_{HH}$ = 7.7 Hz, $H_{o\text{-}tol'}$), 7.61 (dd, 1H, $^3J_{HH}$ = 5.0, 7.7 Hz, H_{bquin3}), 7.53 (t, 1H, $^3J_{HH}$ = 7.7 Hz, $H_{o\text{-}tol}$), 7.36 (d, 1H, $^3J_{HH}$ = 7.7 Hz, H_{bquin9}), 7.30 (d, $^3J_{HH}$ = 7.9 Hz, $H_{o\text{-}tol}$), 7.20 (d, 1H, $^3J_{HH}$ = 7.7 Hz, $H_{o\text{-}tol}$), 6.91 (t, 1H, $^3J_{HH}$ = 7.9 Hz, H_{bquin8}), 6.76 (d, 2H, H_{bquin7}), 5.26, 4.11, 4.09 (m, 4H, H_{2HIm}), 2.79 (s, 3H, *o*-tol-CH_3), 2.28 (s, 3H, *o*-tol-CH_3). Impurities: **cis-IV**.

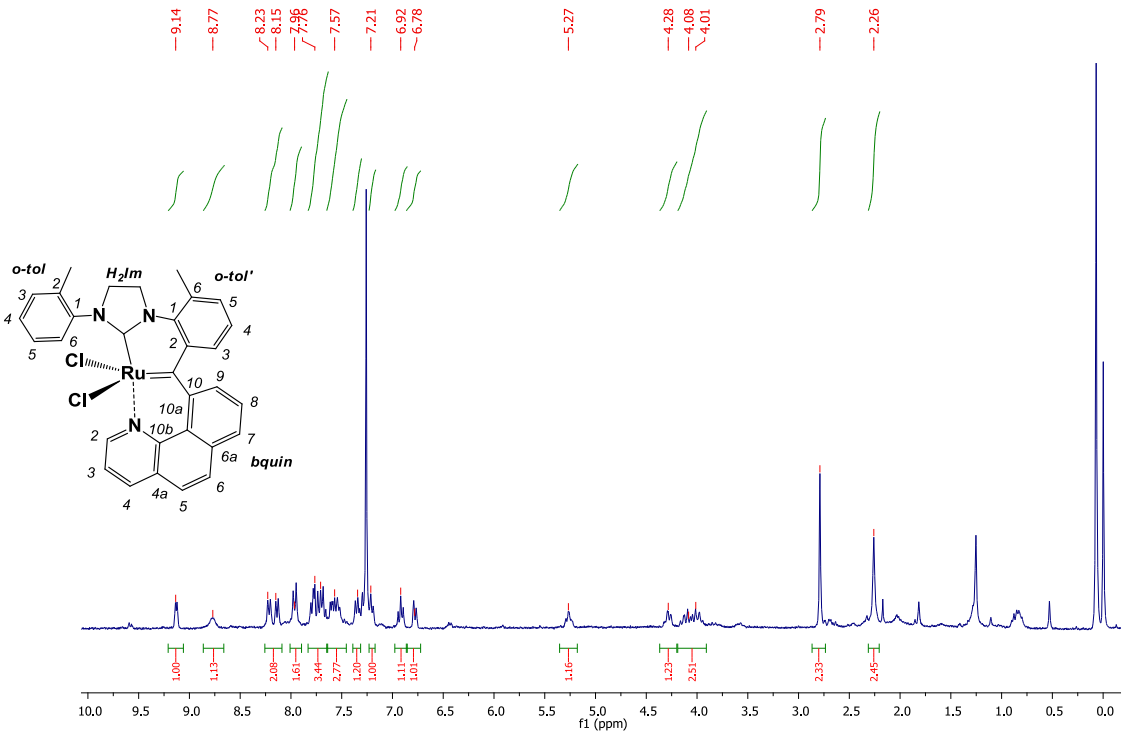

Figure 40. ^{1}H-NMR spectrum of complex **deact-IV** (300 MHz, 25°C, $CDCl_3$).

2. Chapter II[44h]

Scheme 25. General procedure for preparing halide exchanged [Ru] benzylidene complexes.

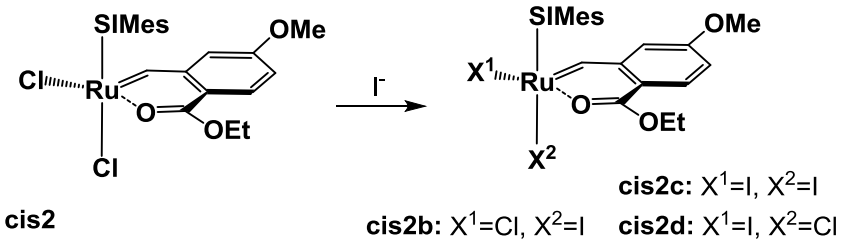

Halide exchange in second generation benzylidene complexes, bearing *cis*-dichloro stereochemistry showed a high tendency to selective halide exchange in the *trans*-position to the NHC ligand. In general a procedure, as shown in Scheme 26 was applied to investigate the behavior of the anionic ligands for this type of initiators.

2.1. Preparation of *cis*-chloro-iodo-(κ²(C,O)-5-methoxy-2-ethylester benzylidene)(SIMes) (cis2b)

Scheme 26. Preparation of monosubstituted complex **cis2b**.

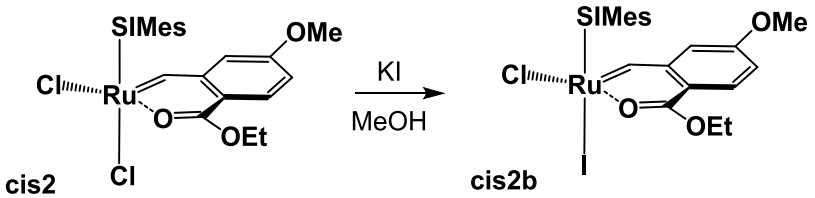

Complex **cis2** (15.0 mg, 0.0224 mmol, 1.0 eq) and KI (111.0 mg, 0.669 mmol, 30 eq) were suspended resp. dissolved in methanol (2 mL). The reaction mixture was stirred for 10 min at room temperature. The methanol was blown off by a N_2 stream and the residue was collected in CH_2Cl_2 (5 mL) was added. Insoluble parts were removed by filtration and the filtrate was evaporated to dryness. The residue was dried in vacuo. Yield: 15.4 mg (90%) grass green solid.

TLC: R_f = 0.7 (CH_2Cl_2:MeOH, 10:1 (v:v)).

Anal.Calcd.for $C_{32}H_{38}ClIN_2O_3Ru$ (762.08): C, 50.43; H, 5.03; N, 3.68; **found**: C, 50.28; H, 5.21; N, 3.52. **^{1}H-NMR** (δ, 25°C, $CDCl_3$, 300 MHz):18.38 (s, 1H, Ru=C*H*), 7.99 (d, 1H, $^3J_{HH}$ = 8.8 Hz, ph^3), 7.21, 7.15, 6.89, 5.99 (s, 4H, mes), 7.14 (dd, 1H, $^3J_{HH}$ = 9.0 Hz,$^4J_{HH}$ = 2.5 Hzph^4), 6.81 (d, 1H, $^4J_{HH}$ = 1.7 Hz, ph^6), 4.75-4.53, 4.48-4.32 (m, 2H, CH_2CH$_3$), 4.32-3.63 (m, 4H, H_2Im), 3.90 (s, 3H, OCH_3), 2.64, 2.57, 2.44, 2.40, 2.06, 1.42 (s, 18H, mes-CH_3), 1.48 (t, 3H, CH_2CH_3). **^{13}C-NMR**(δ, 25°C, $CDCl_3$, 75 MHz): 280.2 (1C, Ru=*C*H), 215.0 (1C, C_q, *C*NN), 175.8 (1C, C_q, COOEt), 165.7 (1C, C_q, ph^5), 144.2 (1C, C_q, ph^1), 140.0, 139.7, 138.5, 137.8, 136.5, 135.0 (6C, C_q, mes-C), 135.7 (1C, C_q, mes-N), 133.2 (1C, ph^3), 131.7 (1C, C_q, mes-N), 131.0, 129.8, 129.5, 128.5 (4C, mes), 114.9 (1C, C_q, ph^2), 114.0, 112.2 (2C, ph^{4,6}), 64.2 (1C, *C*H_2CH$_3$), 55.7 (1C, O*C*H$_3$), 51.3, 50.9 (2C, H_2Im), 21.3, 20.6, 20.1, 18.3, 16.4 (6C, mes-*C*H$_3$), 14.5 (1C, CH_2*C*H$_3$).

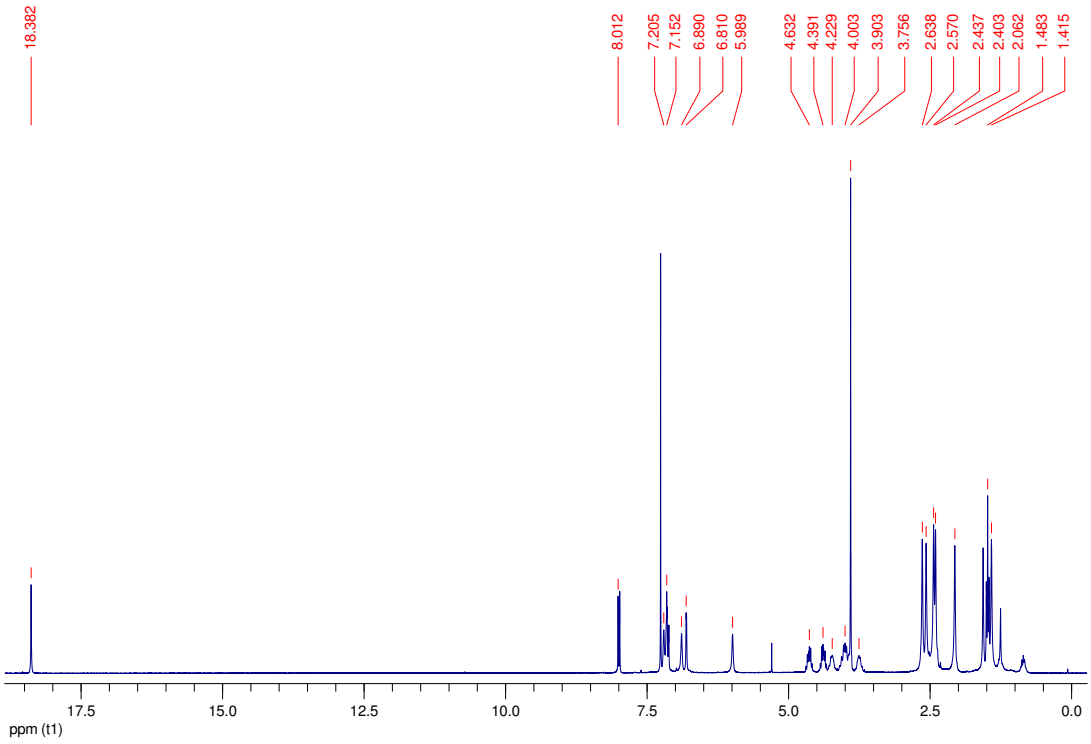

Figure 41. ^{1}H-NMR spectrum of complex **cis2b** (300 MHz, 25°C, $CDCl_3$).

2.1.1. Alternative Protocols for the Preparation of 2b

The product distribution was observed in various solvents after 24 h. Therefore, complex **cis2** (5 mg, 0.0746 mmol, 1.0 eq) and potassium iodide (37.1 mg, 0.224 mmol, 30 eq) were dissolved/suspended in the respective solvent (1 mL). The conversion was monitored every few hours by TLC on silica gel (CH_2Cl_2:MeOH, 10:1 (v:v)). After 24 h the

solvent was blown off by a nitrogen steam. The residue was *re*-dissolved in $CDCl_3$ and immediately subjected to ^{1}H-NMR spectroscopy measurements.

Table 15. Results, obtained from the reaction of **cis2** with 30 eq KI after 24 h in various solvents.

entry	solvent	**cis2**	**cis2b**	**cis2c**	**cis2d**	**decomp.**
1	CH_2Cl_2	0	69	26	0	5
2	methanol	0	83	12	0	5
3	acetone	0	88	3	0	9
4	toluene	77	19	0	0	3

2.1.1.1. Halide Exchange in CH_2Cl_2

Complex **cis2** (15.0 mg, 0.0224 mmol, 1.0 eq) and KI (111.0 mg, 0.669 mmol, 30 eq) were suspended resp. dissolved in dry CH_2Cl_2 (2 mL). The reaction mixture was stirred for 2 h at room temperature. Insoluble parts were removed by filtration and the filtrate was evaporated to dryness. The residue was dried in vacuo and examined by ^{1}H-NMR spectroscopy. A conversion of 5 % towards **cis2b** was found.

2.1.1.2. Halide Exchange by Extraction

An alternative pathway for preparing **cis2b** is the extraction of a solution of **cis2** (10.0 mg, 0.015 mmol, 1.0 eq) in CH_2Cl_2 (10 mL) with aqueous KI (5 w-%, 20 mL). A sudden color change from dark green to grass green was noted upon the first shaking (approx. 5 sec). The organic phase was separated, evaporated to dryness and the residue was examined by ^{1}H-NMR spectroscopy. The extraction was repeated with two further portions of aqueous KI (5 w-%, 20 mL). According conversions after each extraction step are shown in Table 16.

Table 16. Results of extraction of **cis2** after 1-3 repetitions.

repetitions	**cis2**	**cis2b**	**cis2c**	**cis2d**
1	6	94	0	0
2	7	90	3	0
3	9	86	5	0

2.1.1.3. Halide Exchange with an Organic Iodide

Compound **cis2** (3.0 mg, 0.00447 mmol, 1.0 eq) and tetrabutylammonium iodide (16.5 mg, 0.0447 mmol, 10 eq) were dissolved in $CDCl_3$ (0.7 mL) and the reaction was monitored via ^{1}H-NMR spectroscopy. Immediate conversion towards **cis2b** (25%) occurred. The conversion is hardly changing within a period of 24 h.

2.1.1.4. Halide Exchange upon Mixing two Different Complexes

Scheme 27. Formation of all four potential products **cis2**-**cis2d**.

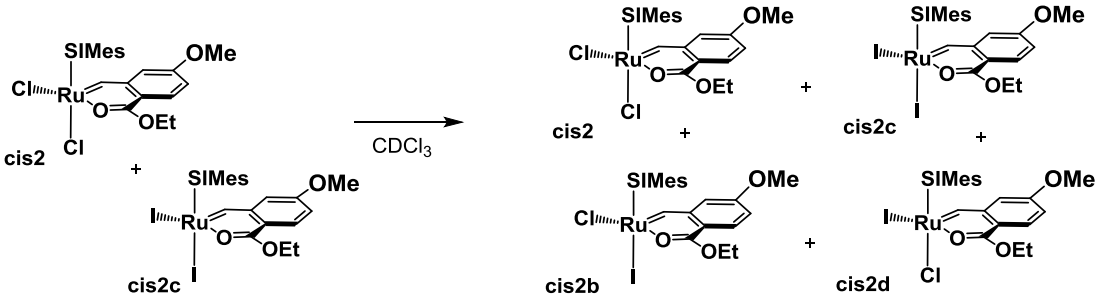

Compound **cis2c** (3.0 mg, 3.5 µmol, 1 eq) was dissolved in $CDCl_3$ (0.35 mL) and added to an equimolar solution of the dichloro complex **cis2** (2.4 mg, 3.5 µmol, 1 eq) in $CDCl_3$ (0.35 mL). The reaction was monitored by ^{1}H-NMR spectroscopy (300 MHz) at 25°C. Figure 42 shows the carbene region of the reaction mixture after 1 h indicating the formation of **cis2** and **cis2c**. Product distribution: 37% **cis2**, 22% **cis2b**, 15% **cis2c** and 21% **cis2d** (5% decomposition).

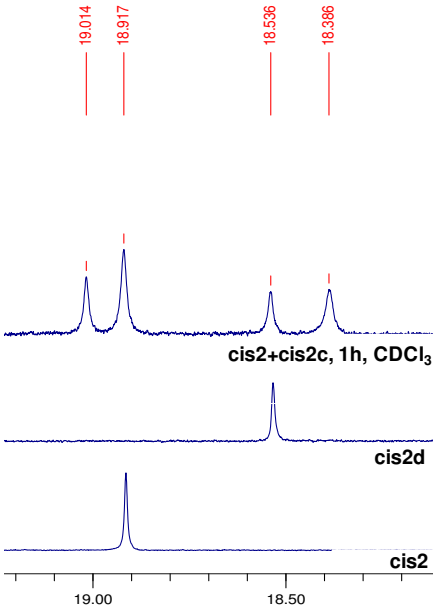

Figure 42. ^{1}H NMR spectroscopy (300 MHz, $CDCl_3$, 25°C) within the carbene region indicates the formation of mixed *cis*-dihalo complexes (**cis2b**, **cis2d**) after mixing **cis2** and **cis2c**.

2.2. Preparation of *cis*-Diiodo-(κ²(C,O)-5-Methoxy-2-Ethylester Benzylidene)(SIMes)Ru (cis2c)

Scheme 28. Preparation of diiodo complex **cis2c**.

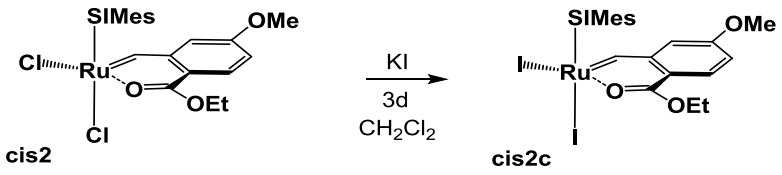

Compound **cis2** (43.5 mg, 0.0648 mmol, 1.0 eq) and KI (323.0 mg, 1.95 mmol, 30 eq) were dissolved respectively suspended in CH_2Cl_2 (water content: 550 ppm) and the reaction was stirred at ambient temperature for 3d. Afterwards, the solvent was destilled off and the residue was purified by column chromatography on silica gel with CH_2Cl_2:MeOH, 10:1 (v:v) as eluent. The volume of the organic fractions containing the product was reduced to 2 mL and 10 mL of CH_2Cl_2 were added. Subsequently, the solution was extracted with aqueous KI (5 w-%). Drying of the CH_2Cl_2 solution over Na_2SO_4, removal of the Na_2SO_4 and evaporation of the solvent. Yield: 23.2 mg (42 %) of yellow crystals.

TLC: R_f = 0.8 (CH_2Cl_2:MeOH, 10:1 (v:v)).

Anal.Calcd.for $C_{32}H_{38}I_2N_2O_3Ru$ (853.53): C, 45.03; H, 4.49; I, 29.74; N, 3.28. **Found**: C, 44.88; H, 4.65; N, 3.04. **^{1}H-NMR** (δ, 25°C, $CDCl_3$, 300 MHz): 18.54 (s, 1H, Ru=C*H*), 8.05 (d, 1H, $^3J_{HH}$ = 9.0 Hz, ph^3), 7.16, 7.09, 6.84, 5.98 (s, 4H, mes), 7.12 (dd, 1H, $^3J_{HH}$ = 8.8 Hz, $^4J_{HH}$ = 2.5 Hz ph^4), 6.71 (s, 1H, ph^6), 4.68, 4.42 (m, 2H, CH_2CH_3), 4.47-3.54 (m, 4H, H_2Im), 3.89 (s, 3H, OMe), 2.67, 2.62, 2.52, 2.38, 2.02, 1.47 (s, 18H, mes-CH_3), 1.52 (t, 3H, $^3J_{HH}$ = 7.1, 7.3 Hz, CH_2CH_3). **^{13}C-NMR** (δ, 25°C, $CDCl_3$, 75 MHz): 280.9 (1C, Ru=*C*H), 216.1 (1C, C_q, CNN), 175.2 (1C, C_q, COOEt), 165.3 (1C, C_q, ph^5), 144.7 (1C, C_q, ph^1), 139.9, 138.4, 138.3, 137.8, 135.9, 134.9 (6C, C_q, mes-C), 135.5, 132.3 (1C, C_q, mes-N), 133.0, 130.9, 130.0, 128.4 (4C, mes), 129.4 (1C, ph^3), 114.3, 112.2 (2C, ph^{4,6}), 113.4 (1C, C_q, ph^2), 64.3 (1C, CH_2CH_3), 55.7 (1C, OCH_3), 51.7, 51.0 (2C, H_2Im), 21.9, 21.3, 20.6, 19.4, 18.5, 16.4 (6C, mes-CH_3), 14.5 (1C, CH_2CH_3).

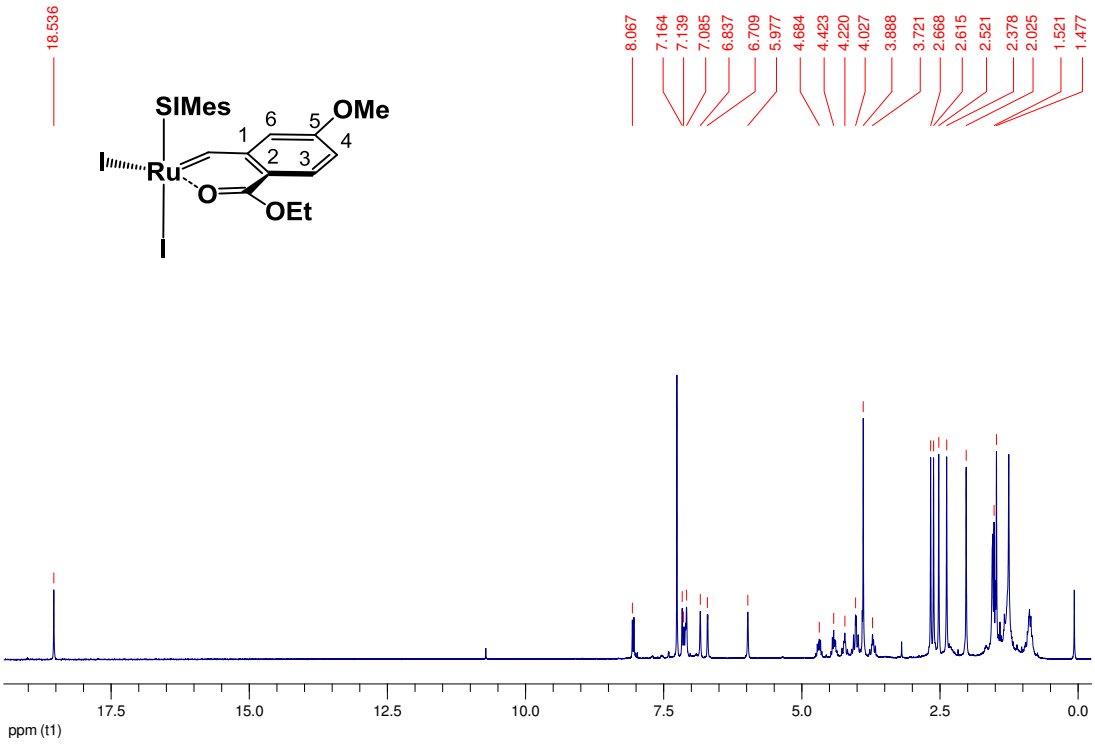

Figure 43. ^{1}H-NMR spectrum of complex **cis2c** (300 MHz, 25°C, $CDCl_3$).

After storing the **cis2c** compound for three days in a NMR tube, isomerization towards the *trans*-species occurred, as evidenced by ^{1}H-NMR spectroscopy (300 MHz, $CDCl_3$, 25°C).

Selected resonances for **trans2c**:

^{1}H-NMR (δ, 25°C, $CDCl_3$, 300 MHz): 17.73 (s, 1H, Ru=C*H*), 8.05 (d, 1H, ph^3), not found (ph^4), 7.06 (s, 4H, mes), 6.26 (d, 1H, ph^6), 4.42 (m, 2H, CH_2CH_3), 4.07 (s, 4H, H_2Im), 3.85 (s, 3H, OCH_3), 2.40 (s, 12H, mes-CH_3), 2.33 (s, 6H, mes-CH_3), 1.52 (t, 3H, CH_2CH_3).

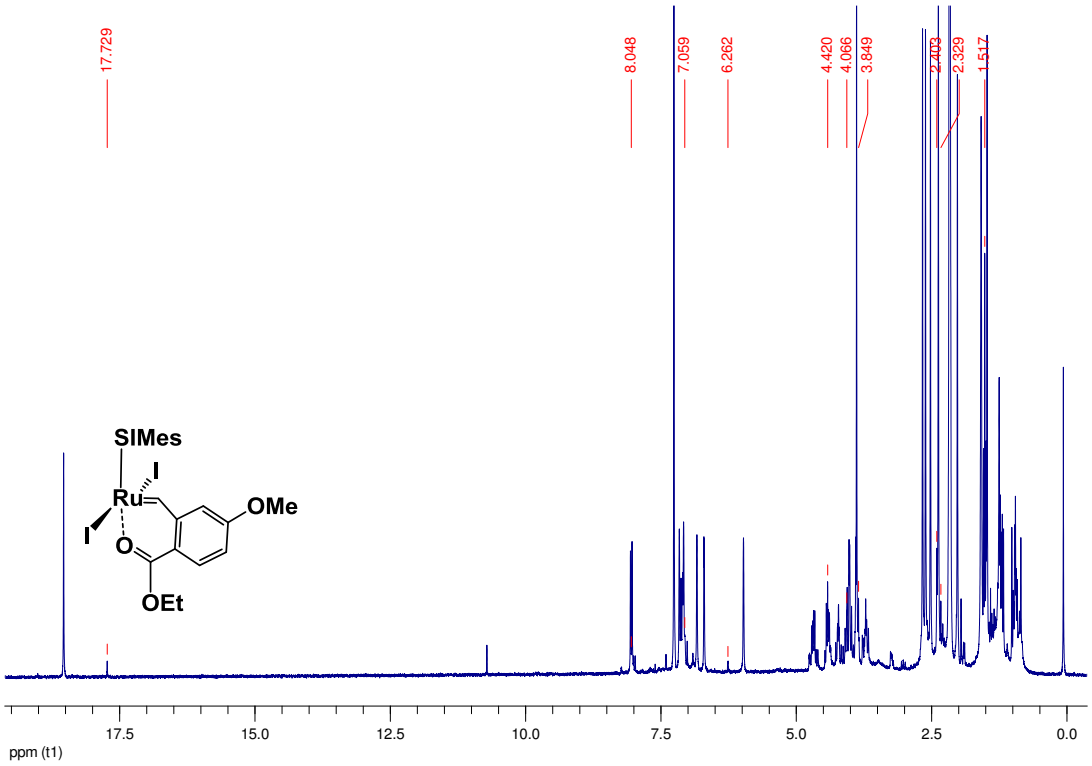

Figure 44. Appearance of **trans2c**, detected when storing **cis2c** in $CDCl_3$ for 3 days.

2.3. Preparation of *cis*-Chloro-Iodo-(κ²(C,O)-5-Methoxy-2-Ethylester Benzylidene)(SIMes)Ru (cis2d)

Scheme 29. Preparation of inverted monosubstituted complex **cis2d**.

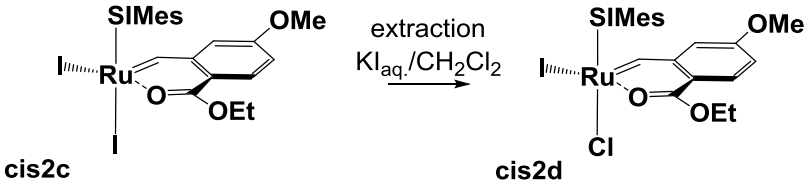

The inverse monosubstitute diodo-compound **cis2d** was obtained by extraction of a solution of **cis2c** (5.0 mg, 0.00586 mmol, 1 eq) in CH_2Cl_2 (5 mL) with a solution of $KCl_{aq.}$ (5 w-

%, 20 mL). The color of the solution immediately changed from yellow to bright green. Afterwards, the organic layer was separated, dried over Na_2SO_4, filtered, evaporated and dried in vacuo. Yield: 3.8 mg (85%) of light green crystals.

TLC: R_f = 0.9 (CH_2Cl_2:MeOH, 10:1 (v:v)).

Anal.Calcd. for $C_{32}H_{38}ClIN_2O_3Ru$ (762.08): C, 50.43; H, 5.03; N, 3.68. **Found**: C, 50.16; H, 4.88; N, 3.43. **^{1}H-NMR** (δ, 25°C, $CDCl_3$, 300 MHz):19.01 (s, 1H, Ru=C*H*), 8.06 (d, 1H, $^3J_{HH}$ = 9.0 Hz, ph^3), 7.17, 7.10, 6.87, 6.01 (s, 4H, mes), 7.13 (dd, 1H, $^3J_{HH}$ = 8.8 Hz, $^4J_{HH}$ = 2.5 Hz, ph^4), 6.64 (d, 1H, $^4J_{HH}$ = 2.5 Hz,ph^6), 4.57, 4.40 (m, 2H, CH_2CH$_3$), 4.33-3.63 (m, 4H, H_2Im), 3.89 (s, 3H, OMe), 2.70, 2.58, 2.52, 2.37, 2.05, 1.44 (s, 18H, mes-CH_3), 1.48 (t, 3H, CH$_2$CH_3).

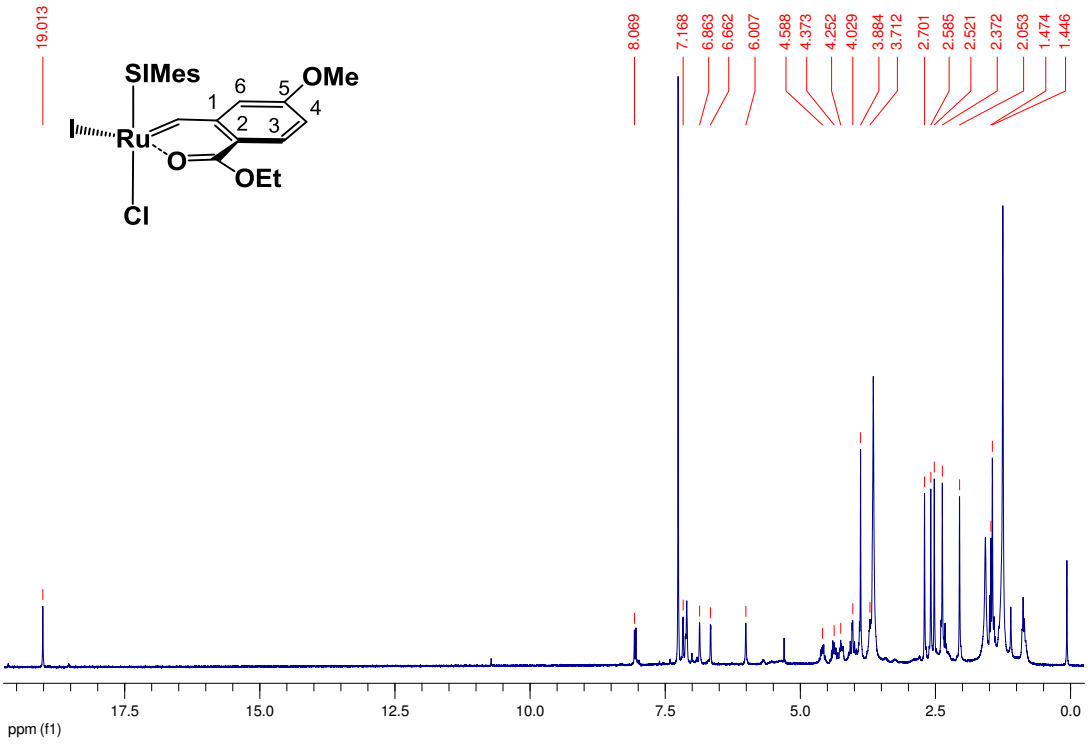

Figure 45. ^{1}H-NMR spectrum of complex **cis2d** (300 MHz, 25°C, $CDCl_3$).

2.4. Preparation of *trans*-Diiodo-(κ^2(C,O)- 2-*iso*-Propoxy Benzylidene)(SIMes)Ru (Hov-I_2)

Scheme 30. Preparation of halide exchanged Hoveyda complexes **Hov-I** and **Hov-I_2**.

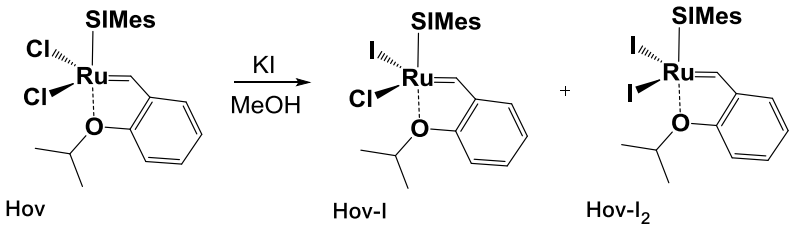

As a reference *trans*-diiodo-(κ^2 (C,O)-(isopropyl benzylidene)-(1,3-bis(2,4,6-trimethylphenyl)-4,5-dihydroimidazol-2-ylidene) ruthenium (Hov-I_2) was prepared according to literature.[19b]

In a Schlenk flask the Hoveyda–catalyst (300 mg, 0.471 mmol, 1.0 eq) was suspended in degassed, dry MeOH and KI (2.35 g; 14.13 mmol; 30 eq) was added. The reaction mixture was stirred under argon atmosphere for 3h. Subsequently, the solvent was removed in vacuo and the dried residue was dissolved in degassed, dry CH_2Cl_2. The salt precipitate was separated by decantation of the organic solvent and the therein dissolved complex. Finally, the remaining CH_2Cl_2 was removed again and a NMR spectrum of the green residue was recorded in $CDCl_3$. Product distribution: 4 % starting material (**Hov**), 12% monosubstituted complex (**Hov-I**), 84% diiodo Hoveyda catalyst (**Hov-I_2**).

Analytical data are in accordance with literature.[19b]

^{1}H-NMR (δ, 20 °C, $CDCl_3$, 300 MHz): 15.66 (s, 1H, Ru=CH), 7.53 (dd, 1H, ph^5), 7.08, 7.00 (s, 4H, mes), 6.96 (d, 1H, ph^2), 6.83 (m, 2H, ph^{3,4}), 5.04 (septet, 1H,C*H*$(CH_3)_2$), 4.14 (s, 4H, H_2Im), 2.68 (s, 6H, mes-C*H*$_3$), 2.52 (s, 6H, mes-CH_3), 2.44 (s, 3H, mes-CH_3), 2.33 (s, 3H, mes-C*H*$_3$), 1.45 (d, 6H, CH(C*H*$_3$)$_2$). Characteristic signal for the mixed halide species: 16.10 (s, Ru=CH).
^{13}C-NMR (δ, 20 °C, $CDCl_3$, 75 MHz): 298.9 (1C, Ru=CH), 214.2 (1C, Ru-C), 153.2, 150.1, 145.3, 139.2, 138.9, 138.7, 138.2, 137.8, 134.7, 130.6, 129.9, 129.7, 123.3, 122.0, 113.5, 75.9, 52.9, 51.2, 23.5, 21.9, 21.24, 21.17, 20.3.

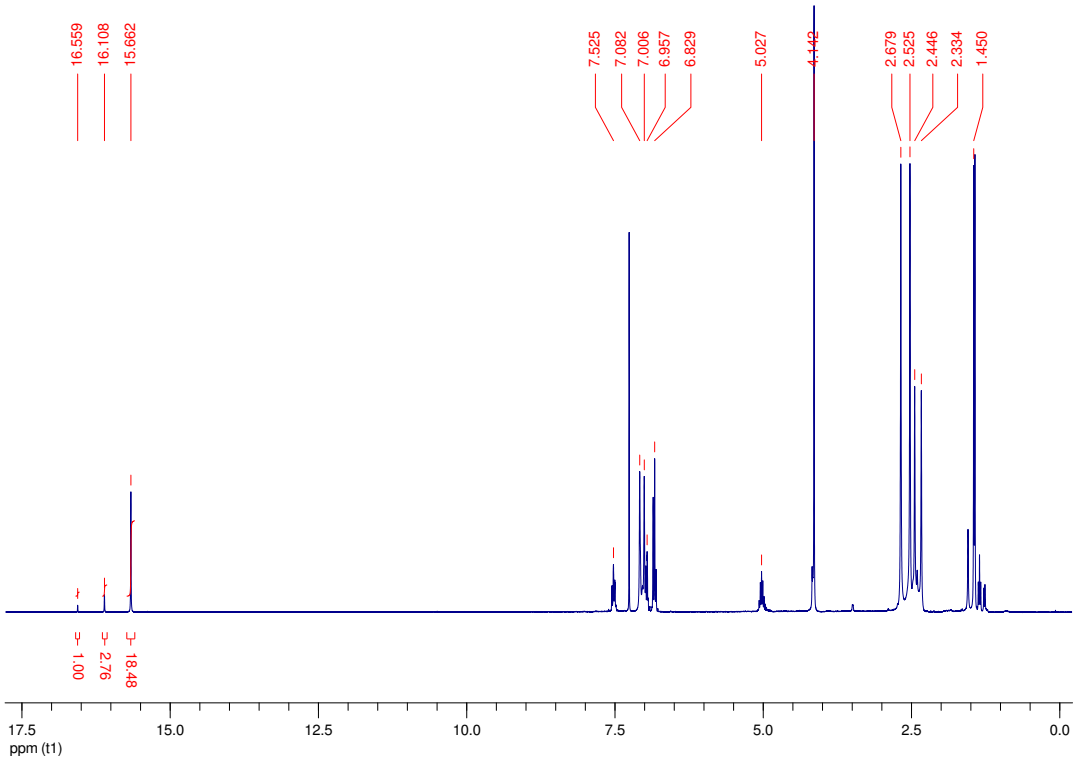

Figure 46. Product distribution after conversion of **Hov** with 30 eq KI in methanol (300 MHz, 25°C, $CDCl_3$).

2.4.1. Alternative Protocols for the Preparation of Hov-I_2

2.4.1.1. Halide Exchange by Extraction

To show the difference between complexes with *cis*- and *trans*-dichloro stereochemistry the extraction procedure for **cis2** was used for exchanging the chlorides in the Hoveyda catalyst (**Hov**). The extraction was repeated three times with aqueous KI (3x shaking for 5 sec for each portion). Subsequently, the organic layer was separated, dried with Na_2SO_4, filtered off, evaporated and finally dried in vacuo. ^{1}H NMR measurement after the third repetition step revealed the formation of 5% mono-iodosubstituted complex **Hov-I** (5%) and **Hov-I_2** was not observed.

2.4.1.2. Halide Exchange with an Organic Iodide

Complex **Hov** (3.0 mg, 0.00447 mmol, 1.0 eq) was dissolved in 0.5 ml $CDCl_3$ and tetrabutylammonium iodide (16.5 mg, 0.0447 mmol, 10 eq), dissolved in 0.2 mL deuterated

solvent was added. The reaction was monitored by ^{1}H-NMR spectroscopy. Results are summarized in Figure 47. After one day a product distribution of 73% **Hov**, 26% **Hov-I** and 1 % **Hov-I$_2$** was observed.

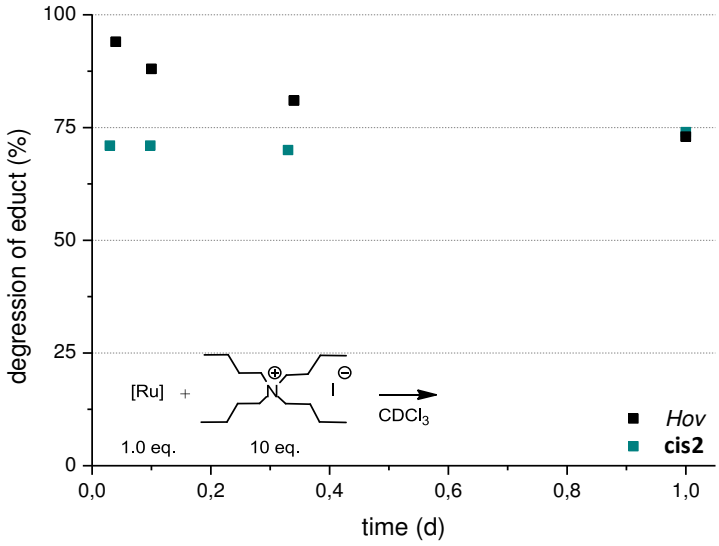

Figure 47. Reaction of **cis2** and Hov with tetrabutylammonium iodide giving the corresponding mono-iodo complexes.

3. Chapter III[84]

Scheme 31. General Procedure for preparing cis-dichloro benzylidene [Ru] complexes.

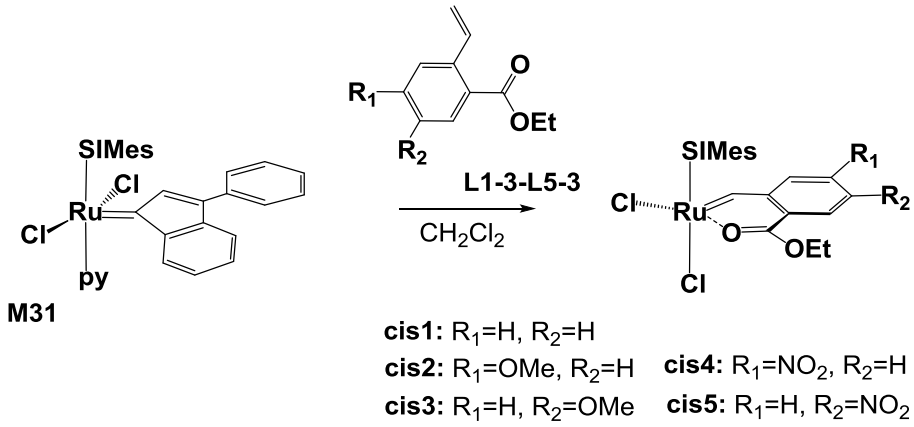

In a Schlenk flask, **M31** (1.0 eq) was dissolved in the appropriate amount of degassed, dry CH_2Cl_2. The desired vinyl benzoyl ethyl ester **L1-3-L5-3** (1.2 - 1.5 eq) was added and the reaction mixture was stirred under argon atmosphere for 20 - 30 h. The color turned from deep red to dark green. Pyridine was removed by extracting the reaction mixture with $HCl_{aq.}$

(5 v-%). Subsequently, the mixture was cleared from traces of water by Na_2SO_4. The solvent was then removed to 1 - 2 mL and precipitated with *n*-pentane. The obtained green solid was filtered, washed with *n*-pentane and dried in vacuo. If needed, column chromatography (silica gel; CH_2Cl_2:MeOH, 20:1 (v:v)) was used for purification.

3.1. Preparation of *cis*-Dichloro-(κ²(C,O)-2-Ethylester Benzylidene)(SIMes)Ru (cis1)

A glass vial containing **M31** (155.5 mg, 0.208 mmol, 1.0 eq) was channeled in an Argon glove box and dissolved in dry, degassed CH_2Cl_2 (4 mL). 2-Vinylbenzoic acid ethyl ester (56.0 mg, 0.318 mmol, 1.5 eq) was dissolved in 1 mL CH_2Cl_2 and added. The reaction mixture was stirred for 22 h, until the color turned from deep red to deep green. The solvent was removed in vacuo to about 1 mL and *n*-pentane was added to precipitate the complexes. The dark green precipitate was filtered and washed with *n*-pentane. The crystals were filtered and dried in vacuo. Yield: 92.5 mg (72 %) greenish crystals.

Analytical data are in accordance to literature.[44b]

^{1}H NMR (δ, 20°C, $CDCl_3$, 300 MHz): 18.96 (s, 1H, Ru=C*H*), 8.08 (d, 1H, $^3J_{HH}$ = 8.9 Hz, ph^3), 7.68 (q, 2H, $^3J_{HH}$ = 8.8 Hz, ph^{4,5}), 7.26 (d, 1H, $^3J_{HH}$ = 8.9 Hz, ph^3), 7.18, 6.98, 5.93 (s, 4H, mes), 4.60, 4.41 (m, 2H, C*H*$_2$CH$_3$), 4.02 (m, 4H, H_2Im), 2.68, 2.52, 2.47, 2.40, 2.08, 1.34 (s, 18H, mes-C*H*$_3$), 1.47 (t, 3H, $^3J_{HH}$ = 6.7 Hz, CH$_2$C*H*$_3$).

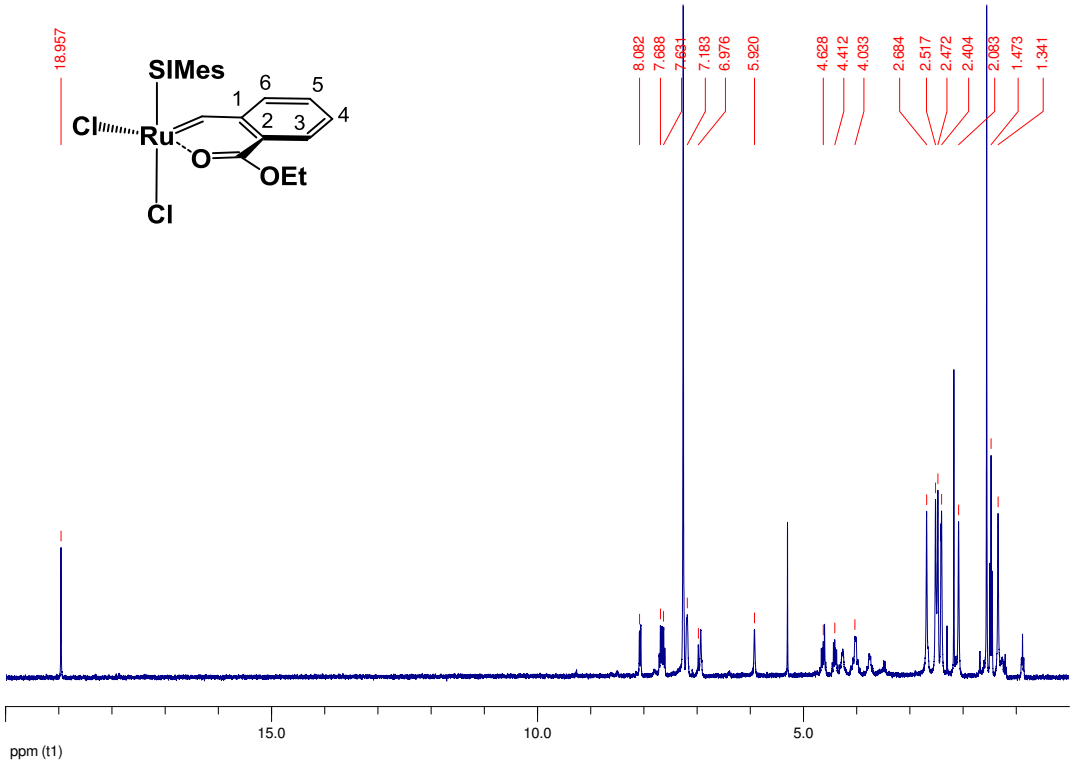

Figure 48. ^{1}H-NMR spectrum of complex **cis1** (300 MHz, 25°C, $CDCl_3$).

3.2. Preparation of *cis*-Dichloro-(κ²(C,O)-5-Methoxy-2-Ethylester Benzylidene)(SIMes)Ru (cis2)

In a Schlenk flask **M31** (400 mg, 0.601 mmol, 1.0 eq) was dissolved in degassed, dry CH_2Cl_2 (5 mL). 2-Vinylbenzoic acid ethyl ester **L2-3** (132.1 mg, 0.641 mmol, 1.2 eq) was added and the reaction mixture was stirred for 8 h until the color turned from deep red to deep green. The solvent was removed in vacuo to about 1 mL and *n*-pentane was added to precipitate the complexes. The dark green precipitate was filtered and washed with *n*-pentane. Afterwards the raw product was purified by column chromatography on silica gel (CH_2Cl_2:MeOH, 20:1 (v:v)). The volume of the organic fractions containing the product was reduced to 2 mL and 10 mL of CH_2Cl_2 were added. Subsequently, the solution was extracted with $NaCl_{aq.}$ (5 w-%). Drying of the CH_2Cl_2 solution over Na_2SO_4, removal of the Na_2SO_4 and evaporation of the solvent yielded upon drying in vacuum **cis-2** as green microcrystals. Yield: 280.9 mg (78%).

Analytical data are in accordance to literature.[44h]

TLC: R_f = 0.3 (CH_2Cl_2:MeOH, 10:1 (v:v)).

Anal. Calcd.for $C_{32}H_{38}Cl_2N_2O_3Ru$ (670.63): C, 57.31; H, 5.71; Cl, 10.57; N, 4.18. **Found:** C, 57.28; H, 5.91; Cl, 10.29; N, 4.01. **^{1}H NMR** (δ, 20°C, $CDCl_3$, 300 MHz): 18.92 (s, 1H, Ru=C*H*), 8.01 (d, 1H, $^3J_{HH}$ = 8.9 Hz, ph^3), 7.19, 7.17, 6.93, 6.03 (s, 4H, mes), 7.12 (dd, 1H, $^3J_{HH}$ = 8.8 Hz, $^4J_{HH}$ = 2.5 Hz, ph^4), 6.74 (d, 1H, $^4J_{HH}$ = 2.5 Hz, ph^6), 4.64 - 4.51 (m, 1H, CH_2CH$_3$), 4.41 - 4.30 (m, 1H, CH_2CH$_3$), 4.34 - 3.67 (m, 4H, H_2Im,), 3.90 (s, 3H, OCH_3), 2.68, 2.52, 2.46, 2.40, 2.10, 1.38 (s, 18H, mes-CH_3), 1.45, 1.43 (t, 3H, $^3J_{HH}$ = 6.7 Hz, CH$_2$CH_3). **^{13}C NMR** (δ, 20°C, $CDCl_3$, 125 MHz): 283.5 (1C, Ru=*C*H), 217.6 (1C, C_q, *C*NN), 176.1 (1C, C_q, COOEt), 165.9 (1C, C_q, ph^5), 144.7 (1C, C_q, ph^1), 140.1, 139.6, 138.4, 138.0, 136.5, 135.1 (6C, C_q, mes-C), 135.6 (1C, C_q, mes-N), 133.3 (1C, ph^3), 132.3 (1C, C_q, mes-N), 131.0, 129.6, 129.5, 128.4 (4C, mes), 113.5 (1C, C_q, ph^2), 113.8, 111.9 (2C, ph^{4,6}), 64.2 (1C, *C*H$_2$CH$_3$), 55.7 (1C, OCH$_3$), 51.02, 50.98 (2C, H_2Im), 21.4, 20.7, 20.1, 18.3, 18.25, 16.3 (6C, mes-*C*H$_3$) 14.2 (1C, CH$_2$*C*H$_3$).

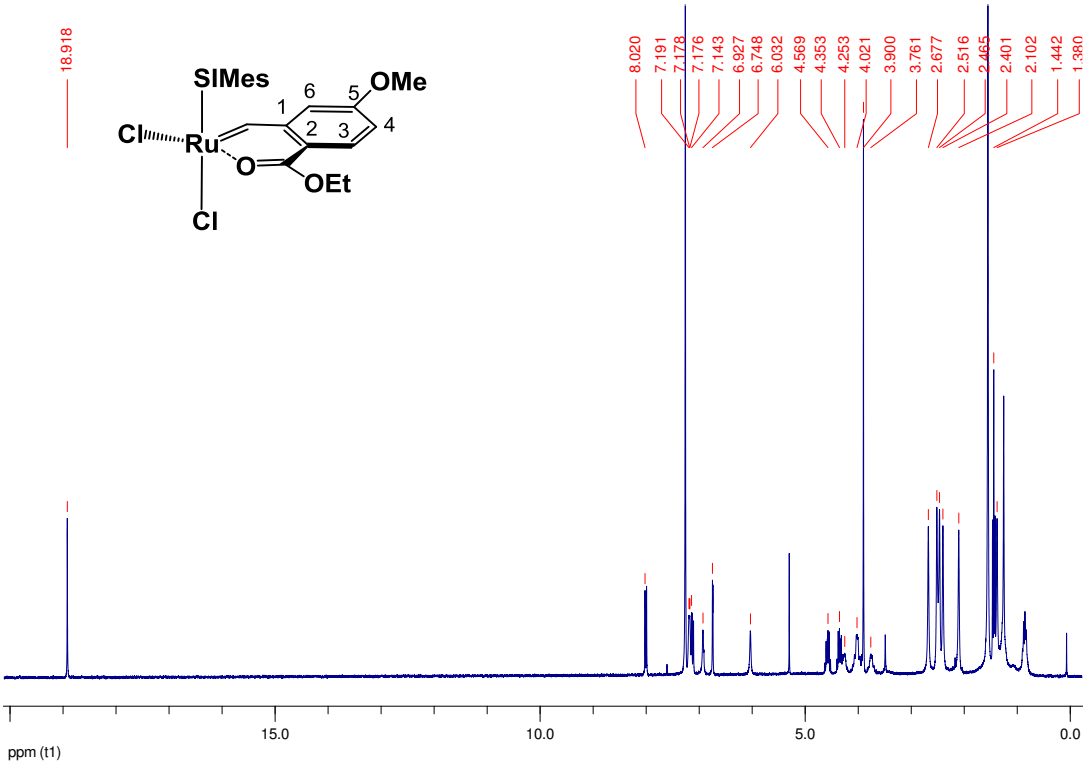

Figure 49.^{1}H-NMR spectrum of complex **cis2** (300 MHz. 25°C, $CDCl_3$).

After storing the **cis2** compound for six days in a NMR tube, isomerization towards the *trans*-species occurs, as evidenced by ^{1}H NMR spectroscopy (300 MHz, $CDCl_3$, 25°C).

Selected resonances for **trans2**:

^{1}H-NMR (δ, 25°C, $CDCl_3$, 300 MHz): 18.71 (s, 1H, Ru=C*H*), 8.01 (d, 1H, ph^3), not found (ph^4), 7.09 (s, 4H, mes), 6.25 (d, 1H, ph^6), 4.35 (m, 2H, CH_2CH_3), 4.10 (s, 4H, H_2Im), 3.86 (s, 3H, OCH_3), 2.48 (s, 12H, mes-CH_3), 2.40 (s, 6H, mes-CH_3), 1.44 (t, 3H, CH_2CH_3).

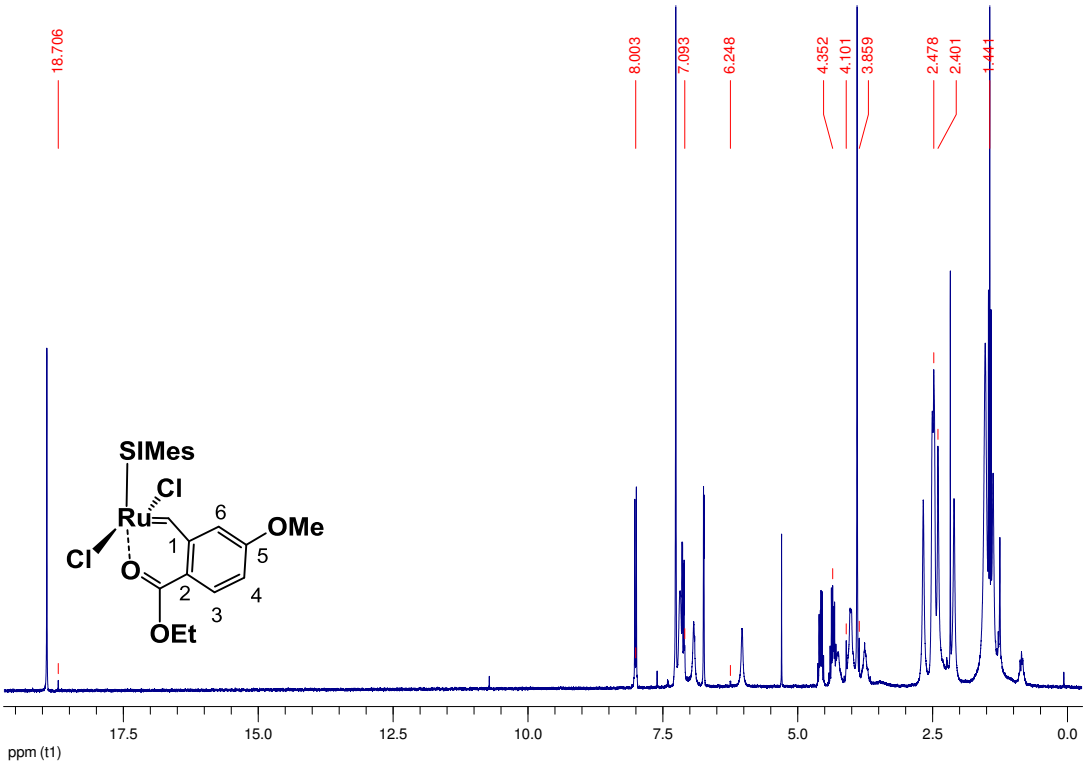

Figure 50. Appearance of **trans2**, detected when storing **cis2** in $CDCl_3$ for 6 days.

3.3. Preparation of *cis*-Dichloro-(κ²(C,O)-4-Methoxy-2-Ethylester Benzylidene)(SIMes)Ru (cis3)

In a Schlenk flask **M31** (148.8 mg, 0.221 mmol, 1.0 eq) was dissolved in degassed, dry CH_2Cl_2 (25 mL). 5-Methoxy-2-vinylbenzoic acid ethyl ester (**L3-3**, 62.9 mg, 0.305 mmol, 1.2 eq) was added. The reaction mixture was stirred under argon atmosphere for 20 h, until the color turned from deep red to deep green. Pyridine was removed by extraction with $HCl_{aq.}$ (5 v-%). The solvent was reduced in vacuo to 1 to 2 mL and the title compound was precipitated with *n*-pentane. The dark green precipitate was filtered and washed with *n*-pentane. For purification column chromatography on silica gel (CH_2Cl_2:MeOH, 20:1 (v:v)) was used. Yield: 95.2 mg (75%) dark green crystals.

TLC: R_f = 0.4 (CH_2Cl_2:MeOH, 20:1 (v:v)).

Anal. Calcd. for $C_{32}H_{38}Cl_2N_2O_3Ru$ (670.64): C, 57.31; H, 5.71; N, 4.18. **Found**: C, 57.28; H, 5.91; N, 4.01. **^{1}H NMR** (δ, 20°C, $CDCl_3$, 300 MHz): 18.57 (s, 1H, Ru=C*H*), 7.54 (d, 1H, $^4J_{HH}$ = 2.5 Hz, ph^3), 7.20 (d, 1H, $^3J_{HH}$ = 8.5 Hz, ph^3), 7.18, 6.94, 6.02 (bs, 4H, mes), 7.08 (dd, 1H, $^3J_{HH}$ = 8.6Hz, $^4J_{HH}$ = 2.5 Hz, ph^5), 6.74 (d, 1H, $^4J_{HH}$= 2.5 Hz, ph^6), 4.62, 4.41 (m, 2H, CH_2CH$_3$), 4.36 - 3.59 (m, 4H, H_2Im,), 3.90 (s, 3H, OCH_3), 2.69, 2.48, 2.39, 2.12, 1.35 (s, 18H, mes-CH_3), 1.47 (t, 3H, $^3J_{HH}$ = 7.1 Hz, CH_2CH_3). **^{13}C NMR** (δ, 20°C, $CDCl_3$, 125 MHz): 282.8 (1C, Ru=*C*H), 217.4 (1C, C_q, *C*NN), 176.7 (1C, C_q, COOEt), 158.8 (1C, C_q, ph^4), 139.8, 138.2, 136.3, 134.8, 130.9, 128.5 (6C, C_q, mes-C), 138.4 (1C, C_q, ph^1), 135.5, 132.5 (1C, C_q, mes-N), 130.2 (1C, ph^5), 129.5 (4 mes-H), 122.5 (1C, C_q, ph^2), 120.2 (1C, ph^6), 115.2 (1C, ph^3), 64.7 (1C, O*C*H$_2$CH$_3$), 55.8 (1C, O*C*H$_3$), 51.0 (2C, H_2Im), 21.2, 20.0, 18.3, 16.4 (6C, mes-*C*H$_3$) 14.1 (1C, OCH$_2$*C*H$_3$).

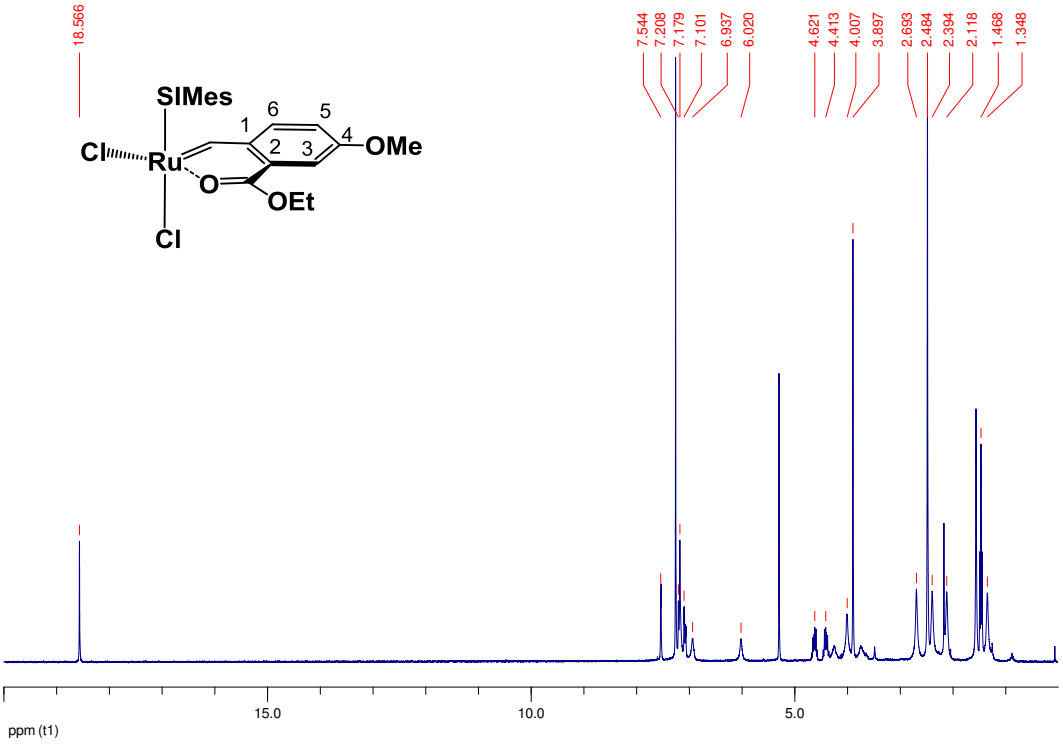

Figure 51. ^{1}H-NMR spectrum of complex **cis3** (300 MHz, 25°C, $CDCl_3$).

3.4. Preparation of of *cis*-Dichloro-(κ²(C,O)-5-Nitro-2-Ethylester Benzylidene)(SIMes)Ru (4)

In a Schlenk flask **M31** (64.0 mg; 0.0859 mmol; 1.0 eq) was dissolved in degassed, dry CH_2Cl_2 (10 mL). The carbene-precursor 4-nitro-2-vinylbenzoic acid ethyl ester (**L4-3**, 22.8 mg; 0.103 mmol; 1.2 eq) was added and the reaction mixture was stirred in a Schlenk flask under nitrogen atmosphere for 17 h. The color turned from deep red to red brown. As described above, the crude product was treated with HCl_{aq} (5 v-%) and subsequently purified by column chromatography with CH_2Cl_2:MeOH 20:1 (v:v), obtaining a red-brownish solid (22.8 mg, 39%).

TLC: 0.4 (CH_2Cl_2:MeOH, 20:1 (v:v)).

Anal. Calcd. for $C_{31}H_{35}Cl_2N_3O_4Ru$ (685.60): C, 54.31; H, 5.15; N, 6.13. **Found**: C, 54.35; H, 5.17; N, 6.09. **^{1}H NMR** (δ, 20°C, $CDCl_3$, 300 MHz): 19.09 (s, 1H, Ru=CH), 8.51 (dd, 1H, $^3J_{HH}$ = 8.6 Hz, $^4J_{HH}$ = 1.9 Hz, ph^4), 8.21 (d, 1H, $^3J_{HH}$ = 8.7 Hz, ph^3), 8.11 (d, 1H, $^4J_{HH}$ = 2.1 Hz, ph^6), 7.19, 7.04, 5.96 (s, 4H, mes), 4.71, 4.50 (m, 1H, C*H*$_2$CH$_3$), 4.38-3.65 (m, 4H, H_2Im),2.67, 2.50, 2.41, 1.99, 1.32 (s, 18H, mes-C*H*$_3$), 1.52 (t, $^3J_{HH}$ = 7.0 Hz, CH$_2$C*H*$_3$). **^{13}C NMR** (δ, 20°C, $CDCl_3$, 75 MHz): 278.0 (1C, Ru=*C*H), 215.3 (1C, C_q, *C*NN), 176.1 (1C, C_q, COOEt), 152.4 (1C, C_q, ph^5), n.d. (8C, C_q, mes-C, mes-N), 142.5 (1C, C_q, ph^1), 132.5 (1C, C_q, ph^3), 131.2, 129.8, 128.2 (4C, mes), 124.0 (1C, C_q, ph^2), 122.3 (1C, ph^4), 121.2 (1C, ph^6), 65.9 (1C, O*C*H$_2$CH$_3$), 51.1 (2C, H_2Im), 18.3 (6C, mes-*C*H$_3$) 14.1 (1C, OCH$_2$*C*H$_3$).

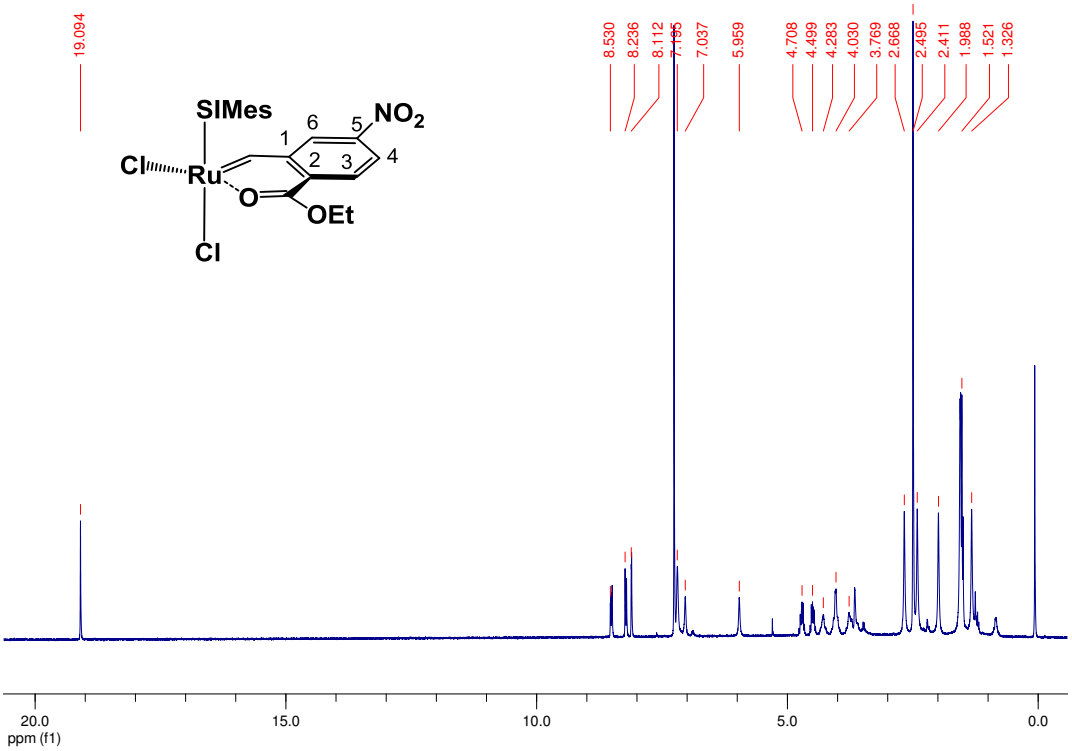

Figure 52. ^{1}H-NMR spectrum of complex **cis4** (300 MHz, 25°C, $CDCl_3$).

3.4.1. Alternative Protocol for the Preparation of 4

In a Schlenk flask **M31** (339 mg; 0.452 mmol; 1.0 eq) was dissolved in degassed, dry CH_2Cl_2 (10 mL). The ligand (100 mg; 0.483 mmol; 1.5 eq) was added and the reaction mixture was stirred in a Schlenk flask under argon atmosphere for 20 h. The color turned from deep red to red green. The complex was then precipitated with *n*-pentane, obtaining a brown solid, which was filtered, washed with *n*-pentane and dried in vacuo. Subsequently the product was separated by column chromatography, leading to two fractions.

Yield of first fraction: 56 g (18 %) of green solid (**trans4**).

^{1}H-NMR (δ, 20°C, $CDCl_3$, 300 MHz): 18.71 (s, 1H, Ru=CH), 8.43 (dd, 1H, $^{3}J_{HH}$ = 8.7 Hz, $^{4}J_{HH}$ = 1.9 Hz, ph^{4}), 8.21 (d, 1H, $^{3}J_{HH}$ = 8.6 Hz, ph^{3}), 7.62 (d, 1H, $^{4}J_{HH}$ = 1.8 Hz, ph^{6}), 7.13 (s, 4H, mes), 4.42 (q, 2H, C*H*$_2$CH$_3$), 4.14 (s, 4H, H$_2$Im), 2.48, 2.46 (s, 18H, mes-C*H*$_3$), 1.34 (t, 3H, $^{3}J_{HH}$ = 7.1 Hz, CH$_2$C*H*$_3$). **^{13}C-NMR** (δ, 20°C, CD_2Cl_2, 75 MHz): 299.7 (1C, Ru=CH), 208.1 (1C, C_q, CNN), 172.9 (1C, C_q, COOCEt), 152.1, 149.0 (1C, C_q, ph^{1,}), 139.4, 138.4, 133.4, 131.0, 129.9 (4C, mes), 124.3, 118.4 (1C, C_q, ph^{2}), 65.1 (1C, O*C*H$_2$CH$_3$), 51.6 (2C, H$_2$Im), 21.1, 19.1 (6C, mes-CH$_3$) 13.7 (1C, OCH$_2$*C*H$_3$).

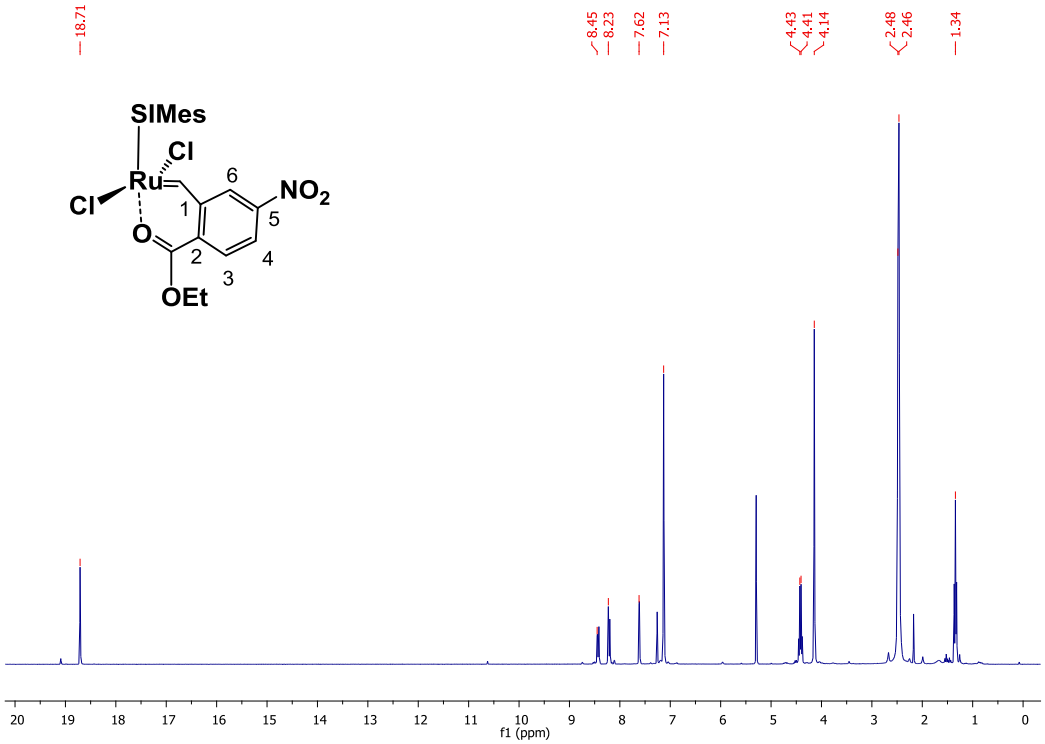

Figure 53. ^{1}H-NMR spectrum of complex **trans4** (300 MHz. 25°C, $CDCl_3$).

Yield of second fraction: 136 g (43 %) of green solid (**trans4$_{py}$**).

^{1}H-NMR (δ, 20°C, $CDCl_3$, 300 MHz): 18.96 (s, 1H, Ru=CH), 8.77 (s, 4H, py^{2,6}), 8.36 (dd, 1H, $^{3}J_{HH}$ = 8.4 Hz, $^{4}J_{HH}$ = 2.1 Hz, ph^{4}), 8.08 (d, 1H, $^{3}J_{HH}$ = 8.8 Hz, ph^{3}), 7.62 (t, 2H, py^{4}), 7.40 (d, 1H, $^{4}J_{HH}$ = 1.8 Hz, ph^{6}), 7.18 (dd, 4H, py^{3,5}), 6.92 (s, 4H, mes), 4.01 (s, 4H, H_2Im), 3.83 (q, 2H, CH_2CH$_3$), 2.44, 2.36 (s, 18H, mes-CH_3), 1.09 (t, 3H, $^{3}J_{HH}$ = 7.3 Hz, CH$_2$CH_3). Impurities: **cis4**.

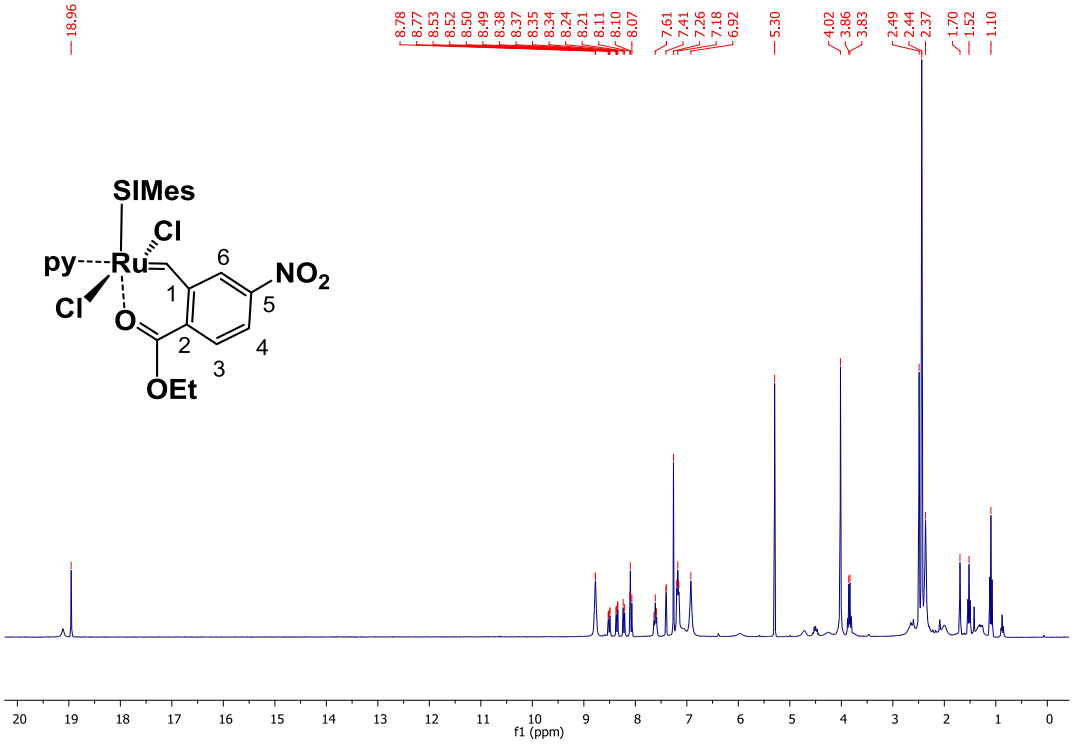

Figure 54. ^{1}H NMR spectrum of complex **trans4$_{py}$** (300 MHz. 25°C, $CDCl_3$).

3.5. Preparation of *cis*-Dichloro-(κ^2(C,O)-4-Nitro-2-Ethylester Benzylidene)(SIMes)Ru (cis5)

In a Schlenk flask **M31** (150.1 mg; 0.200 mmol; 1.0 eq) was dissolved in degassed, dry CH_2Cl_2 (25 mL). 5-Nitro-2-vinylbenzoic acid ethyl ester (**L5-3**, 66.8 mg; 0.300 mmol; 1.5 eq) was added and the reaction mixture was stirred in a Schlenk flask under argon atmosphere until the color turned from deep red to olive, yellowish black. After 20 h of conversion the product was extracted with $HCl_{aq.}$ (5 v-%) to get rid of pyridine. Afterwards the complex was precipitated in CH_2Cl_2 (1-2 mL) with *n*-pentane, obtaining a brown solid, which was filtered and dried in vacuo. The curde product was isolated from side products by column chromatography on silica gel (CH_2Cl_2:MeOH, 20:1 (v:v)). Yield: 88.9 mg ochery solid (65%).

TLC: R_f = 0.4 (CH_2Cl_2:MeOH, 20:1 (v:v)).

Anal Calcd for $C_{31}H_{35}Cl_2N_3O_4Ru$ (685.60): C, 54.31; H, 5.15; N, 6.13. **Found**: C, 54.33; H, 5.20; N, 6.11. **^{1}H-NMR** (δ, 20°C, $CDCl_3$, 300 MHz): 19.37 (s, 1H, Ru=CH), 8.85 (d, 1H, $^4J_{HH}$ = 2.1 Hz, ph^3), 8.45 (dd, 1H, $^3J_{HH}$ = 8.5 Hz, $^4J_{HH}$ = 2.3 Hz, ph^5), 7.47 (d, 1H, $^3J_{HH}$ = 8.5 Hz, ph^6), 7.21, 7.19,

6.96, 5.95 (s, 4H, mes), 4.70, 4.51 (m, 2H, C*H*$_2$CH$_3$), 4.41-3.68 (m, 4H, H$_2$Im), 2.66, 2.52, 2.46, 2.41, 2.09, 1.37 (s, 18H, mes-C*H*$_3$), 1.54 (t, 3H, $^3J_{HH}$ = 7.1 Hz, CH$_2$C*H*$_3$). **^{13}C-NMR** (δ, 20°C, CDCl$_3$, 125 MHz): 276.7 (1C, Ru=*C*H), 215.2 (1C, C$_q$, *C*NN), 175.7 (1C, C$_q$, COOEt), 143.8, 143.6 (2C, C$_q$, ph^{1,5}), 140.5, 139.6, 138.8, 138.2, 136.3, 135.6, 131.1, 128.3 (8C, C$_q$, mes-C, mes-N), 131.7 (1C, ph^4), 128.8 (1C, ph^6), 130.7, 129.9, 129.85, n.d. (4 mes), 126.8 (1C, ph^3), 120.7 (1C, C$_q$, ph^2), 65.9 (1C, O*C*H$_2$CH$_3$), 51.1 (2C, H$_2$Im), 21.3, 20.0, 19.8, 18.2, 16.3 (6C, mes-*C*H$_3$), 14.1 (1C, OCH$_2$*C*H$_3$).

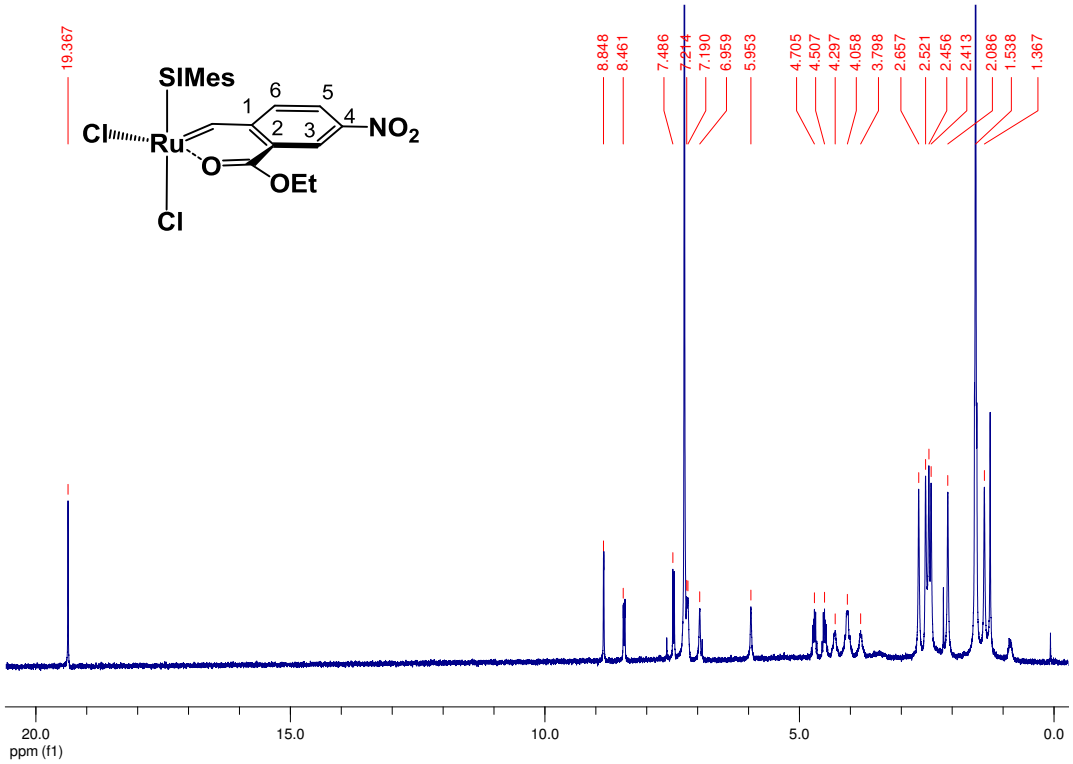

Figure 55. ^{1}H-NMR spectrum of complex **cis5** (300 MHz, 25°C, CDCl$_3$).

4. Chapter IV

4.1. trans-Ester

4.1.1. Preparation of *trans*-Dichloro-(κ²(C,O)-5-Methoxy-2-*iso*-Propylester Benzylidene)(SIMes)Ru(trans2-^{i}Pr)

Scheme 32. Preparation of **trans2-^{i}Pr.**

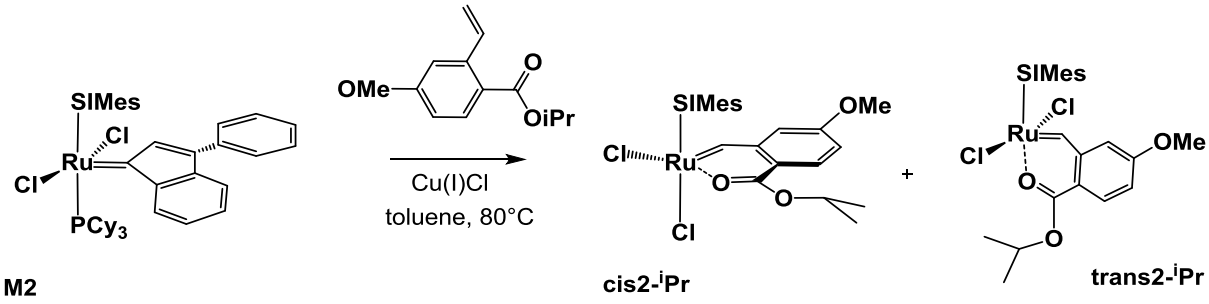

Complex **tran2-^{i}Pr** was isolated using a similar protocol to as for *trans*-dichloro compounds **trans-I**, **trans-IV** and **trans-V**, starting from the respective second generation catalyst. The ligand was prepared similar to literature.[44g] **M2** (4.03 g, 4.24 mmol, 1.0 eq), the ligand (1.12 g, 5.51 mmol, 1.3 eq) and Cu(I)Cl (420.1 mg, 4.21 mmol, 1.0 eq) were dissolved in toluene (60 mL), heated to 80°C and stirred for 17 h. The toluene was removed and the [Cu(I)Cl·PCy_3] complex was precipitated with acetone. The precipitate was filtered and acetone was removed. The *cis*- and *trans*-dichloro isomers were separated using column chromatography on silica gel and CH_2Cl_2:MeOH, 20:1 (v:v) as eluent. Yield: 232 mg (8 %) of green crystals.

TLC: R_f = 0.9 (CH_2Cl_2:MeOH, 10:1 (v:v)).

^{1}H-NMR (δ, 25°C, $CDCl_3$, 300 MHz): 18.71 (s, 1H, Ru=C*H*), 8.01 (d, 1H, $^{3}J_{HH}$ = 8.9 Hz, ph^{3}), 7.09 (s, 4H, mes), 7.05 (dd, 1H, $^{3}J_{HH}$ = 8.9 Hz, $^{4}J_{HH}$ = 2.5 Hz, ph^{4}), 6.25 (d, 1H, , $^{4}J_{HH}$ = 2.5 Hz, ph^{6}), 5.19 (m, 1H, $^{3}J_{HH}$ = 6.3 Hz, C*H*$(CH_3)_2$), 4.10 (s, 4H, H_2Im), 3.85 (s, 3H, OMe), 2.48, 2.40 (s, 18H, mes-CH_3), 1.26 (d, 3H, $^{3}J_{HH}$ = 6.5 Hz, CH(CH_3)$_2$). **^{13}C-NMR** (δ, 25°C, $CDCl_3$, 75 MHz): 305.1 (1C, Ru=*C*H), 211.2 (1C, C_q, CNN), 175.2 (1C, C_q, COOEt), 164.8 (1C, C_q, ph^{5}), 150.6 (1C, C_q, ph^{1}), 138.6, 138.5 (6C, C_q, mes-C), 136.4, 132.6 (2C, C_q, mes-N), 133.9 (1C, ph^{3}), 129.6 (4C, mes-H),

114.8 (1C, C_q, ph[2]), 113.7, 108.2 (1C, C_q, ph[4,6]), 71.3 (1C, *C*H(CH_3)$_2$), 55.7 (1C, O*C*H_3), 51.7 (2C, H_2Im), 21.9, 21.1 (6C, mes-*C*H_3), 19.2 (1C, CH(*C*H_3)$_2$).

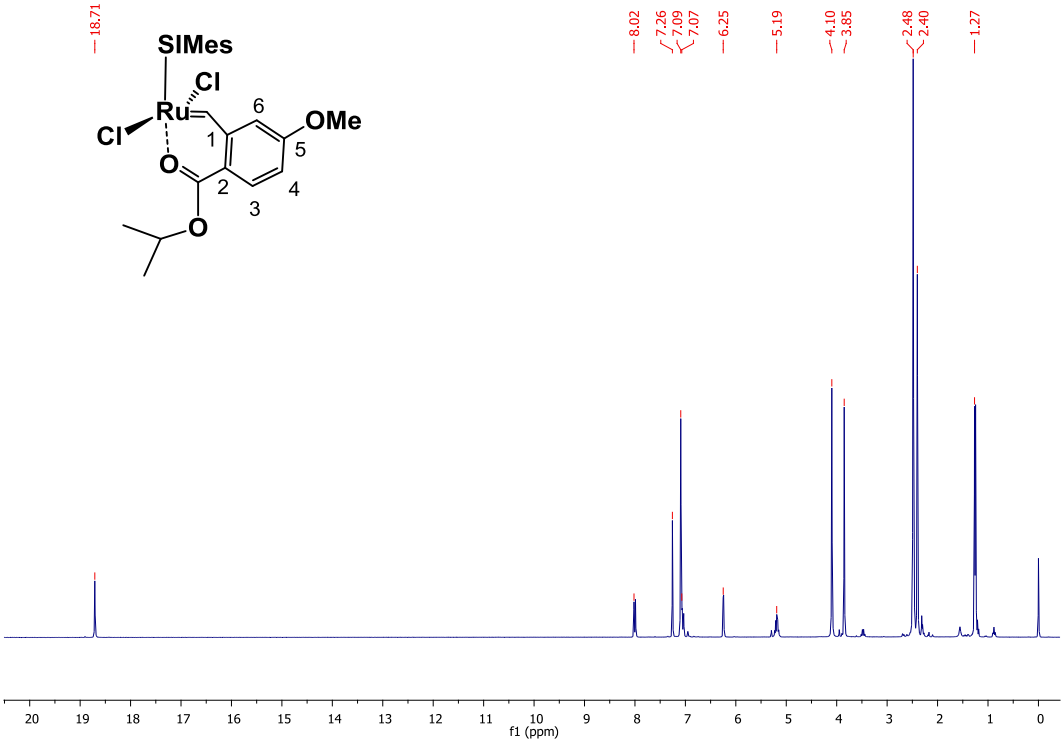

Figure 56. [1]H-NMR spectrum of complex **trans2-^{i}Pr** (300 MHz, 25°C, $CDCl_3$).

4.2. Donor Molecules

In this chapter, complex **cis2** was used for unveiling the role of donor molecules in olefin metathesis when dealing with *cis*-dichloro ruthenium complexes. The impact of pyridine, water, methanol and nitrate was investigated.

4.2.1. Pyridine

4.2.1.1. Preparation of *cis*-Chloro-Pyridino-(κ²(C,O)-5-Methoxy-2-Ethylester Benzylidene)(SIMes)Ru⁺ Cl⁻(cis2⁺$_{py}$)

The cationic pyridine complex **cis2$^{+}_{py}$** was observed as a side product as described in literature,[44g] when using a similar protocol to the one in chapter 3.2. **M31** (242.3 mg, 0.323 mmol, 1.0 eq) and ligand **L2-3** (100 mg, 0.485 mmol, 1.5 eq) were mixed together and stirred

for 22 h under inert N_2 conditions. The crude product showed traces of a cationic compound, which was isolated after column chromatography using CH_2Cl_2:MeOH, 10:1 (v:v) as eluent. Yield: 23 mg (11%) of turquoise-blue crystals.

^{1}H-NMR (δ, 20°C, $CDCl_3$, 300 MHz): 17.96 (s, 1H, Ru=CH), 8.53 (d, 2H, $^3J_{HH}$ = 5.3 Hz, py^{7,11}), 8.05 (d, 1H$^3J_{HH}$ = 8.8 Hz, ph^3), 7.78 (t, 1H, $^3J_{HH}$ = 7.2 Hz, py^9), 7.33 (t, 2H, $^3J_{HH}$ = 6.6 Hz, py^{8,10}), 7.35 (d, 1H, $^4J_{HH}$ = 2.1 Hz, ph^6), 7.22 (dd, 1H, $^3J_{HH}$ = 8.8 Hz, $^4J_{HH}$ = 2.1 Hz, ph4), 7.07, 6.41 (s, 4H, mes), 6.69, 4.47 (m, 2H, $^3J_{HH}$ = 6.2 Hz, CH_2CH_3), 4.19 (s, 4H, H_2Im), 4.01 (s, 3H, OCH_3), 2.67, 2.17, 1.64 (s, 18H, mes-CH_3), 1.57 (t, 6H, $^3J_{HH}$ = 6.2 Hz, CH_2CH_3).

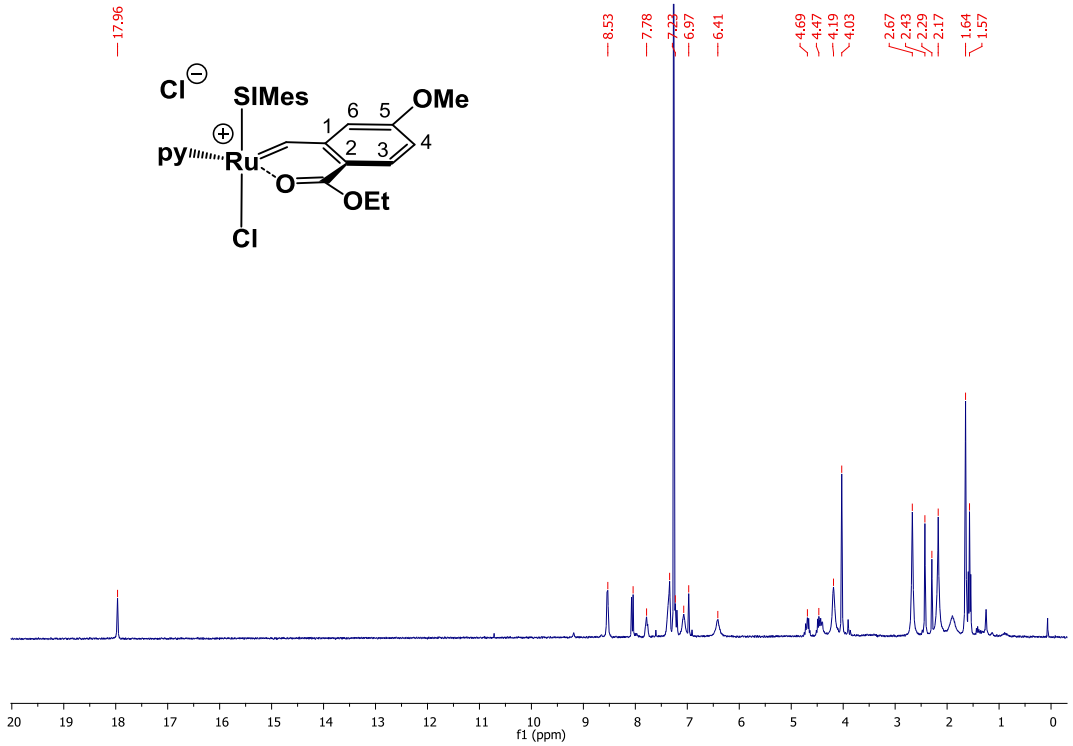

Figure 57. ^{1}H-NMR spectrum of complex **cis2$^+_{py}$** (300 MHz, 25°C, $CDCl_3$).

4.2.1.2. Formation of *cis*-Dichloro-Pyridino(κ^2(C,O)-5-Methoxy-2-Ethylester Benzylidene)(SIMes)Ru (cis2$_{py}$)

Complex **cis2** (9.0 mg, 0.0134 mmol, 1.0 eq) was dissolved in 0.7 mL of $CDCl_3$. Subsequently, 4.2 µL mL of pyridine-d^5 (4.1 mg, 0.0526 mmol, 4.0 eq) were added. A better solubility and a color change from dark green to light green was observed. ^{1}H NMR spectroscopy showed, apart from the pyridine signals, the same peaks as for **cis2**, however broader.

^{1}H NMR (δ, 20°C, $CDCl_3$, 300 MHz): 18.96 (s, 1H, Ru=C*H*), 8.63 (s, 8H, py^{2,6}), 8.01 (d, 1H, $^3J_{HH}$ = 8.9 Hz, ph^3), 7.69 (s, 4H, py^4), 7.19, 7.17, 6.93, 6.06 (bs, 4H, mes), 7.06 (dd, 1H, $^3J_{HH}$ = 8.8 Hz, $^4J_{HH}$ = 2.5 Hz, ph^4), 6.74 (d, 1H, $^4J_{HH}$ = 2.5 Hz, ph^6), 4.62 (m, 1H, C*H*$_2$CH$_3$), 4.40 (m, 1H, C*H*$_2$CH$_3$), 4.02 (bm, 4H, H_2Im,), 3.30 (s, 3H, OC*H*$_3$), 2.85-1.87 (bm, 18H, mes-C*H*$_3$), 1.49 (bs, 3H, CH$_2$C*H*$_3$).

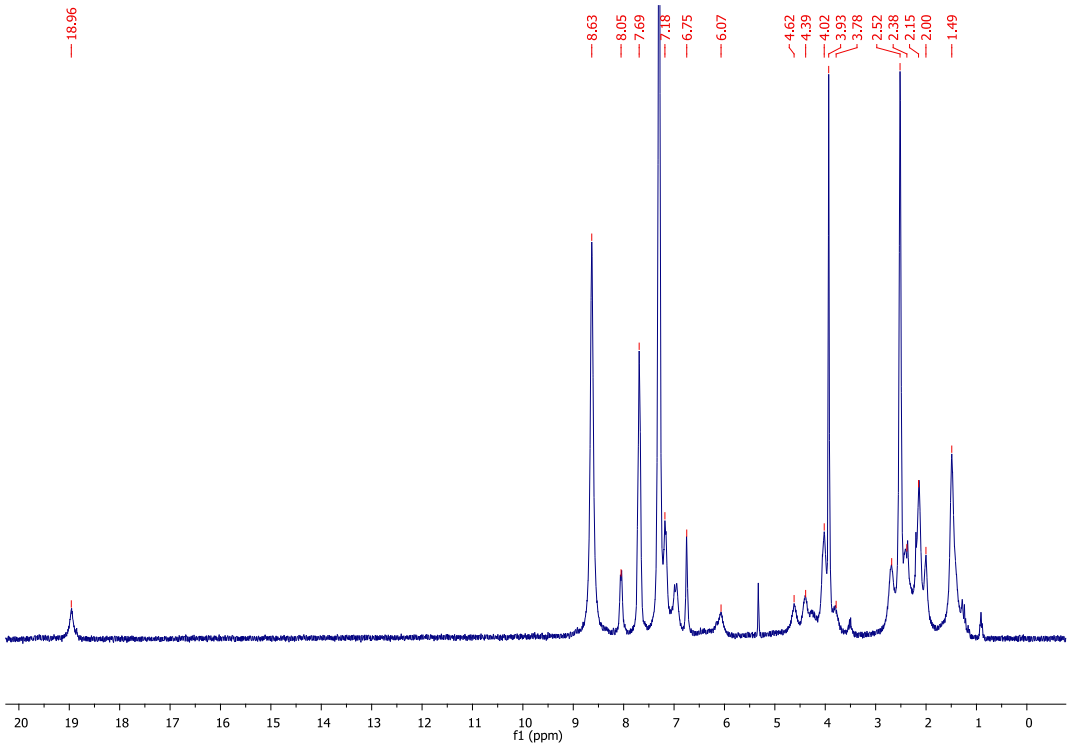

Figure 58. ^{1}H-NMR spectrum of complex **cis2$^+_{py2}$** (300 MHz, 25°C, $CDCl_3$).

A similar experiment was performed, increasing the amount of pyridine: Complex **cis2** (4.3 mg, 0.00642 mmol, 1.0 eq) was dissolved in 0.7 mL of $CDCl_3$ and pyridine-d^5 (16.6 µL, 0.193 mmol, 30 eq) was added. The subsequent appearance of a carbene signal at 19.64 ppm indicates the formation of the neutral 18e complex **cis2$_{py}$**. This indicates also the formation of **cis2$_{py}$** in the previous experiment, however, not completed. Extending the reaction time to three days indicated rearrangment reactions within three days by ^{1}H NMR spectra within the carbene region. Subsequently, the mixture was extracted with 5 mL $HCl_{aq.}$ (5 v-%), yielding to the back formation of **cis2** and the formation of the **cis2$^+_{py}$**.

^{1}H-NMR (δ, 20°C, $CDCl_3$, 300 MHz): 19.69 (s, 1H, Ru=CH), 8.07 (d, 1H, $^3J_{HH}$ = 8.7 Hz, ph^3), 7.16 (dd, 1H, $^3J_{HH}$ = 8.9 Hz, $^4J_{HH}$ = 2.0 Hz, ph^4), 6.75, 6.30 (s, 4H, mes), 6.61 (s, 1H, ph^6), 5.06, 4.59, 4.33 (m, 2H, CH_2CH_3), 3.88 (s, 3H, OCH_3), 3.83 (bs, 4H, H_2Im), 2.47, 2.05 (s, 18H, mes-CH_3), 1.63 (s, 3H, CH_2CH_3).

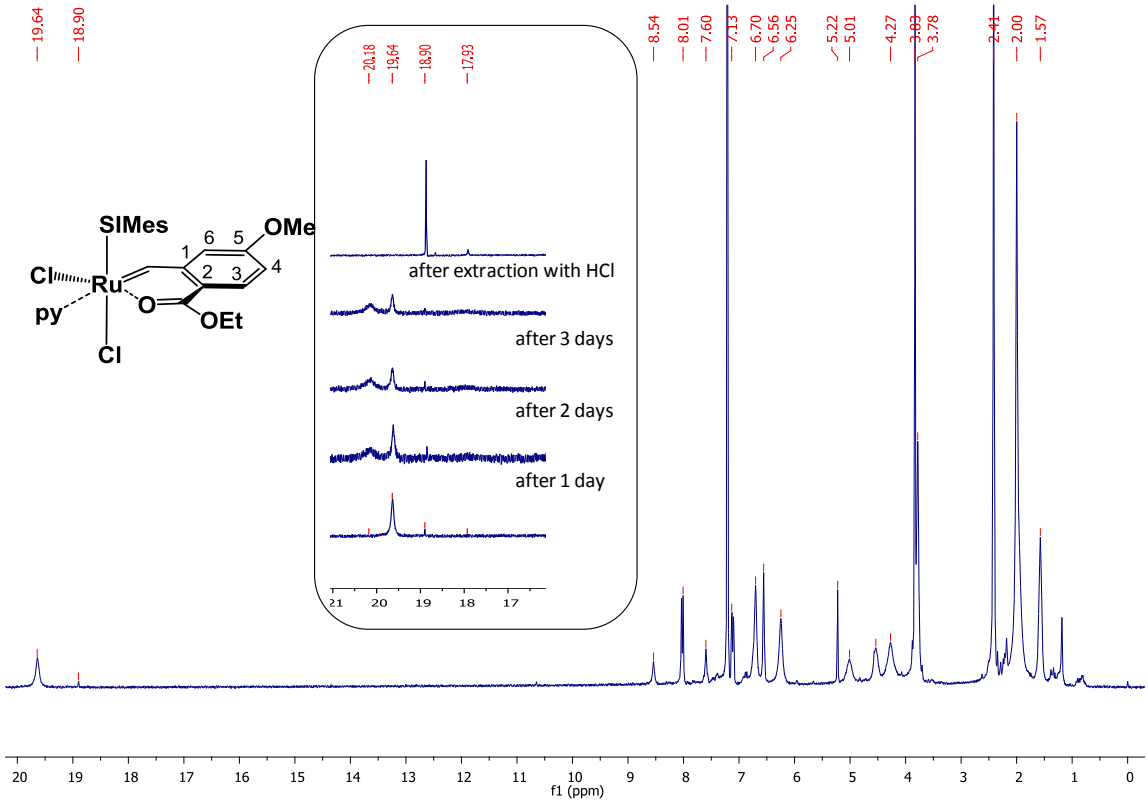

Figure 59. ^{1}H-NMR spectrum of complex **cis2$^+_{py2}$** (300 MHz, 25°C, $CDCl_3$). In the box the product distribution after 3 days and after the extraction with HCl_{aq} (5 v-%) was highlighted.

4.2.1.3. Formation of (κ^2(C,O)-5-Methoxy-2-Ethylester Benzylidene)(SIMes)Cl(py)$_2$Ru$^+$ Cl$^-$(cis2$^+_{2py}$)

Complex **cis2** (3.0 mg, 0.00447 mmol, 1.0 eq) was dissolved in 0.7 mL of pyridine-d^5 (0.7 mL). An immediate color change from dark to light green was observed, indicating that **cis2$^+$-2py** was formed. Extending the reaction time to 24 h yielded in two more carbene signals which might be assigned to two opened chelate complexes.

^{1}H-NMR (δ, 25°C, py-d^5, 300 MHz): 20.12 (s, 1H, Ru=CH), 8.19 (d, 1H, $^4J_{HH}$ = 2.1 Hz, ph^3), 7.29 (dd, 1H, ph^4), 6.89 (d, 1H, ph^6), 6.75, 6.31 (s, 4H, mes), 5.42, 4.83 (bm, 2H, CH_2CH_3), 5.03, 4.83 (m, 2H, CH_2CH_3), 3.88 (bs, 4H, H_2Im), 3.84 (s, 3H, OCH_3), 2.66, 2.18, 2.06 (s, 18H, mes-CH_3), 1.60 (t, 3H, $^3J_{HH}$ = 6.7 Hz, CH_2CH_3).

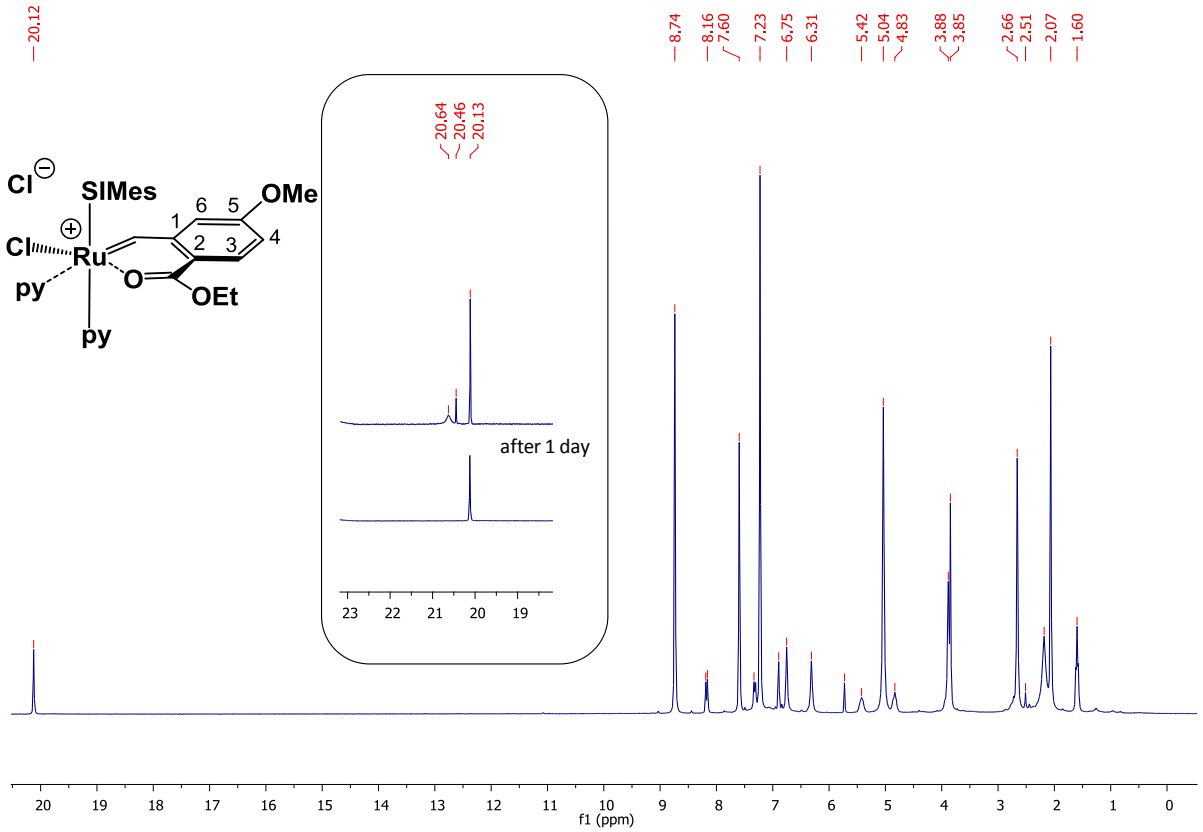

Figure 60. ^{1}H-NMR spectrum of complex **cis2$^+_{2py}$** (300 MHz, 25°C, py-d^5). Down field shifts after one day within the carbene region (box) indicate an opened chelate due to coordination of another pyridine.

4.2.2. Water

4.2.2.1. Formation of *cis*-Dichloro-H_2O-(κ^2(C,O)-5-Methoxy-2-Ethylester Benzylidene)(SIMes)Ru (cis2$_{H2O}$)

Complex **cis2** (3.0 mg, 0.00447 mmol, 1.0 eq) was dissolved in 0.7 mL of $CDCl_3$. Subsequently 3.0 µL of H_2O (3.0 mg, 0.167mmol, 37 eq). A slight color change to turquoise blue was observed after the addition of water. ^{1}H NMR spectroscopy shows no significant changes in shift, however, broader peaks which arise from a constant change of a water and a Cl^- molecule. Moreover, a signal at 4.75 ppm indicates that a water molecule is attached to

the Ru centre.[100] Most probable the signal indicated the interaction with one water molecule to form the neutral 18e complex **cis2$_{H2O}$**, as already discussed for pyridine.

^{1}H NMR (δ, 20°C, $CDCl_3$, 300 MHz): 18.92 (s, 1H, Ru=C*H*), 8.02 (d, 1H, $^3J_{HH}$ = 8.9 Hz, ph^3), 7.19, 7.18, 6.93, 6.04 (bs, 4H, mes), 7.12 (dd, 1H, $^3J_{HH}$ = 8.8 Hz, $^4J_{HH}$ = 2.5 Hz, ph^4), 6.74 (d, 1H, $^4J_{HH}$ = 2.5 Hz, ph^6), 4.75 (s, 2H, H_2O), 4.57 (m, 1H, C*H*$_2$CH$_3$), 4.35 (m, 1H, C*H*$_2$CH$_3$), 4.01 (bm, 4H, H_2Im,), 3.90 (s, 3H, OC*H*$_3$), 2.85-1.87 (bm, 18H, mes-C*H*$_3$), 1.44 (bs, 3H, CH$_2$C*H*$_3$).

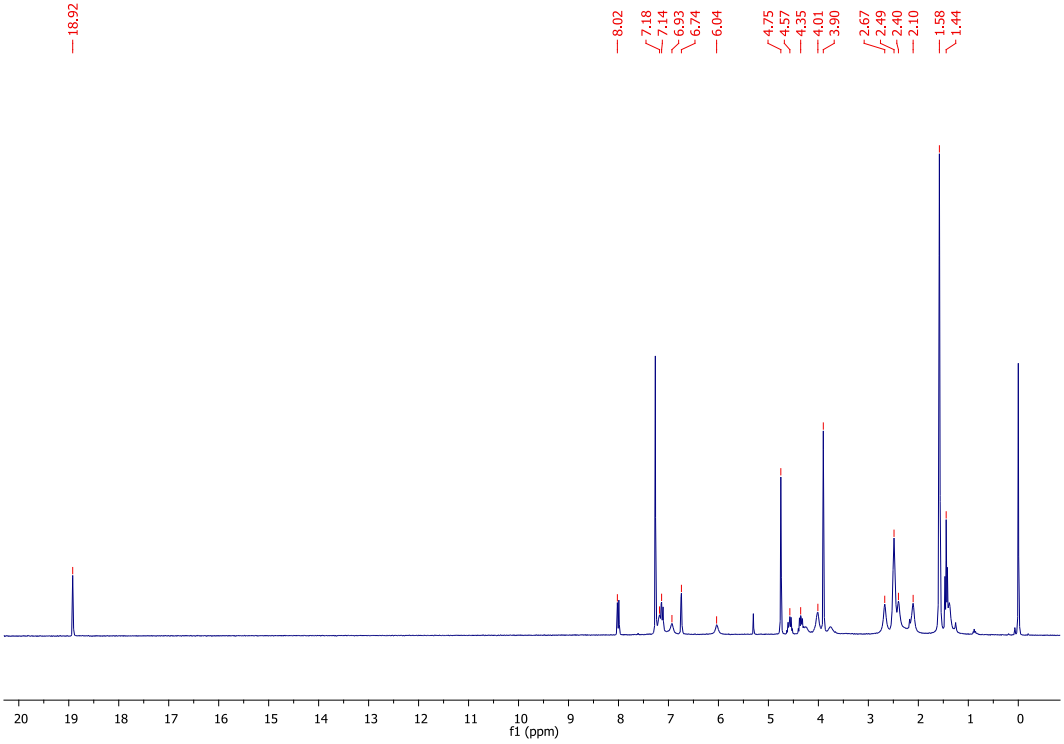

Figure 61. ^{1}H-NMR spectrum of complex **cis2$^+_{H2O2}$** (300 MHz, 25°C, $CDCl_3$).

4.2.3. Methanol

4.2.3.1. Formation of *cis*-Dichloro-Methanol-(κ^2(C,O)-5-Methoxy-2-Ethylester Benzylidene)(SIMes)Ru (cis2$_{MeOD}$)

Complex **cis2** (3.0 mg, 0.00447 mmol, 1.0 eq) was dissolved in 0.6 mL of $CDCl_3$. Subsequently, 0.1 mL of MeOD (79.0 mg, 2.32 mmol, 520 eq). A light color change was indicative for the formation of **cis2$_{MeOD}$**.

(100) Gemel, C.; Trimmel, G.; Slugovc, C.; Kremel, S.; Mereiter, K. Schmid, K.; Kirchner, K. *Organometallics* **1996**, *15*, 3998-4004.

^{1}H NMR (δ, 20°C, $CDCl_3$, 300 MHz): 18.88 (s, 1H, Ru=C*H*), 7.96 (d, 1H, $^3J_{HH}$ = 8.9 Hz, ph^3), 7.69 (s, 4H, py^4), 6.52 (bs, 4H, mes), 6.99 (dd, 1H, $^3J_{HH}$ = 8.8 Hz, $^4J_{HH}$ = 2.5 Hz, ph^4), 6.69 (s, 1H, ph^6), 4.49 (m, 1H, C*H*$_2$CH$_3$), 4.32 (m, 1H, C*H*$_2$CH$_3$), 3.94 (bm, 4H, H$_2$Im,), 3.85 (s, 3H, OC*H*$_3$), 3.40 (s, 3H, MeOH), 2.39, 2.18, 2.11, 1.95 (bs, 18H, mes-C*H*$_3$), 1.37 (t, 3H, CH$_2$C*H*$_3$).

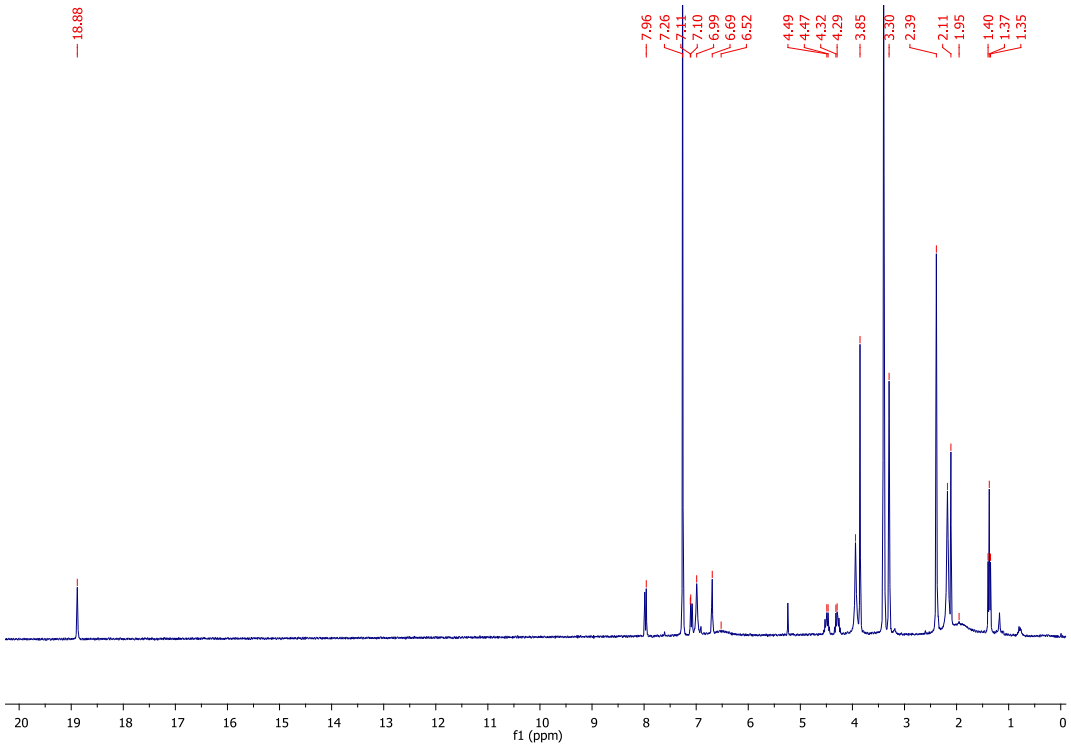

Figure 62. ^{1}H-NMR spectrum of complex **cis2$^+_{MeOD2}$** (300 MHz, 25°C, $CDCl_3$).

4.2.3.2. Formation of *cis*-chloro-dimethanol-(κ^2(C,O)-5-methoxy-2-ethylester benzylidene)(SIMes)Ru$^+$ Cl$^-$(cis2$^+_{2MeOD}$)

Complex **cis2** (3.0 mg, 0.00447 mmol, 1.0 eq) was dissolved in 0.7 mL of $CDCl_3$. Subsequently, 0.1 mL of MeOD (79.0 mg, 2.32 mmol, 520 eq) was added. A light color change was indicative for the formation of **cis2$^+_{2MeOD}$.**

^{1}H-NMR (δ, 20°C, MeOD, 300 MHz): 19.56 (s, 1H, Ru=CH), 8.20 (d, 1H, $^3J_{HH}$ = 8.9 Hz, ph^3), 7.39 (dd, 1H, $^3J_{HH}$ = 8.9 Hz, $^4J_{HH}$ = 2.4 Hz, ph^4), 6.86 (d, 1H, $^4J_{HH}$ = 2.5 Hz, ph^6), 6.50, 4.47 (s, 4H, mes), 4.53 (m, 2H, C*H*$_2$CH$_3$), 4.00 (s, 3H, OCH$_3$), 3.90 (s, 4H, H$_2$Im), 2.38, 2.25, 1.96 (s, 18H, mes-C*H*$_3$), 1.43 (t, 3H, $^3J_{HH}$ = 7.2 Hz, CH$_2$C*H*$_3$).

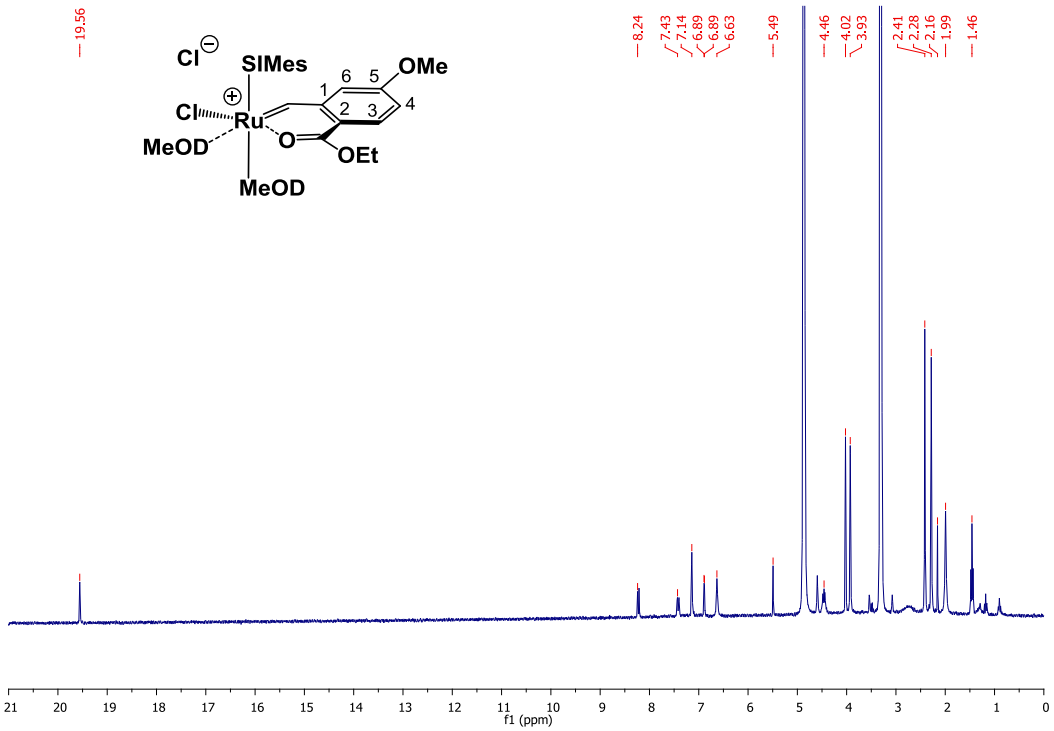

Figure 63. ^{1}H-NMR spectrum of complex **cis2**$^{+}_{\mathbf{2MeOD}}$ (300 MHz, 25°C, MeOD).

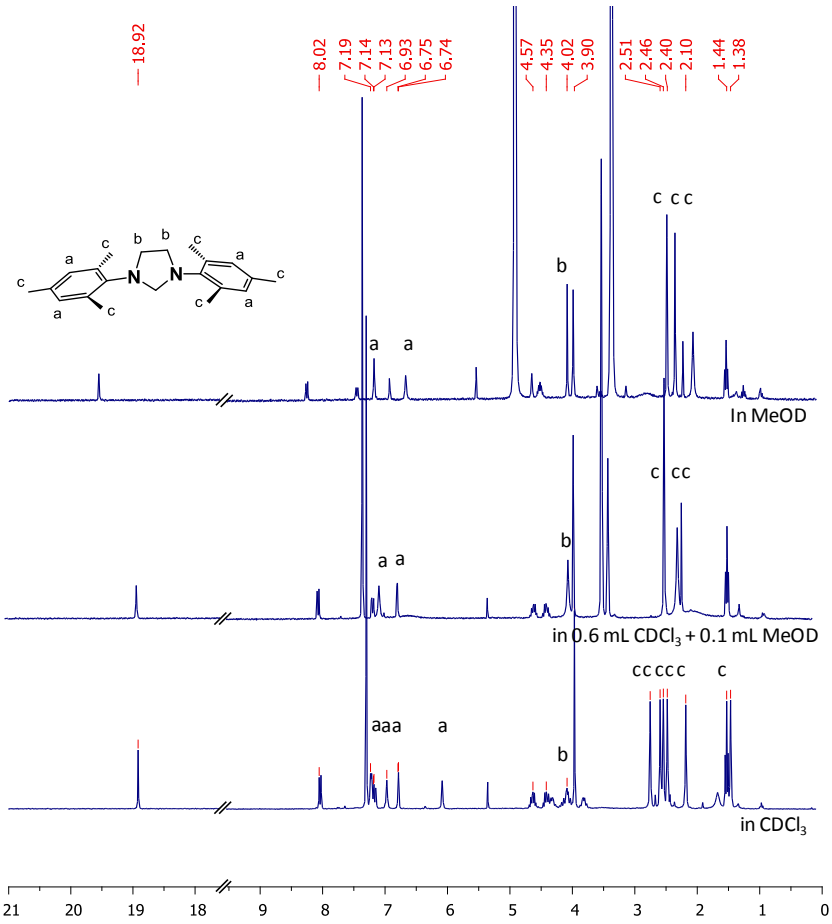

Figure 64. Distinctive changes of NHC shifts for **cis2** after the addition of MeOD (300 MHz, 25°C, $CDCl_3$/MeOD).

In Figure 64 distinctive differences between **cis2** were outlined, dependent on the amount of methanol in dependency of the solvent. Distinctive mesityl signals were outlined with **a**, the protones of the imidazol were signed with **b** and the mes-CH_3 residues were marked with a **c**. Generally it can be concluded that with higher MeOH content NHC-ligand rotation increases, leading to a gain in symmetry.

4.2.4. Nitrate

4.2.4.1. Preparation of Chloro-Nitrate-(κ²(C,O)-(2-Ethylester-5-Methoxy Benzylidene)-(SIMes)Ru (cis2$_{NO3}$)

Scheme 33. Preparation of **cis2$_{NO3}$**.

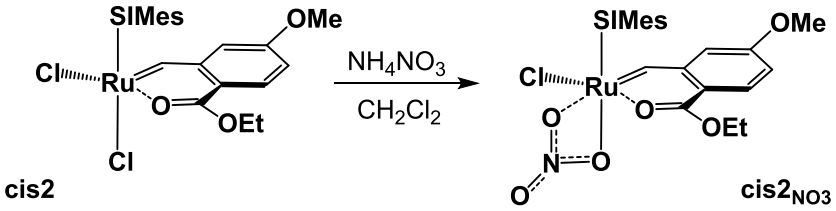

In a Schlenk flask **cis2$_{NO3}$** (9.3 mg, 0.0139 mmol, 1.0 eq) and ammonium nitrate (34.7 mg, 0.434 mmol, 30 eq) were suspended resp. dissolved in methanol (2 mL). The reaction mixture was stirred for 5 min, until the color changed from turquoise-green to turquoise-blue. The reaction solution was blown off by a nitrogen steam and *re*-dissolved in CH_2Cl_2. Subsequently, the salt residue was filtered, the solvent was blown off with a nitrogen stream and the product was dried in vacuo. Yield: 8.9 mg (92 %) turquoise-blue crystals.

^{1}H-NMR (δ, 25°C, $CDCl_3$, 300 MHz): 19.81 (s, 1H, Ru=C*H*), 8.03 (d, 1H, $^3J_{HH}$ = 8.8 Hz, ph^3), 7.30 - 6.87 (bs, 3H, mes), 7.19 (dd, 1H, $^3J_{HH}$ = 8.7 Hz, $^4J_{HH}$ = 2.2 Hz, ph^4), 6.77 (d, 1H, $^4J_{HH}$ = 2.2 Hz, ph^6), 6.04 (bs, 1H, mes), 4.37, 4.27 (m, 2H, C*H*$_2$CH$_3$), 4.40-3.47 (m, 4H, H_2Im), 3.93 (s, 3H, OC*H*$_3$), 3.02-1.81 (bs, 15H, mes-C*H*$_3$), 1.74-1.50 (bs, 3H, mes-C*H*$_3$), 1.36 (t, 3H, CH$_2$C*H*$_3$). **^{13}C-NMR** (δ, 25°C, $CDCl_3$, 75 MHz): 309.2 (1C, Ru=*C*H), 216.2 (1C, C_q, CNN), 177.7 (1C, C_q, COOEt), 166.3 (1C, C_q, ph^5), 144.3 (1C, C_q, ph^1), 138.8 (s, C_q, ph^2), 140.4-136.3 (bs, C_q, mes-CH_3), 133.7 (1C, ph^3), 136.0-134.4 (bs, 2C, mes-N), 131.6-127.4 (bs, 4C, mes), 114.3, 113.1 (2C, ph^{4,6}),

64.2 (1C, *C*$H_2$$CH_3$), 55.8 (1C, O*C*$H_3$), 51.0 (bs, 2C, H_2Im), 21.0, 18.1 (bs, 6C, mes-*C*H_3), 14.0 (1C, CH_2*C*H_3).

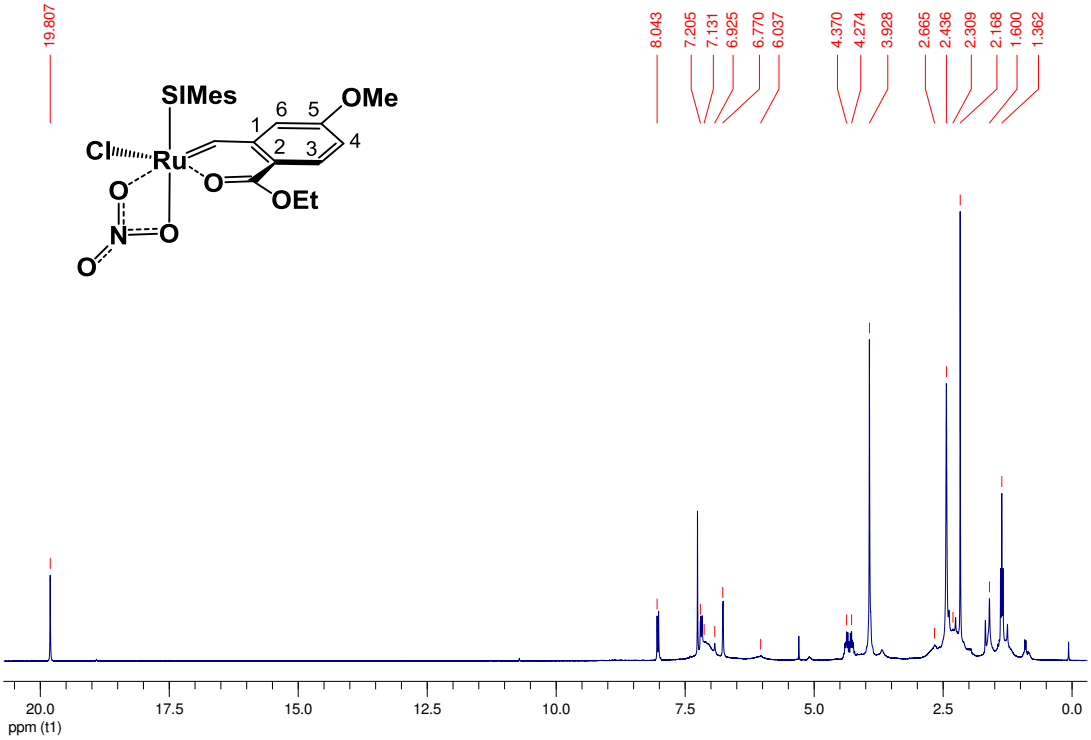

Figure 65. ^{1}H-NMR spectrum of complex **cis2$_{NO3}$** (300 MHz, 25°C, $CDCl_3$).

X-ray Crystallography

All crystals suitable for single crystal X-ray diffractometry were removed from a vial and immediately covered with a layer of silicone oil. A single crystal was selected, mounted on a glass rod on a copper pin, and placed in the cold N_2 stream provided by an Oxford Cryosystems cryometer. Single crystal data collection was performed on a BRUKER APEX II diffractometer with use of Mo Kα radiation (λ= 0.71073 Å) and a CCD area detector. Empirical absorption corrections were applied using SADABS.[101] The structures were solved with use of either direct methods or the Patterson option in SHELXS and refined by the full-matrix least-squares procedures in SHELXL.[102] The space group assignments and structural solutions were evaluated using PLATON.[103] The solvent of crystallization for compound **cis5** was removed from the refinement by using the "squeeze" option available in the PLATON program suite.[104] Non-hydrogen atoms were refined anisotropically. Hydrogen atoms were located in calculated positions corresponding to standard bond lengths and angles.

(101) (a) Bruker. APEX2 and SAINT. Bruker AXS Inc., Madison, Wisconsin, USA. **2012**. (b) Blessing, R. H. *Acta Crystallogr. A.* **1995**, *51*, 33–38.

(102) (a) Sheldrick, G. M. SADABS, Version 2.10, Siemens Area Detector Correction, Universität Göttingen,Germany; **2003**. (b) Sheldrick, G. M. SHELXL2013. Universität Göttingen, Germany, **2013**.

(103) Sheldrick, G. M. SHELXL2013. Universität Göttingen, Germany, **2013**.

(104) Van der Sluis, P., Spek, A. L. *Acta Crystallogr. Sect. A.* **1990**, *46*, 194–201.

1. Chapter I

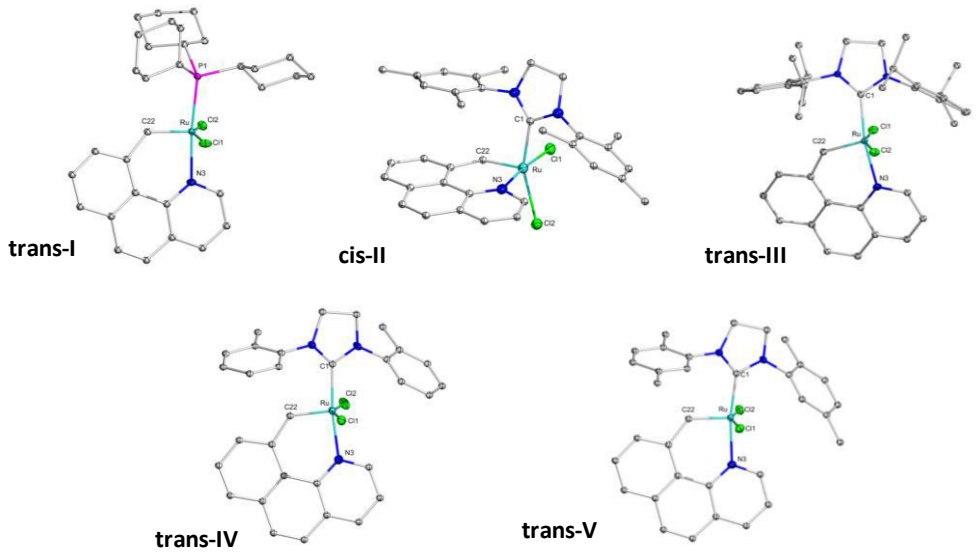

Figure 66. Crystal structures of **trans-I**, **cis-II**, **trans-III**, **trans-IV** and **trans-V**. All non-carbon atoms are shown as 30% ellipsoids. Hydrogen atoms were removed for clarity.

Important bond lengths and angles of complexes **trans-I**, **trans-II, cis-II**, **trans-III**, **trans-IV** and **trans-V** (Figure 66) can be found in Table 17, crystallographic data and details of measurements are summarized in

Table 18 and Table 19.

Table 17. Selected bond lengths (Å) and bond angles (deg) for complexes **trans-I** - **trans-V** and **cis-II**.

	trans-I	**trans-II**	**cis-II**	**trans-III**	**trans-IV**	**trans-V**
Ru–C(22)	1.825(2)	1.814(4)	1.817(4)	1.827(2)	1.826(2)	1.824(1)
Ru–X(1)	2.3465(5)	2.039(4)	2.033(4)	2.039(8)	2.026(2)	2.027(2)
Ru–N(3)	2.127(2)	2.107(3)	2.055(4)	2.116(6)	2.118(2)	2.118(1)
Ru–Cl(1)	2.3572(5)	2.339(1)	2.3991(11)	2.374(3)	2.3554(5)	2.3522(4)
Ru–Cl(2)	2.3527(5)	2.346(1)	2.3983(11)	2.356(3)	2.3640(5)	2.3581(4)
X(1)-Ru-C(22)	95.58(6)	99.42(18)	95.63(18)	100.98(9)	97.49(8)	99.0(2)
N(1)–Ru–Cl(2)	86.04(4)	84.46(9)	85.83(10)	89.78(6)	86.81(5)	87.34(4)
C(22)–Ru–N(3)	90.04(8)	88.82(17)	91.60(17)	89.40(9)	90.16(8)	90.14(5)
C(22)–Ru–Cl(1)	101.50(6)	99.22(13)	91.32(14)	96.82(7)	97.57(6)	99.37(4)
C(22)–Ru–Cl(2)	103.32(6)	99.29(13)	106.01(13)	102.09(7)	104.21(6)	100.08(4)
Cl(1)–Ru–Cl(2)	154.41(2)	160.28(5)	88.66(4)	160.22(3)	157.59(2)	160.16(2)

Table 18. Crystallographic data and details of measurements for compounds **trans-**I, **cis-II** and **trans-III**. (Mo Kα (λ=0.71073Å). $R_1 = \Sigma/ |F_o| - |F_c|/|\Sigma|F_d$; wR2 = $[\Sigma_w(F_o^2-F_2^2)^2/\Sigma_w(F_o^2)^2]^{1/2}$).

Properties	**trans-I**	**cis-II**	**trans-III**
Formula	$C_{32}H_{42}Cl_2NPRu\cdot CH_2Cl_2$	$C_{35}H_{35}Cl_2N_3Ru\cdot CH_2Cl_2$	$C_{41}H_{47}Cl_2N_3Ru\cdot CH_2Cl_2$
Fw (g mol^{-1})	728.53	754.55	838.71
a (Å)	11.2034(3)	10.0672(4)	10.5939(19)
b (Å)	25.0424(7)	12.6689(5)	28.939(6)
c (Å)	11.8440 (3)	27.2270(11)	12.949(3)
α(°)	90	83.981(2)	90
β (°)	101.066(1)	89.056(2)	93.682(9)
γ (°)	90	72.580(2)	90
V (Å^3)	3261.17(15)	3294.6(2)	3961.7(14)
Z	4	4	4
Crystal habit	Green block	Green plate	Green block
Crystal system	Monoclinic	Triclinic	Monoclinic
Space group	$P2_1/c$	*P*-1	$P2_1/n$
d_{calc} (mg/m^3)	1.484	1.521	1.406
μ (mm^{-1})	0.88	0.83	0.70
T (K)	100(2)	100(2)	100(2)
2ϑ range (°)	2.4–27.1	2.2–27.2	2.4–27.2
F(000)	1504	1544	1736
R_{int}	0.056	0.083	0.053
independent reflns	7209	11396	8083
No. of params	361	805	459
R1, wR2 (all data)	R1 = 0.0348 wR2 = 0.0613	R1 = 0.0665 wR2 = 0.1563	R1 = 0.0437 wR2 = 0.0839
R1, wR2 (>2σ)	R1 = 0.0262 wR2 = 0.0571	R1 = 0.0525 wR2 = 0.1437	R1 = 0.0321 wR2 = 0.0781

Table 19. Crystallographic data and details of measurements for compounds **trans-IV** and **trans-V**. (Mo Kα (λ=0.71073Å). $R_1 = \Sigma / |F_o| - |F_c| / |\Sigma| F_d$; $wR2 = [\Sigma_w(F_o^2 - F_2^2)^2 / \Sigma_w(F_o^2)^2]^{1/2}$).

Properties	**trans-IV**	**trans-V**
Formula	$C_{31}H_{27}Cl_2N_3Ru$	$C_{33}H_{31}Cl_2N_3Ru$
Fw (g mol^{-1})	613.52	641.58
a (Å)	12.8239(4)	13.8160(4)
b (Å)	13.4359(4)	13.4312(4)
c (Å)	16.8249(5)	16.4223(5)
α(°)	90	90
β (°)	110.8190(12)	107.6010(12)
γ (°)	90	90
V (Å^3)	2709.66(14)	2904.75(15)
Z	4	4
Crystal habit	Green block	Green block
Crystal system	Monoclinic	Monoclinic
Space group	$P2_1/c$	$P2_1/c$
d_{calc} (mg/m^3)	1.504	1.467
μ (mm^{-1})	0.80	0.75
T (K)	100(2)	100(2)
2ϑ range (°)	2.5–27.1	2.6–27.1
F(000)	1248	1312
R_{int}	0.030	0.022
independent reflns	5523	5935
No. of params	336	356
R1, wR2 (all data)	R1 = 0.0296 wR2 = 0.0531	R1 = 0.0195 wR2 = 0.0474
R1, wR2 (>2*σ*)	R1 = 0.0233 wR2 = 0.0504	R1 = 0.0181 wR2 = 0.0464

2. Chapter II[44h]

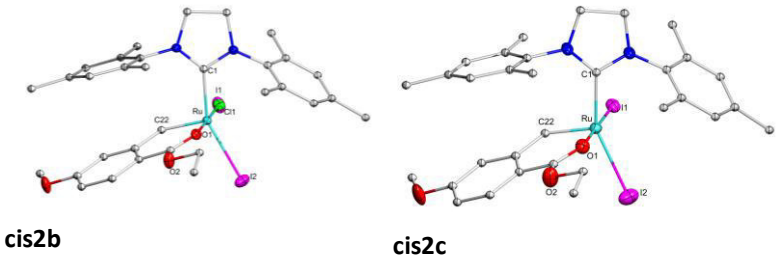

cis2b **cis2c**

Figure 67. Crystal structures of **cis2b** and **cis2c**. All non-carbon atoms are shown as 30% ellipsoids. Hydrogen atoms wereremoved for clarity.

Important bond lengths and angles of complexes **cis2-cis2d** (Figure 67) can be found in Table 21, crystallographic data and details of measurements are summarized in Table 21.

Table 20. Selected bond lengths (Å) and bond angles (deg) for complexes **cis2** - **cis2d**.

	cis2	**cis2b**[b]	**cis2c**	**cis2d**
Ru–C(22)	1.824(3)	1.823(4)	1.823(7)	1.82(3)
Ru–C(1)	2.010(2)	2.009(4)	2.026(6)	2.05(5)
Ru–O(1)	2.076(2)	2.089(3)	2.083(4)	2.11(2)
Ru–X(1)	2.3632(6)	2.366(9)	2.6715(5)	2.651(3)
Ru–X(2)	2.3447(9)	2.6603(5)	2.6983(7)	2.35(5)
C(1)-Ru-C(22)	98.7(1)	100.7(2)	100.0(3)	-
O(1)–Ru–X(2)	85.53(6)	86.06(9)	85.0(1)	-
C(22)–Ru–O(1)	89.9(1)	90.0(2)	89.6(2)	-
C(22)–Ru–X(1)	89.6(1)	89.9(3)	90.0(1)	-
C(22)–Ru–X(2)	111.3(1)	106.9(1)	103.8(2)	-
X(1)–Ru–X(2)	91.21(3)	94.0(2)	94.91(2)	-

[a]Complex **cis2b**, **cis2c**, and **cis2c** from an isostructural series with two Ru-complexes and one CH_2Cl_2 molecule in the asymmetric unit. Only the bond lengths of the first of these two complexes are given.[b]partial occupation of X1 with 11% iodide; [c] partial occupation of X2 with 50% iodide; twinned crystals of poor quality, bond angles therefore omitted.

Table 21. Crystallographic data and details of measurements for compounds **cis2b** and **cis2c** (Mo Kα (λ=0.71073Å). $R_1 = \Sigma / |F_o| - |F_c| / |\Sigma| F_d$; $wR2 = [\Sigma_w(F_o^2 - F_2^2)^2 / \Sigma_w(F_o^2)^2]^{1/2}$).

Properties	**cis2b**	**cis2c**
Formula	$C_{32.50}H_{39}Cl_{1.89}I_{1.1}N_2O_3Ru$	$C_{32.50}H_{39}ClI_2N_2O_3Ru$
Fw (g mol^{-1})	814.75	895.98
a (Å)	8.0758(9)	8.3539(3)
b (Å)	20.4880(19)	21.1185(7)
c (Å)	21.520(2)	21.0212(8)
α (°)	108.225(3)	107.5010(10)
β (°)	97.870(4)	98.358(2)
γ (°)	96.013(4)	95.7310(10)
V ($Å^3$)	3308.7(6)	3458.6(2)
Z	4	4
Crystal habit	Green Block	Green Block
Crystal system	Triclinic	Triclinic
Space group	*P*-1	*P*-1
d_{calc} (mg/m^3)	1.635	1.721
μ (mm^{-1})	1.697	2.350
T (K)	100(2)	100(2)
2*ϑ* range (°)	2.57–26.49	2.52–27.96
F(000)	1628	1756
R_{int}	0.062	0.0384
independent reflns	12954	14269
No. of params	796	783
R1, wR2 (all data)	R1 = 0.0720 wR2 = 0.0876	R1 = 0.0541 wR2 = 0.1400
R1, wR2 (>2*σ*)	R1 = 0.0387 wR2 = 0.0805	R1 = 0.0456 wR2 = 0.1326

3. Chapter III[84]

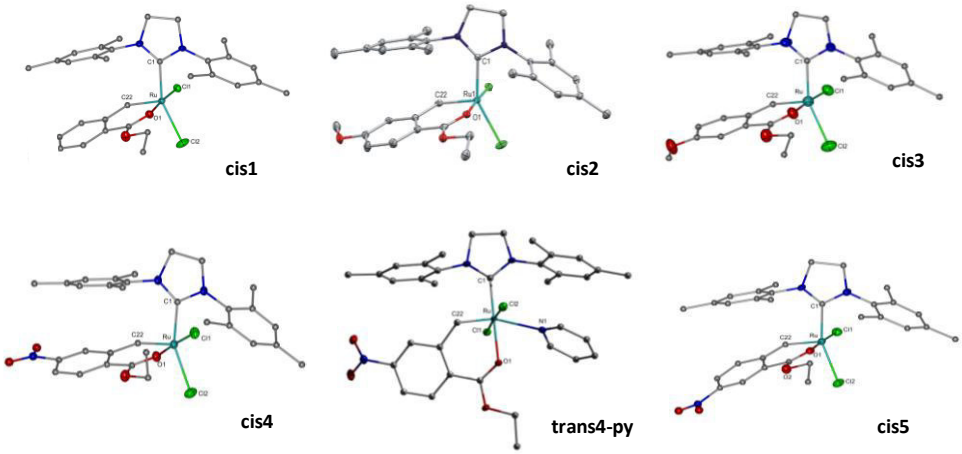

Figure 68. Crystal structures of **cis1** - **cis5** and **trans4$_{py}$**. All non-carbon atoms are shown as 30% ellipsoids. Hydrogen atoms were removed for clarity.

Important bond lengths and angles of complexes **cis1** - **cis5** and **trans4$_{py}$** (Figure 68) can be found in Table 22, crystallographic data and details of measurements are summarized in Table 23 and Table 24.

Table 22. Selected bond lengths (Å) and bond angles (deg) for complexes **cis1** – **cis5** and **trans4$_{py}$**.

	cis1	**cis2**	**cis3**	**cis4**	**trans4$_{py}$**	**cis5**
Ru–C(22)	1.821(2)	1.824(3)	1.833(9)	1.813(3)	1.839(2)	1.805(5)
Ru–C(1)	2.024(2)	2.010(2)	2.008(8)	2.022(3)	2.023(2)	2.033(5)
Ru–O(1)	2.088(1)	2.076(1)	2.072(6)	2.093(2)	2.1743(1)	2.083(3)
Ru–Cl(1)	2.368(1)	2.363(2)	2.374(3)	2.352(1)	2.3926(4)	2.356(1)
Ru–Cl(2)	2.356(2)	2.344(2)	2.354(3)	2.367(2)	2.3724(4)	2.351(1)
Ru-N(1)	-	-	-	-	2.378(2)	-
C(1)-Ru-C(22)	98.68(7)	98.7(1)	97.7(4)	97.5(1)	95.22(8)	99.0(2)
O(1)–Ru–Cl(2)	85.81(4)	85.53(6)	84.6(2)	85.63(6)	89.39(4)	86.1(1)
C(22)–Ru–O(1)	89.86(7)	89.9(1)	89.4(3)	90.2(1)	86.51(7)	90.1(2)
C(22)–Ru–Cl(1)	91.88(6)	89.6(1)	92.4(3)	90.6(1)	85.56(6)	92.4(2)
C(22)–Ru–N(1)	-	-	-	-	157.73(7)	-
C(22)–Ru–Cl(2)	106.15(6)	111.3(1)	107.9(3)	107.8(1)	96.76(6)	102.8(2)
Cl(1)–Ru–Cl(2)	90.49(2)	91.21(3)	92.08(9)	91.69(3)	176.81(2)	91.92(5)
Cl(1)-Ru-N(1)	-	-	-	-	87.33(4)	-

Table 23. Crystallographic data and details of measurements for compounds **cis1**, **cis2** and **cis3** (Mo Kα (λ=0.71073Å). $R_1 = \Sigma/ |F_o| - |F_c|/|\Sigma|F_d$; $wR2 = [\Sigma_w(F_o^2-F_2^2)^2/\Sigma_w(F_o^2)^2]^{1/2}$).

Properties	**cis1**	**cis2**	**cis3**
Formula	$C_{31}H_{36}Cl_2N_2O_2$ Ru	$C_{32}H_{38}Cl_2N_2O_3Ru$	$C_{32}H_{38}Cl_2N_2O_3Ru$
Fw (g mol^{-1})	640.59	670.61	670.61
a (Å)	8.0672(4)	7.9196(3)	11.9390(7)
b (Å)	17.3773(8)	14.5983(5)	33.3485(18)
c (Å)	20.6993	25.8440(9)	8.0047(5)
α (°)	90	90	90
β (°)	90	90	101.181(4)
γ (°)	90	90	90
V ($Å^3$)	2901.8(3)	2987.89(18)	3126.6(3)
Z	4	4	4
Crystal size (mm)	0.30 x 0.21 x 0.20	-	0.37 × 0.21 × 0.05
Crystal habit	green plate	green block	green plate
Crystal system	orthorhombic	Orthorhombic	Monoclinic
Space group	$P2_12_12_1$	$P2_12_12_1$	$P2_1/c$
d_{calc} (mg/m^3)	1.466	1.491	1.425
μ (mm^{-1})	0.755	0.740	0.71
T (K)	100(2)	100(2)	100(2)
2*ϑ* range (°)	1.53-31.50	2.69–27.09	2.5–19.5
independent reflns	63107	6569	5817
No. of params	350	369	369
R1, wR2 (all data)[a]	R1 = 0.0280 wR2 = 0.0626	R1 = 0.0280 wR2 = 0.0703	R1 = 0.1320 wR2 = 0.222
R1, wR2 (>2*σ*)[b]	R1 = 0.0255 wR2 = 0.0618	R1 = 0.0390 wR2 = 0.0742	R1 = 0.093 wR2 = 0.2047

Table 24. Crystallographic data and details of measurements for compounds **cis4**, **trans4$_{py}$** and **cis5** (Mo Kα (λ=0.71073Å). $R_1 = \Sigma / |F_o| - |F_c| / |\Sigma| F_d$; $wR2 = [\Sigma_w(F_o^2 - F_2^2)^2 / \Sigma_w(F_o^2)^2]^{1/2}$).

Properties	**cis4**	**trans4$_{py}$**	**cis5**
Formula	$C_{31}H_{35}Cl_2N_3O_4Ru$	$C_{109}H_{122}Cl_8N_{12}O_{12}\ Ru_3$	$C_{31}H_{35}Cl_2N_3O_4Ru$
Fw (g mol^{-1})	685.59	2379.00	685.59
a (Å)	8.1955(3)	20.3265(8)	23.7001(11)
b (Å)	11.4563(4)	22.5318(9)	16.9338(7)
c (Å)	17.3420(8)	23.4639(9)	7.9974(4)
α (°)	101.894(2)	90	90
β (°)	100.549(2)	99.179(2)	90
γ (°)	105.261(2)	90.	90
V (Å^3)	1487.73(10)	10608.7(7)	3209.6(3)
Z	2	4	4
Crystal size (mm)	0.26 × 0.07 × 0.05	0.23 x 0.10 x 0.09	0.08 × 0.07 × 0.02
Crystal habit	brown block	brown block	orange plate
Crystal system	Triclinic	monoclinic	Orthorhombic
Space group	*P*-1	$P2_1/c$	$Pca2_1$
d_{calc} (mg/m^3)	1.530	1.490	1.419
μ (mm^{-1})	0.75	0.71	0.69
T (K)	100(2)	100(2) K	100(2)
2*ϑ* range (°)	2.6–27.7	1.4-27.5.	1.7–27.2
independent reflns	5778	4896	7107
No. of params	377	377	377
R1, wR2 (all data)[a]	R1 = 0.0439 wR2 = 0.0867	R1 = 0.0440 wR2 = 0.0688	R1 = 0.0607 wR2 = 0.0920
R1, wR2 (>2*σ*)[b]	R1 = 0.0338 wR2 = 0.0813	R1 = 0.0285 wR2 = 0.0613	R1 = 0.0430 wR2 = 0.0855

4. Chapter IV

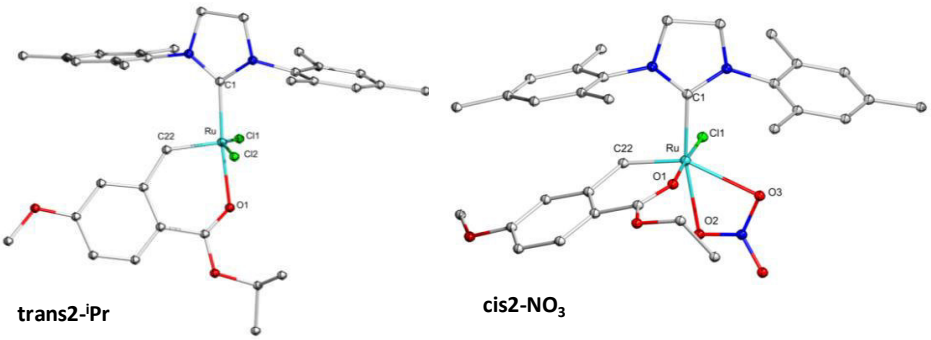

Figure 69. Crystal structures of **trans2-^{i}Pr** and **cis2-NO_3**. All non-carbon atoms are shown as 30% ellipsoids. Hydrogen atoms were removed for clarity.

Important bond lengths and angles of complexes **trans2-^{i}Pr** and **cis2$_{NO3}$** (Figure 69) can be found in Table 25, crystallographic data and details of measurements are summarized in Table 26.

Table 25. Selected bond lengths (Å) and bond angles (deg) for complexes **trans2-^{i}Pr** and **cis2$_{NO3}$**.

	trans2-^{i}Pr	**cis2$_{NO3}$**
Ru–C(22)	1.822(4)	1.828(3)
Ru–C(1)	2.022(4)	1.995(4)
Ru–O(1)	2.171(2)	2.060(3)
Ru–Cl(1)	2.3523(9)	2.3676(9)
Ru–X(2)	2.3202(9)	2.183(3)
Ru-O(3)	-	2.365(2)
C(1)-Ru-C(22)	96.1(1)	97.6(1)
C(1)–Ru–O(3)	-	110.2(1)
O(1)-Ru-X(2)	83.56(6)	83.87(9)
C(22)–Ru–O(1)	88.9(1)	91.0(1)
C(22)–Ru–Cl(1)	102.9(1)	90.5(1)
C(22)–Ru-X(2)	99.7(1)	95.4(1)
C(22)–Ru-O(3)	-	151.9(1)
Cl(1)–Ru–X(2)	154.33(4)	93.15(7)

Table 26. Crystallographic data and details of measurements for compounds **trans2-^{i}Pr** and **cis2$_{NO3}$.** (Mo Kα (λ=0.71073Å). $R_1 = \Sigma/ |F_o| - |F_c|/|\Sigma|F_d$; wR2 = $[\Sigma_w(F_o^2-F_2^2)^2/\Sigma_w(F_o^2)^2]^{1/2}$).

Properties	**trans2-^{i}Pr**	**cis2$_{NO3}$**
Formula	$C_{33}H_{40}Cl_2N_2O_3Ru$	$C_{32}H_{38}ClN_3O_6Ru$, CH_2Cl_2
Fw (g mol^{-1})	684.64	747.23
a (Å)	16.9121(11)	8.1303(5)
b (Å)	9.1769(7)	23.7524(12)
c (Å)	20.5583(13)	17.8450(11)
α (°)	90	90
β (°)	100.842(3)	96.797(2)
γ (°)	90	90
V (Å^3)	3133.7(4)	3421.9(3)
Z	4	4
Crystal habit	Green block	Green block
Crystal system	Monoclinic	Monoclinic
Space group	$P2_1/n$	$P2_1/n$
d_{calc} (mg/m^3)	1.451	1.450
μ (mm^{-1})	0.71	0.59
T (K)	100(2)	100(2)
2ϑ range (°)	2.5–26.9	1.4-28.1
F(000)	1416	1544
R_{int}	0.088	0.054
independent reflns	6408	4648
No. of params	379	423
R1, wR2 (all data)	R1 = 0.0741 wR2 = 0.0886	R1 = 0.0601 wR2 = 0.0696
R1, wR2 (>2σ)	R1 = 0.0417 wR2 = 0.0781	R1 = 0.0325 wR2 = 0.0627

Isomerization

1. Chapter I

Scheme 34. *cis-trans* Isomerization of **trans-I** – **trans-V.**

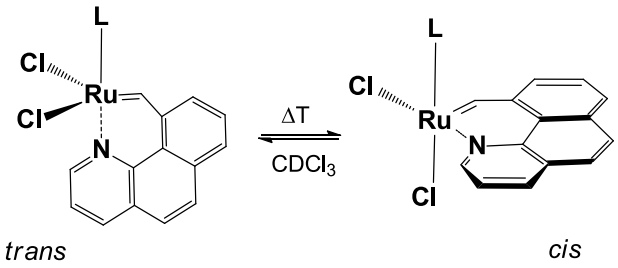

7.0 mM stock solutions of the respective *trans*-compounds **trans-I – trans-V** in degassed $CDCl_3$ were prepared under inert atmosphere (N_2) and subsequently exposed. The composition of the solution was determined by recording ^{1}H NMR spectra (300 MHz) of each system. Moreover, different exposure times (10 min, 4 h, 8 h) were applied for the above-mentioned protocol at 140°C. Also lower reaction temperatures (80°C) were applied for 1 h to investigate the isomerization behavior, whereas just in case of **trans-IV** isomerization was observed. Characteristic ^{1}H NMR spectra of product mixtures **III**, **IV** and **V** can be found in Figure 70-Figure **72**. Typical carbene signals for all new compounds **I - IV** are summarized in Table 27.

Table 27. Characteristic ^{1}H NMR signals for isomerization and decomposition products, recorded in $CDCl_3$.

Initiator	cis	trans	decomp
6	n.d.	19.53	11.28[a]
7	19.19	19.19	11.28
8	19.20	19.06	11.28
9	19.20	19.01	11.28[b]
10	19.22	19.05	11.28[b]

[a]decomposition material not identified; [b]deactivation

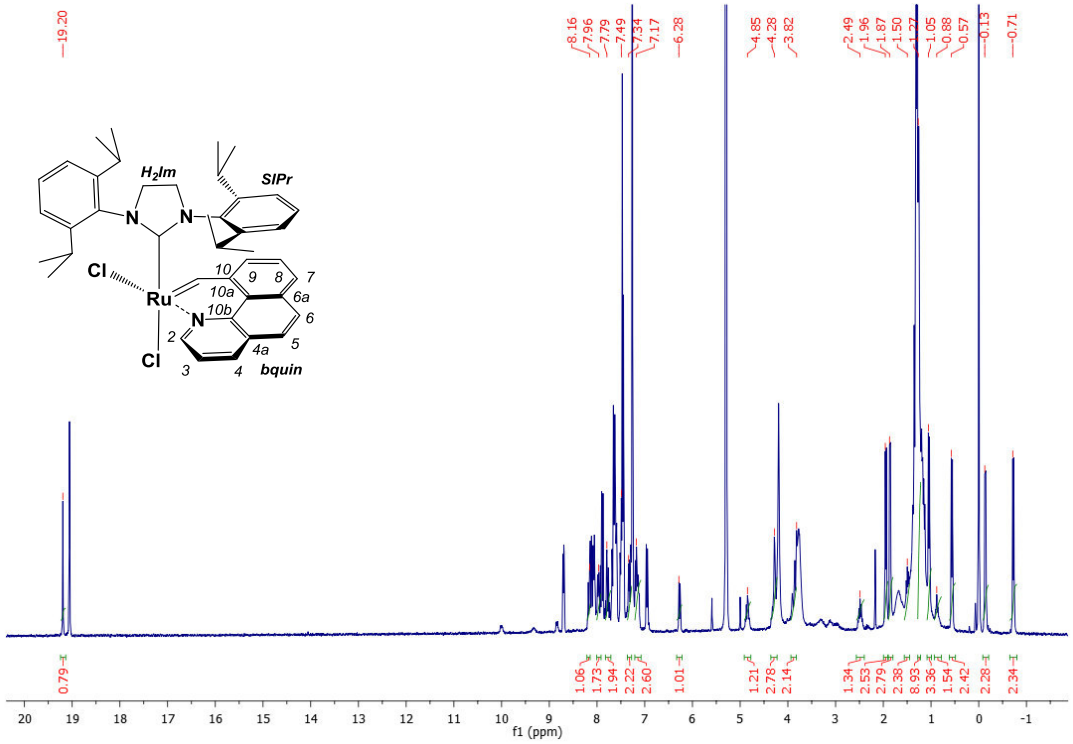

Figure 70. Characteristic ^{1}H-NMR signals of complex **cis-III** (300 MHz, 25°C, $CDCl_3$).

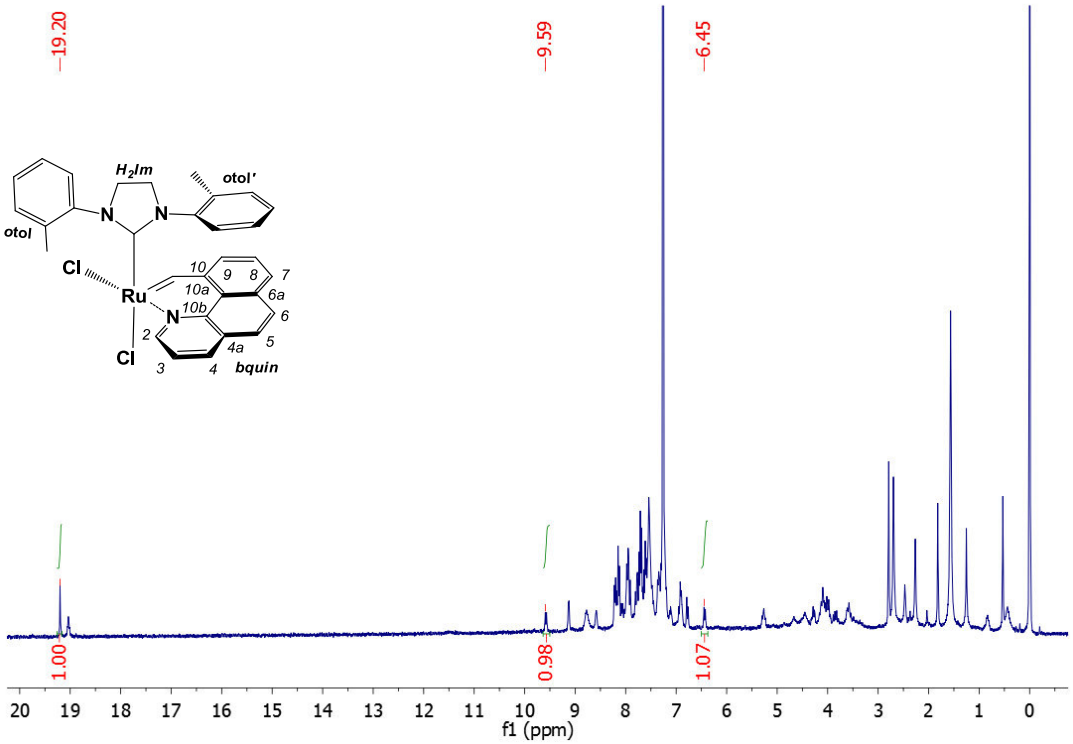

Figure 71. Characteristic ^{1}H-NMR signals of complex **cis-IV** (300 MHz, 25°C, $CDCl_3$).

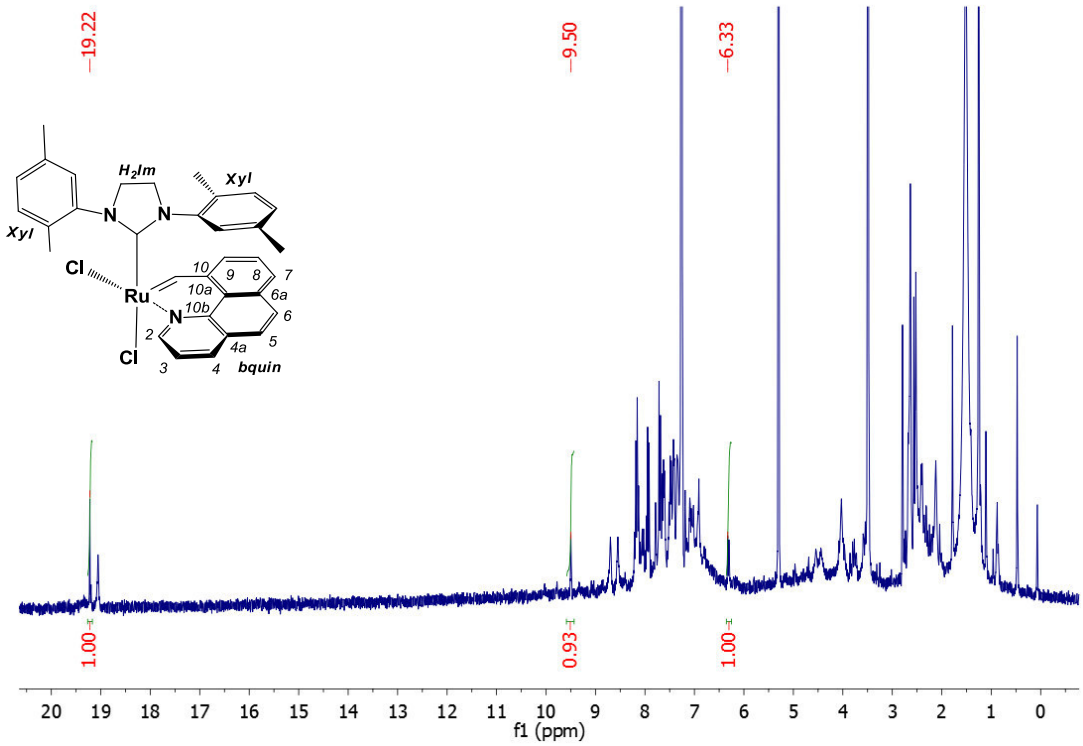

Figure 72. Characteristic ^{1}H-NMR signals of complex **cis-V** (300 MHz, 25°C, $CDCl_3$).

2. Chapter II[44h]-III[84]

2.1. General Protocol for Isomerization

A stock solution of 5.5 µM of initiators **cis1-5** was prepared in 0.7 mL degassed $CDCl_3$ under inert conditions. Changes in the composition of the solution were monitored by ^1H NMR spectroscopy (300 MHz) at 25°C by recording spectra every few hours. For complexes **cis2**-**cis2d**, the respective compound was prepared in 0.8 mL degassed $CDCl_3$ ($c_{[Ru]}$ = 5.0 mM). Rearrangement reactions for this series were monitored by ^1H NMR spectroscopy (500 MHz). In case of the NHC series, 7.0 mM stock solutions of the respective *trans*-compounds **6**-**10** were dissolved in degassed $CDCl_3$ under inert atmosphere (N_2) and subsequently exposed for 1 h in the microwave at 140°C. For all experiments, the final distribution of the respective complex was then evaluated until the equilibrium was balanced. Isomerization reactions were characterized by signals within the carbene region. Decomposition was assigned to the appearance of an aldehyde (**decomp**), with a significant peak between 10 and 11 ppm. Signals for new compounds **1-5** are summarized in Table 28. Typical *cis*- and *trans*-signals were explained in the respective publications.

Scheme 35. Isomerization of benzylidene [Ru] complexes at rt in $CDCl_3$.

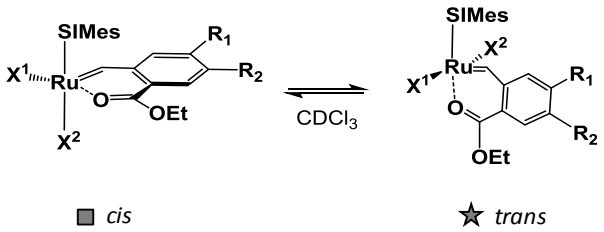

Table 28. Characteristic ^1H NMR signals for isomerization and decomposition products, recorded in $CDCl_3$.

Initiator	cis	trans	decomp
1	18.96	18.72	10.62
2	18.92	18.71	10.72
2b	18.38	18.28	10.72
2c	18.54	17.73	10.72
2d	19.01	18.28	10.72
3	18.57	18.35	10.48
4	19.09	18.71	10.62
5	19.37	19.02	10.72

Exemplary characterization of ethyl 2-formyl-4-methoxy benzoate (**decomp2**):

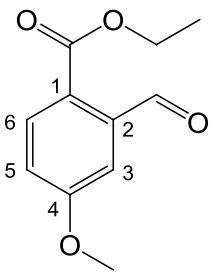

^{1}H-NMR (δ, 25°C, $CDCl_3$, 300 MHz): 10.71 (s, 1H, C*H*O), 7.99 (d, 1H, $^3J_{HH}$ = 8.7 Hz, ph^3), 7.40 (d, 1H, $^4J_{HH}$ = 2.7 Hz, ph^6), 7.11 (d, 1H, $^3J_{HH}$ = 8.8 Hz, ph^5), 4.40 (m, 2H, CH_2CH_3), 3.90 (s, 3H, OCH_3), 1.41 (t, 3H, CH_2CH_3).

2.1.1. Isomerization in $CDCl_3$

Results of the abovementioned experiments with **cis2**-**cis2d** are summarized in Figure 73.

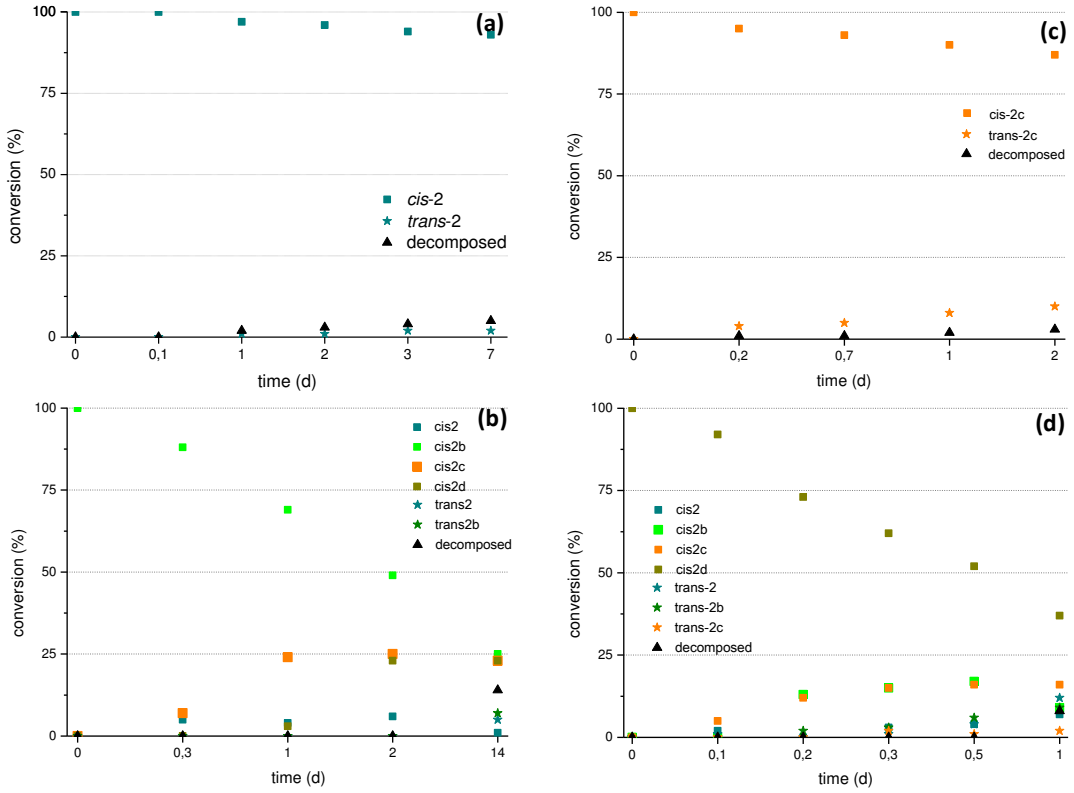

Figure 73. Isomerization of **cis2** - **cis2d** ($CDCl_3$) within 1 - 14 days.

Results of abovementioned experiments with **cis1** - **cis5** and **trans4** are summarized in Figure 74.

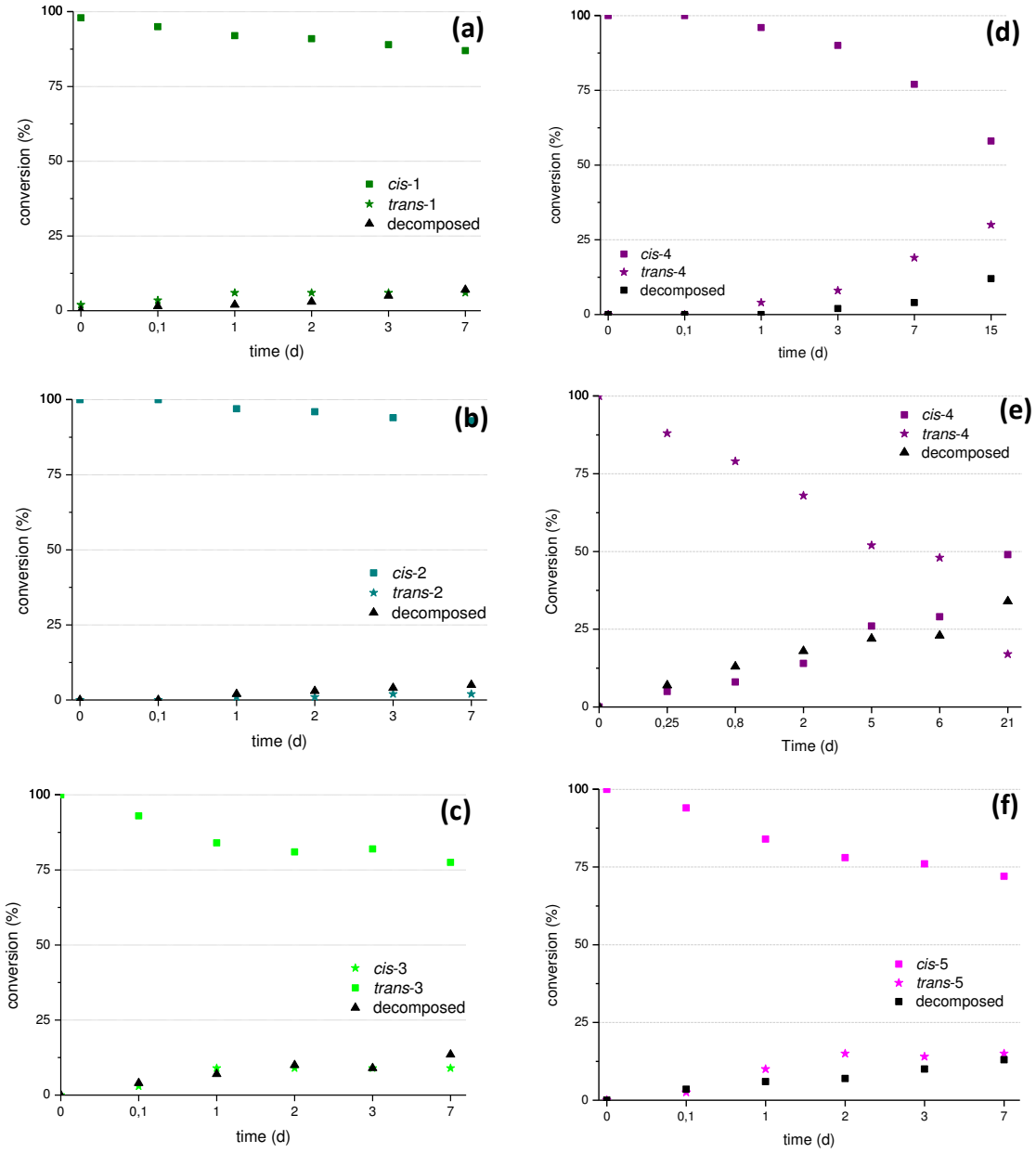

Figure 74. Isomerization of **cis1** (a), **cis2** (b), **cis3** (c) **cis4** (d), **trans4** (e) and **cis5** (f) in $CDCl_3$ within 7 - 21 days.

The same thermodynamic equilibrium was found for **4** in both caseswhen starting from **cis4** and when starting from **trans4**, as shown in Figure 74, entry (**d**) and (**e**).

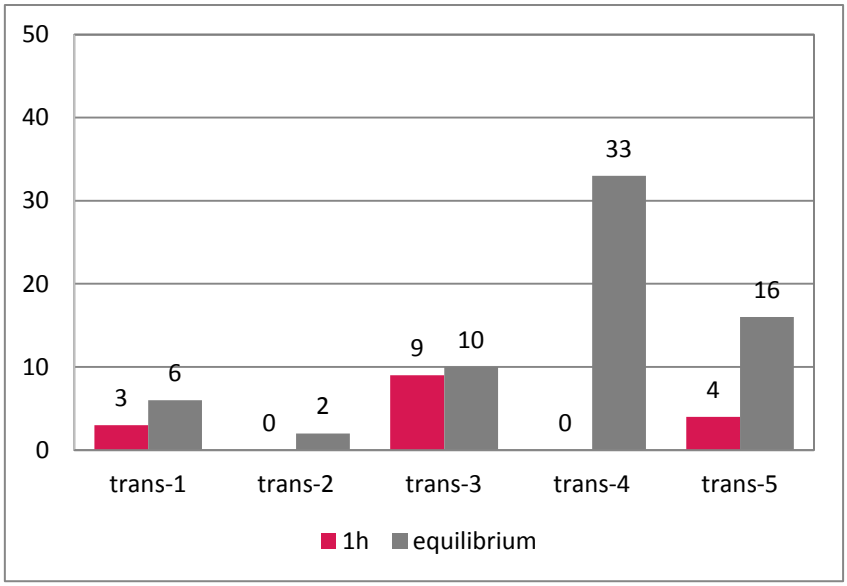

Figure 75. Percentage of **trans1-5** after 1 hour and after equilibrium has balanced.

Thermodynamic equilibrium constants for isomerization were calculated at 298.15 K from $\Delta G_{trans\text{-}cis} = -RT \cdot \ln K$ and are found to be conform to theoretically calculated values. Used values are shown in Table 29.

Table 29. Relevant values for determining the thermodynamic equilibrium constant ($\Delta G_{trans\text{-}cis}$).

Initiator	cis (%)	trans (%)	K	$\Delta G_{trans\text{-}cis}$ (kcal/mol)
1	94	6	0.064	1.6
2	98	2	0.020	2.3
3	90	10	0.111	1.3
4	67	33	0.492	0.4
5	84	16	0.190	1.0

2.1.2. Isomerization during Synthesis

Scheme 36. Investigation of the impact of pyridine on the isomerization during the synthesis, starting from **M31**.

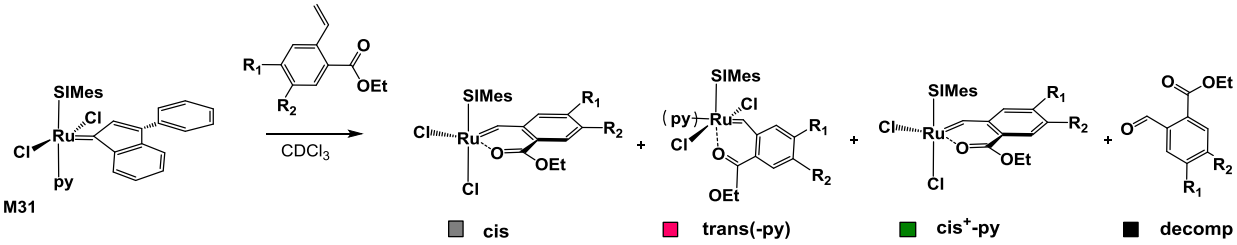

1.0 eq of **M31** (5.5 mg, 0.00734 mmol, 1.0 eq) was weighed in a NMR tube under nitrogen atmosphere and dissolved in 0.4 mL degassed $CDCl_3$. The respective amount of ligand **L1-3** – **L5-3** (0.00880 mmol, 1.2 eq) was dissolved in 0.3 mL deuterated solvent and injected. The formation of **cis**, **trans$_{py}$**, **cis$^{+}_{py}$** and **decomp** were followed by ^{1}H-NMR spectroscopy (300 MHz) at 25°C, recording spectra every few hours. Results are summarized in Figure 76 - Figure 80.

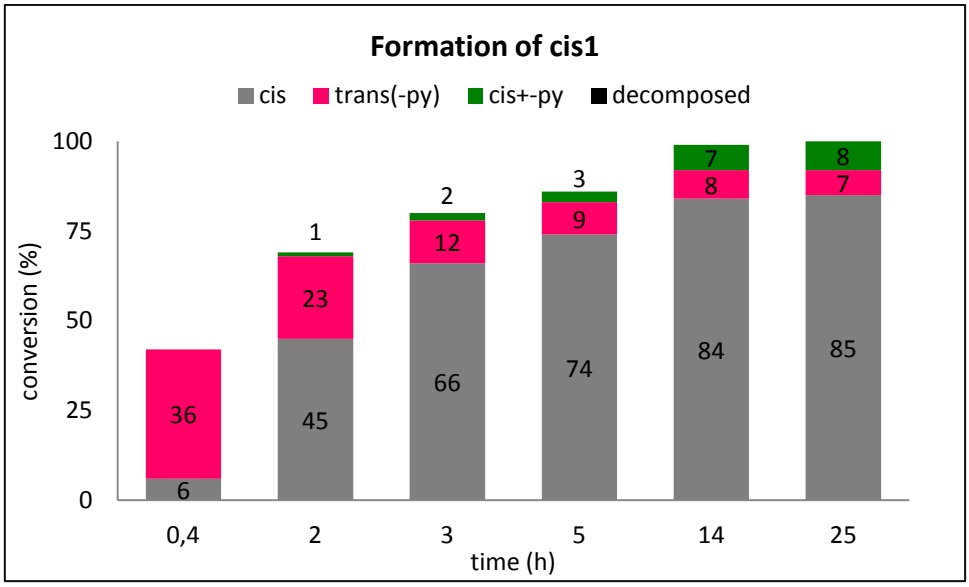

Figure 76. Product distribution during preparing **cis1** followed by ^{1}H NMR spectroscopy (300 MHz, $CDCl_3$, 25°C).

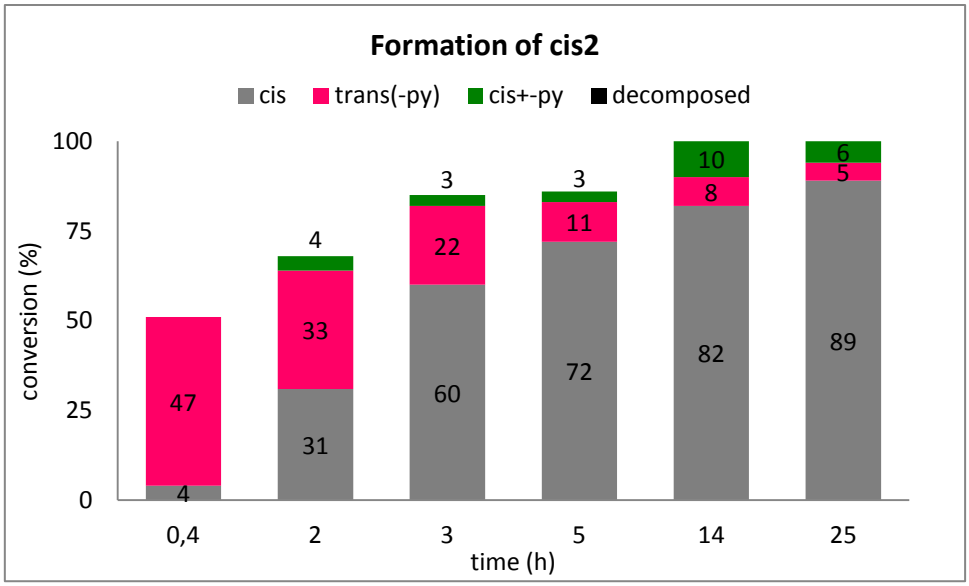

Figure 77. Product distribution during preparing **cis2**, followed by ^{1}H NMR spectroscopy (300 MHz, $CDCl_3$, 25°C).

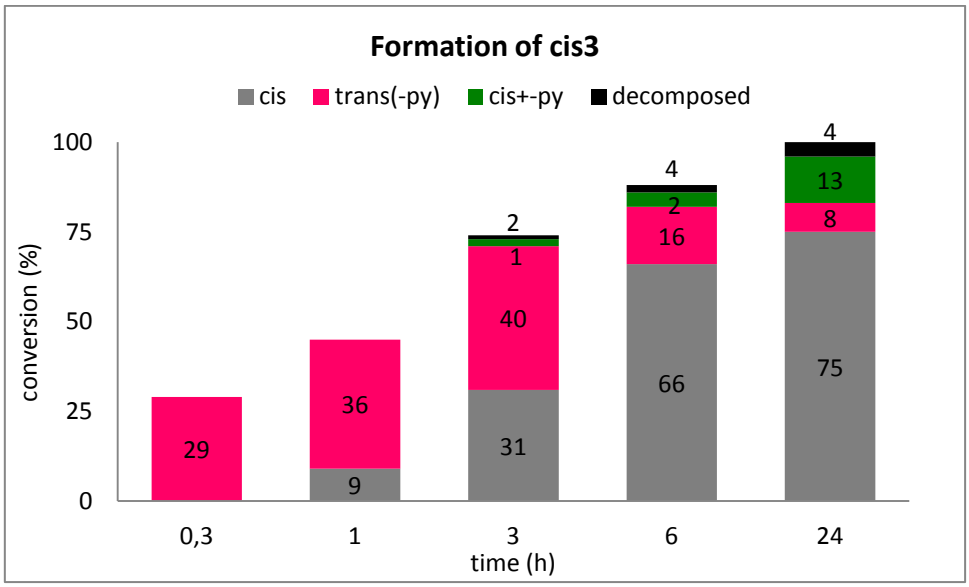

Figure 78. Product distribution during preparing **cis3**, followed by ^{1}H NMR spectroscopy (300 MHz, $CDCl_3$, 25°C).

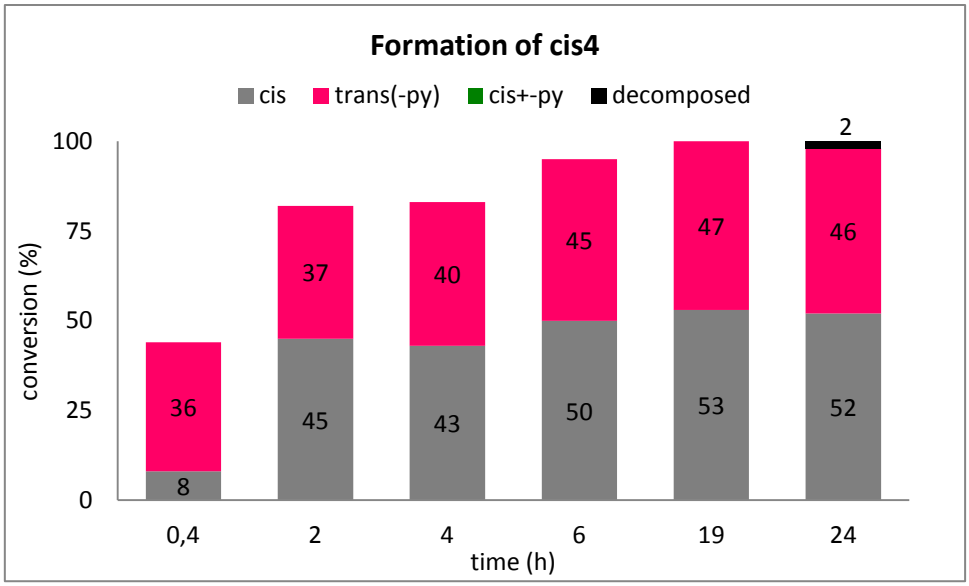

Figure 79. Product distribution during preparing **cis4**, followed by ^{1}H NMR spectroscopy (300 MHz, $CDCl_3$, 25°C)

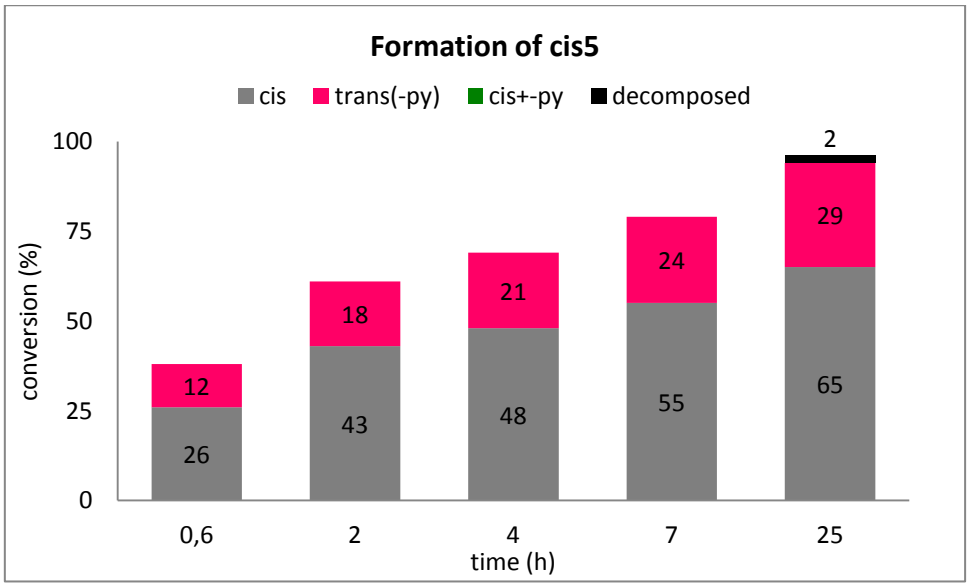

Figure 80. Product distribution during preparing **cis5**, followed by ^{1}H NMR spectroscopy (300 MHz, $CDCl_3$, 25°C).

Polymerization

1. Chapter I-IV

1.1. Polymerization in Solution (**mon1**)

Scheme 37. Polymerization with monomer **mon1**.

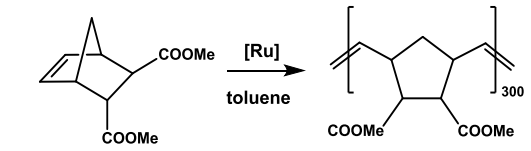

mon1 **poly1**

Monomer **mon1** ((±)-*endo*-*exo*-bicycle[2.2.1]hept-2-ene-2,3-dicarboxylic acid dimethyl ester) was selected as **poly1** is not prone to secondary metathesis reactions (e.g. back-biting) and is consequentially not degraded by the initiators.[105] In a Schlenk flask, the respective initiator (1.27 µmol, 1.0 eq) was dissolved in toluene (3.8 mL, $c_{[8]}$=0.1 M). Subsequently, the mixture was heated to 80°C then **mon1** (100.0 mg, 0.38 mmol, 300 eq) was added, dissolved in 1 mL toluene. The reaction was followed by TLC using Cy:EA, 3:1 (v:v) and $KMnO_4$-solution for staining. After complete conversionm the reaction was quenched with an excess of ethyl vinylether (200 µL) and stirred for 15 more minutes. Further, the solvent was evaporated to a volume of 2-3 mL and the polymer was precipitated in cold, stirred methanol. The white solid was sampled and dried in vacuum. Characteristic polymer properties were examined by gel permeation chromatography (GPC) in THF against polystyrene standards.

(105) (a) Riegler, S.; Demel, S.; Trimmel, G.; Slugovc, C.; Stelzer, F. *J. Mol. Catal.A-Chem.* **2006**, *257*, 53-58; (b) Slugovc, C.; Demel, S.; Riegler, S.; Hobisch, J.; Stelzer, F. *J. Mol. Catal. A*-Chem. **2004**, *213*, 107-113.

1.2. Kinetic Measurement (**mon1**)

Scheme 38. Kinteic measurement with monomer **mon1**.

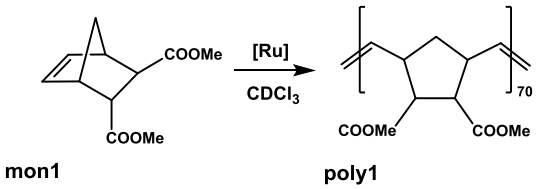

1.0 eq of the respective initiator was weighed in a NMR tube under nitrogen atmosphere and dissolved in 0.5 mL degassed $CDCl_3$. The appropriate amount of **mon1** (22.0 mg, 0.10 mmol, 70 eq) was dissolved in 0.3 mL deuterated solvent and injected. The propagation was monitored by ^1H NMR spectroscopy (500 MHz) at 25°C, recording spectra every few hours.

1.3. STA measurements (**mon2**)

Scheme 39. Polymerization with monomer **mon2**.

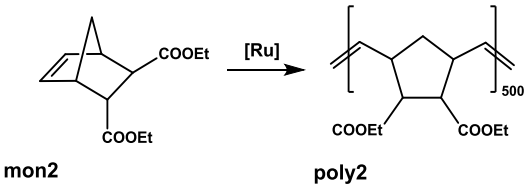

A stock solution of the initiator with a concentration $c_{[Ru]}$ = 1-3 mM was prepared. 60 µL of this stock solution (0.83 µmol) were transferred into a 2 mL glass vial and 100 µL of liquid (±)-*endo*-*exo*-5,6-bis(ethoxymethyl)bicycle[2.2.1]hept-2-ene **mon2** (d = 1.0 g/mL, 0.42 mmol) were added and well-mixed. The solvent was removed by a N_2-stream and then immediately shock frozen by liquid nitrogen to avoid any premature activation. For transportation the vial was stored in a Styropfoam container. About 8-12 mg of the mixture were transferred into a cooled DSC pan, which was then subjected to the STA run. The analysis was run with a constant He gas stream of 50 mL/min at a heat rate of 3 K/min, starting at 20°C.

Mechanical Properties of *poly*-DCPD

Scheme 40. Polymerization with monomer **mon3**.

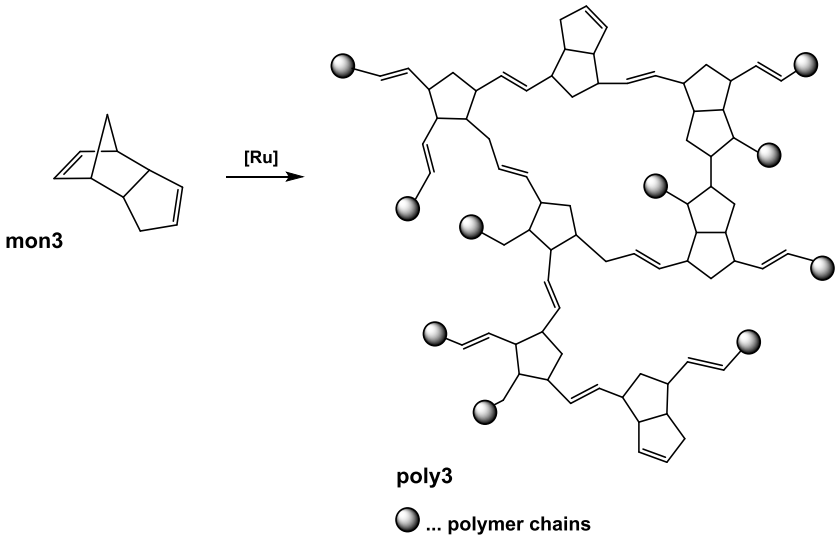

1. Chapter I

1.1. Compression Tests

Initiator **M2** (4.4 mmol, 20 ppm) and **trans-I - trans-V** ($c_{[Ru]}$ = 11 mM) were weighed each into 50 mL Eppendorf tubes and dissolved in 900 µL toluene. 30.9 mL of *pre*-prepared, liquid **mon3** (30 $\mu L_{toluene}/mL_{DCPD}$) were added and well-mixed. Half of the solution (15.9 mL) was transferred to a 20 mL glass vial (d = 25 mm) and heated for 24 h at 80°C, 110°C (I) or 140°C. For determining mechanical properties, 8 mm slices of properly polymerized samples were prepared for compression tests (Shimadzu Autograph AGS-X). The analysis was performed with a speed rate of 5 mm/min until either a force of 5000 N or a sample height of 2 mm was reached. The second part of the sample was stored at rt for 2 weeks and then again reacted at 110°C (II).

1.2. Tensile Strength

Initiator **M2** (4.4 mmol, 20 ppm) and **trans-II** (11 mmol, 50 ppm) were weighed each into a 50 mL Eppendorf tube. The catalyst was dissolved in 900 µL toluene and subsequently mixed with 30.9 mL of liquid monomer **mon3** (30 $\mu L_{toluene}/mL_{DCPD}$). Afterwards the mixture was poured into a test bar mould, which was immediately covered with a glass plate for providing the evaporation of volatile monomer **mon3**. The mould was heated in an oven for 24 h at 80°C for **M2** and at 110°C for **trans-II** (I). The same procedure was applied for an identical sample of **trans-II**, after storing the monomer/initiator formulation for 1 week at room temperature (II). Tests were performed on a Shimadzu Autograph AGS-X, with a force measuring range from 1-10 kN. The clamping length of the samples was 80 mm; an initial tension of 10 N was applied. The area of the shoulder test bars was 35.2 mm^2 in the reduced section; samples were measured with a speed of 1 mm/min.

DFT Calculations

1. Energy Surface

The DFT geometry optimizations were performed at the GGA level with the Gaussian09 package,[106] using the BP86 functional of Becke and Perdew.[107] No symmetry constraint was used in the geometry optimizations, and the final geometries were confirmed to be minimum potential energy structures through frequency calculations. The electronic configuration of the molecular systems was described with the standard splitvalence basis set with a polarization function of Ahlrichs and co-workers for H, C, N, O, and Cl (SVP keyword in Gaussian09),[108] for Ru we used the small-core, quasirelativistic Stuttgart/Dresden effective core potential, with the associated valence basis set (standard SDD keywords in Gaussian09).[109] The reported energies have been obtained through single point calculations with the M06 functional of Truhlar. In these single point calculations the electronic configuration of the molecular systems was described by a triple-ζ basis set for main group atoms (TZVP keyword in Gaussian09).[110] Solvent effects including contributions of non-electrostatic terms have been estimated in zero point calculations on the gas phase

(106) Gaussian 09, Revision D.01, Frisch, M. J.; Trucks, G. W.; Schlegel, H. B.; Scuseria, G. E.; Robb, M. A.; Cheeseman, J. R.; Scalmani, G.; Barone, V.; Mennucci, B.; Petersson, G. A.; Nakatsuji, H.; Caricato, M.; Li, X.; Hratchian, H. P.; Izmaylov, A. F.; Bloino, J.; Zheng, G.; Sonnenberg, J. L.; Hada, M.; Ehara, M.; Toyota, K.; Fukuda, R.; Hasegawa, J.; Ishida, M.; Nakajima, T.; Honda, Y.; Kitao, O.; Nakai, H.; Vreven, T.; Montgomery, J. A., Jr.; Peralta, J. E.; Ogliaro, F.; Bearpark, M.; Heyd, J. J.; Brothers, E.; Kudin, K. N.; Staroverov, V. N.; Kobayashi, R.; Normand, J.; Raghavachari, K.; Rendell, A.; Burant, J. C.; Iyengar, S. S.; Tomasi, J.; Cossi, M.; Rega, N.; Millam, N. J.; Klene, M.; Knox, J. E.; Cross, J. B.; Bakken, V.; Adamo, C.; Jaramillo, J.; Gomperts, R.; Stratmann, R. E.; Yazyev, O.; Austin, A. J.; Cammi, R.; Pomelli, C.; Ochterski, J. W.; Martin, R. L.; Morokuma, K.; Zakrzewski, V. G.; Voth, G. A.; Salvador, P.; Dannenberg, J. J.; Dapprich, S.; Daniels, A. D.; Farkas, Ö.; Foresman, J. B.; Ortiz, J. V.; Cioslowski, J.; Fox, D. J. Gaussian, Inc., Wallingford CT, **2009**.

(107) (a) Becke, A. D. Phys. Rev. A 1988, 38, 3098-3100. (b) Perdew, J. P. *Phys. Rev. B* **1986**, *33*, 8822–8824. (c) Perdew, J. P. *Phys. Rev. B* **1986**, *34*, 7406-7406.

(108) Schaefer, A.; Horn, H.; Ahlrichs, R. *J. Chem. Phys.* **1992**, *97*, 2571-2577.

(109) (a) Leininger, T.; Nicklass, A.; Stoll, H.; Dolg, M.; Schwerdtfeger, P. *J. Chem. Phys.* **1996**, *105*, 1052–1059. (b) Kuechle, W.; Dolg, M.; Stoll, H.; Preuss, H. *J. Chem. Phys.* **1994**, *100*, 7535-7535. (c) Haeusermann, U.; Dolg, M.; Stoll, H.; Preuss, H. *Mol. Phys.* **1993**, *78*, 1211–1224.

(110) Schaefer, A.; Huber, C.; Ahlrichs, R. *J. Chem. Phys.* **1994**, *100*, 5829-5835.

optimized structures, based on the polarizable continuum solvation model PCM, using toluene ($2.4 \cdot 10^{-30}$ Cm), benzene ($2.3 \cdot 10^{-30}$ Cm), CCl_4 ($2.2 \cdot 10^{-30}$ Cm), $CHCl_3$ ($4.8 \cdot 10^{-30}$ Cm), THF ($7.5 \cdot 10^{-30}$ Cm), CH_2Cl_2 ($9.1 \cdot 10^{-30}$ Cm) as the solvent.[111] Diffusion coefficients for Cl and O were involved using Def2-TZVPD basis set for Gaussian94.[112]

2. NMR Simulations

For NMR simulations zero point calculations on the BP86 optimized geometries were done, using B3LYP functional, including the keyword NMR and CHLOROFORM as solvent. An individual basis set based on IGLO-II (specific for NMR simulation) was used, considering special parameters for C, H, Cl, O and N.[112]

(111) Tomasi, J.; Persico, M. *Chem. Rev.* **1994**, *94*, 2027-2094.

(112) https://bse.pnl.gov/bse/portal

appendix

1. List of Abbreviations

Anal. Calcd.	analytical calculated
BP86	hybrid functional method, applied in DFT
BuVe	butyl vinylether
Cu(I)Cl	copper chloride
Cy	cyclohexane
DCM	dichloromethane
DEDAM	diethyl diallyl malonate
DFT	density functional theory
dtbpm	bis(di-tert-butylphosphanyl)methane
CH_2Cl_2	dichloromethane
EA	ethyl acetate
Et_2O	diethyl ether
eq	equivalent
GGA	generalized gradient approximation (DFT)
GPC	gel permeation chromatography
H_2Im	4,5-dihydroimidazol-2-ylidene
Ind	indenylidene
k_i	initiation rate constant
k_p	propagation rate constant
M06	hybrid functional method, applied in DFT
MeOH	methanol
M:I	monomer:initiator
M_n	number molecular weight
MWD	molecular weight distribution
NHC	N-heterocyclic carbene
NMR	nuclear magnetic resonance
pcm	polarizable continuum model (DFT)
PCy_3	tricyclohexylphosphine
PDI	poly dispersity index

$Pd(PPh_3)_4$	tetrakis(triphenylphosphine)palladium
py	pyridine
ROMP	ring opening metathesis polymerization
rt	room temperature
STA	simulatnous thermal analysis
SIMes	saturated 1,3-bis-mesityl-imidazol-2-ylidene
SI*o*tol	saturated 1,3-bis-bis-*o*-toluyl-imidazol-2-ylidene
SIPr	saturated 1,3-bis-(2',6'-di-*iso*-propyl)phenyl
SIXyl	saturated 1,3-bis-bis-xylyl-imidazol-2-ylidene
SPY	square pyramidal
SVP	single polarized valance (basis set DFT)
UV	ultra violet
TLC	thin layer chromatography
TZVP	triple zeta polarized valance (basis set DFT)
XRD	X-ray diffraction

2. List of Figures

3. List of Schemes

4. List of Tables